Aristotle University of Thessaloniki
School of Electrical and Computer Engineering
Telecommunications Department

Alexandros-Apostolos A. Boulogeorgos
Diploma in Electrical and Computer Engineering

INTERFERENCE MITIGATION TECHNIQUES IN MODERN WIRELESS COMMUNICATION SYSTEMS

Ph.D Thesis

Thessaloniki
September 2016

INTERFERENCE MITIGATION TECHNIQUES IN MODERN WIRELESS COMMUNICATION SYSTEMS.

by

ALEXANDROS-APOSTOLOS A. BOULOGEORGOS

A Dissertation submitted to the
Aristotle University of Thessaloniki
in partial fulfillment of the requirements
for the Degree of Doctor of Philosophy

September 2016

Approved by the Thesis Committee:

- Dr. George K. Karagiannidis, Supervisor
  Professor, Aristotle University of Thessaloniki, Greece
- Dr. Leonidas G. Georgiadis, Advisory Committee Member
  Professor, Aristotle University of Thessaloniki, Greece
- Dr. Stavros Kotsopoulos, Advisory Committee Member
  Professor, University of Patras, Greece
- Dr. Fotini-Niovi Pavlidou, Examination Committee Member
  Professor, Aristotle University of Thessaloniki, Greece
- Dr. Traianos Yioultsis, Examination Committee Member
  Associate Professor, Aristotle University of Thessaloniki, Greece
- Dr. Nikolaos Kantartzis, Examination Committee Member
  Associate Professor, Aristotle University of Thessaloniki, Greece
- Dr. Harilaos G. Sandalidis, Examination Committee Member
  Assistant Professor, University of Thessaly, Greece

Interference Mitigation Techniques In Modern Wireless Communication Systems.

To my family
To my teacher

Abstract

During the last decades, wireless communications have evolved from a scarce technology, used by professionals for niche applications to a rapidly advancing research field. Ever increasing proliferation of smart devices, introduction of new emerging multimedia applications, together with an exponential rise in wireless data (multimedia) demand and usage is already creating a significant burden on existing wireless systems. Future wireless networks, with improved data rates, capacity, latency and quality of service (QoS) requirements, are expected to be the panacea of most of the current wireless systems' problems. Interference management is critical towards this goal, whereas transceiver design and implementation is expected to play an important role.

This thesis investigates the influence of interference in wireless systems, revisits promising network- and user-side interference management solutions, as well as studies the impact of interference, caused by hardware imperfections, on the performance of the wireless link and propose countermeasures. The thesis is divided into two parts.

In the first part of the thesis, different types of interference and modern interference management solutions, which are expected to be used in the future wireless networks, are reviewed. Moreover, the influence of fading and interference, due to the existence of multiple possible users operating simultaneously in the same carrier frequency, on the spectrum sensing capability of a low-complexity energy detector (ED) is investigated. Analytical tools for the performance evaluation of this problem, i.e., the false alarm and detection probabilities, are derived, while the problem of appropriately selecting the energy detection threshold and the spectrum sensing duration, in order to satisfy a specific requirement, is discussed. The results reveal the detrimental effect of interference and the importance of taking into consideration the wireless environment, when evaluating the ED spectrum sensing performance and selecting the ED threshold. Finally, the offered analytical framework can be applied in cognitive radio systems, which are include in several wireless standards, and are expected to be employed in ultra-dense wireless environments.

The second part of this thesis investigates the impact of transceivers radio frequency (RF) front-end imperfections on the performance of the wireless system. RF imperfections generally result to signal distortion in single-carrier communications, while, in multi-carrier communications, they additionally cause interference. In both cases, RF imperfections may cause significant degradation to the quality of the wireless link, which becomes more severe as the data rates increases. Motivated by this, after briefly illustrating the influence of different types of RF imperfections, namely in-phase and quadrature imbalance (IQI), phase noise, and amplifiers non-linearities, the analytical framework for the evaluation and quantification of the effect of IQI on wireless communications in the context of cascaded fading channels, is derived. To this end, closed form expressions for the outage probability over $N*$Nakagami-m channels for both the cases of single- and multi-carrier communications, when at least one communication node suffers from IQI, are provided. To justify the importance and practical usefulness of the analysis, the offered expressions along with several deduced corresponding special cases are employed in the context of vehicle-to-vehicle communications. This study gives critical insight for the performance degradation in wireless communications, due to RF imperfections, and indicates the need of designing proper RF imperfections compensation techniques. Next, the impact of IQI and partial successive interference suppression (SIS) in the spectrum sensing of full duplex CR systems, for both the cases of single- and multi-carrier ED, is studied. In this context, closed form expressions are derived for the false alarm and detection probabilities, in the general case, where partial SIS and joint transmitter and receiver IQI are considered. The derived expressions can be used in order to properly select the energy detection threshold that maximizes the ED spectrum sensing capabilities. Additionally, the joint influence of fading and several RF impairments on energy detection based spectrum sensing for CR systems in multi-channel environments is investigated. After assuming flat-fading Rayleigh channels and complex

Gaussian transmitted signals, as well as proving that, for a given channel realization, the joint effect of RF impairments can be modeled as a complex Gaussian process, closed form expressions for the probabilities of false alarm and detection are derived. Based on these expressions, the impact of RF impairments and fading on the spectrum sensing capability of the ED is studied. The results illustrated the degrading influence of RF imperfections on the ED spectrum sensing performance, which bring significant losses in the utilization of the spectrum. Furthermore, the impact of uncompensated IQI on orthogonal frequency division multiple access (OFDMA) systems, in which a power allocation (PA) policy is employed in order to maximize each user's capacity, is demonstrated. To overcome, the user's capacity loss, due to IQI, a novel, low-complexity PA strategy is presented, which, by taking into account the levels of IQI of the served users, notably enhance each user's achievable capacity. Finally, a novel low-complexity scheme, which improves the performance of single-antenna multi-carrier communication systems, suffering from IQI at the receiver, is proposed. The proposed scheme, which we refer to as I/Q imbalance self-interference coordination (IQSC), not only mitigate the detrimental effect of IQI, but, through appropriate signal processing, also coordinates the self-interference terms produced by IQI, in order to achieve second-order frequency diversity. In order to evaluate the performance of IQSC, closed form expressions for the resulting outage probability and symbol error rate are derived. The findings reveal that IQSC is a promising low-complexity technique for significantly increasing the reliability of low-cost devices that suffer from high levels of IQI.

Acknowledgements

This dissertation is the product of my research activity at the Department of Electrical and Computer Engineering of Aristotle University of Thessaloniki, during the years 2012-2016. This research activity corresponds to four productive, educational and demanding years.

My choice to conduct research and seek a Ph.D in Electrical Engineering was very important to me, not only because of the experience and skills that I acquired in research, but also due to the general approach of my everyday life, since pursuing a Ph.D taught me how to face any problem with critical thinking and careful strategy. The experience of forming and sustaining productive collaborations was also very valuable to me, a fact that showed me that the power of collaboration cannot be replaced by the power of oneself.

At this point, I would like to thank all those people who helped me through these years.

I would first like to wholeheartedly thank my advisor and mentor, Dr. George Karagiannidis, Professor at the Department of Electrical and Computer Engineering of Aristotle University of Thessaloniki. His guidance and insight were the catalyst for the completion of this dissertation, while his way of thinking significantly influenced my the way of thinking.

I would like to thank the members of my advisory committee, Dr. Leonidas Georgiadis, Professor at the Department of Electrical and Computer Engineering of Aristotle University of Thessaloniki, and Dr. Stavros Kostopoulos, Professor at the Department of Electrical and Computer Engineering of the University of Patras, for our constructive conversations and valuable collaboration that were necessary for the preparation of this thesis.

My special thanks to Dr. Nestor Chatzidiamantis, Dr. Paschalis Sofotasios, Dr. Koralia Pappi and Dr. Vasileios Kapinas, colleagues and friends, who offered much needed help during my first steps as a researcher, and they are still always happy to discuss any scientific concern I have.

My special thanks also to Dr. Robert Schober, Professor at the Institute for Digital Communications of Friedrich-Alexander University Erlangen-Nürnberg, for believing in me and supporting my efforts.

I would like to thank my colleagues and friends, Mr. Dimitrios Karas, Mr. Panagiotis Diamantoulakis, and Ms. Georgia Ntouni, for our excellent collaboration and their valuable company.

Finally, I would like to express my gratitude to the people who I am lucky to have in my everyday life.

To my friend Dimitra, who stood by me when I needed her, discussed with me several of my concerns, supported my decisions and helped me achieve my goals.

To my friends Dimitrios, Konstantinos, Dora, Panos, Christoforos, Rafaila, Manolis, Georgios, Nikos, Xanthipi, Dimitris, Apostolos, and Alkis, for their support.

To Ms. Dimitra and Mr. Christos, for their moral support and our zestful discussions.

To my aunt Maria, who is always there for me, for her wise counsel and sympathetic ear.

To my family, who stood by me throughout my studies, and helped me achieve my goals.

Alexandros-Apostolos A. Boulogeorgos
September 13, 2016

Contents

List of Figures

List of Tables

Abbreviations

3GPP	Third generation partnership project
4G	Forth generation
5G	Fifth generation
A-IQSC	Alternative I/Q imbalanced self-interference coordination
ABSFs	Almost blank subframes
ACI	Adjacent channel interference
ADC	Analog-to-digital converter
AF	Amplify-and-forward
AM	Amplitude modulation
AM-AM	Amplitude-to-amplitude modulation
AM-PM	Amplitude-to-phase modulation
AWGN	Additive white Gaussian noise
BER	Bit error rate
BPSK	Binary phase shift keying
BS	Base station
CA	Collision avoidance
CB	Coordinated beam forming
CCC	Common control channel
CCI	Co-channel interference
CD	Collision detection
CDD	Cyclic delay diversity
CDF	Cumulative distribution function
CDMA	Code-division-multiple-access
CoMP	Coordination multipoint
CPE	Common phase error
CR	Cognitive radio
CRN	Cognitive radio network
CS	Coordinating scheduling
CSCWG	Circularly symmetric complex white Gaussian
CSI	Channel state information
CSMA	Carrier sense multiple access
DAC	Digital-to-analog converter
DC	Direct current
DCA	Direct conversion architecture
DCR	Direct conversion radio
DF	Decode-and-forward
DFE	Decision feedback equalizer
DoF	Degrees of freedom

DPB	Dynamic point blanking
DPS	Dynamic point selection
DPSK	Differential phase shift keying
DSP	Digital signal processing
DSSS	Direct sequence spectrum sensing
DVB	Digital video broadcasting
ED	Energy detector
eICIC	Enhanced inter-cell interference coordination
FC	Fusion center
FD	Full duplex
FDM	Frequency domain multiplexing
FDMA	Frequency domain multiple access
FHSS	Frequency-hopping spread spectrum
FI	Frequency independent
FM	Frequency modulated
FS	Frequency selective
FTBC	Frequency time block code
HD	Half-duplex
HetNet	Heterogeneous network
HIPERLAN	High performance radio local are network
I	In-phase
i.i.d.	Independent and identically distributed
I/Q	In-phase and quadrature
IA	Interference alignment
IBO	Input back-off factor
IC	Integrated circuit
ICI	Inter-carrier interference
IEEE	Institute of Electrical and Electronics Engineers
IF	Intermediate frequency
IMD	Intermodulation distortion
INR	Interference to noise ratio
IRC	Interference combining
IRR	Image rejection ratio
ISI	Intersymbol interference
ITS	Intelligent transportation system
ITU-R	International telecommunication union's radio communication sector
IQI	In-phase and quadrature imbalance
IQSC	I/Q imbalanced self-interference coordination
JR	Joint reception
JT	Joint transmission
LINCs	Linear amplification using nonlinear components
LLR	Log-likelihood ratio
LM	Lagrange multiplier
LNA	Low noise amplifier
LO	Local oscillator
LoS	Line of sight

LPF	Low pass filter
LTE	Long-term evolution
LTE-A	Long-term evolution advanced
MA	Multiple access
MAP	Maximum a posteriori probability
MFD	Mirror frequency diversity
MIMO	Multiple-input multiple-output
MISO	Multiple-input single-output
ML	Maximum likelihood
MLSE	Maximum-likelihood sequence estimation
MMSE	Minimum mean square error
MRC	Maximum ratio combining
NOMA	Non-orthogonal multiple access
OC	Optimum combining
OFDM	Orthogonal frequency division multiplexing
OFDMA	Orthogonal frequency division multiple access
OSA	Opportunistic spectrum access
P/S	Parallel to serial
PA	Power allocation
PAm	Power amplifier
PDF	Probability density function
PIC	Parallel interference cancellation
PM	Phase modulated
PR	Primary
PSD	Power spectrum density
PSK	Phase shift keying
PU	primary user
Q	Quadrature
QAM	Quadrature amplitude modulation
QoS	Quality of service
QPSK	Quadrature phase-shift keying
RC	Repetition coding
RE	Range extension
RF	Radio frequency
ROC	Receiver operation curves
RV	Random variable
RX	Receiver
SC	Selection combine
SDR	Software define radio
SEP	Symbol error probability
SER	Symbol error rate
SFN	Single frequency network
SIC	Successive interference cancellation
SIMO	Single-input multiple-output
SINR	Signal to interference plus noise ratio
SIS	Self-interference suppression

SISO	Single-input single-output
SNR	Signal to noise ratio
STBC	Space-time block coding
SU	Secondary user
TDM	Time domain multiplexing
TDMA	Time division multiple access
TX	Transmitter
UE	User equipment
UWB	Ultra-wideband
V2V	Vehicle-to-vehicle
WCDMA	Wide-band code division multiple access
WiFi	Wireless Fidelity
WiMAX	Worldwide interoperability for microwave access
WLAN	Wireless local area networks
WWRF	Wireless word research forum
ZF	Zero-forcing

List of Symbols

$*$	convolution
$\ln(x)$	natural logarithm of x
$\log_2(x)$	base-2 logarithm of x
$\log_{10}(x)$	base-10 logarithm of x
$\exp(x)$	exponential of x
$\sin(x)$	sine of x
$\cos(x)$	cosine of x
$\tan(x)$	tangent of x
$\frac{df(x)}{dlx}$	derivative of function f with respect to x_i
$\frac{\partial f(x_1,\cdots,x_i,\cdots,x_m)}{\partial x_i}$	partial derivative of function f with respect to x_i
$\tan^{-1}(x)$	arc tangent of x
$\lvert\cdot\rvert$	absolute value
$(\cdot)^*$	conjugate
$(\cdot)^T$	transpose
$\mathbf{0}_{M\times N}$	$M \times N$ zero matrix
$\text{rank}(\cdot)$	rank function
$\{a_1,\ldots,a_n\}$	a set of n terms
$[a_1,\ldots,a_n]$	a tuples-type set of n terms
$(a_1,\ldots,a_n)$	a sequence of n terms
$\mathcal{A}\cup\mathcal{B}$	union of the sets $\mathcal{A}$ and $\mathcal{B}$
$\mathcal{A}\cap\mathcal{B}$	intersection of the sets $\mathcal{A}$ and $\mathcal{B}$
$\mathcal{A}\subseteq\mathcal{B}$	$\mathcal{A}$ is a subset of $\mathcal{B}$
$\max(\cdot)$	maximum value of a set of elements
$\min(\cdot)$	minimum value of a set of elements
$\text{med}(\cdot)$	median value of a set of elements
$E[\cdot]$	expected value
$\text{Var}[\cdot]$	variance

$\mathrm{card}(\cdot)$	cardinality of a set
$k!$	factorial of k
$\binom{a}{b}$	binomial coefficient
$\Re\{\mathbf{x}\}$	real part of complex vector $\mathbf{x}$
$\Im\{\mathbf{x}\}$	imaginary part of complex vector $\mathbf{x}$
$\mathcal{CN}\left(\mu, \sigma^2\right)$	complex Gaussian process with mean μ and variance σ^2
N_0	noise power spectral density
P_e	probability of error
$P_r(\cdot)$	probability
$f_x(x)$	probability density function of x
$F_x(x)$	cumulative distribution function of x
$\lfloor \cdot \rfloor$	floor function
$\lceil \cdot \rceil$	ceil function
$\mathrm{sgn}(\cdot)$	sign function
$\gcd(\cdot)$	greatest common division function
$U(\cdot)$	step function
$\mathrm{erfc}(\cdot)$	complementary error function
$Q(\cdot)$	Q-function
$Q^{-1}(\cdot)$	inverse Q-function
$\Gamma(\cdot)$	Gamma function
$\Gamma(\cdot, \cdot)$	upper incomplete Gamma function
$\gamma(\cdot, \cdot)$	lower incomplete Gamma function
$\Gamma(\cdot, \cdot, \cdot, \cdot)$	extended incomplete Gamma function
$E_n(\cdot)$	exponential integral function
$K_n(\cdot)$	modified Bessel function of the second kind
${}_mF_n(a_1, \cdots, a_m; b_1, \cdots, b_n; x)$	generalized hypergeometric function
$G_{p,q}^{m,n}\left[x \middle\vert \begin{matrix} \alpha_1, \ldots, \alpha_p \\ \beta_1, \ldots, \beta_q \end{matrix}\right]$	Meijer's G-function
$\lim_{x \to x_o}(g(x))$	limiting value of $g(x)$ when x approaches x_o

Part I

Introduction

Chapter 1

Thesis Layout

During the last decades, wireless communications have been a subject of much hype, due to their increasing integration in everyday life. As a result, they have evolved significantly from early voice systems to today's highly sophisticated integrated communication platforms that provide numerous services, which are used by billions of people around the world. These services, coupled with an expanding cache of bandwidth hungry applications, have triggered demands for higher data rates. Moreover, by 2020, it is expected that approximately 6×10^9 wireless devices will serve the global population. Consequently, the mobile data traffic has been forecasted to grow more than 24−fold between 2010 and 2015, and more than 500−fold between 2010 and 2020 [1]. On the other hand, as wireless systems evolve, we are confronting more and more inherent limitations preventing further performance improvements. Among all the limitations of wireless systems, interference is one of the biggest concerns, since it can significantly constrain the throughput and reliability of the wireless link [2–7]. Therefore, interference identification and mitigation or coordination have become critical issues for modern wireless systems.

1.1 Cornerstones in the history of interference identification and management

The problem of interference, due to the transmission medium limitations, dates back at least to 1858, when it was observed during the first transatlantic communication through the telegraph cable, and led Lord Kelvin to the formulation of *the theory of dispersion* [8]. In later decades, Heaviside and Pupin understood the source of this type of interference by analyzing the nature of the propagation medium and laid the groundwork in confronting this problem, which is now called intersymbol interference (ISI). After this, several researcher studied the impact of ISI in different wired and wireless systems, and proposed ISI mitigation solutions (see for example [9–21] and references therein). The major approaches for the ISI elimination are based on appropriately designing the transmission and reception filters, applying coding schemes, adding guard periods between consecutive transmissions, employing channel equalization at the receiver (RX), and using sequence detector at the RX. Nowadays, due to the evolution on the design of communications systems and devices, ISI is considered to be easily avoided and canceled. For example, in multi-carrier systems, guard periods are widely employed in order to fully mitigate the influence of ISI.

Another handicap for the performance of the wireless systems is interference from neighboring communication devices operating simultaneously at the same frequency. Claude E. Shannon was the first one to discuss the problem of the interaction between two user equipments (UEs), which share the same channel [22]. His work was followed by several researchers, who investigated the so-called co-channel interference (CCI) problem and presented system- and RX-design avoidance, suppression or mitigation approaches. In system-design approaches, transmission of co-channel signals is properly managed so that the power of received CCI is maintained below an acceptable level [23–25]. In contrast, RX-design approaches actively mitigate the CCI, which cannot be separated by the preemptive system-design approaches. In practical systems, both approaches are employed in joint fashions to reduce the interference.

The first part of the dissertation is devoted in reviewing the main types of interference and presenting network- and device-side approaches in order to manage the impact of interference in the fifth generation (5G) wireless systems.

1.2 Dirty RF

In 1948, Claude E. Shannon published his impact treatise and put a clear border around the region within which reliable communication is feasible [26]. The notion of capacity was born, followed by

the obsession to design and deploy systems capable of reaching such capacity [27]. After this, great amount of effort was put in the theoretical characterization of the capacities of several channel settings of interest, with the inclusion of fading and multiple-input multiple-output (MIMO) [28–33]. However, most of these efforts ignore the impact of transceiver radio frequency (RF) chain. As a result, doubts about the feasibility and viability of physical layer research have naturally arisen. Specifically, in [27], the authors highlighted the need for *"more realistic theory and more holistic designs"* that takes into consideration the influence of RF impairments.

The history of identifying and compensating the RF imperfections dates back at least to 1940, when Morisson observed the impact of power amplifiers nonlinearities in wide-band frequency modulated (FM) transmissions and proposed a hardware based solution in order to suppress their detrimental effect [34]. Two decades later, Edson highlighted the influence of phase noise in the transceiver's performance, and presented an oscillator design methodology, which aims in reducing its impact [35]. At the same time, Love discussed the intermodulation effect, due to amplifiers nonlinearities, in FM and phase modulated (PM) systems [36]. In 1990, Casadevall and Olmos studied the influence of gain and phase mismatches between the two RF paths, and the different nonlinear characteristics of both RF power amplifiers in linear amplification using nonlinear components (LINCs) transmitter (TX) [37]. More recently, the impact of RF impairments in the performance of terrestrial [38–54] and satellite [55–61] communication systems was presented.

All previously mentioned research efforts conclude that RF impairments may cause significant degradation to the quality of the wireless link, which becomes more severe as the data rates increases. Therefore, it is important to suppress their effect. Early approaches in mitigating the impact of RF imperfections were circuit-based solution that aimed in improving the hardware quality and/or suppressing the detrimental influence of the imperfections (see for example [62–69] and references therein). However, circuit-based approaches often increase the communication device cost and energy consumption, while, at the same time, reduce the device's compactness. Motivated by this, the concept of *Dirty RF* was born [49]. The main idea behind this concept is to design digital signal processing (DSP) solutions to cope with RF impairments, allowing lee-way in the requirements set of the communication devices, i.e., to live with imperfect RF and compensate the resulting effects using digital baseband processing [49, 66, 70–73]. More details about this approach are presented in the second part of the dissertation.

1.3 Thesis Layout

This dissertation is divided into two main parts. The first part, which consists of two chapters, extensively reviews the different types of interference and discusses interference management solutions that are used (or expected to be used) in modern wireless communication systems. Additionally, it investigates the impact of CCI and fading in energy detection spectrum sensing. The second part, which is comprised of six chapters, focuses in the interference caused to the devices, due to RF imperfections, presents the analytical framework that is needed in order to quantify and evaluate the impact of RF imperfections, as well as two novel RF imperfections mitigation techniques. The dissertation's chapters are briefly described below.

1.3.1 Types of interference and interference managment

Chapter 2 serves as an introduction to the different types of interference and modern interference management techniques, which are expected to be widely used in the 5G communication systems. In this context, the definitions of different types of interference as well as their influence in the quality of the communication link is revisited. Finally, key technologies and techniques, which will possibly be included in 5G and will enable significant interference suppression are highlighted.

Chapter 3 studies the influence of fading and CCI, which is caused by multiple primary users (PUs), on the spectrum sensing of a classical energy detector (ED). Specifically, novel closed form expressions for the false alarm and detection probabilities in a multiple PUs environment, assuming Nakagami-m fading and complex Gaussian PUs transmitted signals, are derived. The results reveal the importance of taking into consideration the wireless environment, when evaluating the ED spectrum sensing performance and selecting the ED threshold.

1.3.2 Interference due to hardware impairments

Chapter 4 serves as an introduction to the major RF impairments, namely in-phase (I) and quadrature (Q) imbalance (IQI), phase noise, and amplifier nonlinearities. In this chapter, the source of imperfections on modern transceivers are identified. Additionally, the model of each RF impairment is extensively described, as well as their influence in the transmitted and received signal in both single- and multi-carrier communications.

In Chapter 5, the analytical framework for the quantification and evaluation of the impact of IQI on wireless single- and multi-carrier communications, in the context of cascaded fading channel, is presented. To this end, closed form expressions are firstly derived for the outage probability over N*Nakagami$-m$ channels for the cases of ideal TX and RX, ideal TX and IQI RX, IQI TX and ideal RX, and joint TX/RX IQI. To justify their importance and practical usefulness, the offered expressions along with several deduced corresponding special cases are subsequently employed in the context of vehicle-to-vehicle (V2V) communications. Extensive numerical and simulation results are presented, which give insight for the detrimental effect of IQI in the quality of the wireless link.

In Chapter 6, the influence of IQI in the energy-based spectrum sensing is investigated. In more details, this chapter is focused in quantifying and evaluating the impact of IQI in single- and multi-carrier EDs operating in full duplex (FD) mode, under both cooperative and non-cooperative sensing. Tractable closed form expressions for the false alarm and detection probabilities are derived in the most general case, in which partial self-interference suppression (SIS) and joint TX/RX IQI are considered. Additionally, simplified closed form expressions for the special cases, where either the RF front-end is ideal or the SIS technique is perfect, are also presented. The offered expressions can be used in order to appropriately set the energy threshold, as well as the sensing duration. The derived results indicate that the IQI and partial SIS can significantly affect spectrum sensing accuracy in FD-based cognitive radio (CR) networks (CRNs).

In Chapter 7, the joint effect of RF impairments, namely IQI, phase noise and low noise amplifier (LNA) nonlinearities, on energy detection based spectrum sensing for CR systems in multi-channel environments, is studied. In particular, novel closed-form expressions for the evaluation of the detection and false alarm probabilities, assuming Rayleigh fading, are provided. Furthermore, the analysis is extended to the case of CRNs with cooperative sensing, where the secondary users (SUs) suffer from different levels of RF imperfections, considering both the scenarios of error free and imperfect reporting channel. Numerical and simulation results demonstrate the accuracy of the analysis as well as the detrimental impact of RF imperfections on the spectrum sensing performance, which bring significant losses in the spectrum utilization.

In Chapter 8, the power allocation (PA) problem in an orthogonal frequency-division multiple access (ODFMA) system, when the served UEs suffer from different levels of IQI, is addressed. In this context, novel low-complexity solution with directly calculated PA policies, given the Lagrange multiplier, is presented, which, by taking into account the influence of IQI, achieves fairness in terms of capacity for the served UEs, by maximizing the minimum achievable capacity of the UEs. Simulation results show that, by using the proposed PA strategy, the achievable rate of each UE drastically enhanced, while the system's computational complexity is the same as the conventional PA strategy.

Chapter 9, presents a novel low-complexity scheme, which improves the performance of single-antenna multi-carrier communication systems, suffering from IQI at the RX. We refer to the proposed scheme as I/Q-imbalance self-interference coordination (IQSC). IQSC does not only mitigate the detrimental effect of IQI, but, through appropriate signal processing, also coordinates the self-interference terms produced by IQI, in order to achieve second-order frequency diversity. However, these benefits come at the expense of a reduction in transmission rate. More specifically, IQSC is a simple transmit diversity scheme that improves the signal quality at the receiver by elementary signal processing operations across symmetric (mirror) pairs of subcarriers. Thereby, the proposed transmission protocol has a similar complexity as Alamouti's space-time block coding (STBC) scheme and does not require extra transmit power nor any feedback. To evaluate the performance of IQSC, closed form expressions for the resulting outage probability and symbol error rate are derived. Interestingly, IQSC outperforms not only existing IQI compensation schemes, but also the ideal system without IQI for the same spectral efficiency and practical target error rates, while it achieves almost the same performance as ideal (i.e., IQI-free) equal-rate repetition coding. The findings reveal that IQSC is a promising low-complexity technique for significantly increasing the reliability of low-cost devices that suffer from high levels of IQI.

The dissertation is completed with Chapter 10, where the main conclusions of the presented research are drawn, while possible future extensions of this work are also proposed.

Part II

Types of interference and interference management

Chapter 2

Introduction to interference

The next generation wireless networks are envisioned to deal with the expected thousand-fold increase in total mobile broadband data and the hundred-fold increase in connected devices. In order to provide higher data rates, improved end-to-end performance and coverage, low latency, and low energy consumption at low cost per transmission, 5G systems are required to overcome various hadicaps of current cellular networks and wireless links [6, 74, 75]. One of the key handicaps of 5G systems is the performance degradation of the communication link, due to the increased level of interference.

In general, interference is a fundamental phenomenon in wireless communication systems. It is a result of the superposition and broadcast nature of wireless transmission along with spectrum shared among multiple users. Uncoordinated interference may cause significant reduction in the wireless system throughput. As a result, it is essential to understand and manage interference to achieve the highest system performance [76].

Motivated by this, the objection of this chapter is to define interference as a signal that affects communications, identify its source, and then point out methods that can be used in the design of modern wireless systems, in order to mitigate or even align its negative impact. Specifically, in Section 2.1, the major type of interference in wireless systems are reviewed. Section 2.2 is devoted in presenting CCI management techniques that are expected to be used in 5G systems, whereas Section 2.3 is focused in interference alignment approaches. Finally, in Section 2.4, self-interference cancellation techniques for FD systems are discussed.

2.1 Types of interference

In this section, we revisit the different types of interference. In more details, CCI and adjacent channel interference (ACI) are respectively presented in subsections 2.1.1 and 2.1.2. Likewise, in subsection 2.1.3, self-interference, which is the main drawback of FD systems, is reviewed, whereas subsections 2.1.4 and 2.1.5 focuses in demonstrating the influence of intermodulation interference and ISI, respectively. Moreover, in subsection 2.1.6, the interference caused in both downlink and uplink non-orthogonal multiple access (NOMA) systems, due to the use of common access resources by the UEs, is defined and examined. Finally, in subsection 2.1.7, the problem of near-to-far-end ratio interference is illustrated.

2.1.1 Co-channel interference

Spectral efficiency is of primary importance in the design of current and future wireless systems. This is achieved in cellular mobile radio networks by reusing the same sets of frequency channels in cells spatially separated by a predetermined reuse distance. However, while frequency-reuse provides more efficient use of the scarce radio spectrum it introduces CCI, which ultimately limits the QoS offered to the users [25, 77]. Especially, in 5G systems, where ultra dense small cells are expected to be deployed [3, 78–80], the influence of CCI is expected to be decisive for the quality of the communication link [81–86]. As a result, great amount of effort has been put to analyze, quantify and suppress the detrimental effect of CCI (see for example [77, 87–100], and reference therein).

To provide an insight of the impact of CCI, we consider a wireless system, which, as illustrated in Fig. 2.1, consists of a desired TX, a RX, and N_{CI} neighboring TXs that cause CCI. Under these assumptions, the $n-$th sample of the base band equivalent received signal can be expressed as

$$r(n) = \sqrt{E_0} h_0(n) s_0(n) + \sum_{m=1}^{N_{\mathrm{CI}}} \sqrt{E_m} h_m(n) \theta_m s_m(n) + w(n), \tag{2.1}$$

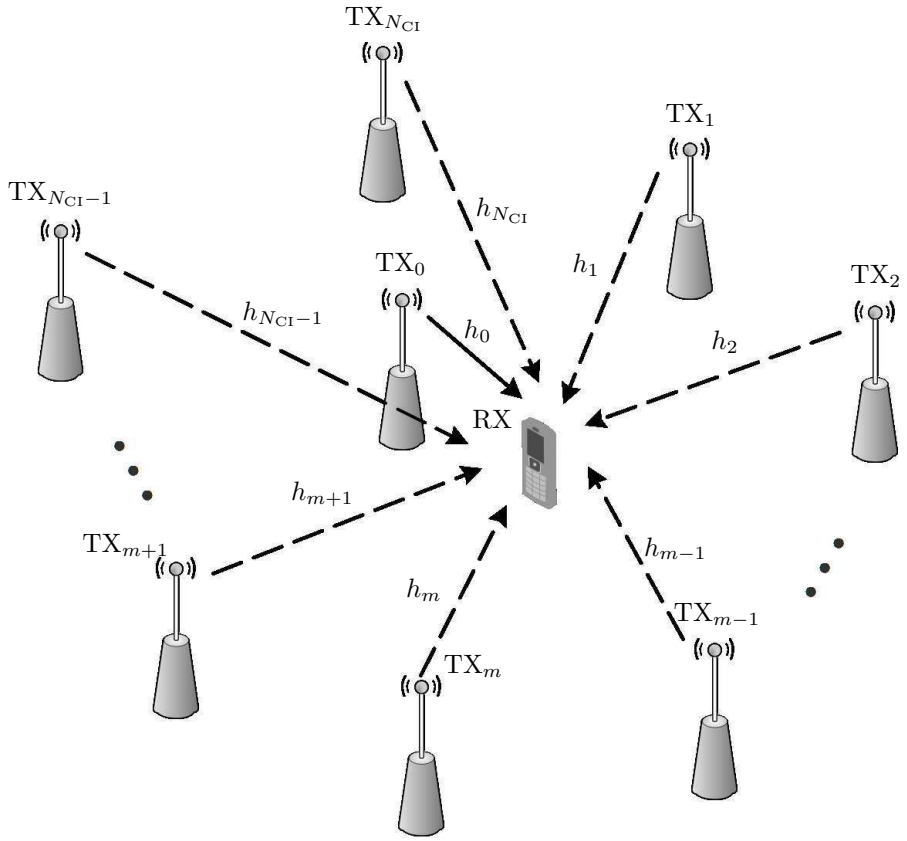

Figure 2.1 Typical system model for the investigation of the influence of ICI.

where E_0 and E_m $(m = 1, \cdots, N_{\rm CI})$ represent the average received signal power from the desired TX and the $m-$th interference TX, respectively, whereas $s_0(n)$ and $s_m(n)$ $(m = 1, \cdots, N_{\rm CI})$ stand for the $n-$th sample of the desired and the signal transmitted by the $m-$th interferer, respectively. Moreover, $h_0(n)$ and $h_m(n)$ $(m = 1, \cdots, N_{\rm CI})$ are the channel responses from the desired TX and the $m-$th neighboring TX to the receiver[1], respectively, while $w(n)$ denotes the additive noise component. Finally, θ_m characterize the state of the $m-$th possible interferer, i.e., if $\theta_m = 0$ the $m-$th TX is silent (does not transmit any signal), while if $\theta_m = 1$ the $m-$th TX is active.

From (2.1), it is observed that the impact of interference depends on the number and the state of the possible interferers, the received signal power from the desired TX and the interferers, as well as the statistics of the wireless environment. Therefore, to quantify the influence of CCI to the quality of the communication link, the outage probability is traditionally used. For example, in [101–103], the authors approximately evaluated the outage probability in log-normally shadowed environments. In most of these works, the impact of small scale scale fading was neglected. On the other hand, in [104, 105], the authors provided analytical expressions for the outage probability for different small scale fading scenarios. Specifically, in [104], the authors considered Rician fading, while in [105], the outage probability in the case of Nakagami-m fading signals was derived. The impact of CCI in more complex systems, such as MIMO and relaying communications, was investigated in [87, 88, 90, 92, 95–97].

All of the above references concluded that, unless CCI is appropriately compensated or managed, its influence can be detrimental for the quality of the communication link. Consequently, a broad range of interference mitigation techniques have been employed at TX and/or RX [106–115], as illustrated in Fig. 2.2. Generally, CCI mitigation techniques can be separated into two categories, i.e., system- and RX-design techniques. In system-design techniques, transmission of co-channel signals is properly managed so that the power of received CCI is maintained below an acceptable level. In contrast, RX-design techniques actively mitigate the CCI, which cannot be separated by the preemptive system-design

[1]Note that in case of multi-carrier transmission, $h_0(n)$ and $h_m(n)$ represent the channel responses on a specific subcarrier from the desired TX and the $m-$th neighboring TX to the RX, respectively.

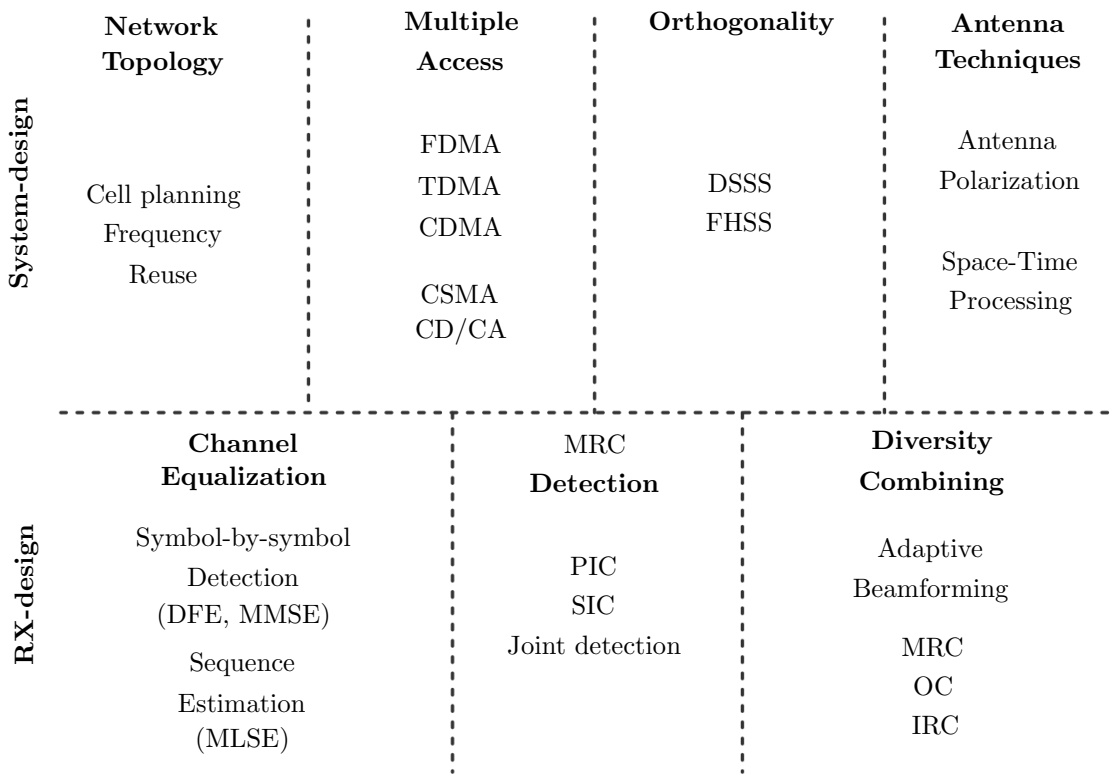

Figure 2.2 Typical interference mitigation techniques. In this figure, TDMA, CDMA, CSMA, CD/CA, DSSS, FHSS, DFE, MLSE, PIC, OC, and IRC respectively stand for time division multiple access, code division multiple access, carrier sense multiple access, collision detection/collision avoidance, direct-sequence spread spectrum, frequency-hopping spread spectrum, decision feedback equalizer, maximum-likelihood sequence estimation, parallel interference cancellation, optimum combining, and interference combining.

approaches. In practical implementations, both approaches are employed in joint fashions to manage the effect of CCI.

2.1.2 Adjacent channel interference

ACI is the interference caused by extraneous power from a signal in a neighboring channel [116]. The adjacent-channel interference is created by two phenomenos [117]:

- The TX transmission is not limited to the nominal frequency range. Depending on the type of modulator, and various properties of the TX hardware, the spectrum of a generated signal may extend over a larger frequency range. Since the transmit filters are not ideal, this out-of band leakage is not completely suppressed. Therefore, at the RX, which listens in an adjacent frequency channel, this leakage cannot be suppressed. Since the adjacent channel signals lie in the frequency band of the desired signal, they pass to the demodulator essentially without attenuation.
- At the RX, the radiation from the desired channel is suppressed insufficiently by the RX filter. Thus, the signals in adjacent channels is passed on to the demodulator, where they act as interference.

Generally, ACI can be classified as either in-band or out-of-band interference [118]. The term in-band is applied when the center of the interfering signal bandwidth falls within the bandwidth of the desired signal, while the term out-of-band is applied when the center of the interfering signal bandwidth falls outside the bandwidth of the desired signal.

Due to the large dynamic range of mobile radio signals, the impact of ACI can be significant. In this context, there are several works in the technical literature that focus in quantifying the degradation

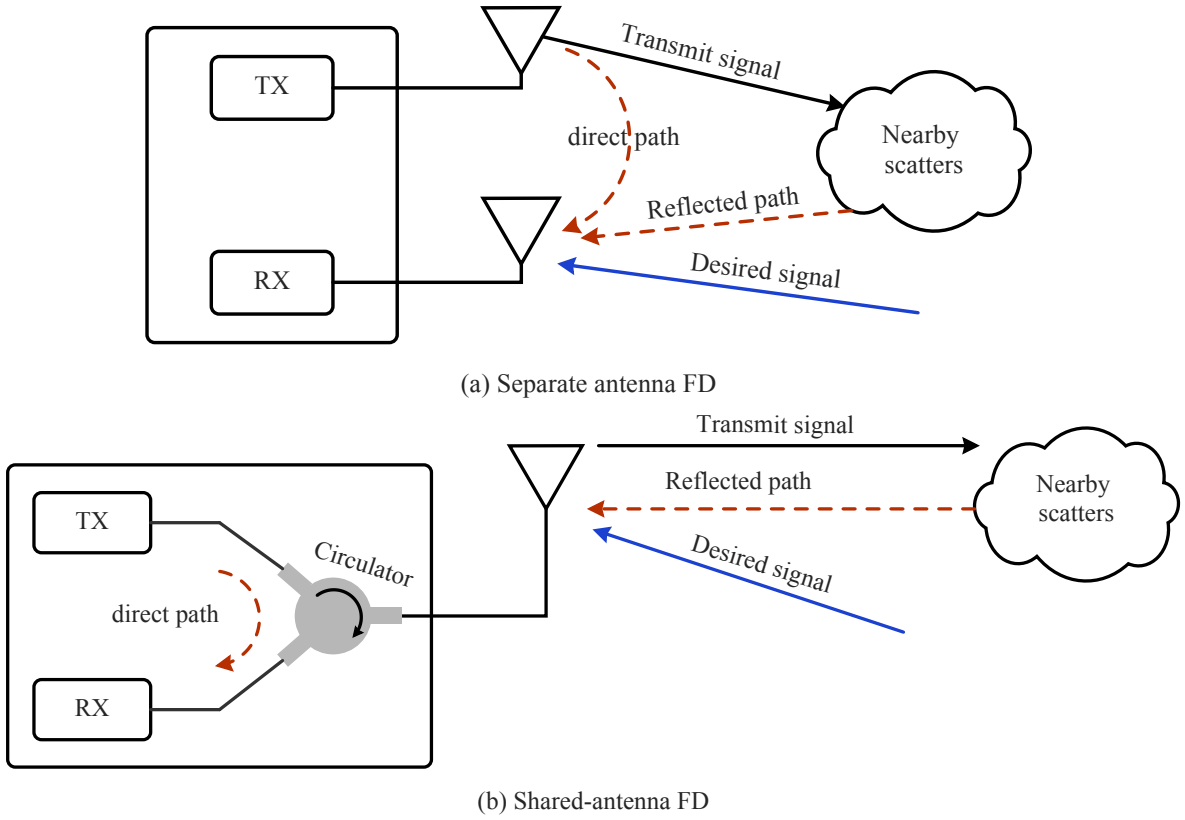

Figure 2.3 Anatomy of FD devices.

of ACI in the quality of the wireless communication link [119–124]. Specifically, the effect of ACI on the capacity of frequency domain multiple access (FDMA) cellular systems was presented in [119], while the influence of ACI on the capacity of wide-band code-division multiple-access (WCDMA) systems, was investigated in [120]. Likewise, in [121], the impact of ACI on several the broadcasting long term evolution (LTE) systems was illustrated through Monte Carlo simulations. In [122], the authors described the statistical properties of ACI, by presenting an analytical probability density function (PDF) of ACI in a single cell environment. Moreover, the effect of ACI, when different modulation methods are used, was demonstrated in [123]. Finally, in [124], the impact of different types of interference, including ACI, on the symbol error rate (SER) was quantified.

2.1.3 Self-interference

Until recently, the concept of simultaneous transmission and reception over the same frequency channel, i.e., operating in FD mode, was deemed impossible [125]. A traditional radio can either transmit or receive over a given channel, but not simultaneously; in other words, it can operate in half-duplex (HD) mode. As illustrated in Fig. 2.3, the problem of achieving FD communications over the same channel is that the transmitted power from a given node is typically much larger than the received power of another signal to be captured by the same node. As a result, the FD device receives its transmitted signal as interference. This type of interference is called self-interference, and may be detrimental for the performance of FD wireless systems [126]. Consequently, to utilize FD systems, it is important to understand the nature and the properties of self-interference.

Based on the structure of the FD device, the base band equivalent received signal at the RX can been obtained as

$$r = h_r s_r + \alpha h_t s_t + n, \tag{2.2}$$

where s_r and s_t stand for the desired signal and transmitted signals from the FD device, respectively, whereas h_r and h_t are the channel responses of the desired and the self-interference signals. Moreover, α

denotes the SIS level, while n represents the additive noise. From (2.2), it is evident that the performance of FD system depends not only on the signal to noise ratio and the statistics of the fading channel, but also on the level of the transmitted signal, the self-interference suppression capabilities of the FD device, as well as the statistic of the self-interfernce channel.

To appreciate the impact of the level of self-interference, we consider the following indicative example in the context of contemporary femto-cell cellular systems [127]. Based on the data provided in [127, Table 10-2], both the femto base stations and mobile UE transmit at 21 dBm, while their RX noise floor level is -100 dBm. Assuming 20 dB isolation between the base station (BS) TX and RX signal paths, the self-interference at the BS will be $21 - 20 - (-100) = 101$ dB above the noise floor. In other words, in order for the FD BS to achieve the link signal to interference plus noise ratio (SINR) equal to the signal to noise ratio (SNR) of the corresponding HD system, it must suppress self-interference by more than 101 dB. However, in practice, the typical isolation between the TX and RX in FD systems is in the order of $20 - 40$ dB [128–130]. In other words, the effect of self-interference in FD systems, cannot fully compensated. This example indicates the importance of quantifying the impact of imperfect SIS, in order to decide whether to deploy a FD system or a HD, as well as the demand of presenting more efficient SIS techniques.

The performance of FD systems have been analyzed in several published papers, assuming different fading channels (see [131–142] and references therein). For instance, in [132, 133] the self-interference channel gain was modeled as a constant value. This is a very coarse approximation and is only meaningful when digital cancellation is applied. Moreover, in [134] the authors presented the performance degradation due to imperfect SIS, considering a pair of separate antenna FD devices that communicate with each other through Ricean self-interference channel gain, while in [135], this analysis was extended in MIMO systems. Additionally, by assuming passive SIS implemented in the analogue domain via antenna separation and shielding to suppress the line-of-sight (LoS) paths, the authors, in [136], modelled the self-interference channel gain as Rayleigh and investigated the effect of imperfect SIS in MIMO relay systems. In [137], a bit error rate (BER) analysis of a FD relaying scheme that employs binary phase shift keying (BPSK) and a single decode-and-forward (DF) relay, in the presence of Rayleigh self-interference gain, was conducted, whereas, in [138], the impact of imperfect SIS on the outage probability of three-terminal FD relay channel that adopts a selective DF protocol was presented. The effect of imperfect SIS in cascaded multiple FD DF relaying systems was studied in [139], assuming again Rayleigh self-interference channel gain. Furthermore, in [140], the authors investigated the influence of residual self-interference in FD amplify-and-forward (AF) relaying systems, assuming that the residual self-interference is a zero-mean complex Gaussian process, while in [141] the impact of imperfect SIS in selection FD AF relaying systems with self-interference subject to Rayleigh fading was presented. Finally, in [142], the authors studied the impact of imperfect SIS in two-way FD relaying systems with AF protocol, assuming that the residual self-interference is a zero-mean complex Gaussian process.

2.1.4 Intermodulation interference

Non-linear system components cause spurious signals, which may play the role of interference in adjacent channels [118, 143]. When a non-linear device (e.g. an amplifier) is used simultaneously by a number of carriers, intermodulation products are generated, which result to distortion in the desired signals. To gain an insight of the spurious frequency profile of a non-linear element, we assume that it can be modelled as a memoryless polynomial of degree N [144–149], i.e.,

$$y(t) = \sum_{i=1}^{N} a_i x^i(t), \tag{2.3}$$

where $x(t)$ and $y(t)$ stand for the input and the output to the non linear component signals, respectively. Generally, the intermodulation distortion (IMD) profile is defined based on the single- or two-tone response of the non-linearity, i.e., the output of the non-linear element, when the input is sinusoidal signal consisted of one or two tones, respectively. In the case of a two-tone signal, say f_1 and f_2, it is well-known in the literature [150–153] that the output of the non-linearity is a signal that consists of two groups of frequencies:

- the harmonics in the form nf_1, mf_2; and
- the intermodulation frequencies, namely $\pm nf_1 \pm mf_2$,

where m and n are integers. Note that the order of the intermodulation product is the sum of the integers $m + n$.

Although, this "pure-tone" IMD profile provide information on the spurious components center frequencies, it does not provide information about the spurious components envelops and phases, which are essential for understanding the nature of this type of interference. To obtain a more realistic IMD profile, the band pass modulated signals are used as the input of the non-linear component [154]. In other words, the non-linear component input, $x(t)$, consists of M band pass signals centered at f_i $(i = 1, \cdots, M)$, and can be expressed as

$$x(t) = \sum_{i=1}^{M} A_i(t) \cos\left(2\pi f_i t + \phi_i(t)\right), \tag{2.4}$$

where $A_i(t)$ and $phi_i(t)$ represent the amplitude and the phase of the $i-$th band pass modulated signal.

To further demonstrate the influence of interference due to the non-linearity, the IMD profile of a non-linear element with $N = 3$, and a band pass signal with $M = 3$ as input, is presented. In this scenario, according to (2.3) and (2.4), the output signal is given by

$$\begin{aligned} y(t) = a_1 x(t) + y_{\mathrm{DC}}(t) + y_{\mathrm{SD}}(t) + y_{2f}(t) + y_{f_1 \pm f_2}(t) + y_{f_1 \pm f_3}(t) + y_{f_2 \pm f_3}(t) \\ + y_{3f}(t) + y_{2f_1 \pm f_2} + y_{2f_1 \pm f_3} + y_{2f_2 \pm f_3} + y_{2f_3 \pm f_2} + y_{2f_2 \pm f_1} + y_{2f_3 \pm f_1} + y_{f_1 \pm f_2 \pm f_3}, \end{aligned} \tag{2.5}$$

where

$$y_{\mathrm{DC}}(t) = \frac{a_2}{2} \sum_{i=1}^{3} A_i^2(t), \tag{2.6}$$

stand for the output signal components around the direct current (DC),

$$\begin{aligned} y_{\mathrm{SD}}(t) = a_3 \left(\frac{3}{4} A_1^3(t) + \frac{3}{2} A_2^2(t) A_1(t) + \frac{3}{2} A_3^2(t) A_1(t) \right) cos\left(2\pi f_1 + \phi_1(t)\right) \\ + a_3 \left(\frac{3}{4} A_2^3(t) + \frac{3}{2} A_3^2(t) A_2(t) + \frac{3}{2} A_1^2(t) A_2(t) \right) cos\left(2\pi f_2 + \phi_2(t)\right) \\ + a_3 \left(\frac{3}{4} A_3^3(t) + \frac{3}{2} A_2^2(t) A_1(t) + \frac{3}{2} A_1^2(t) A_3(t) \right) cos\left(2\pi f_3 + \phi_3(t)\right), \end{aligned} \tag{2.7}$$

represent self-distortion components,

$$y_{2f}(t) = a_2 \frac{A_1^2(t)}{2} cos\left(2\pi 2 f_1 + 2\phi_1(t)\right) + a_2 \frac{A_2^2(t)}{2} cos\left(2\pi 2 f_2 + 2\phi_2(t)\right) + a_2 \frac{A_3^2(t)}{2} cos\left(2\pi 2 f_3 + 2\phi_3(t)\right), \tag{2.8}$$

are the output signal components of the output signal at the frequencies $2f_i$, $i = 1, 2, 3$,

$$\begin{aligned} y_{f_1 \pm f_2}(t) &= a_2 A_1(t) A_2(t) \cos\left(2\pi (f_1 + f_2) t + \phi_1(t) + \phi_2(t)\right) \\ &\quad + a_2 A_1(t) A_2(t) \cos\left(2\pi (f_1 - f_2) t + \phi_1(t) - \phi_2(t)\right), \end{aligned} \tag{2.9}$$

$$\begin{aligned} y_{f_1 \pm f_3}(t) &= a_2 A_1(t) A_3(t) \cos\left(2\pi (f_1 + f_3) t + \phi_1(t) + \phi_3(t)\right) \\ &\quad + a_2 A_1(t) A_3(t) \cos\left(2\pi (f_1 - f_3) t + \phi_1(t) - \phi_3(t)\right), \end{aligned} \tag{2.10}$$

$$\begin{aligned} y_{f_2 \pm f_3}(t) &= a_2 A_2(t) A_3(t) \cos\left(2\pi (f_2 + f_3) t + \phi_2(t) + \phi_3(t)\right) \\ &\quad + a_2 A_2(t) A_3(t) \cos\left(2\pi (f_2 - f_3) t + \phi_2(t) - \phi_3(t)\right), \end{aligned} \tag{2.11}$$

are the output signal components of the output signal at the frequencies $f_m \pm f_n$, $m, n \in \{1, 2, 3\}$, $m \neq n$,

$$y_{3f}(t) = a_3 \frac{A_1^3(t)}{4} cos\left(2\pi 3 f_1 + 3\phi_1(t)\right) + a_3 \frac{A_2^3(t)}{4} cos\left(2\pi 3 f_2 + 3\phi_2(t)\right) + a_3 \frac{A_3^3(t)}{4} cos\left(2\pi 3 f_3 + 3\phi_3(t)\right), \tag{2.12}$$

are the output signal components at the frequencies $3f_i$, $i = 1, 2, 3$,

$$\begin{aligned} y_{2f_1 \pm f_2}(t) &= \frac{3}{4} a_3 A_1^2(t) A_2(t) \cos\left(2\pi \left(2f_1 + f_2\right) t + 2\phi_1(t) + \phi_2(t)\right) \\ &\quad + \frac{3}{4} a_3 A_1^2(t) A_2(t) \cos\left(2\pi \left(2f_1 - f_2\right) t + 2\phi_1(t) - \phi_2(t)\right), \end{aligned} \tag{2.13}$$

$$y_{2f_1\pm f_3}(t) = \frac{3}{4}a_3A_1^2(t)A_3(t)\cos\left(2\pi\left(2f_1+f_3\right)t+2\phi_1(t)+\phi_3(t)\right) + \frac{3}{4}a_3A_1^2(t)A_3(t)\cos\left(2\pi\left(2f_1-f_3\right)t+2\phi_1(t)-\phi_3(t)\right), \tag{2.14}$$

$$y_{2f_2\pm f_3}(t) = \frac{3}{4}a_3A_2^2(t)A_3(t)\cos\left(2\pi\left(2f_2+f_3\right)t+2\phi_2(t)+\phi_3(t)\right) + \frac{3}{4}a_3A_2^2(t)A_3(t)\cos\left(2\pi\left(2f_2-f_3\right)t+2\phi_2(t)-\phi_3(t)\right), \tag{2.15}$$

$$y_{2f_2\pm f_1}(t) = \frac{3}{4}a_3A_2^2(t)A_1(t)\cos\left(2\pi\left(2f_2+f_1\right)t+2\phi_2(t)+\phi_1(t)\right) + \frac{3}{4}a_3A_2^2(t)A_3(t)\cos\left(2\pi\left(2f_2-f_1\right)t+2\phi_2(t)-\phi_1(t)\right), \tag{2.16}$$

$$y_{2f_3\pm f_1}(t) = \frac{3}{4}a_3A_3^2(t)A_1(t)\cos\left(2\pi\left(2f_3+f_1\right)t+2\phi_3(t)+\phi_1(t)\right) + \frac{3}{4}a_3A_3^2(t)A_1(t)\cos\left(2\pi\left(2f_3-f_1\right)t+2\phi_3(t)-\phi_1(t)\right), \tag{2.17}$$

$$y_{2f_3\pm f_2}(t) = \frac{3}{4}a_3A_3^2(t)A_2(t)\cos\left(2\pi\left(2f_3+f_2\right)t+2\phi_3(t)+\phi_2(t)\right) + \frac{3}{4}a_3A_3^2(t)A_2(t)\cos\left(2\pi\left(2f_3-f_2\right)t+2\phi_3(t)-\phi_2(t)\right), \tag{2.18}$$

are the output signal components at the frequencies $|2f_m - f_n|$, $m, n \in \{1, 2, 3\}$, $m \neq n$, and

$$\begin{aligned} y_{f_1\pm f_2\pm f_3}(t) = {} & \frac{6}{4}a_3A_1(t)A_2(t)A_3(t)\cos\left(2\pi\left(f_2-f_1-f_3\right)t+\phi_2(t)-\phi_1(t)-\phi_3(t)\right) \\ & + \frac{6}{4}a_3A_1(t)A_2(t)A_3(t)\cos\left(2\pi\left(f_1+f_2-f_3\right)t+\phi_1(t)+\phi_2(t)-\phi_3(t)\right) \\ & + \frac{6}{4}a_3A_1(t)A_2(t)A_3(t)\cos\left(2\pi\left(f_2+f_3-f_1\right)t+\phi_2(t)+\phi_3(t)-\phi_1(t)\right) \\ & + \frac{6}{4}a_3A_1(t)A_2(t)A_3(t)\cos\left(2\pi\left(f_1+f_2+f_3\right)t+\phi_1(t)+\phi_2(t)+\phi_3(t)\right) \end{aligned} \tag{2.19}$$

are the output signal components at the frequencies $|f_1 \pm f_2 \pm f_3|$. Note that $y_{\mathrm{DC}}(t)$, $y_{2f}(t)$, $y_{f_1\pm f_2}$, $y_{f_1\pm f_3}$, and $y_{f_2\pm f_3}$ are generated due to the second order non-linearity, i.e., $a_2x^2(t)$, while $y_{\mathrm{SD}}(t)$, $y_{3f}(t)$, $y_{2f_1\pm f_2}(t)$, $y_{2f_1\pm f_3}(t)$, $y_{2f_2\pm f_3}(t)$, $y_{2f_2\pm f_1}(t)$, $y_{2f_3\pm f_1}(t)$, $y_{2f_3\pm f_2}(t)$, and $y_{f_1\pm f_2\pm f_3}(t)$ are generated due to the third order non-linearity, i.e., $a_3x^3(t)$. In other words, the second order non-linearity causes a distortion around the DC, interference in the second harmonics, and interference in the intermodulation frequencies, $\omega_m \pm \omega_n$ $(m, n \in \{1, 2, 3\}, m \neq n)$, whereas the third order non-linearity causes self-distortion the the original signal, interference in the third harmonics, and interference in the intermodulation frequencies $\omega_m \pm \omega_n$ $(m, n \in \{1, 2, 3\}, m \neq n)$ and $\omega_1 \pm \omega_2 \pm \omega_3$.

2.1.5 Intersymbol interference

ISI is a form of distortion of a signal in which one symbol interferes with subsequent symbols. This is an unwanted phenomenon as the previous symbols have similar effect as noise, thus making the communication less reliable. The spreading of the pulse beyond its allotted time interval causes it to interfere with neighboring pulses [116]. ISI is usually caused by multipath propagation or the inherent non-linear frequency response of a channel causing successive symbols to "blur" together.

To understand the nature of ISI is, let us consider the transmission of a sequence of symbols with the basic waveform, $g_T(t)$. To send the $n-$th symbol, x_n, we transmit $x_n g_T\left(t - nT\right)$, where T is the symbol interval. Therefore, the transmitted signal can be expressed as

$$s(t) = \sum_{n=-\infty}^{\infty} x_n p\left(t - nT\right), \tag{2.20}$$

while the received signal can be obtained as

$$r(t) = \sum_{n=-\infty}^{\infty} x_n v(t - nT) + n(t), \tag{2.21}$$

where $n(t)$ stands for the additive noise and

$$v(t) = g_T(t) * h(t), \tag{2.22}$$

with $h(t)$ be the impulse response of the dispersive channel.

Let us consider that the RX uses a matched filter, with impulse response $g_R(t)$, for demodulation, and the output of the filter is sampled at $t = mT$. Then, the sampled signal at the RX is

$$z_m = b_m x(0) + \sum_{\substack{n=-\infty \\ n \neq m}}^{\infty} b_n y\left(mT - nT\right) + w_n, \tag{2.23}$$

where w_n is the noise component at the output of the sampler, and

$$y(t) = v(t) * g_R(t). \tag{2.24}$$

In (2.23), the first term is the desired signal contribution due to the symbol b_m, whereas the second term contains contributions from the other symbols. On conceptual level, this is demonstrated in Fig. 2.4, where the transmitted and received signal are plotted. From this figure, it is shown that the dispersive channel creates a tail of energy that lasts much longer than intended. As a result, each symbol interferes with one or more of the subsequent symbols. These unwanted contribution to a symbol from other subsequent symbols is the ISI.

The problem of ISI arose with the early attempts at telegraph transmission in the mid-nineteenth century. Since that time, the problem has been considered from many viewpoints [20, 21, 155–166]. For example, in [155], a method for specifying an optimum linear, time invariant receiving filter for a digital data transmission system was derived, assuming that the transmission medium introduces intersymbol interference and additive Gaussian noise, while, in [156], the impact of ISI on the error performance in binary differentially-coherent phase-shift-keying (PSK) systems was evaluated. Additionally, in [20], an upper bound for the probability of error of a digital communication system, subjected to ISI and Gaussian noise, was derived, whereas, in [21], an analytical method for the exact evaluation of the impact of ISI in binary differentially coherent phase-shift-keying (DPSK) systems, in the presence of thermal noise and a known channel filter, was presented. In [157], the impact of ISI in the capacity of a Gaussian channel was studied. Moreover, in [158], the authors investigated the error performance of M-PSK systems in the presence of Gaussian noise and ISI, while in [159], this analysis was extended in order to include the influence of non-selective fading. Likewise, the joint effect of ISI and Rayleigh fast fading channel was investigated in [161]. The influence of ISI in the capacity region of broadcast channels in the presence of colored Gaussian noise was studied in [162], whereas the impact of ISI on the capacity of frequency-selective channels in training-based transmission schemes was presented in [160]. Furthermore, the impact of ISI and additive colored Gaussian noise on the capacity of relay channels was examined in [163]. In [164], the authors presented the impact of ISI on the performance of diversity systems with multiple branches, in the presence of multipath Rayleigh, Nakagami-m and Rician fading. Finally, the effect of ISI in multiple access systems, in which the users employ STBC was revealed in [165], whereas in [166], the authors analyzed the performance of multi-band orthogonal frequency division multiplexing (OFDM) ultra-wideband (UWB) systems, in the presence of ISI.

2.1.6 Interference in non-orthogonal multiple access systems

One of the key technologies of 5G, which is expected to increase the spectal efficiency and the system throughput, as well as accommodate massive connectivity, is NOMA [167, 168]. The idea of NOMA is to realize multiple access (MA) in the power domain, which is fundamentally different from conventional orthogonal MA technologies (e.g., time/frequency/code division MA). In other words, in the downlink, the BS uses different power levels for the messages intended to different UEs, while, in the uplink, each

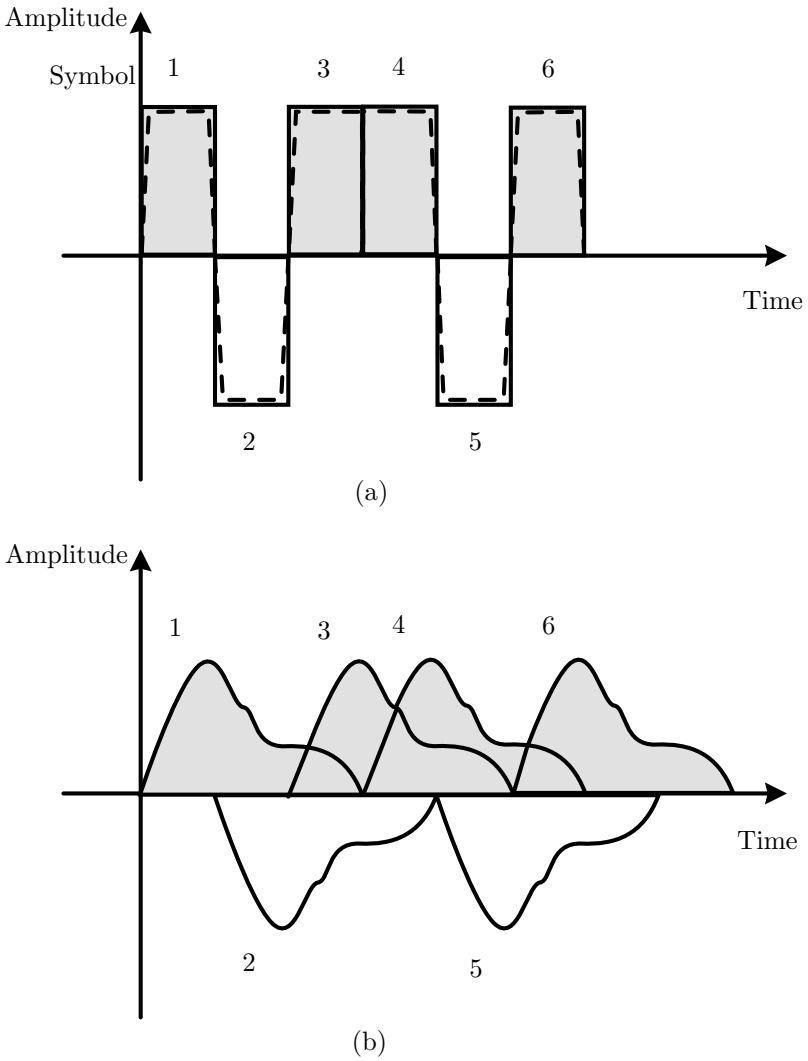

Figure 2.4 Transmitted (a) and received (b) signal in the presence of ISI.

UE transmits in different power level its information to the BS. The motivation behind this approach lies in the fact that NOMA can use spectrum more efficiently by opportunistically exploring users' channel conditions [169–178]. However, since all the nodes of the communication system employ the same access resources, inevitable interference arises to the RXs.

To understand the nature of this type of interference, the downlink and the uplink of a single-cell topology with one BS and M UE, as illustrated in Fig. 2.5, is considered.

2.1.6.1 Downlink NOMA

In the downlink, based on the NOMA protocol, the transmitted signal can be expressed as

$$x = \sum_{m=1}^{M} \sqrt{P_s(m)} s_m, \tag{2.25}$$

where s_m and $P_s(m)$ stand for the signal intended and the transmitted power for the $m-$th UE, respectively. The base band equivalent received signal at the $m-$th UE, can be obtained as

$$y_m = h_m^d \sqrt{P_s(m)} s_m + h_m^d \sum_{\substack{i=1 \\ i \neq m}}^{M} \sqrt{P_s(i)} s_i + n_m, \tag{2.26}$$

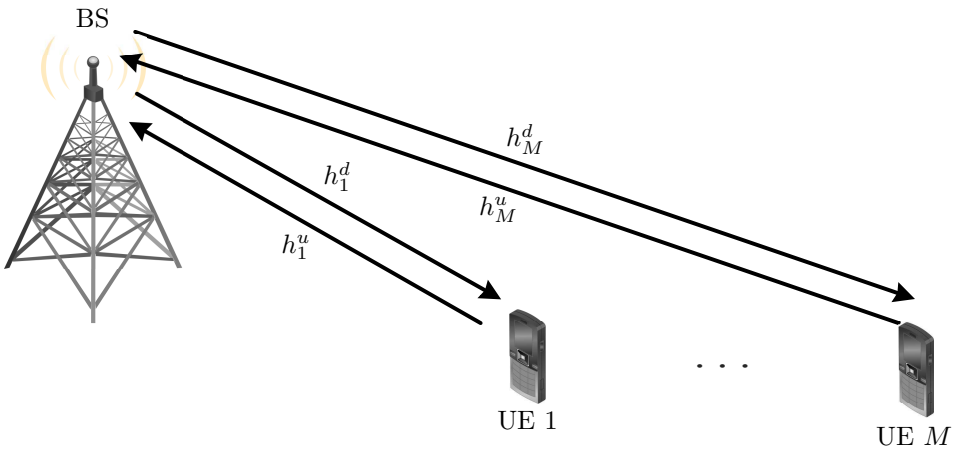

Figure 2.5 Topology of a single-cell multiple UE NOMA system.

where h_m^d and n_m denote the downlink fading channel between the BS and the $m-$th UE, and the additive noise, respectively.

Without loss of generality, it is assumed that the downlink channel gains are sorted as

$$|h_1^d| \leq |h_2^d| \leq \cdots \leq |h_m^d|; \tag{2.27}$$

hence, according to NOMA protocol

$$P_s(1) \geq P_s(2) \geq \cdots \geq P_s(M). \tag{2.28}$$

Consequently, the $m-$th UE can detect and remove the messages intended for the $k-$th UE, with $k < m$, but it cannot remove the messages intended fot the $l-$th UE, with $l > m$. As a result, the observation of the $m-$th UE can be written as

$$\tilde{y}_m = h_m^d \sqrt{P_s(m)} s_m + h_m^d \sum_{i=m+1}^{M} \sqrt{P_s(i)} s_i + n_m, \tag{2.29}$$

while the instantaneous SINR can be obtained as

$$\gamma_m^d = \frac{|h_m^d|^2 P_s(m)}{|h_m^d|^2 \sum_{i=m+1}^{M} P_s(i) + N_0}, \tag{2.30}$$

where N_0 denotes the noise single-sided power spectrum density (PSD). From (2.30), it can be observed that the level of interference at the $m-$th UE depends from the total transmit power to the UEs, with index $l > m$. Moreover, by comparing (2.29) with (2.1), someone can consider that the interference in the downlink of a NOMA system is a special case of CCI. However, this abstraction is incorrect, since there are three fundamental differences between CCI and interference in downlink NOMA:

- In downlink NOMA, the source of interference is a single TX, which can control the level of interference in the $m-$th UE by appropriately allocating the power intended for the UEs with index $l > m$. Moreover, as observed by (2.30), both the intended message for the $m-$th UE and the interference are carried by the same wireless channel. On the other hand, CCI is caused by multiple TXs that transmits simultaneously at the same frequency band. As a result, the intended message for the UE and the CCI are carried by different channels. Therefore, more sophisticated schemes need to be used in order to reduce the level of CCI in a UE.

- In downlink NOMA, the reduction of $P_s(i)$, $i > m$, may result to an increase of the SINR at the $m-$th UE, but, in the same time, it causes a reduction to the power received by the $i-$th UE, $i > m$. On the other hand, in the case of CCI, the reduction of the interference level at the UE does not necessarily affect the performance of the other UEs.

- NOMA is based on the channel ordering, described by (2.27), and the capabilities of the $m-$th UE to decode and remove the message intended for the $i-$th UE, with $i > m$. Therefore, an outage event, Ω_m, in a downlink NOMA system occurs at the $m-$th UE, when the $m-$th UE cannot detect its own message or the message intended for the $i-$th UE ($i < m$) [179], i.e.,

$$\Omega_m = \left\{ \{R_{m,1} \leq \tilde{R}_1\} \cup \cdots \cup \{R_{m,m} \leq \tilde{R}_m\} \right\}, \tag{2.31}$$

  where $R_{m,i}$ and R_i denote the achievable rate for the $m-$th UE to detect the $i-$th UE message, and the targeted rate for the message intended for the $i-$th UE, respectively. On the other hand, in case of CCI, there is no ordering condition and an outage event occurs only when the UE cannot detect its own message.

2.1.6.2 Uplink NOMA

In the uplink, it is assumed that the M UEs share the same channel simultaneously. Consequently, the received signal at the BS can be obtained as [180]

$$y_{\text{BS}} = \sum_{m=1}^{M} h_m^u \sqrt{P_s^u(m)} s_m^u + n, \tag{2.32}$$

where s_m^u and $P_s^u(m)$ represent the transmit messages and the transmit power from the $m-$th UE, respectively, whereas h_m^u and n denote the uplink fading channel between the $m-$th UE and the BS, and the additive noise, respectively.

Again, without loss of generality, it is assumed that the uplink channel gains are sorted as

$$|h_1^u| \leq |h_2^u| \leq \cdots \leq |h_m^u|; \tag{2.33}$$

therefore, according to NOMA protocol

$$P_s^u(1) \geq P_s^u(2) \geq \cdots \geq P_s^u(M). \tag{2.34}$$

In order to split the overlapped signals, successive interference cancellation (SIC) is carried out at the BS. In other words, before the BS detects the $m-$th UE's message, it decodes the prior $i-$th ($i < m$) UEs' message first, then remove the message from its observation, in a successive manner. The rest ($M - m$) UEs' messages are regarded as interference. This type of interference can be seen as a special type of CCI, since it is caused by multiple TXs that transmits simultaneously in the same frequency band. However, there are some differences between this type of interference and CCI:

- Although, both types of interference is caused by multiple TXs that transmits in the simultaneously in the same frequency band, in case of uplink NOMA, the level of interference can be controlled by appropriately determining the transmit power of each UE. However, this might not be possible in case of CCI.

- In uplink NOMA there is a trade-off between the level of interference at the $m-$th UE and the achievable rate of the UEs, with index $l > m$. This trade-off does not usually occur in the case of CCI.

- Finally, as in the case of downlink NOMA, in case of uplink NOMA, the outage performance of the system depends on the capability of the BS to detect not only the message transmitted by the m UE, but also the messages transmitted by the UEs, with index $i < m$. On the other hand, in the case of CCI, the outage performance of the systems depends only on the capability of the BS to detect the message transmitted by the $m-$th UE.

2.1.7 Near-to-far-end ratio interference

Near to far end ratio interference appears only in mobile communications, when the distance between the receive UE, UE_r and the transmit BS becomes critical with respect to another transmit UE, UE_t, which is close to UE_r and transmits simulataneously at the same frequency with the BS [181–186].

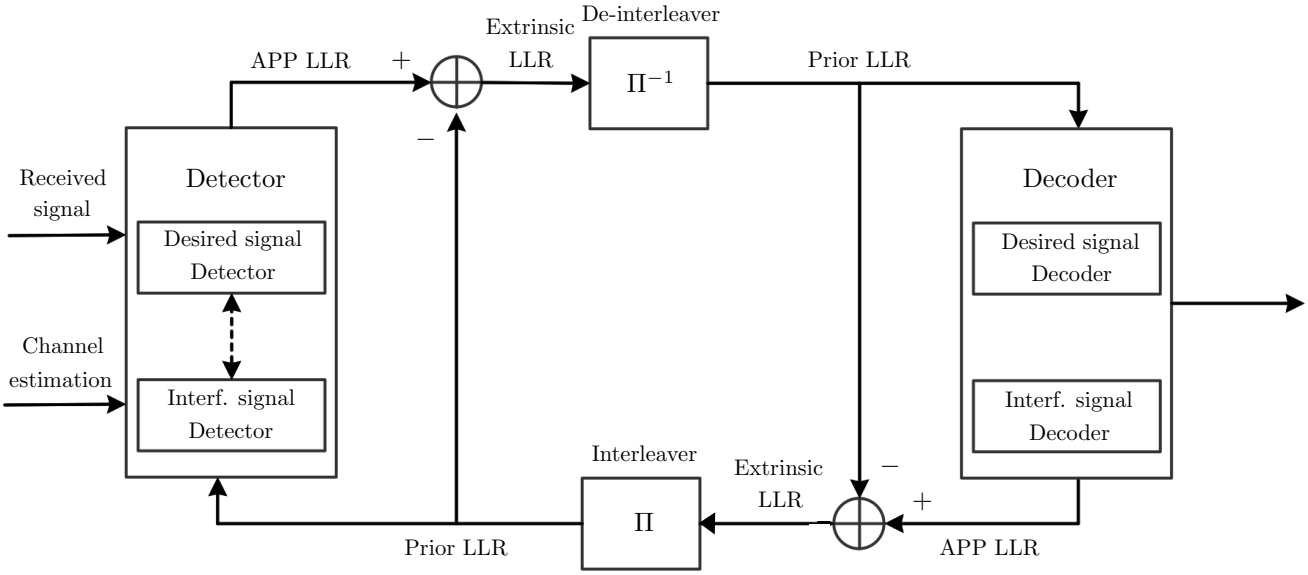

Figure 2.6 Iterative RX architecture. In this figure, APP and LLR stand for the a posteriori probability and the log likelihood ratio, respectively.

Additionally, this type of interference may occur at the BS, when signals are received simultaneously at the same frequency from at least two UEs [187].

In cellular systems using frequency domain multiplexing (FDM) and time domain multiplexing (TDM), a frequency or a time slot is not shared by another user in the cell; consequently, near-to-far-end ratio interference is not a problem. On the other hand, in systems such as direct sequence spread spectrum (DSSS), where all the mobiles within a cell share the same carrier frequency, near-to-far-end ratio interference is of a major concern and efforts are made so that none of the signals arriving at the BS dominates the others [188–190].

2.2 Co-channel interference management in 5G systems

The densification of wireless networks are expected to be a key tool to improve traffic capacity and user throughput in 5G systems. For instance, heterogeneous overlay deployment of low-power cells within the coverage of a macrocell brings additional enhancement by efficient load sharing between macrocells and local access networks. However, all the benefits are not free: as the density and load of the network grow, the network's RX terminals suffer from increased CCI, particularly at the boundaries of cells. As a result, enhanced inter-cell interference coordination (eICIC) and coordination multipoint (CoMP) [191–194] has been introduced to LTE releases in order to manage CCI. Both ICIC and CoMP are network-side operations and are transparent to the RXs. Network-side interference management is beneficial to ensure backward compatibility with legacy users and easy to deploy by extending the legacy network. However, putting the responsibility for interference management solely on the network entails lots of practical issues and limitations, such as backhaul and feedback overheads [195]. Consequently, to overcome the issues and the limitations of network-side interference management, several researchers proposed UE-side interference management techniques that are expected to provide significant synergy with the network-side counterpart [196–198]. Motivated by this, in the following subsections, the concepts of UE-side interference management as well as eICIC and CoMP are presented.

2.2.1 UE-side interference management

In conventional cellular systems, the RXs mainly presume a noise-limited operation scenario. Therefore, RXs are designed based on either optimal approaches, such as maximum-likelihood (ML) and maximum a posteriori probability (MAP) criteria, or suboptimal, such as zero-forcing (ZF) or minimum mean square error (MMSE) equalization-based architectures [195]. However, modern wireless systems are usually dominated by strong CCI among neighboring cells. The interference signals have a similar

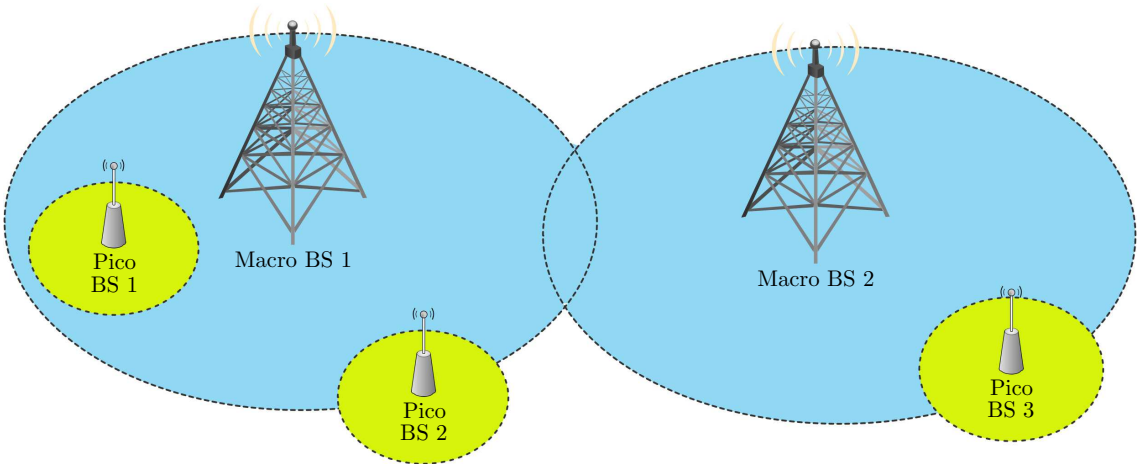

Figure 2.7 Typical LTE HetNet architecture with macro and pico access BSs. Pico-cell 1 is used for throughput enhancement in a possible traffic hotspot location. Pico-cell 2 and pico-cell 3 are used for improving edge throughput or extending the range.

structure to the desired signal, since they are desired signal on their own in other cells. Consequently, to suppress CCI, the RXs should be capable to take advantage of the structure of the interference signals, including modulation constellation, coding scheme, channel, and resource allocation. For example, the RX can try to detect the symbols of the interference signal within their constellation, or even try to decode them. Then, the interference signals can be reconstructed based on the detected/decoded signal and subtracted from the received signal in order to enhance the desired signal decoding performance. Another approach, which is used for negligible levels of interference at the RX, is to jointly decode the desired and the interference signals.

To support such functionalities, advanced RXs have been proposed, which are based in the iterative architecture [199–201], presented in Fig. 2.6. These RXs attempt to detect and decode the interference signal jointly with the desired signal. In each step of the procedure, soft information on both the desired and the interference signals, as a form of log-likelihood ratio (LLR), is iteratively exchanged between the detector and the decoder. After completion of the procedure, only the decoder output for the desired signal is taken.

The complexity of such a RX is relatively high. Especially, if the iterative RX uses the MAP detection criteria, which is the optimal one, the computational load grows exponentially with the number of joint detection signals. A significant complexity reduction can be achieved by replacing the MAP decoder with a SIC type decoder [202–204]. Additionally, in the high SNR regime, performing interference detection only, without decoding, can be sufficient.

2.2.2 Enhanced inter-cell interference coordination (eICEC)

A typical heterogeneous network (HetNet) with pico and macro access nodes is shown in Fig. 2.7. The high-power macro-cell network nodes are deployed for blanket coverage of urban, suburban, or rural areas, whereas the pico-cell nodes with small RF coverage areas aim to complement the macro network nodes for filling coverage holes or enhancing throughput. Consequently, the downlink pico-cell transmissions to its associated UEs could be severely interfered by high-power macro-cell BS transmissions [99]. For example, in Fig. 2.7 downlink transmissions to UEs associated with pico-cell 1 could be interfered by downlink transmissions of macro-cell 1.

To manage the interference in a HetNeT, the eICIC techniques was included in Release 10 of the third generation partnership projrct (3GPP) LTE advanced (LTE-A), and can be grouped under three major categories, namely [205]:

- Time-domain techniques;
- Frequency-domain techniques;
- Power control techniques.

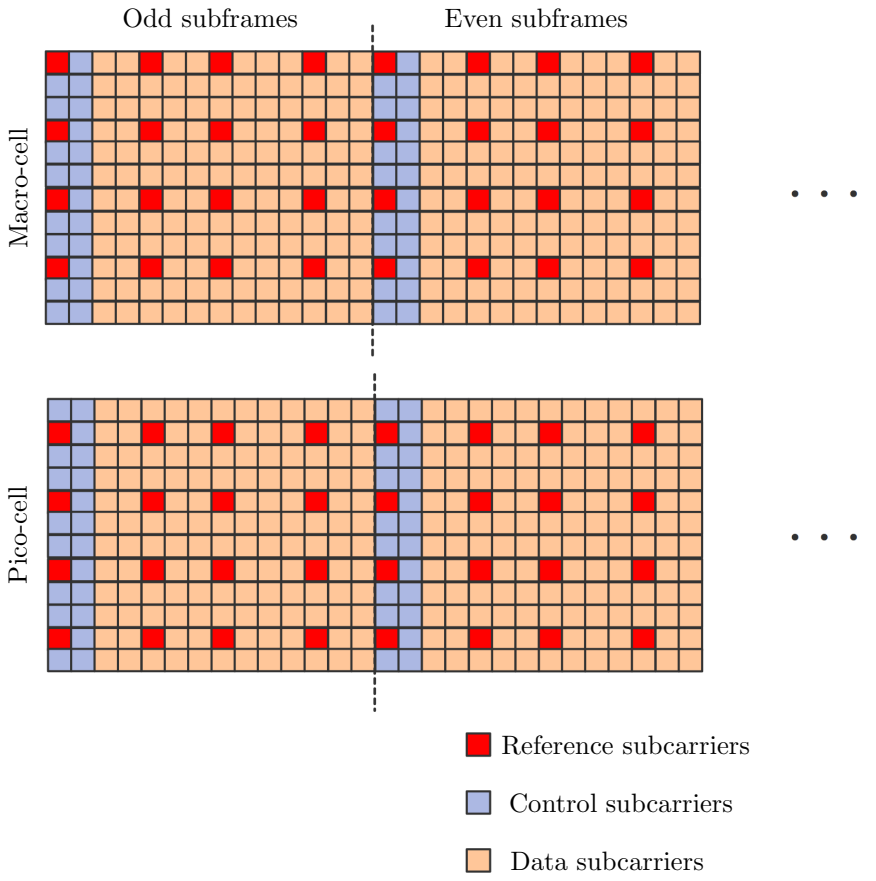

Figure 2.8 Illustration of macrocell and picocell subframes without any eICIC.

In the following subsections, the basic eICIC techniques are presented.

2.2.2.1 Time-domain technique

The main idea behind time-domain eICIC techniques is to schedule the transmission to victim UEs in time-domain resources, in which the interference from other nodes is suppressed. The following approaches of time-domain eICIC can be discerned:

- *Subframe alignment*: If the subframes of the macro-cell BS and the pico BS used for throughput enhancement are aligned, as illustrated in Fig. 2.8, their control and data channels overlap with each other. In order to suppress the interference to the control channels of the macro UEs, eICIC can be implemented in the pico-cells. Specifically, the pico-cell BSs reduces the interference to its surrounding neighbors, including the macro BS, by minimizing its transmission, i.e., the pico-cell BS stop its transmission in some subframes. These muted subframes are called almost blank subframes (ABSFs) approach. As presented in Fig. 2.9, during ABSFs, the signals that are mainly transmitted are common reference signals, as well as other mandatory system information, synchronization channels and paging channels. Note that, although in Fig. 2.9 the even subframes are configures as ABSFs, different patterns are also included in 3GPP LTE (e.g. with ABSF duty cycles of 1/8, 2/8, 3/8, and 3/20 [206]). The number of subframes configured as ABSFs need to be carefully chosen in order to maximize the overall system performance, as the use of ABSFs in the pico-cell has negative impact in terms of lost pico-layer capacity.

  A similar eICIC approach using ABSFs can also be used to mitigate the interference problems in pico-cells (and relays) that implement range expansion (RE). In this case, as depicted in Fig. 2.10, ABSFs is applied in the macro BS. As a result, the pico-cell UEs are obviously exposed to much less interference, which allows the pico-cell to serve UEs from a larger geographical area, as whould

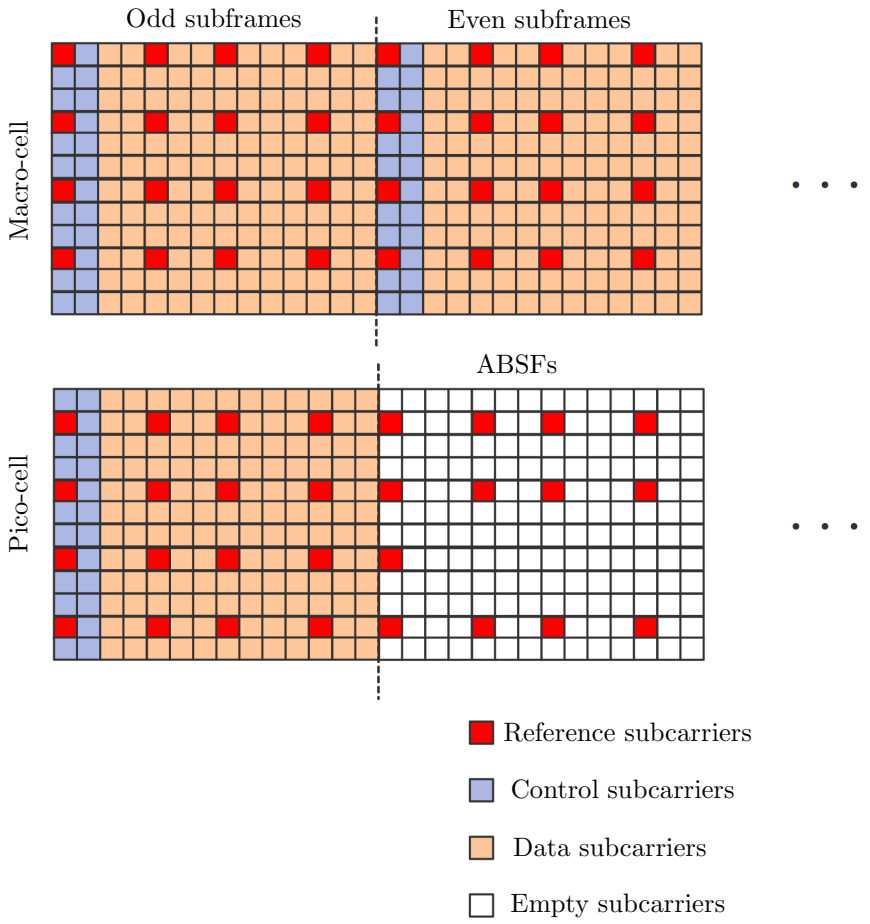

Figure 2.9 Illustration of macrocell and picocell, used for throughput enhancement, subframes with ABSFs.

otherwise have been feasible. Therefrore, the use of ABSFs at the macro-cell offers enhanced opportunities for load balancing between the macro- and pico-cells [207].

To appreciate the effectiveness of ABSFs approach, note that it can reduce the interference level of a BS in a UE by approximately 10 dB, assuming that the BSs use two transmit antennas [99]. The aforementioned 10 dB reduction of interference, due to ABSFs, can in some cases still result in interference problems. As a result, advanced UE RXs are employed in order to further suppress the residual interference from ABSFs, such that the UEs virtually experience close to zero interference from BS that uses ABSFs [208].

- *OFDM Symbol Shift*: In this case, the subframe boundary of a pico-cell BS is shifted by one or more OFDM symbols relative to that of the macro BS, in order to prevent overlap between the control channels of the pico- and macro-cell signals [209]. However, this approach does not mitigate the interference from the data channels of the pico-cell UEs to the control channels of macro-cells UEs [210]. There are two different proposed approaches to address this problem, namely *shared-channel symbol muting* and *consecutive subframe blanking*.

  In the shared-channel symbol muting approach, the OFDM symbols that overlap with the control channel of the victim macro-cell UEs are muted. By this muting, the macro UE can receive and decode its control information with no or mitigated interference from the pico-cell BS. The main drawback of this approach is that it leads to throughput loss in the pico-cell. To overcome this, rate matching can be used around the muted symbols [209]. Rate Matching is the process, in which bits are selected for transmission from the rate 1/3 turbo encoder via puncturing and/or repetition. Rate matching increases or decreases the coding rate, and hence the data rate. By rate matching that aims at increasing the code rate around the muted symbols, the throughput loss

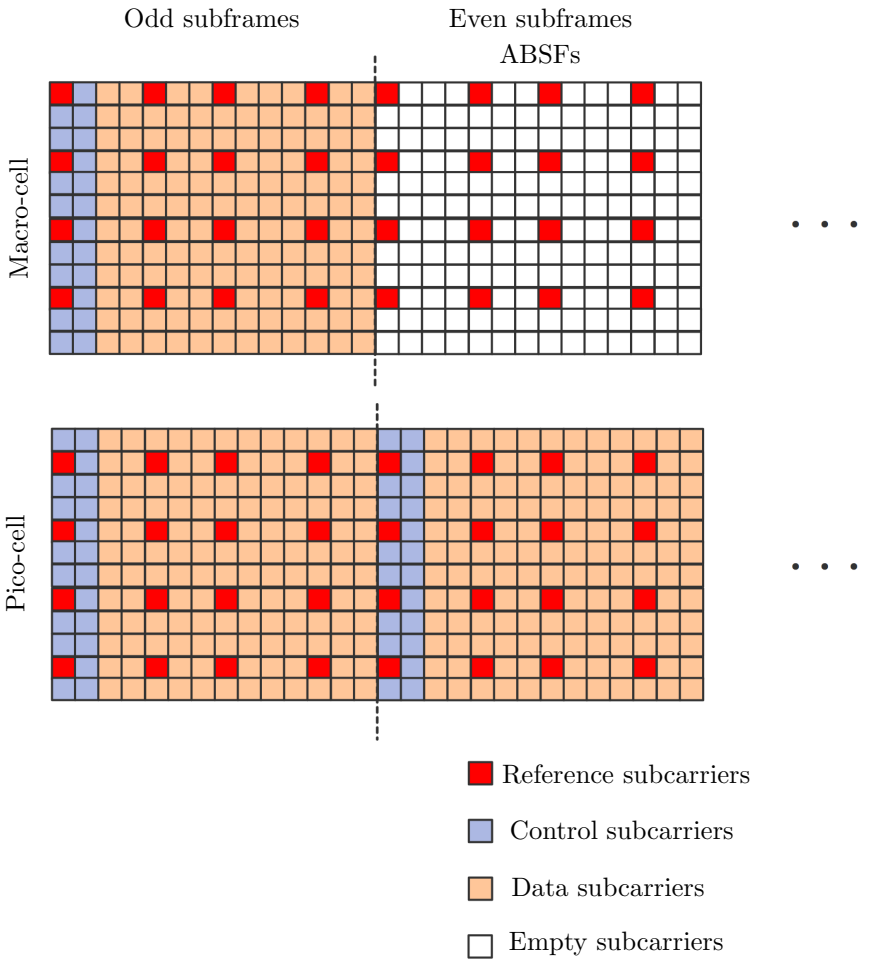

Figure 2.10 Illustration of macrocell and picocell, used for RE, subframes with ABSFs.

can be compensated [211].

In contrast with shared-channel symbol muting approach, in the consecutive subframe blanking approach, the whole subframes of the pico-cell that overlaps with the control channels of macro-cell UEs are to be blank, i.e., are configured as ABSFs. The main drawback of this approach is the loss of resources at the pico-cell BS.

2.2.2.2 Frequency-domain techniques

The main idea behind the frequency-domain eICIC techniques is to schedule the control channels and the physical signals in reduced bandwidth, in order to have totally orthogonal transmission of at different cells. In frequency-domain orthogonalization, the BS determines whether a UE suffers from unacceptable levels of interference, by utilizing the measurement reports of the UE. The identification of a victim UE is signaled by the macro (pico) cell BS to the pico (macro) cell BS through the backhaul. Then, the BSs schedule their transmissions over the entire bandwidth. Note that the orthogonality in frequency-domain is usually used only for control channels, whereas data channels may be scheduled over the entire bandwidth available for the serving cell.

2.2.2.3 Power control techniques

This approach depends mainly upon reducing the radiated power of pico-cells, which are used for throughput enhancement, to improve the performance of victim macro-cell UEs. However, this may sacrifice the total throughput of the pico-cell UEs.The different approaches can be listed as follows:

- *Strongest macro-cell BS received power at the pico-cell BS*: This power control technique restrict the transmit power of the pico-cell BS to a value that guarantees a certain SINR at the victim macro-cell UE that is in close proximity to the pico BS. This protects the reception of the control channels at the macro-cell UE. According to [205], the power setting of the pico-cell BS can be obtained as

$$P_t = \max\left(\min\left(\alpha P_M + \beta, P_{\max}\right), P_{\min}\right), \tag{2.35}$$

  where $P_{\max}$ and $P_{\min}$ represent the maximum and minimum allowed transmit power of the pico-cell BS, respectively, while P_M denote the received power from the strongest co-channel macro-cell BS at the pico-cell BS. Moreover, α is a linear scalar that allows altering the slope of power control mapping curve in order to adjust in different sizes of macro-cells. Finally, β is a parameter expressed in dB that can be used for altering the exact range of P_M covered by dynamic range of power control [212]. Note that in (2.35), all the values are in dBm.

  It is important to notice that this power control approach affects only the implementation for the pico-cell and rely on pico-cell measurements only. Hence, no additional signalling between macro- and/or pico-cell BSs is required for this solution and also no extra measurements or support from UEs is required [212].

- *Path loss between the pico-cell BS and the macro-cell UE*: For the power control approach based on the measurement of path loss between pico-cell BS and macro-cell UE, the transmit power of the pico-cell BS should be set as

$$P_t = \mathrm{med}\left(P_M + P_o, P_{\max}, P_{\min}\right), \tag{2.36}$$

  where the power offset P_o can be expressed as

$$P_o = \mathrm{med}\left(P_i, \max(P_o), \min(P_o)\right), \tag{2.37}$$

  with P_i denoting a power offset value that captures the indoor path loss and the penetration loss between the pico-cell BS and the nearest macro-cell UE.

- *Objective* SINR *of pico-cell UE*: The aim of this method is to depress the interference suffered at the macro-cell UE by restricting the received power at the pico-cell UE to a desired relatively low, but acceptable level. In more details, the value of the received SINR at pico-cell UE is restricted to a target value and the transmit power of the pico-cell BS is reduced to achieve this target SINR leading to lower interference levels to the neighbor macro-cell UEs [205, 210, 213]]. The transmission power of the pico-cell BS can be set as

$$P_t = \max\left(P_{\min}, \min\left(PL + P_{IN}, P_{\max}\right)\right), \tag{2.38}$$

  with PL being an estimation of the path loss between the pico-cell BS and the pico-cell UE, and

$$P_{IN} = 10\log_{10}\left(10^{I/10} + 10^{N_0/10}\right) + \gamma_t, \tag{2.39}$$

  where I and N_0 are the interference detected by the served UE and the background noise, respectively, whereas γ_t stand for the targeted SINR at the pico-cell UE.

- *Objective* SINR *of macro-cell UE*: This power control technique restricts the transmit power of the pico-cell BS to a value, which guarantees a certain SINR at the victim macro-cell UE that is in close proximity to the pico-cell BS. In this case, the transmission power of the pico-cell BS can be obtained as

$$P_t = \max\left(\min\left(\alpha P_\gamma + \beta, P_{\max}\right), P_{\min}\right), \tag{2.40}$$

  where P_γ is the SINR of the macro-cell UE considered only the nearest pico-cell interference.

Notice that the aforementioned power control approaches deal with the interference caused to a macro-cell UE, due to the existence of a pico-cell BS, which is used for throughput enhancement. As a result, they aim at reducing the level of interference in the macro-cell UE, by appropriately controlling the transmit power of the pico-cell BS. Similar approaches can be used in order to reduce the interference in pico-cells that are used for RE. However, in this case, the approaches will aim at reducing the transmit power of the macro-cell BS.

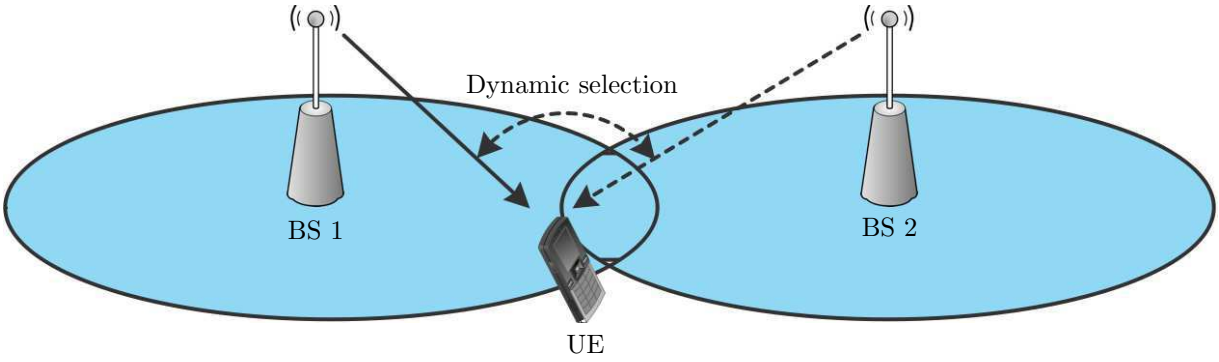

Figure 2.11 Illustration of CoMP DPS transmission scheme.

2.2.3 Coordination multipoint (CoMP) for interference management

The main idea of CoMP (also referred to as collaborative MIMO (co-MIMO), network MIMO, etc.) is to allow geographically separated BSs to cooperate in serving the UEs. Specifically, in CoMP a number of TX points provide coordinated transmission in the downlink, and a number of RX points provide coordinated reception in the uplink. A TX/RX-point constitutes of a set of co-located TX/RX antennas providing coverage in the same sector. The set of TX/RX-points used in CoMP can either be at different locations, or co-sited but providing coverage in different sectors. They can also belong to the same or different BSs. CoMP can be performed in a number of ways, and the coordination can be done for both the downlink and the uplink in homogenous as well as heterogeneous networks [210].

2.2.3.1 Downlink CoMP

According to the 3GPP, downlink CoMP transmission is categorized as dynamic point selection (DPS), dynamic point blanking (DPB), joint transmission (JT) and coordinated scheduling/beamforming (CS/CB) [214]. The four categories of the transmission schemes are demonstrated in Figs. 2.11-2.14.

In the case of DPS, the quality of the link between the BSs and the UE are checked on per-subframe basis, and the BS with the best channel conditions is dynamically selected. In other words, DPS exploits the channels variations opportunistically in order to achieve selection diversity gain. However, the achievable selection diversity gain may be marginal in comparison with the already achieved frequency and spatial diversity gain. To enhance the achievable gain, DPB, which is depicted in Fig. 2.12, can be used in addition to DPS. DPB aims to identify and instantaneously mute the dominant interferers in the coordination area. This results in a significant increase in the instantaneous SINR of the UE, since the number of the dominant interferers decreases. Muting a BS may reduce the interference in the UE, but it also causes performance loss of the particular BS. Therefore, it is important to compare the performance improvements of those beneficiaries with the performance loss of the BS, before muting a BS. If the performance improvements outweigh the loss, then the BS can be mute; otherwise, it should remain active. Someone might argue that the use of DPB seams to be unfair for the UE served by the muted BS. However, since scheduling is dynamically performed, those UE might also benefit from muting other BSs in subsequent subframes. This indicates the importance of carefully design the scheduling algorithm in order to be beneficial to all the UEs.

As illustrated in Fig. 2.13, in the case of JT, two or more BSs are transmitting a signal to a single UE using the same access (time and frequency) resources. The UE combines the signals received the multiple BSs, either coherently or non-coherently. Non-coherent JT may use techniques like single-frequency network (SFN) or cyclic delay diversity (CDD) schemes, which target diversity gains and also enable increased transmit power to the UE. Although, the SINR at UE could be boosted by non-coherent JT, it is not able to nulify interference across multiple BSs, due to the lack of relative phase information across the BSs. On the other hand, coherent transmission could be based on spatial channel state information (CSI) feedback relative to two or more BSs, which can be used to perform MIMO transmissions from the corresponding antennas. However, better synchronization and much smaller timing error differences between transmission points are needed to realize the full potential gains of coherent JT schemes, which may limit their applicability only to BSs connected by a fast backhaul [215, 216]. Moreover, coherent

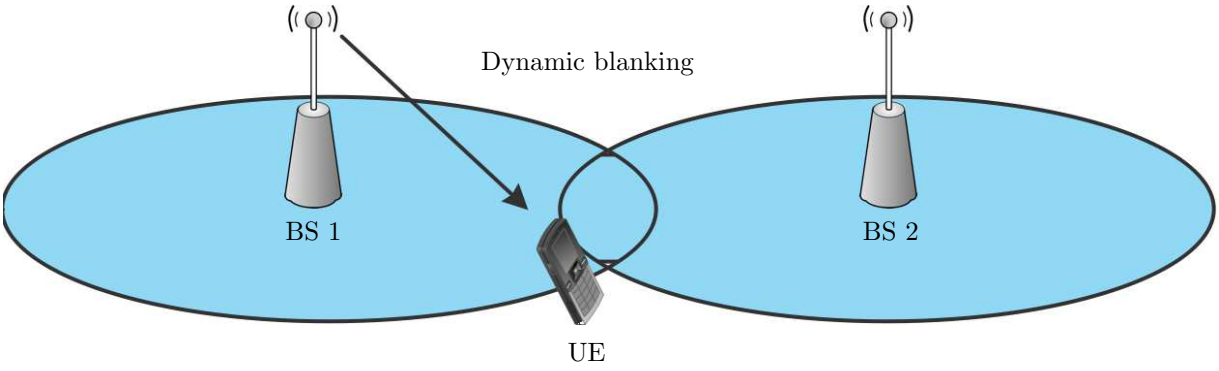

Figure 2.12 Illustration of CoMP DPB transmission scheme.

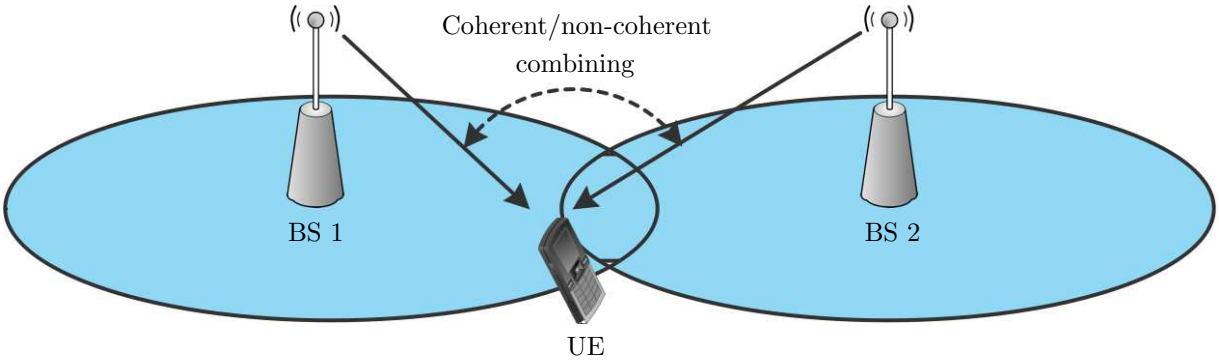

Figure 2.13 Illustration of CoMP JT transmission scheme.

JT allows multiple BSs to completely nullify interference towards co-schedule UEs. Therefore, it offers the best performance among all the considered CoMP schemes. However, coherent JT is sensitive to imperfects of CSI knowledge [217].

CS/CB CoMP transmission scheme, presented in Fig. 2.14, aims at mitigating interference by beamforming and scheduling across different BSs. A wise selection of beamforming weight may contribute to increase the SINR of a specific UE, by exploiting the channel knowledge, in order to support directional transmission across a specific UE, while at the same time it can reduce the interference to other UEs. Additionally, by selecting the UE for transmission through through a coordinated scheduling algorithm, interference at the UEs can be further suppressed. CS/CB CoMP requires joint decisions on UE and beams across multiple BSs, which might be not be feasible in practice, due to the high complexity of such a joint decision algorithm. Therefore, an iterative scheduling process is generally used. According to this scheduling process, each cell revisits the selection of both the UE and the transmit beam(s), based on the scheduling decisions and beamforming matrices decided by other cells in the previous iteration. An updated scheduling decision not only accounts for the utility of the scheduled UE, but also for the utility of the victim UE that has been tentatively scheduled by other cells in the previous iteration. The goal of each updating is to maximize a global utility (e.g., the total weighted throughput with the coordination area). Note that only a few numbers of iterations are needed to reach a near-optimal solution [214].

2.2.3.2 Uplink CoMP

Uplink CoMP is more straightforward than downlink coordination, since uplink CSI is available in the network without resource-consuming transmission, and the UE terminals need almost no modification. Joint reception (JR) of the received signal at multiple BSs and/or CS decisions among UEs in order to manage the interference level and enhance the coverage, are included in uplink CoMP [218].

The basic idea behind JR is to jointly process different copies of signal received by antennas at different sites to produce the final output signal. The process in JR is similar to the one in JT; however, in the case of JR, the received data need to be transferred between the BSs, i.e., a backhaul infrastructure

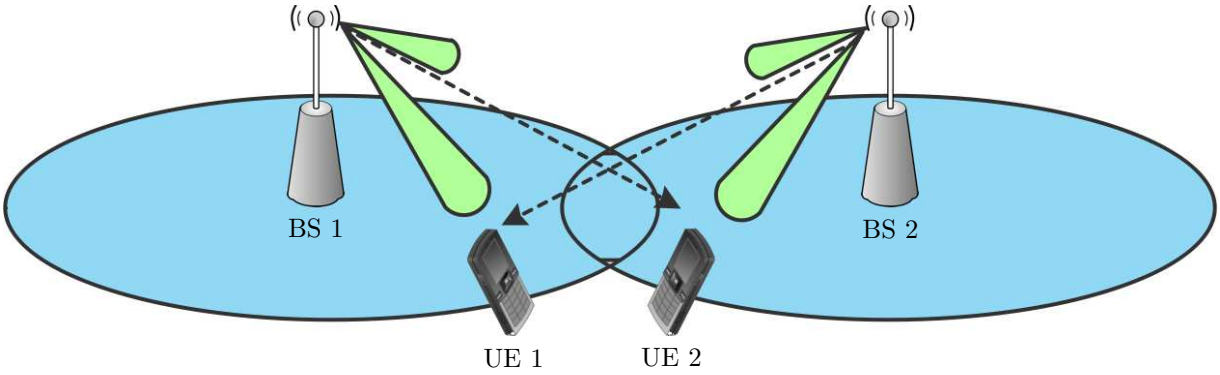

Figure 2.14 Illustration of CoMP CS/CB transmission scheme.

is needed. The amount of exchange information between cooperating BSs depends on what extend the received signals are pre-processed before information exchange. Although, quantized baseband samples are the most complete information for joint processing, as their processing leads to the best performance, the load on the backhaul is the highest. On the other hand, further processing at the BSs can lower the load of the backhaul, but, at the same time, the CoMP gain is constrained. In other words, there is a trade-off between the CoMP gain and backhaul overhead.

CS aims at mitigating interference by appropriately align UE scheduling and precoding decisions among BSs in the coordination area. In comparison with JR, CS requires only CSI and resource allocation information to be shared among the BSs, i.e., the load in the backhaul network is significantly reduced.

2.3 Interference alignment

Interference alignment (IA) is a cooperative interference management strategy that exploits the availability of multiple signaling dimensions provided by multiple time slots, frequency blocks, or antennas [219–221]. The TXs jointly design their transmitted signals in the multidimensional space, such that the interference observed at the RXs occupies only a portion of the full signaling space. By doing so, IA maximizes the number of non-interfering symbols that can be simultaneously communicated over the interference channel.

To illustrate the IA concept, we consider a K transmit/receive pair system, as demonstrated in Fig. 2.15. It is assumed that the signal transmitted by the $i-$th $(i = 1, \cdots, K)$ TX is intended to the $i-$th RX, while the signal transmitted by the $k-th$ $(k \neq i)$ TX causes interference to the $i-$th RX, i.e., each RX observes a total of $K-1$ interference signal. The user i transmits a set of S_i information symbols encoded in the $S_i \times 1$ vector, $\mathbf{s}_i$. The symbols $\mathbf{s}_i$ are precoded using the precoding matrix $\mathbf{F}_i$, and are observed at each RX k after propagating over the $N_1 \times N_2$ matrix channel $\mathbf{H}_{k,i}$. Note that in the case of multiple-input multiple-output systems with N_T and N_R transmit and receive antennas, respectively, $N_1 = N_R$ and $N_2 = N_T$, whereas in the case in which the time or the frequency domain are used to transmit the symbols (e.g. when OFDM is employed), $\mathbf{H}_{k,i}$ is a diagonal matrix with $N_1 = N_2$. For such a system, the received signal at the i RX can be obtained as

$$\mathbf{r}_i = \mathbf{H}_{i,i}\mathbf{F}_i\mathbf{s}_i + \sum_{\substack{k=1 \\ k \neq i}}^{K} \mathbf{H}_{i,k}\mathbf{F}_k\mathbf{s}_k + \mathbf{n}_i, \tag{2.41}$$

where $\mathbf{n}_i$ is the noise vector at the $i-$th RX. From (2.41), it is observed that without careful design of the precoding matrix, $\mathbf{F}_i$, the $K-1$ interference signals at the $i-$th RX occupy all the signal dimensions at the RX, i.e., the signals do not align. On the other hand, the arbitrary RX i can fully cancel the interference without nullifying or destroying its desired signal, by using a simple linear RX filter $\mathbf{W}_i$, by calculating a set of precoders that have the following properties:

$$\begin{cases} \mathbf{W}_i^*\mathbf{H}_{i,k}\mathbf{F}_k = \mathbf{0}_{S_i \times S_k}, & \text{for } i \neq k, \\ \text{rank}\left(\mathbf{W}_i^*\mathbf{H}_{i,k}\mathbf{F}_k\right) = S_i, & \text{for } i = k, \end{cases} \tag{2.42}$$

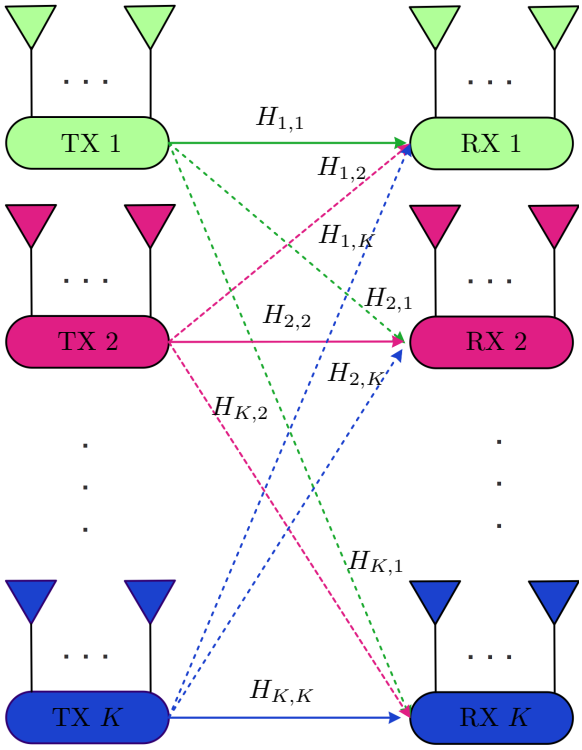

Figure 2.15 K-user IA-based network.

where $\mathbf{0}_{S_i \times S_k}$ is the $S_i \times S_k$ zero matrix, and rank $(\cdot)$ represent the rank function. Of the two conditions in (2.42), the first one may be interpreted as the condition for the existence of an interference free space of desired dimensions, whereas the second one is the condition that ensures that the desired signal is visible and resolvable within the interference-free space. Additionally, from (2.42), it is evident that the IA capability of a system depends of the ability to find appropriate IA precoders. This ability is directly related to the number of signal dimensions over which it can code [219–223].

To intuitively understand the concept of IA, we present the following insightful example [224].

Example 2.1. We consider that the system observe the following expressions:

$$y_1 = 3x_1 + 2x_2 + 3x_3 + x_4 + 5x_5, \tag{2.43}$$
$$y_2 = 2x_1 + 4x_2 + x_3 - 3x_4 + 5x_5, \tag{2.44}$$
$$y_3 = 4x_1 + 3x_2 + 5x_3 + 2x_4 + 8x_5. \tag{2.45}$$

Our objection is to solve a five-unknowns problem in a three-dimensional space. In order to derive all the five unknowns, we will need five independent observations. However, let us consider that the RX only wants to recover x_1. From (2.43)-(2.45), we observer that, even though the number of expressions is smaller than the number of unknowns, x_1 can be recovered, because the interfering beams span only a two-dimensional vector space, leaving one dimension free from interference. The received signal can be projected along the interference free dimension to recover x_1. This can be achieved by multiplying $\mathbf{u} = [17 \ -1 \ -10]$ with the observation vector $\mathbf{y} = [y_1 \ y_2 \ y_3]^T$, as

$$\mathbf{uy} = 17y_1 - y_2 - 10y_3 = 9x_1. \tag{2.46}$$

From (2.46), it is observed that the value of x_1 can be recovered from the observed values y_1, y_2 and y_3 in the three dimensional space, even when the number of unknowns is 5.

This example indicates that IA allows many interfering users to communicate simultaneously over a small number of signaling dimensions by consolidating the space spanned by the interference at each receiver within a small number of dimensions, while keeping the desired signals separable from interference so that they can be projected into the null space of the interference and thereby recovered free from interference.

2.3.1 Feasibility of IA

The problem of characterizing the number of signaling/coding dimensions, the DoF, that are needed in order to guarantee the feasibility of IA, has been extensively investigated (see [225] and references therein). The necessary condition for IA-based MIMO interference networks was derived in [226], based on the fact that the generic polynomial systems can be solved, if and only if the number of variables is no less than the number of equations from Bezout's therorem. Following the pioneering work of [226], several research efforts have been concentrated on the development of sufficient condition of feasibility [223, 227–230]. For example, in [223], the authors presented feasibility conditions for IA in a $K-$users interference network, in which each UE is equipped with multiple antennas. A necessary condition and a sufficient condition on the IA feasibility for a FD MIMO cellular networks were established in [228]. Moreover, in [229], the authors provided closed form feasibility conditions for relaying systems, in which the relay nodes are equipped with multiple-antennas. Likewise, a study of the feasibility of IA for the selective fading interference channel with time-frequency selective links was conducted in [230]. Finally, the feasibility of IA for OFDM systems was investigated in [231], where it was shown that in order to guarantee feasibility in OFDM systems that employ IA, the conditions presented in [227] should be valid for the signals carried by each subcarrier.

In general, in the K users $N_R \times N_T$ MIMO interference channel, the DoF equal [232]

$$D_{KM} = \frac{R}{R+1}, \tag{2.47}$$

where

$$R = \left\lfloor \frac{\max(N_R, N_T)}{\min(N_R, N_T)} \right\rfloor, \tag{2.48}$$

with $\lfloor \cdot \rfloor$ being the floor function, provided that the following condition is valid:

$$K > \frac{N_T + N_R}{\gcd(\mathrm{N_T}, \mathrm{N_R})}, \tag{2.49}$$

where $\gcd(\cdot)$ refers to the greatest common divisor function. For the special case in which $N_T = N_R = N$, simply by splitting each node into N separate nodes, the K users $N \times N$ MIMO interference channel can be transformed into the KN users 1×1 interference channel. Consequently, since the DoF of the K users interference channel equals $K/2$, the the $N \times N$ MIMO interference channel can achieve a DoF of

$$D_{KN} = \frac{KN}{2}. \tag{2.50}$$

2.4 Self-interference cancellation (SIC) in full duplex systems

Since the FD device knows the signal being transmitted, subtracting it from the received signal should be relatively simple to implement. However, in practice, this abstraction is incorrect. Although, the FD device knows the clean transmitted digital base band signal, once the signal is converted to analog and up-converted to the carrier frequency, the transmitted signal looks quite different from its base band incarnation. The numerous analog components in the radio TX chain distort the signal in both linear and nonlinear ways, add their own noise, are slightly inaccurate , or delay it by different amounts at different frequencies, and so on. In other words, the transmitted signal is a complicated nonlinear function of the ideal transmitted signal along with unknown noise. Interestingly, naively subtracting the "known" base band version of the transmit signal without accounting for all these analog distortions does not work [233, 234]. In other words, the effectiveness of self-interference cancellation highly depends on the accuracy with which the transmitted signal can be copied, modified and subtracted from the received signal [235].

There are three main categories of self-interference cancellation architectures that are described in the open technical literature [128, 236–239]. The first one, called *digital cancellation* and illustrated in Fig 2.16, processes the signals completely in the digital domain, i.e., after the analog-to-digital converter (ADC), by applying sophisticated DSP techniques to the received signal [128, 133, 240, 241]. The advantage of working in the digital domain is that sophisticated processing becomes relatively easy;

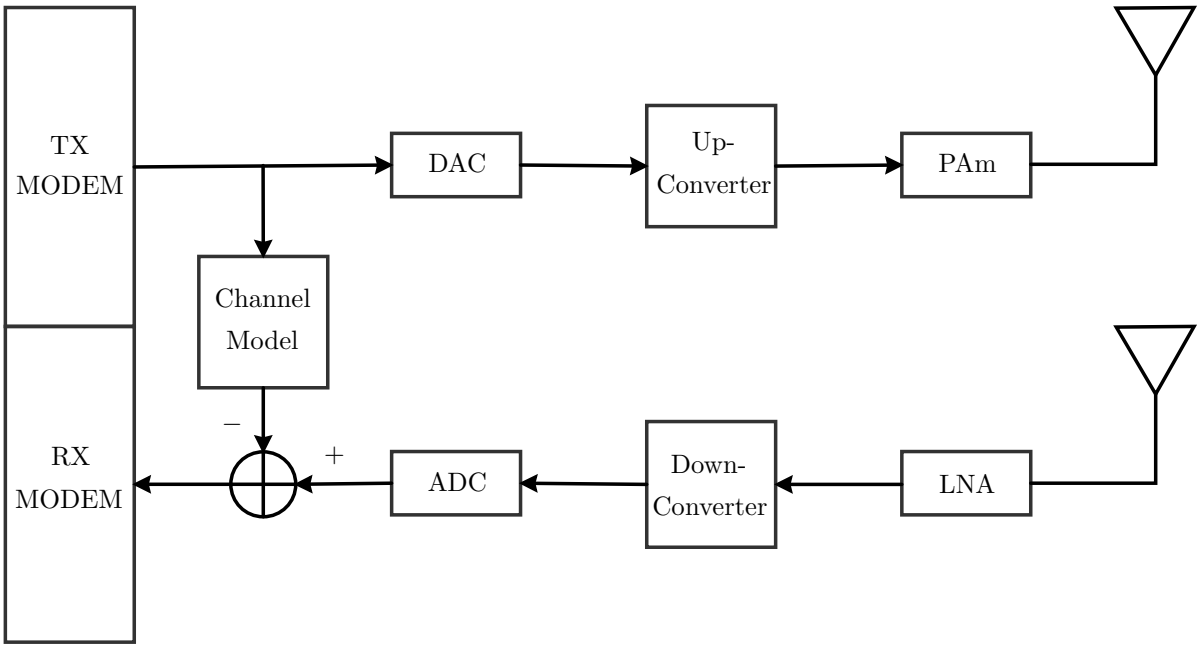

Figure 2.16 Digital self-interference cancellation architecture. In this block diagram, ADC, DAC, PAm and LNA stand for the analog-to-digital converter, the digital-to-analog converter, the power amplifier and the low-noise amplifier, respectively.

hence, the circuit complexity and the power consumption are reduced. However, the digital cancellation architecture cannot remove self-interference in the analog RX chain; therefore, it is unable to prevent the analog circuitry to block the reception due to nonlinear distortion or saturation. As a result, in practice, digital cancellation cannot provide more than $30 - 35$ dB cancellation [237, 238]. The second architecture is the *analog cancellation*, which uses a copy of the actual RF transmitted signal in order to subtract it from the RF received signal. This suppression may occur either before or after the down-converter and the LNA. Fig. 2.17 shows the analog self-interference cancellation architecture, where the transmit signal is tapped at the transmit antenna feed, electronically processed in the analog-circuit domain, and subtracted from the receive-antenna feed in order to cancel self-interference. Since, in the case of analog cancellation, the signal includes all TX impairments, this architecture can provide cancellation performance up to 60 dB [233]. The main drawback of analog cancellation is that it requires processing of the cancellation signal in the analog RF domain. The third architecture is called *mixed-signal cancellation*. In this architecture, the digital TX signal is processed in the base band and then is converted to analog RF, where subtraction occurs. As demonstrated in Fig. 2.18, this requires a dedicated additional up-converter, which, in practice, introduces its own noise and distortions. As a results, the mixed-signal self-interference cancellation architecture can provide a self-interference rejection ratio of about 35 dB [239].

To achieve even higher self-interference rejection ratio, in shared-antenna systems, a circulator can be used, while in separate-antennas FD devices, a combination of cancellation techniques with wireless-propagation-domain isolation mechanisms can be employed [128, 236–239, 242]. Wireless-propagation-domain isolation techniques aim to electromagnetically isolate the transmit chain from the receive chain, i.e., to suppress the self-interference before it manifests in the receive chain circuitry. The primary advantage of this type of self-interference suppression is that the downstream RX hardware does not need to faithfully process signals with a huge dynamic range. The key mechanisms for wireless-propagation-domain isolation are *absorptive shielding, cross-polarization*, and *directional isolation* [243, 244]. Absorptive shielding is realized by placing a RF absorber material between the TX and RX antennas. Although, this is an attractive approach, due to its simplicity, its effectiveness and feasibility depends on the FD device form-factor, i.e., the smaller the device, the less room there is to implement such mechanism. Cross-polarization offers an additional mechanism to electromagnetically isolate the transmit and receive antennas of the FD device. The main idea behind this approach is that the self-interference channel can be passively suppressed, if the FD device transmits with one polarization and receives with

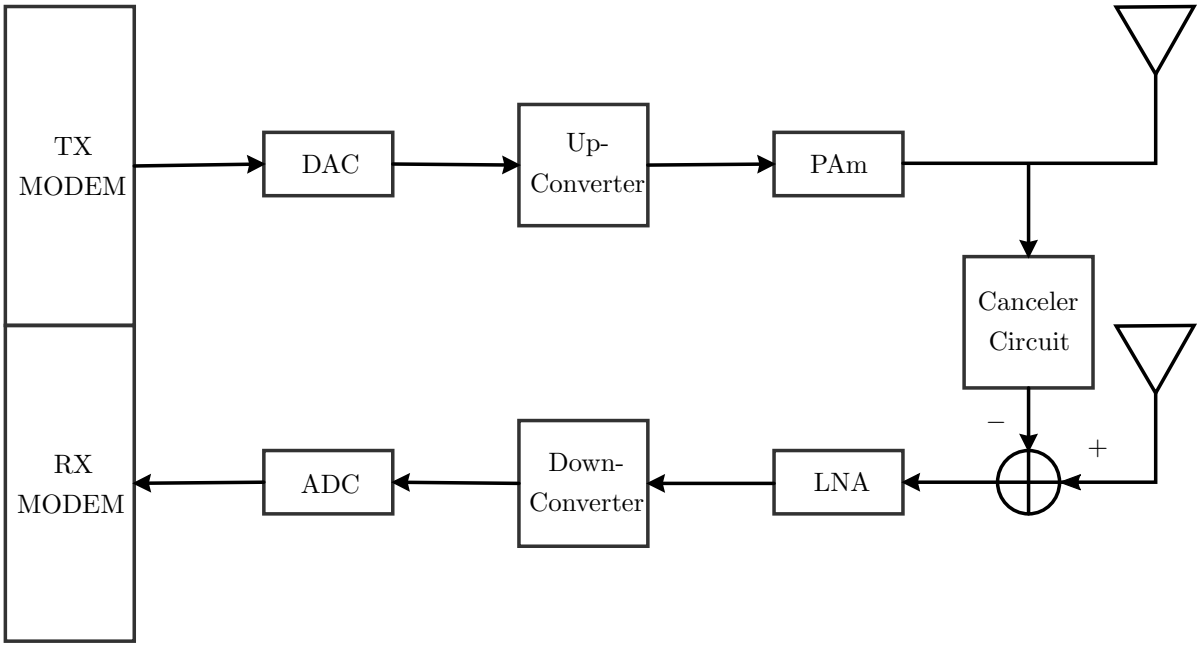

Figure 2.17 Analog self-interference cancellation architecture. In this block diagram, ADC, DAC, PAm and LNA stand for the analog-to-digital converter, the digital-to-analog converter, the power amplifier and the low-noise amplifier, respectively.

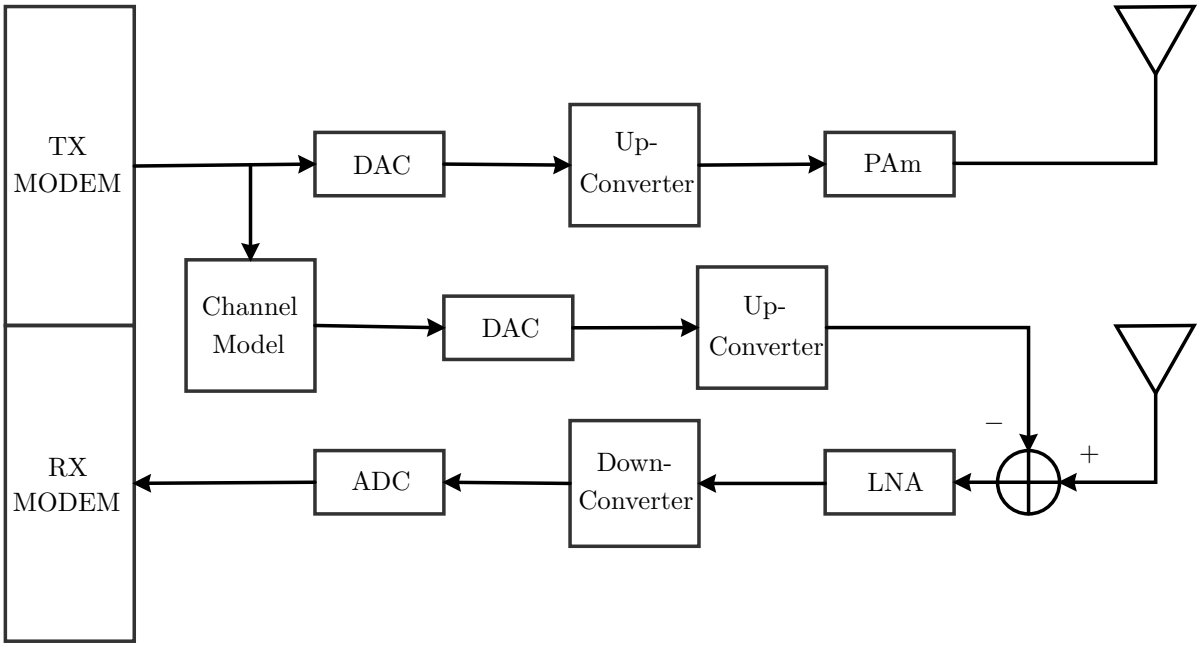

Figure 2.18 Mixed-signal self-interference cancellation architecture. In this block diagram, ADC, DAC, PAm and LNA stand for the analog-to-digital converter, the digital-to-analog converter, the power amplifier and the low-noise amplifier, respectively.

an orthogonal polarization. For example, a FD device can transmits only horizontally polarized signal, and receives only vertically polarized signal in order to avoid interference between them [243, 245, 246]. Finally, directional isolation can be implemented by using a highly directional TX antenna and placing the RX antenna at precisely a location, where the carrier waveforms are exactly 180^o out of phase. This will result to a near-perfectly cancellation of any narrow-band signal modulated in those carriers.

Chapter 3

Spectrum sensing with multiple primary users under Nakagami-m fading channel

This chapter investigates the impact of fading and CCI, which is caused due to the existence of multiple PUs, on the spectrum sensing of a classical ED. Specifically, novel closed form expressions for the false alarm and detection probabilities in a multiple PUs environment, assuming Nakagami-m fading and complex Gaussian PUs transmitted signals, are presented. The results reveal the importance of taking into consideration the wireless environment, when evaluating the ED spectrum sensing performance and selecting the ED threshold.

The research results of this chapter are included in [247].

3.1 Introduction

The rapid growth of wireless communications and the foreseen spectrum occupancy problems, due to the exponentially increasing consumer demands on mobile traffic and data, inspired the evolution of the concept of CR [248]. CRs are wireless devices with re-configurable hardware and software (including transmission parameters and protocols) that are able to intelligently sense and adapt to their spectral environment [249, 250]. One fundamental task in CR that allows the exploitation of the under-utilized spectrum, is spectrum sensing. As a result, great amount of effort has been put to derive optimal, sub-optimal and ad-hoc solutions to the spectrum sensing problem and investigate their performance [251–268].

3.2 Related work

Scanning the open technical literature, most of the related works have neglected the impact of multiple PUs and fading on the spectrum sensing performance of the CR's ED. However, in several widely used wireless communication standards, such as LTE-A, WiFi and WiMAX, where code-division-multiple-access (CDMA) is used, users simultaneously operate in the same frequency band [269–271]. These applications motivated a general investigation of the effect of PU traffic on the sensing performance, when multiple PUs are present. To the best of the author's knowledge, there is only one published work in the open literature [272], where the effect of multiple PUs on spectrum-sensing performance was investigated, considering only the impact of additive white Gaussian noise (AWGN) channels. Moreover, in [273], the authors derived the sensing time and the transmission time that jointly maximize the sensing efficiency and the sensing accuracy in a multiple mobile PU network. However, in [273], the spectrum sensing method and the effect of fading channels was neglected.

3.3 Contribution

In this chapter, we present an analytical framework to evaluate and quantify the joint effect of multiple PUs and fading on the spectrum sensing performance of a classical ED. In particular, we present novel closed form expressions for the false alarm and detection probabilities in a multiple PUs environment, assuming Nakagami-m channels and complex Gaussian transmitted signals. Those expressions can be used not only to determine the spectrum sensing capabilities of the ED, but also to select the appropriate energy detection threshold and the spectrum sensing duration of the ED.

3.4 Organization

The remainder of the chapter is organized as follows. The system and signal model are described in Section 3.5. Section 3.6 is devoted to the derivation of the analytical expressions for the false alarm and detection probabilities. Respective numerical results evaluated by computer simulations are provided in Section 3.7. Finally, Section 3.8 concludes the chapter by summarizing the main findings.

3.5 System and signal model

We consider a multiple PUs/secondary user (SU) environment, where M static PUs operate in the same frequency band, which is sensed by a single CR device. The two possible states, i.e., busy or idle, of the $i-$th PU are denoted with the parameters $\theta_i \in \{0,1\}$, where $i = 1, 2, \ldots, M$. Suppose that the n-th sample of the transmitted signal of the $i-$th PU, $s_i(n)$, is conveyed over a flat-fading wireless channel, with channel gain, $h_i(n)$. Hence, at the SU detector the $n-$th sample of the baseband equivalent received signal can be expressed as

$$y(n) = \sum_{i=1}^{M} \theta_i h_i(n) d_i^{-\xi_i/2} s_i(n) + w(n), \tag{3.1}$$

where d_i and ξ_i stand for the distance between the $i-$th PU and the SU, and the corresponding link path-loss exponent, respectively, while $w(n)$ represents the AWGN. We assume that s_i and w are zero-mean circular symmetric complex white Gaussian processes with variances $\sigma_{s_i}^2$ and σ_w^2. Furthermore, h_i is a zero mean complex random variable (RV) with variance $\sigma_{h_i}^2$ and $|h_i|$ follows Nakagami-m_i distribution. Without loss of generality, it is assumed that SU is located in the first ($i = 1$) PU cell.

Next, the basic symbols, which are used in this chapter, are defined. Specifically,

$$\Theta = [\theta_1, \theta_2, \cdots, \theta_M], \tag{3.2}$$

represents the set of M PUs (busy and idle) located at distances

$$d = [d_1, d_2, \cdots, d_M] \tag{3.3}$$

from the SU, while

$$\tilde{\Theta} = \left[\tilde{\theta}_1, \tilde{\theta}_2, \cdots, \tilde{\theta}_L\right] \subseteq \Theta, \tag{3.4}$$

denotes the set of the $L \leq M$ active PU located at distances

$$\tilde{d} = \left[\tilde{d}_1, \tilde{d}_2, \cdots, \tilde{d}_L\right] \subseteq d. \tag{3.5}$$

Additionally,

$$\Theta_0 = [0, 0, \cdots, 0], \tag{3.6}$$

stands for the all idle PU occupancy set, while

$$\Theta_1 = [1, \theta_2, \cdots, \theta_M], \tag{3.7}$$

with $\theta_j \in \{0,1\}$, $j = 2, \cdots, M$, represents the PU occupancy set, in which the first PU is active. Moreover,

$$\Theta_{0,1} = [0, \theta_2, \cdots, \theta_M], \tag{3.8}$$

in which at least one $\theta_l = 1$, $l \in \{2, \cdots, M\}$, denotes the PU occupancy set in which the first PU is idle and at least one PU is busy. Finally, $\tilde{\Theta}_1$ and $\tilde{\Theta}_{0,1}$ denote the corresponding to Θ_1 and $\Theta_{0,1}$ sets of active PUs.

3.6 False alarm and detection probabilities

In the classical ED, the energy of the received signals is used to determine whether a channel is idle or busy. Based on the signal model described in Section 3.5, ED calculates the energy test statistics as

$$\begin{aligned} T &= \frac{1}{N_s}\sum_{n=0}^{N_s-1} \left|y\left(n\right)\right|^2 \\ &= \frac{1}{N_s}\sum_{n=0}^{N_s-1} \Re\left\{y\left(n\right)\right\}^2 + \Im\left\{y\left(n\right)\right\}^2, \end{aligned} \tag{3.9}$$

where N_s is the number of samples used for spectrum sensing. The energy test statistic, T, is compared against a threshold γ to yield the sensing decision, i.e., the ED decides that the channel is busy if $T > \gamma$ or idle, otherwise.

For a given channel realization set

$$H = \{h_1, h_2, \cdots, h_M\} \tag{3.10}$$

and PUs occupation set

$$\Theta = \{\theta_1, \theta_2, \cdots, \theta_M\}, \tag{3.11}$$

the real and imaginary parts of the received signals are uncorrelated, i.e.,

$$E\left[\Re\left\{y\right\}\Im\left\{y\right\}\right] = 0, \tag{3.12}$$

with variances

$$\sigma^2 = E\left[\Re\left\{y\right\}^2\right] = E\left[\Im\left\{y\right\}^2\right] = \sum_{i=1}^{M} \theta_i \left|h_i\right|^2 d_i^{-\xi_i} \frac{\sigma_{s_i}^2}{2} + \frac{\sigma_w^2}{2}, \tag{3.13}$$

the received energy test statistic follows chi-square distribution with $2N_s$ DoF and cumulative distribution function (CDF) given by

$$F_T\left(x\left|H,\Theta\right.\right) = \frac{\gamma\left(N_s, \frac{N_s x}{2\sigma^2}\right)}{\Gamma\left(N_s\right)}. \tag{3.14}$$

Furthermore, since N_s is an integer, (3.14) can be re-written as [274, Eq. (8.352/2)]

$$F_T\left(x\left|H,\Theta\right.\right) = 1 - \sum_{n=0}^{N_s-1} \frac{1}{n!}\left(\frac{N_s x}{\sigma^2}\right)^n \exp\left(-\frac{N_s x}{\sigma^2}\right). \tag{3.15}$$

Next, we present Theorem 3.1, which returns closed form expressions for the CDFs of the test statistics for a given PUs occupancy set, and Lemma 1 that evaluates the CDF of the test statistics, when all the PUs are idle.

Theorem 3.1. *The CDF of the energy test statistics for a given channel set, $\tilde{\Theta} \subseteq \Theta$, with $L \in [1, M]$ active PUs, can be evaluated by*

$$\begin{aligned} F_T\left(x\left|\Theta\right.\right) = 1 - \sum_{n=0}^{N_s-1}\sum_{i=1}^{L}\sum_{k=1}^{a_i}\sum_{j=0}^{k-1} \frac{(-c)^{k-1-j}\,\Xi(i,k)}{n! b_i^{k+n-j-1}(k-1)!} \binom{k-1}{j} \left(\frac{N_s x}{2}\right)^n \exp\left(\frac{c}{b_i}\right) \\ \times \Gamma\left(-n+j+1, \frac{c}{b_i}, \frac{N_s x}{2b_i}, 1\right), \end{aligned} \tag{3.16}$$

where $\Gamma\left(\cdot,\cdot,\cdot,\cdot\right)$ stand for the extended incomplete Gamma function, which is defined as in [275, Eq. (6.2)], while

$$a = \{\tilde{m}_1, \tilde{m}_2, \cdots, \tilde{m}_L\}, \tag{3.17}$$

$$b = \left\{ \frac{\tilde{d}_1^{-\tilde{\xi}_1} \sigma_{\tilde{h}_1}^2 \sigma_{\tilde{s}_1}^2}{2\tilde{m}_1}, \frac{\tilde{d}_2^{-\tilde{\xi}_2} \sigma_{\tilde{h}_2}^2 \sigma_{\tilde{s}_2}^2}{2\tilde{m}_2}, \cdots, \frac{\tilde{d}_L^{-\tilde{\xi}_L} \sigma_{\tilde{h}_L}^2 \sigma_{\tilde{s}_L}^2}{2\tilde{m}_L} \right\}, \tag{3.18}$$

and

$$c = \frac{\sigma_w^2}{2}. \tag{3.19}$$

Furthermore, $\tilde{d}_i$ and $\tilde{\xi}_i$, represent the distance and the corresponding link path-loss exponent between the $i-th$ active PU and the ED, whereas $\sigma_{\tilde{s}_i}^2$, and $\sigma_{\tilde{h}_i}^2$ stand for the variances of the $i-th$ active PU's transmitted signal and $i-th$ fading channel. The shape factor of the fading channel between the $i-th$ active PU and the CR device is denoted as $\tilde{m}_i$. Moreover, note that in (3.16)*, $\Xi(i,k)$ is defined in [276, Eqs. (8) and (9)]* [1].

Proof. Please refer to Appendix A. ■

Note that $\Gamma(\cdot,\cdot,\cdot,1)$ can be evaluated by Theorem B.1 given at Appendix B.

Lemma 3.1. *The CDF of the energy test statistic assuming all the PUs are idle can be evaluated by*

$$F_T(x\,|\Theta_0) = 1 - \sum_{n=0}^{N_s-1} \frac{1}{n!} \left(\frac{N_s x}{\sigma_w^2}\right)^n \exp\left(-\frac{N_s x}{\sigma_w^2}\right). \tag{3.20}$$

Proof. If $\Theta = \Theta_0$, according to (3.13),

$$\sigma^2 = \frac{\sigma_w^2}{2}, \tag{3.21}$$

which is independent of the channel realization set H. Substituting this value into (3.15), we get (3.20). This concludes the proof. ■

Based on the above analysis the detection and false alarm probabilities can be respectively obtained as

$$P_{\mathbf{d}}(\gamma) = \sum_{i=1}^{\mathrm{card}\left(\tilde{\Theta}_1\right)} P_r(\Theta_1) \left(1 - F_T\left(\gamma \left| \tilde{\Theta}_1 \right.\right)\right) \tag{3.22}$$

and

$$P_{\mathbf{fa}}(\gamma) = \sum_{i=1}^{\mathrm{card}\left(\tilde{\Theta}_{0,1}\right)} P_r(\Theta_{0,1}) \left(1 - F_T\left(\gamma \left| \tilde{\Theta}_{0,1} \right.\right)\right) + P_r(\Theta_0) \sum_{n=0}^{N_s-1} \frac{1}{n!} \left(\frac{N_s x}{\sigma_w^2}\right)^n \exp\left(-\frac{N_s x}{\sigma_w^2}\right), \tag{3.23}$$

where $P_r(\Theta)$ stands for the probability of the PU occupancy set Θ, and $\tilde{\Theta}$ denote the set of active PUs. According to (3.22), (3.23) and (3.16), the detection and false alarm probabilities depend not only take on the PU that is located in the same cell as the SU, but also the interference and the fading characteristics of the neighbor PUs-SU links. Consequently, in order to select the energy detection threshold and the number of samples that will be used to achieve a detection and/or false alarm probabilities requirements, ED should take into consideration not only the variances of the PU signal, noise and channel, but also the variances of the neighbor PUs' signals, and channels, as well as the probabilities of active PU existence. Note that in practice, the CR device has certain noise measurements and has only an estimate for the noise variance. However, in our analysis, we assume that the ED has perfect knowledge on the noise variance, which is obtained from calibration measurements. This is a typical assumption ([277–279] and

[1] Note that there is a typo in [276, Eq. (8)]. The correct expression is

$$\Xi(i, a_i - k) = \frac{1}{k} \sum_{\substack{q=1 \\ q \neq i}}^{L} \sum_{j=1}^{k} \frac{a_q}{b_i^j} \left(\frac{1}{b_i} - \frac{1}{b_q}\right)^{-j} \Xi(i, a_i - k + j).$$

references therein) in order to be able to quantify the performance degradation due to the effects of multiple PUs, independently of the classical noise uncertainty problem. Next, we study two important special cases.

Special Case 1 (Rayleigh fading): In the special case in which all the PUs-SU links are Rayleigh distributed, the CDF of the energy test statistics for the given set $\tilde{\Theta}$ can be obtained, by setting

$$a = \{1, 1, \cdots, 1\} \tag{3.24}$$

into (3.16), as

$$F_T\left(x\,|\Theta\right) = 1 - \sum_{n=0}^{N_s-1} \sum_{i=1}^{L} \frac{\Xi(i,1)}{n! b_i^n} \left(\frac{N_s x}{2}\right)^n \exp\left(\frac{c}{b_i}\right) \Gamma\left(-n+1, \frac{c}{b_i}, \frac{N_s x}{2b_i}, 1\right). \tag{3.25}$$

Special Case 2 (single PU scenario): In the special case of a single PU, the CDF of the energy test statistic assuming that the PU is active can be obtained, by setting

$$L = 1, \tag{3.26}$$

$$a = \{m\}, \tag{3.27}$$

and

$$b = \left\{ \frac{d^{-\xi}\sigma_h^2\sigma_s^2}{2m} \right\} \tag{3.28}$$

into (3.16), as

$$F_T\left(x\,|\theta\right) = 1 - \frac{2m^m}{\left(\sigma_h^2 d^{-\xi}\sigma_s^2\right)^m \Gamma(m)} \exp\left(\frac{m\sigma_w^2}{\sigma_h^2 d^{-\xi}\sigma_s^2}\right) \sum_{k=0}^{m-1} \sum_{n=0}^{N_s-1} \binom{m-1}{k} \frac{2^{k-n}}{n!} \left(-\sigma_w^2\right)^{m-1-k} \left(N_s x\right)^n \times \left(\frac{\sigma_h^2 d^{-\xi}\sigma_s^2}{2m}\right)^{k-n+1} \Gamma\left(k-n+1, \frac{m\sigma_w^2}{\sigma_h^2 d^{-\xi}\sigma_s^2}, \frac{mN_s x}{\sigma_h^2 d^{-\xi}\sigma_s^2}, 1\right). \tag{3.29}$$

Furthermore, the CDF of the energy test statistics assuming that the PU is idle can be derived by (3.20). Therefore, the detection and false alarm probabilities in the single PU scenario can be respectively expressed as

$$P_{\mathbf{d}}(\gamma) = P_r\left(T_k > \gamma\,|\theta_k = 1\right) = \frac{2m^m}{\left(\sigma_h^2 d^{-\xi}\sigma_s^2\right)^m \Gamma(m)} \exp\left(\frac{m\sigma_w^2}{\sigma_h^2 d^{-\xi}\sigma_s^2}\right) \times \sum_{k=0}^{m-1} \sum_{n=0}^{N_s-1} \binom{m-1}{k} \frac{2^{k-n}}{n!} \left(-\sigma_w^2\right)^{m-1-k} \left(N_s\gamma\right)^n \left(\frac{\sigma_h^2 d^{-\xi}\sigma_s^2}{2m}\right)^{k-n+1} \times \Gamma\left(k-n+1, \frac{m\sigma_w^2}{\sigma_h^2 d^{-\xi}\sigma_s^2}, \frac{mN_s\gamma}{\sigma_h^2 d^{-\xi}\sigma_s^2}, 1\right) \tag{3.30}$$

and

$$P_{\mathbf{fa}}(\gamma) = \sum_{n=0}^{N_s-1} \frac{1}{n!} \left(\frac{N_s\gamma}{\sigma_w^2}\right)^n \exp\left(-\frac{N_s\gamma}{\sigma_w^2}\right). \tag{3.31}$$

In order to meet the requirements for the detection and/or false alarm probabilities, the ED should appropriately set the detection threshold and the number of samples, by taking into consideration parameters as the PU signal variance, the noise variance, the fading characteristics and the path-loss exponent of the PU-SU link, as well as the distance between the PU and the SU.

Note that the single PU scenario has been extensively studied in the open literature, considering deterministic PU transmission signal. However, to the best of the authors' knowledge, this is the first work, in which a closed form expression for the CDF of the energy statistics, under the assumptions of Nakagami-m fading and complex Gaussian distributed PU transmitted signal, is presented. Therefore, the derived expressions can be used to quantify the effects of Nakagami-m fading, by neglecting the impact of multiple PUs. Finally, in Section 3.7, the single PU scenario, is used as a benchmark to demonstrate the impact of multiple PUs on the spectrum sensing performance of the ED.

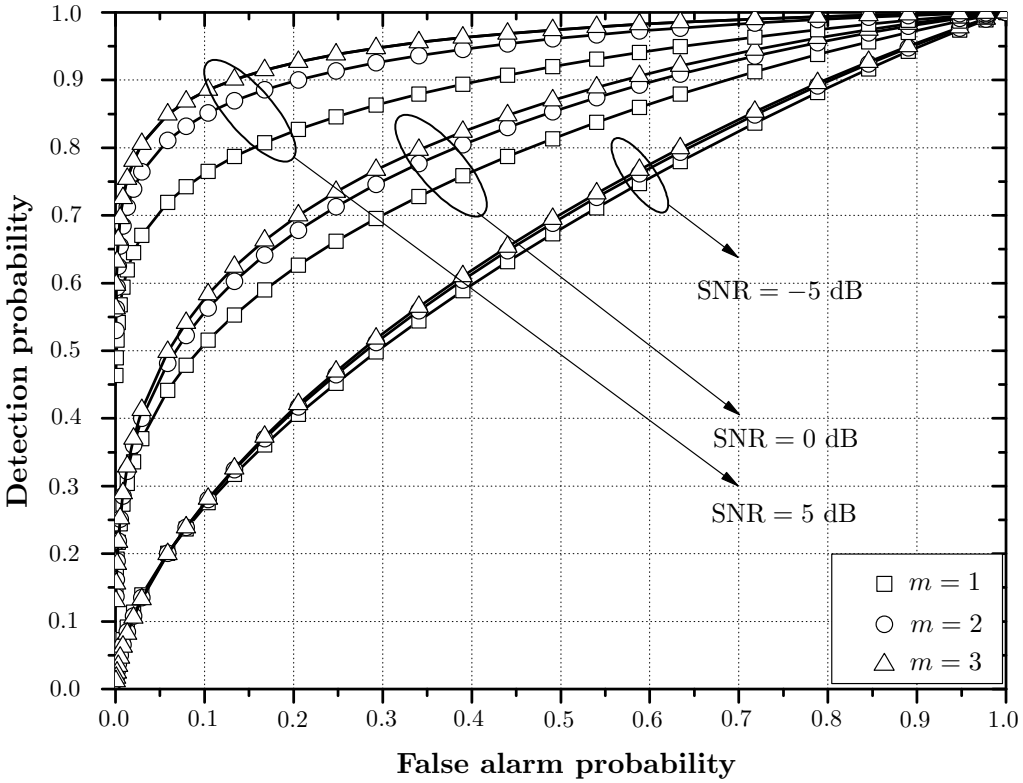

Figure 3.1 ROCs for systems with a single PU and different values of m and SNR.

3.7 Numerical and simulation results

In this section, using the previous results, we investigate the impact of fading and the existence of multiple PUs on the spectrum sensing performance of EDs. In particular, we present three insightful scenarios. In the first scenario, demonstrated in Fig. 3.1, we illustrate the impact of the fading statistics on the spectrum sensing performance of an ED operating in the presence of a single PU. In the second scenario, illustrated in Fig. 3.2, the impact of the probability of existence of multiple active PUs on the spectrum sensing capabilities of an ED operating in the presence of six PUs is demonstrated. To further investigate the effect of the existence of multiple PUs on the spectrum sensing performances, in the third scenario (3.3), we illustrate the impact of the number of PUs in the spectrum sensing capabilities of the ED, considering fixed PU existence probabilities. For all figures, the number of samples is set to 5 ($N_s = 5$), while it is assumed that $\sigma_{h_i}^2 = \sigma_w^2 = 1$, $i = 1, \ldots, M$. In all the illustrations, the solid curves represent analytical values obtained through the derived formulas, while the markers represent Monte-Carlo simulation results.

In Fig. 3.1, receiver operation curves (ROCs) are demonstrated for different signal-to-noise ratios (SNRs) and m values, in the presence of a single PU, i.e., $M = 1$. We observe that for low SNR values, the characteristics of the fading channels do not significantly affect the ED performance. However, as SNR increases, the effects of the fading statistics become more detrimental. In addition, it is seen that for a fixed m and false alarm probability, the detection probability of the ED increases as the SNR increases. Moreover, for a fixed SNR and false alarm probability, as m increases, the effects of fading become less severe; hence, the detection probability increases, while, for a fixed SNR and detection probability, as m increases the false alarm probability decreases. In other words, for a fixed SNR, as m increases the spectrum sensing performance of the ED increases. This is expected, because the effects of fading become less severe as m increases.

Next, we consider that the CR device operates in a 6-PUs environment, where all the fading channels are assumed to be Rayleigh distributed ($m_i = 1$, $i \in \{1, \ldots, 6\}$) and each PU causes a different level of interference to the CR. We assume that the SU belongs to the first PU's cell, while the other 5 PUs are interferers from neighbor cells. In particular, in Fig. 3.2, ROCs are plotted for different probabilities

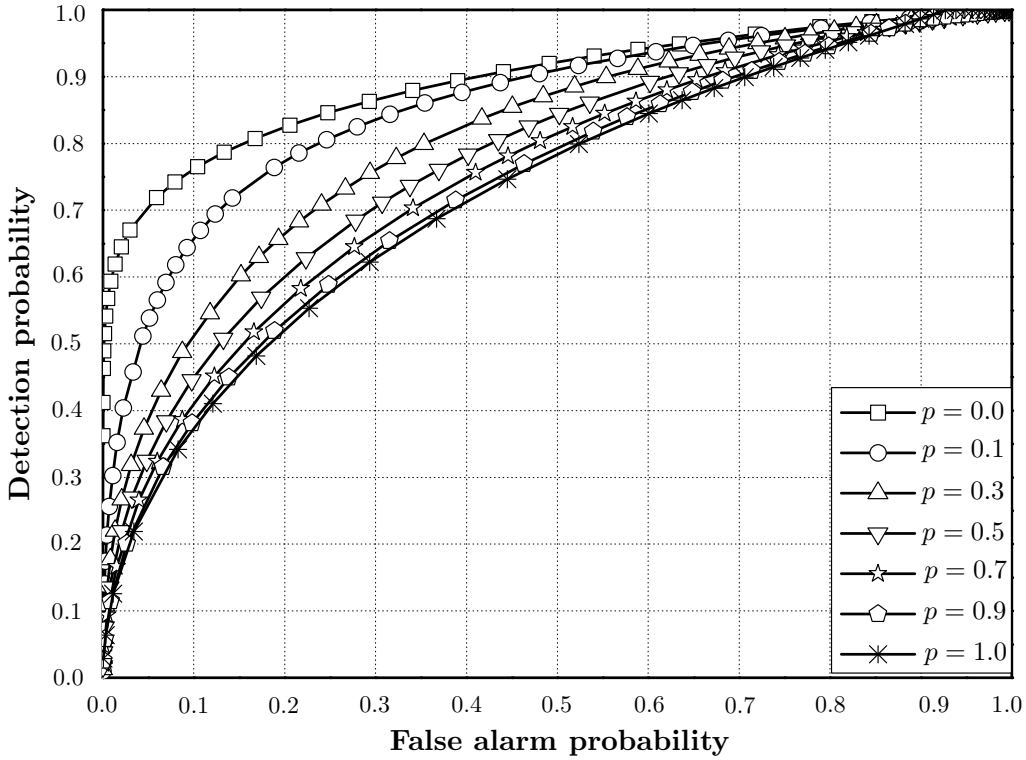

Figure 3.2 ROCs for systems with 6 PUs and different values of p.

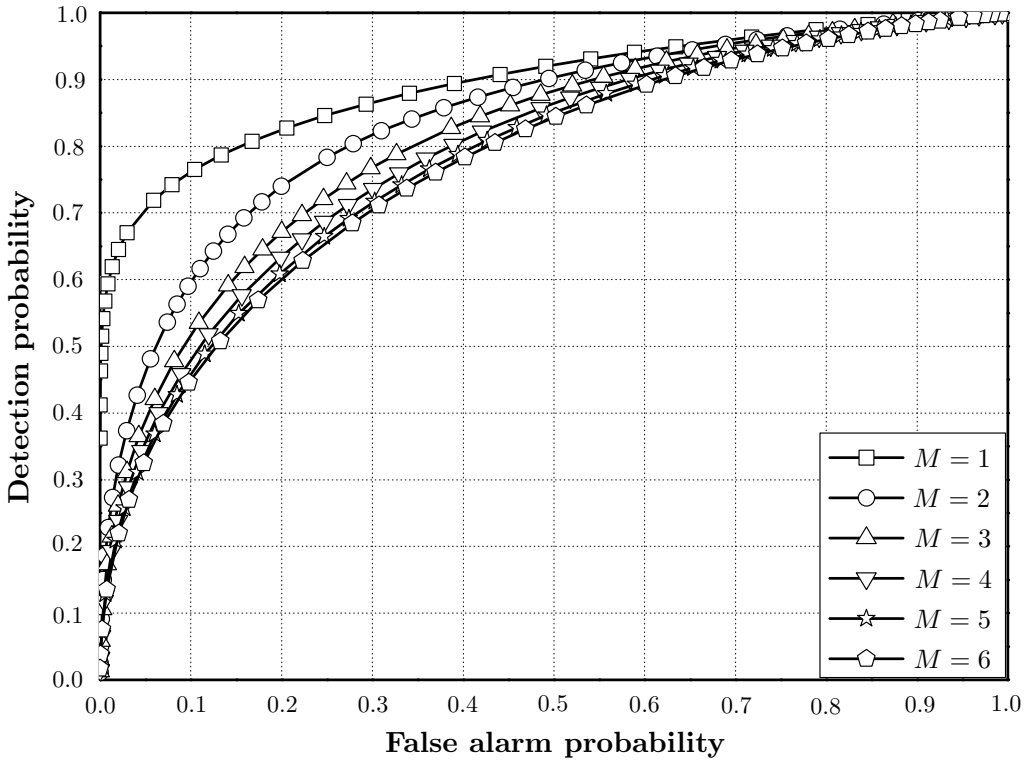

Figure 3.3 ROCs for systems with M PUs with $p = 0.5$.

of active interfering PU existence, p, considering that the received SNR from the PU, which is located in the same cell with the SU, is equal to 0 dB, while the interference-to-noise ratios (INRs) from the other 5 PUs are 0 dB, -1 dB, -2 dB, -3 dB and -5 dB. Note that we assume the same p for the 5 interfering PUs. It is observed that as p increases, the probability of interference of an neighbor PU increases; consequently, the spectrum sensing capabilities of the ED are constrained. For example, for a fixed $\mathrm{P_{fa}} = 0.1$, the detection probability is decreased about 41.8% for $p = 0.5$ in comparison with the case in which $p = 0$. Notice that the $p = 0$ case corresponds to the single PU scenario.

In Fig. 3.3, ROCs are illustrated for different number of PUs, M, considering that $m_i = 1$, for $i = 1, \ldots, 6$, and the probability of existence of the $j-$th PU, $j \in \{2, \ldots, M\}$ is equal to 0.5, i.e., $p = 0.5$. We observe that as the number of PUs increases, the interference from neighbor PUs increases; hence the false alarm probability increases and the spectrum sensing capabilities of the ED are constrained. For example, $\mathrm{P_{fa}} = 0.1$, the detection probability is decreased about 41.6% for $M = 6$ in comparison with the case in which $M = 1$. This finding reveals the importance of taking into consideration the number of PU, when deploying a CR system.

3.8 Conclusions

In this chapter, we studied the impact of multiple PUs in the spectrum sensing performance of a classical ED, assuming Nakagami-m channels and complex Gaussian PUs' transmitted signals. Our results revealed the importance of taking into consideration the fading statistics, especially in the medium to high SNR regime. Furthermore, we observed that the spectrum sensing performance is constrained as the probability of interference from neighbor PUs increases. Therefore, when selecting the operational energy detection threshold, we should not only take into consideration the PU that is located in the same cell as the SU, but also the wireless environment, i.e., interference, as well as the fading characteristics of the PUs-SU links.

Part III

Interference due to hardware impairments

Chapter 4

Introduction to RF impairments

In the last three decades, wireless communication has evolved from a scarce technology used by professionals (e.g. government, military or aerospace) for niche applications to consumer electronics [74, 280–282]. With the advent of data-centric applications, such as the Internet, mobile communication, or wireless local area networks (WLANs), in the early nineties, wireless communication started its way into everybody's daily life. Moreover, according to the wireless world research forum (WWRF), by 2020, it is expected that about 7×10^9 wireless devices will be serving the global population [283], while the number of mobile-connected devices per capita will reach 1.5 [284]. Motivated by the variety of wideband multimedia applications, which are supported by the 5G wireless systems, the data transfer capacity per wireless device has been dramatically growing [5, 285–290]. As a result, the international telecommunication union's radiocommunication sector (ITU-R) has specified that the device peak data rate should be between 100 MBit/s and 1 GBit/s (depending on mobility), for the forth generation (4G) cellular wireless standards [291–293], while 5G systems might require even 10 GBit/s, in order to support mobile cloud services [3, 80, 285, 294].

From a technology point of view, in order to achieve the increased data rates, radio transceivers need to be flexible and software-reconfigurable devices [295–298]. By definition, flexible radios are characterized by the ability to operate over multiple-frequency bands, and to support different types of waveforms, as well as various air interface technologies of currently existing and emerging wireless systems [299]. In this context, the terms multi-mode, multi-band, and multi-standard are commonly used. The flexibility of transceivers, in line with the software define radio (SDR) principle, will enable the use of emerging standards and waveforms though software updates, without hardware changes [297, 300–302]. Moreover, SDR is considered one of the key technologies that enables the use of CRs, which are expected to bring significant improvements in spectral efficiency through opportunistic spectrum access [303–305].

From an economical point of view, the advantages in integrated circuit (IC) technologies and the adoption of low-complexity transceiver structures, such as the direct-conversion radio (DCR) architecture, allowed improvements in manufacturing efficiency and automation that resulted in reducing the cost-per-device. Moreover, the use of low-complexity transceiver structure enable the reduction of the power consumption in battery-powered devices, without sacrificing too much performance.

In general, the demands for multi-standards operation, flexibility, and higher data rate, as well as the constraints of product cost, device size, and energy efficiency, lead to the use of simplified radio architectures and low-cost radio electronics [27, 306–311]. In this context, the DCR architecture of such systems provides an attractive front-end solution [312–317], as it requires neither external intermediate frequency filters nor image rejection filters [307, 318]. Instead, the essential image rejection is achieved through signal processing methods [319]. DCRs architectures are low cost and can be easily integrated on chip, which render them excellent candidates for modern wireless technologies [320–322]. However, direct-conversion transceivers are typically sensitive to front-end related impairments, such as IQI, local oscilator (LO) phase noise and amplifiers nonlinearities, which are often inevitable due to components imperfections and manufacturing defects [49, 72, 323–336].

Motivated by this, this chapter is devoted in modelling the effect of IQI, phase noise and amplifiers nonlinearities in single- and multi-carrier communication systems. Specifically, Section 4.1 presents the single- and multi-carrier signal model for the TX and RX IQI. Section 4.2 focuses in the TX and RX LO phase noise effect in single- and multi-carrier systems. Finally, Section 4.3 is devoted to the demonstration of the signal models that takes into consideration the nonlinearity effect of the power amplifiers.

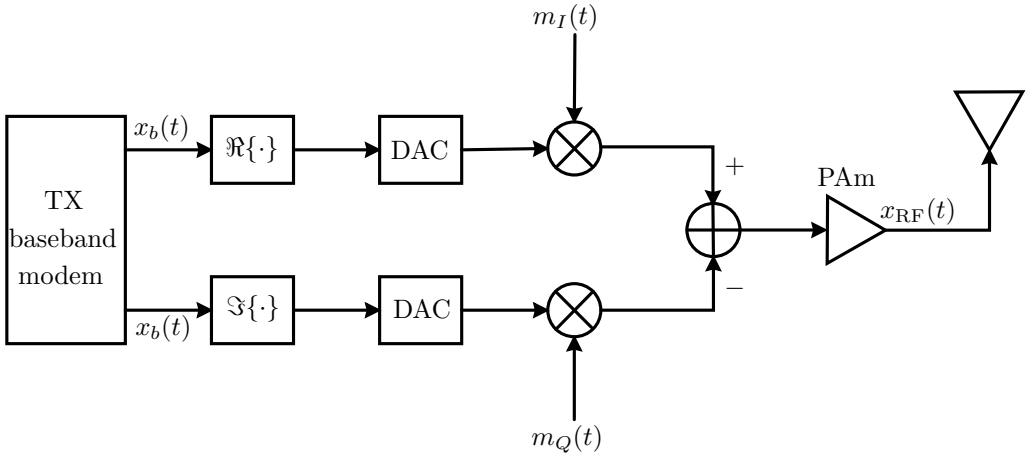

Figure 4.1 Block diagram of a typical direct-conversion transmitter. In this block diagram, PAm and DAC denote the power amplifier and the digital-to-analog converter, respectively.

4.1 In-phase and quadrature imbalance (IQI)

IQI stems from the unavoidable amplitude and phase differences between the physical analog in-phase (I) and quadrature (Q) signal paths at the up- and down-converter of the TX and RX, respectively. In particular, IQI occurs due to the error in the nominally 90^o error shifter and the mismatch between the amplitudes of the LO I and Q outputs. This problem arises mainly due to the finite tolerances of the capacitors and the resistors used in the implementation of the analog front-end components [277, 299, 319, 320, 334, 337–380].

4.1.1 Up-conversion in the presence of IQI

In this subsection, the up-conversion process of a time domain baseband signal, $x_b(t)$, in a direct-conversion TX, is considered. As illustrated in Fig. 4.1, the real and imaginary part of $x_b(t)$ are first passed through the digital-to-analog converters (DACs). The signal is then up-converted to RF, f_c. In the case of imperfect matching between the I and Q branches, the imbalanced LO signals used for up-conversion can be expressed as [320]

$$m_Q(t) = \epsilon_t \sin(\omega_c t + \phi_t), \tag{4.1}$$

and

$$m_I(t) = \cos(\omega_c t), \tag{4.2}$$

where ϵ_t and ϕ_t model the TX amplitude and phase mismatch, respectively, while

$$\omega_c = 2\pi f_c. \tag{4.3}$$

From (4.1) and (4.2), it is observed that in the case of perfect matching, the imbalance parameters are $\epsilon_t = 1$ and $\phi_t = 0$.

Based on (4.1) and (4.2), the RF signal , $x_{\mathrm{RF}}(t)$, can be obtained as

$$x_{\mathrm{RF}}(t) = 2\Re\{x_b(t)\} m_Q(t) - 2\Im\{x_b(t)\} m_I(t), \tag{4.4}$$

or, equivalently

$$x_{\mathrm{RF}}(t) = \left(K_1^t x_b(t) + \left(K_2^t\right)^* x_b^*(t)\right) \exp(j\omega_c t) + \left(\left(K_1^t\right)^* x_b^*(t) + K_2^t x_b(t)\right) \exp(-j\omega_c t), \tag{4.5}$$

where

$$K_1^t = \frac{1}{2}\left(1 + \epsilon_t \exp(j\phi_t)\right) \tag{4.6}$$

and

$$K_2^t = \frac{1}{2}\left(1 - \epsilon_t \exp\left(-j\phi_t\right)\right). \tag{4.7}$$

In what follows, we refer to K_1^t and K_2^t as TX IQI coefficients. It is also noted that the TX IQI coefficients are algebraically linked to each other as

$$K_2^t = 1 - \left(K_1^t\right)^*. \tag{4.8}$$

Moreover, the TX IQI coefficients are associated with the TX image rejection ratio (IRR), which determines the amount of attenuation of the image signal and is expressed as

$$\mathrm{IRR}_t = \frac{|K_1^t|^2}{|K_2^t|^2}. \tag{4.9}$$

It is recalled here that for practical analog RF front-end electronics, the values of IRR_t is typically in the range of 20 dB − 40 dB [277, 278, 314, 321, 355, 367, 374–379, 381–384].

From (4.5), it is observed that the base band equivalent transmitted signal in the presence of IQI can be obtained as

$$x(t) = K_1^t x_b(t) + \left(K_2^t\right)^* x_b^*(t). \tag{4.10}$$

Note that for perfect TX matching, $K_1^t = 1$, $K_2^t = 0$, and (4.10) reduces to $x(t) = x_b(t)$.

4.1.2 Down-conversion in the presence of IQI

In this subsection, the down-conversion process of a time domain RF signal, $y_{\mathrm{RF}}(t)$, in a direct-conversion RX, is considered. As demonstrated in Fig. 4.2, the received RF signal is first pass through the LNA, and then is down-converted to base band by a quadrature mixer. Low-pass filtering is applied in both the I and Q branched to remove higher order modulation products. Finally, both signal are passed though an analog-to-digital converter (ADC) and combined to form the base band signal. In the case of imperfect matching between the I and Q branches, the imbalanced LO signals used for down-conversion can be expressed as [320]

$$d_Q(t) = -\epsilon_r \sin\left(\omega_c t + \phi_r\right) \tag{4.11}$$

and

$$d_I(t) = \cos\left(\omega_c t\right), \tag{4.12}$$

where ϵ_t and ϕ_t model the TX amplitude and phase mismatch, respectively.

According to (4.11) and (4.12), the down-converted signal can be obtained as

$$y(t) = \mathrm{LPF}\left\{d_I(t) y_{\mathrm{RF}}(t)\right\} + j\mathrm{LPF}\left\{d_Q(t) y_{\mathrm{RF}}(t)\right\}, \tag{4.13}$$

where $\mathrm{LPF}\{\cdot\}$ denotes the low-pass filtering operation. After some algebraic manipulations, (4.13) can be rewritten as

$$y(t) = K_1^r y_{\mathrm{id}}(t) + K_2^r y_{\mathrm{id}}^*(t), \tag{4.14}$$

where $y_{\mathrm{id}}(t)$ denote the base band IQI-free signal. Furthermore, K_1^r, K_2^r are the RX IQI coefficients, which can be obtained as

$$K_1^r = \frac{1}{2}\left(1 + \epsilon_r \exp(-j\phi_r)\right) \tag{4.15}$$

and

$$K_2^r = \frac{1}{2}\left(1 - \epsilon_r \exp(j\phi_r)\right). \tag{4.16}$$

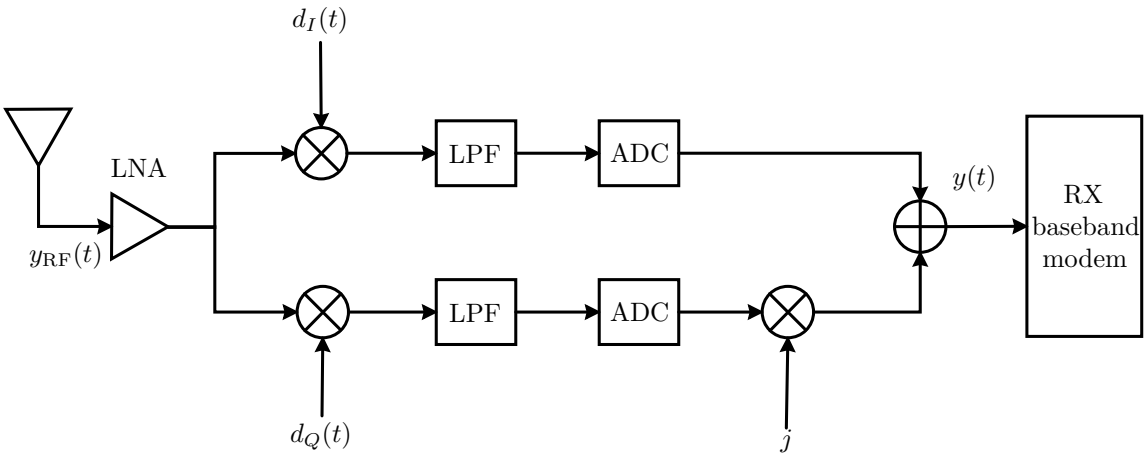

Figure 4.2 Block diagram of a typical direct-conversion receiver. In this block diagram, LNA, LPF and ADC denote the low power amplifier, low pass filter and the analog-to-digital converter, respectively.

From (4.15) and (4.16), it is evident the the RX IQI coefficients are connected to each other as

$$K_2^r = 1 - \left(K_1^r\right)^* . \tag{4.17}$$

Furthermore, the RX IQI coefficients are associated with the RX IRR as

$$\mathrm{IRR}_r = \frac{|K_1^r|^2}{|K_2^r|^2}. \tag{4.18}$$

It is recalled here that for practical analog RF front-end electronics, the values of IRR_r is typically in the range of 20 dB − 40 dB.

4.1.3 Influence of IQI in single-carrier communications

The second terms in (4.10) and (4.14), namely $\left(K_2^t\right)^* x_b^*(t)$ and $K_2^r y_{\mathrm{id}}^*(t)$, respectively, are caused by the associated imbalances, and in the case of single-carrier transmission, they represent the self-interference effect. This is illustrated on a conceptual level in Fig. 4.3, where the spectra of single carrier transmission for both cases of IQI-free and IQI RF front-end is presented.

Furthermore, Fig. 4.4 depicts the effect of IQI on noiseless quadrature phase-shift keying (QPSK), 16 quadrature amplitude modulation (QAM), and 64-QAM symbol constellation. The rectagulars represent the ideal symbols, whereas the circles and the stars stand for the TX and RX I/Q imbalanced symbols, respectively. From this figure, it is evident that for the single-carrier transmission, the constellation is expanded and skewed. Additionally, it is observed that as the constellation order increases, the impact of IQI become more severe. In other words, IQI can be seen as a limiting factor for increasing the spectral efficiency of wireless systems.

4.1.4 Influence of IQI in multi-carrier communications

In the case of multi-carrier communications, the second terms in (4.10) and (4.14), namely $\left(K_2^t\right)^* x_b^*(t)$ and $K_2^r y_{\mathrm{id}}^*(t)$, denote the image aliasing effect and result to crosstalk between mirror-frequencies at the TX and RX in the up-converted and down-converted signals, respectively. This is illustrated in Fig. 4.5, where the spectral of the noise-free received signal is presented for both cases of IQI and IQI-free RX. Form this figure, we observe that subcarrier k experience interference from the signal received on the mirror subcarrier $-k$, and vice versa. Since complex conjugate in the time domain corresponds to complex conjugate and mirroring in the frequency domain, the spectrum of the imbalanced signal at the $k-$th subcarrier at the TX and RX can be respectively obtained as

$$X(k) = K_1^t X_b(k) + \left(K_2^t\right)^* X_b^*(-k). \tag{4.19}$$

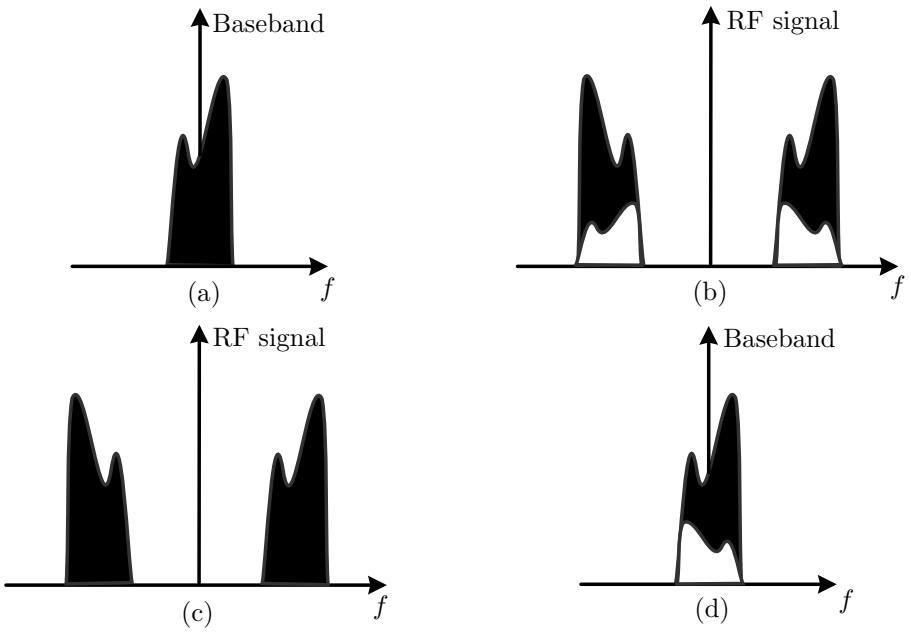

Figure 4.3 Spectra of the (noise-free) I/Q imbalanced transmitted and received signal: (a) at the TX, before up-conversion, (b) at the TX, after up-conversion, when the TX RF front-end suffers from IQI, where the intermixing of the image signal (in white) and the desired signal (in black) is clearly visible, (c) at the TX, before down-conversion, (d) at the TX, after down-conversion, when the RX RF front-end suffers from IQI, where the intermixing of the image signal (in white) and the desired signal (in black) is clearly visible.

and

$$Y(k) = K_1^r Y_{\rm id}(k) + K_2^r Y_{\rm id}^*(-k), \tag{4.20}$$

where $X_b(k)$ and $X_b(-k)$ denote the spectrum of the IQI free transmitted signal at the k and $-k$ subcarriers, respectively, whereas $Y_{\rm id}(k)$ and $Y_{\rm id}^*(-k)$ represent the spectrum of the IQI free received signal at the k and $-k$ subcarriers, respectively.

Fig. 4.6 demonstrates the impact of TX and RX IQI on noiseless 16-QAM symbol constellation, for multi-carrier communications. From this figure, it is observed that, in the case of multi-carrier systems, IQI results to mirror subcarrier interference, as well as gain and common phase errors. The mirror subcarrier interference is pure noise, whose level depends on the power difference between the mirror signal subcarriers and the level of IRR.

4.1.5 Frequency selective IQI

From (4.19) and (4.20), it can be seen that the modelled IQI has a frequency independent (FI) behavior. Although the main source of IQI is generally FI, in multi-carrier transceivers IQI may have a frequency selective (FS) behavior. FS IQI arises due to mismatches between filters and differences in group delay in the I and Q branches [320, 342, 347, 353, 355, 385]. Hence, this subsection is devoted in presenting the signal model of FS IQI. Specifically, we present the signal model of FS RX IQI; however, the same results apply and for the case of FS TX IQI.

In the case of FS RX IQI, the received baseband signal can be expressed as [320, Eq. (5.37)]

$$\tilde{y}(t) = g_I(\tau) * (d_I(t) y_{RF}(t)) + j g_Q(\tau) * (d_Q(t) y_{RF}(t)), \tag{4.21}$$

where $g_I(\tau)$ and $g_Q(\tau)$ model the impulse response of the LPFs of the I and Q branches, respectively. Moreover, note that we assume that the LPFs can fully suppress the term at the double frequency. Therefore, (4.21) can be equivalently written as

$$\tilde{y}(t) = g_I(\tau) * \frac{y_{\rm id}(t) + y_{\rm id}^*(t)}{2} + j g_Q(\tau) * \frac{\epsilon_r \exp(-j\phi_r)\, y_{\rm id}(t) - \epsilon_r exp(j\phi_r)\, y_{\rm id}^*(t)}{2}. \tag{4.22}$$

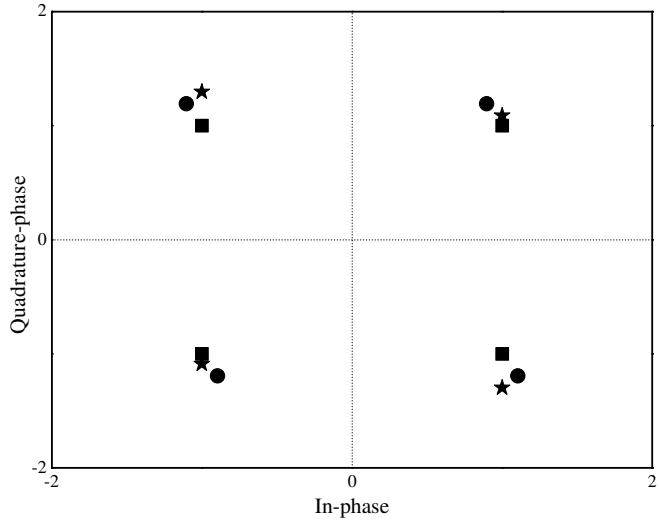

(a) QPSK

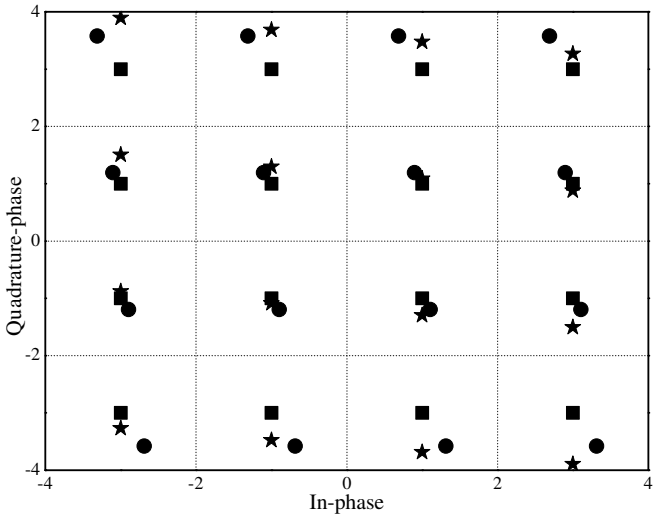

(b) 16-QAM

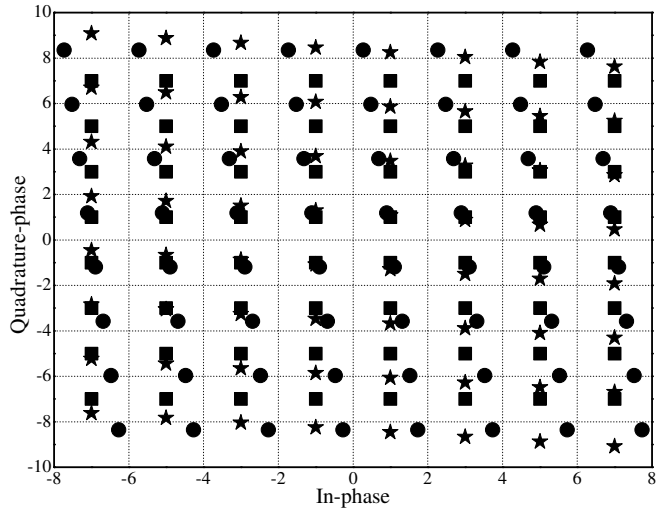

(c) 64-QAM

Figure 4.4 Scatter plots of noiseless M-QAM signal, for single-carrier transmission. The rectangulars denote the ideal symbols, while the circles and the stars represent the TX and RX imbalanced symbols, respectively, with $\text{IRR}_r = \text{IRR}_t = 20$ dB and $\phi_r = \phi_t = 5^o$.

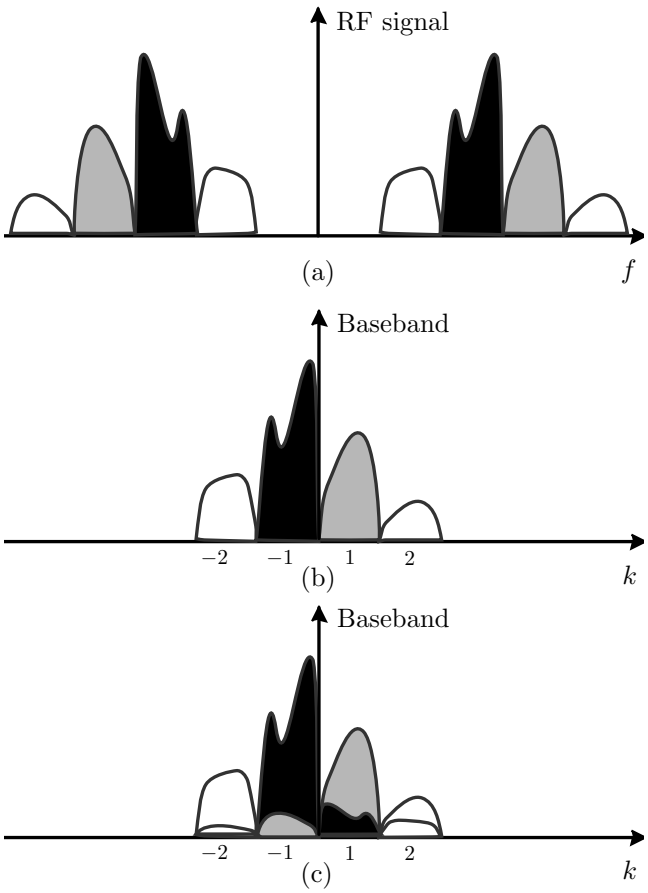

Figure 4.5 Spectra of the (noise-free) received signals: (a) before down-conversion (passband RF signal), (b) after down-conversion, when ideal RF front-end is considered, and (c) after down-conversion, when the RX RF front-end suffers from IQI, where for the 1st subcarrier, the intermixing of the image signal (in black) and the desired signal (in grey) is clearly visible, while for the −1st subcarrier, the image and desired signals are depicted in grey and black colors, respectively.

Next, by transforming (4.22) in the frequency domain, and after some algebraic manipulations, we get the received signal at the $k-$th subcarrier

$$\tilde{Y}(k) = \tilde{K}_1^r(k) Y_{\text{id}}(k) + \tilde{K}_2^r(k) Y_{\text{id}}^*(-k), \tag{4.23}$$

where

$$\tilde{K}_1^r(k) = \frac{1}{2}\left(G_I(k) + j\epsilon_r \exp(-j\phi_r) G_Q(k)\right) \tag{4.24}$$

and

$$\tilde{K}_2^r(k) = \frac{1}{2}\left(G_I(k) - j\epsilon_r \exp(j\phi_r) G_Q(k)\right). \tag{4.25}$$

In (4.24) and (4.25), $G_I(k)$ and $G_Q(k)$ stand for the frequency responses of the low pass filters (LPFs) for the $k-$th subcarrier for the I and Q branches. Moreover, note that since G_I and G_Q are frequency responses of real filters, $G_I(k) = G_I^*(-k)$ and $G_Q(k) = G_Q^*(-k)$. Consequently, $\tilde{K}_1^r(k)$ and $\tilde{K}_2^r(-k)$ are linked through

$$\tilde{K}_2^r(-k) = G_I(k) - \left(\tilde{K}_1^r(k)\right)^*. \tag{4.26}$$

Additionally, in case the case of FS IQI, the IRR is defined as

$$\text{IRR}_r(k) = \frac{|\tilde{K}_1^r(k)|^2}{|\tilde{K}_2^r(k)|^2}. \tag{4.27}$$

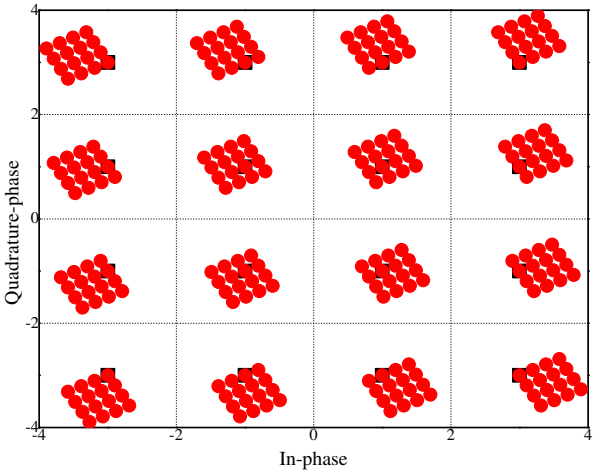

(a) TX IQI

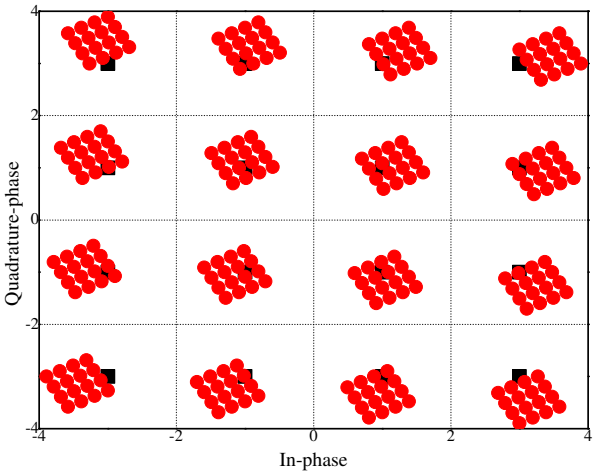

(b) RX IQI

Figure 4.6 Scatter plots of noiseless 16-QAM signal, for multi-carrier transmission. The black rectangulars denote the ideal symbols, while the red circles and the stars represent the TX and RX imbalanced symbols, respectively, with $\text{IRR}_r = \text{IRR}_t = 20$ dB and $\phi_r = \phi_t = 5^o$.

From (4.27), it is evident that the IRR varies as a function of the subcarrier index k.

By comparing (4.23) with (4.20), it is observed that the structure of the received frequency domain signal in the case of FS IQI is very similar to the one in the case of FI IQI. The only difference is that the IQI coefficients in the case of FS IQI is a function of the subcarrier index. Therefore, in what follows, we assume FI IQI; however, the generalization to the SI case is straightforward using the methodology presented in this section.

4.2 Phase noise

Noise is of major concern in LOs, because introducing even small noise into a LO leads to dramatic changes in its frequency spectrum and timing properties. This phenomenon, peculiar to LOs, is known as phase noise or timing jitter, and it was identified as one of the major performance limiting factors of communication systems in several studies, see for example [49, 72, 277, 323, 328, 334, 336, 349, 380, 386–425]. Generally, the disturbance of the amplitude of the oscillator output is marginal. As a result, most influence of the oscillator imperfection is noticeable in random deviation of the frequency of the oscillator output [320]. These frequency deviations are often modelled as a random excess phase, and therefore referred to as phase noise. Phase noise will more and more appear to be a performance limiting factor

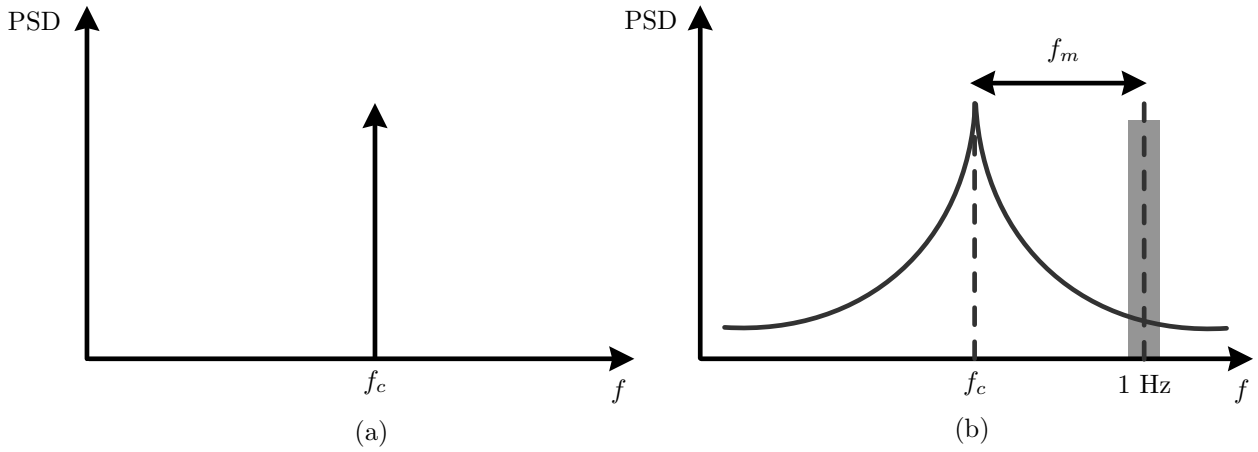

Figure 4.7 PSD of (a) an ideal LO, and (b) a realistic LO.

especialy in the case of multi-carrier communications, when low-cost implementations or systems with high carrier frequencies are considered [49, 336, 391], since, in those cases, it is harder to produce an oscillator with sufficient stability [424, 426].

4.2.1 Phase noise modelling

In TX, the complex baseband signal is up-converted around a carrier frequency f_c, while, in RX, it is down-converted, using a mixer and a LO. A perfect LO has localized tones at discrete frequencies (i.e., harmonics). In other words, without phase noise, the oscillator processes at the TX and RX can be respectively expressed as [320]

$$a_{\mathrm{id},t}(t) = \exp\left(j2\pi f_c t\right) \tag{4.28}$$

and

$$a_{\mathrm{id},r}(t) = \exp\left(j2\pi f_c t\right). \tag{4.29}$$

On the other hand, in case of imperfect LO, these perfect tones are spread, resulting in high power levels at neighboring frequencies. Now, by taking into consideration the LO phase noise, the LO processes can be respectively obtained as

$$a_t(t) = p_t a_{\mathrm{id},t}(t) \tag{4.30}$$

and

$$a_r(t) = p_r a_{\mathrm{id},r}(t), \tag{4.31}$$

with

$$p_t(t) = \exp\left(j\theta_t(t)\right) \tag{4.32}$$

and

$$p_r(t) = \exp\left(j\theta_r(t)\right) \tag{4.33}$$

where $\theta_t(t)$ and $\theta_r(t)$ are the TX and RX phase noise processes, respectively. Note that the phase noise is commonly described in the frequency domain by its PSD, i.e., the ratio between the noise power measured in 1 Hz bandwidth at a frequency offset, f_m, and the power of the carrier [386, 398, 427]. As illustrated in Fig. 4.7, in the frequency domain, the ideal LO process is a Dirac function, while the realistic LO process present a kind of "skirt", due to the effect of phase noise. Moreover, by using

the discrete time equivalent baseband model, the LO processes, $p_{\mathcal{X}}(n)$ ($\mathcal{X} \in \{t, r\}$), for the $n-$th time sample can be obtained as

$$p_{\mathcal{X}}(n) = \exp\left(j\theta_{\mathcal{X}}(n)\right). \tag{4.34}$$

Next, by assuming that the LOs, which are used for up- and down-conversion, are built as free-running oscillators, $\theta_{\mathcal{X}}(t)$ ($\mathcal{X} \in \{t, r\}$) can be modeled as Brownian phase noise process[1] (also known as Wiener or random walk process), i.e.,

$$\theta_{\mathcal{X}}(n) = \sum_{m=1}^{n} \theta_{\mathcal{X}}(m-1) + \epsilon(n), \tag{4.35}$$

where $\epsilon(n)$ is a zero-mean real Gaussian random variable with variance

$$\sigma_{\epsilon}^2 = \frac{4\pi\beta}{W}, \tag{4.36}$$

and W, β are the bandwidth of the RF signal and the the $3-$dB bandwidth of the LO process. Note that for typical LOs, the $3-$dB bandwidth is in the order of few tens or hundreds of Hz.

4.2.2 Influence of phase noise in single-carrier communications

In the case of single-carrier communication systems, phase noise is multiplicative. Therefore, the base band equivalent signal at the output of the LO can be expressed as

$$v_{\mathrm{o}} = \exp\left(j\theta_{\mathcal{X}}\right) v_{\mathrm{i}}, \tag{4.37}$$

where $\mathcal{X} \in \{t, r\}$ and v_{i} stands for the base band equivalent signal at the input of the LO. From (4.37), it is evident that, unless the phase noise parameters are accurately estimated and compensated [432], phase noise results in time-varying rotation of the signal constellation from symbol to symbol and erroneous data detection [415, 429]. This is illustrated in Fig. 4.8, where a QPSK symbol constellation in the presence of phase noise is plotted. Note that such effect, if small, is relatively easily compensated by constellation de-rotation.

4.2.3 Influence of phase noise in multi-carrier communications

In the case of multi-carrier communication systems, the $n-$th sample of the base band equivalent signal carried by the sub-carrier k at the output of the LO, which is used either for up- or down-conversion, can be obtained as [277, 278, 417]

$$\begin{aligned} y_k(n) &= \exp\left(j\theta_{\mathcal{X}}(n)\right) \sum_{l \in \mathbf{S}_K} x_l(n) \exp\left(j2\pi(f_l - f_k)n\right) * b(n) \\ &= \exp\left(j\theta_{\mathcal{X}}(n)\right) x_k(n) * b(n) + \exp\left(j\theta_{\mathcal{X}}(n)\right) \sum_{\substack{l \in \mathbf{S}_K \\ l \neq k}} x_l(n) \exp\left(j2\pi(f_l - f_k)n\right) * b(n), \end{aligned} \tag{4.38}$$

where

$$\mathbf{S}_K = \{-K/2, \cdots, -1, 1, \cdots, K/2\} \tag{4.39}$$

stands for the set of the K sub-carriers carried by the RF signal, $b(n)$ is the channel impulse response of a base band selection filter, and f_k is the normalized frequency that can be expressed as

$$f_k = \mathrm{sgn}(k)\frac{2|k| - 1}{2K}. \tag{4.40}$$

[1] Note that this model is commonly used to describe the behavior of practical oscillators [391, 401, 419, 424, 427–431], since it comes from the integration of the system perturbation over time.

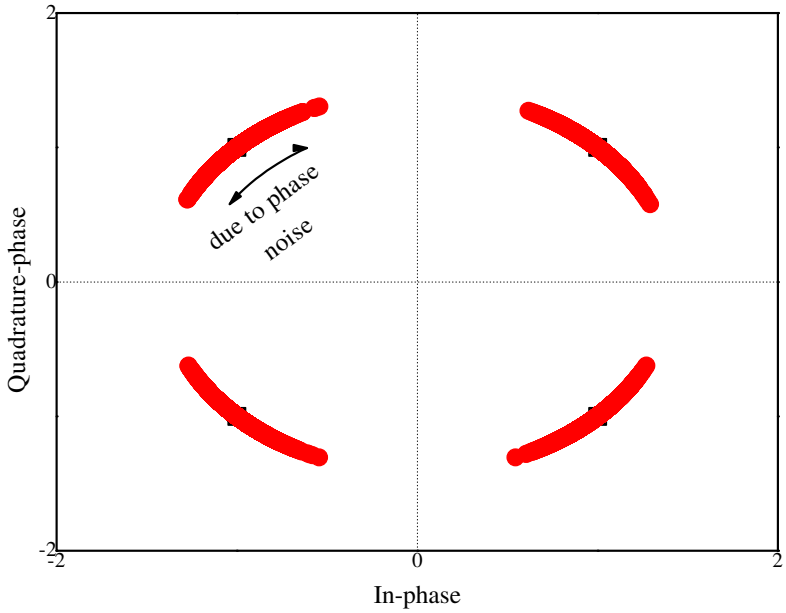

Figure 4.8 Scatter plot of single-carrier QPSK signal with and without phase noise. The black rectangulars denote the ideal symbols, while the red circles stand for the case imperfect LO with $\sigma_\epsilon^2 = 0.076$.

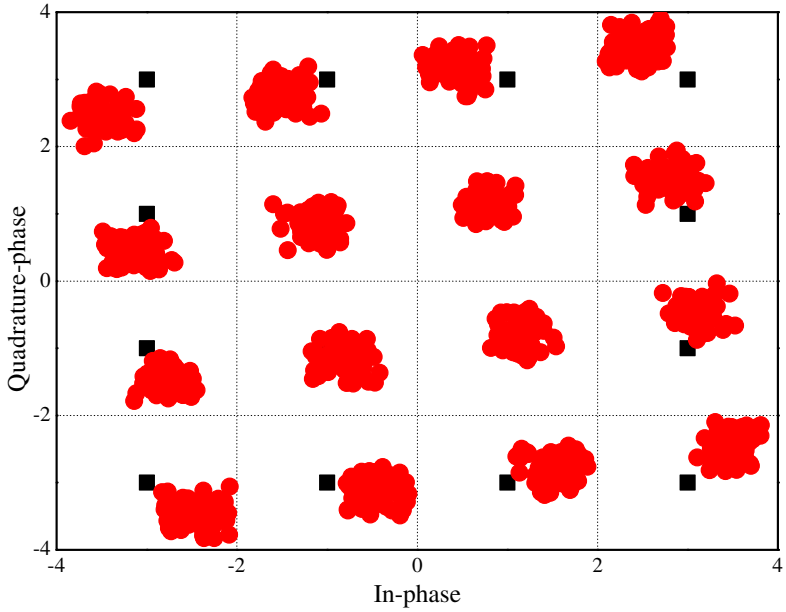

Figure 4.9 Scatter plot of multi-carrier 16-QAM signal with and without phase noise. The black rectangulars denote the ideal symbols, while the red circles stand for the case imperfect LO.

From (4.38), it is observed that in case of multi-carrier systems, the effect of phase noise is much more complex and severe, compared to the single-carrier scenarios. This is because in the frequency domain, the effect can been seen as spread of the received signals [320, 427]. Therefore, in addition that every multi-carrier symbol is phase rotated (similarly to a single-carrier symbol), also the subcarriers spread on top of each other causing inter-carrier interference (ICI) [277, 278, 391, 392, 417, 433]. This is illustrated in Fig. 4.9, where a 16-QAM symbol constellation in the presence of phase noise is plotted.

4.3 Amplifier non-linearities

In order to incorporate the impact of amplifier non-linearities, we first need to explain the input/output relation of the amplifier. In general, for a complex base band input signal represented as

$$u_{\text{in}}(t) = A(t)\exp\left(j\phi(t)\right), \tag{4.41}$$

the signal at the output of an amplifier with amplitude gain $g_A\left(A(t)\right)$ and phase gain $g_\phi\left(A(t)\right)$, can be obtained as [153, 320, 427]

$$u_{\text{out}}(t) = g_A\left(A(t)\right)\exp\left(\left(j\phi(t) + jg_\phi\left(A(t)\right)\right)\right). \tag{4.42}$$

There are various types of amplifier models for the amplitude and phase gains, such as ideal clipping, traveling wave tube, and solid-state amplifier model [153]. Fortunately, all the models can be encompassed under the umbrella of a polynomial amplifier model. In general, a polynomial amplifier model can simultaneously mode amplitude-to-amplitude modulation (AM-AM) and amplitude-to-phase modulation (AM-PM) distortion, by the following curve fitting of degree N:

$$g(u_{\text{in}}) = \exp\left(jg_\phi\right)\sum_{n=1}^{N}\beta_n A^n, \tag{4.43}$$

where the model parameters β_n are generally complex coefficients. Note that for the special case of only AM-AM distortion, the distortion coefficients, β_n, are real.

By this preamble and regarding the Bussgang's theorem [320, 434–437], the distorted signal at the output of the non-linearity can be written as [325, 438–443]

$$u_{\text{out}}(t) = \alpha u + e, \tag{4.44}$$

where u is the input signal, whereas α and e represent the non-linearity parameters, which model the amplitude/phase distortion and the non-linear distortion, respectively. Note that the distortion noise term ϵ is statistically independent of u, i.e.,

$$E\left[ue^*\right] = 0. \tag{4.45}$$

Moreover, according to Bussgang's theorem, e is a zero-mean random variable[2] with variance σ_e^2. Considering the polynomial amplifier model, the amplification factor, α, and the variance, σ_e^2, can respectively obtained as [320]

$$\alpha = \sum_{n=0}^{N-1}\beta_{n+1}2^{-n/2}\sigma_u^2\Gamma\left(1+n/2\right), \tag{4.46}$$

and

$$\sigma_e^2 = \sum_{n=2}^{2M}\gamma_n 2^{-n/2}\sigma_u^2\Gamma\left(1+n/2\right) - \left|a\right|^2\sigma_u^2, \tag{4.47}$$

where

$$\gamma_n = \sum_{m=1}^{n-1}\widehat{\beta}_m\widehat{\beta}_{n-m}^*, \tag{4.48}$$

and

$$\widehat{\beta}_m = \begin{cases} \beta_m, & 1 \le m \le M+1 \\ 0, & m > M+1 \end{cases}, \tag{4.49}$$

[2]Based on the Bussgang's theorem, if the input to the non-linearity is a zero-mean Gaussian process, the error term can be modelled as a Gaussian random variable[320, 434, 435]. Moreover, note that this special case was also stated in Price's theorem [444].

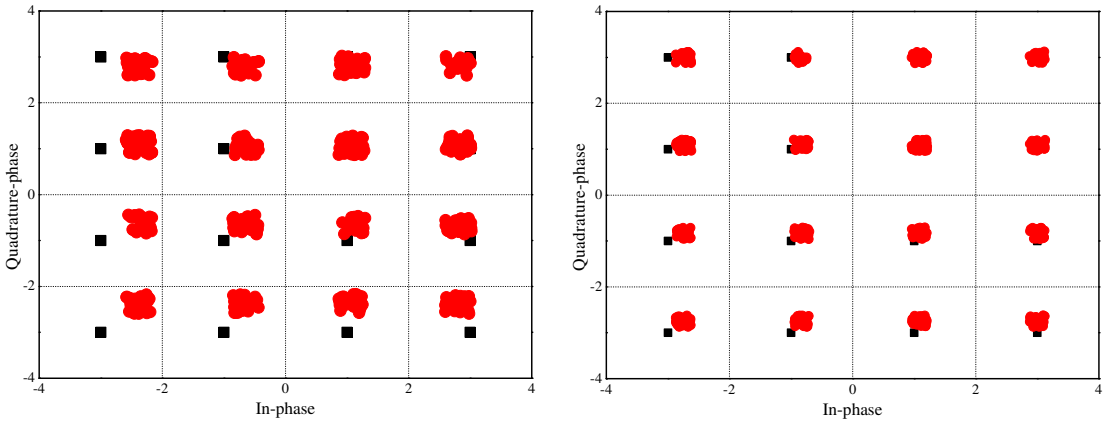

(a) IBO = 3dB (b) IBO = 5dB

Figure 4.10 The influence of the ideal clipping non-linearity on the 16-QAM symbol constellation.

where σ_u^2 represent the variance of the signal u. Furthermore, if an ideal clipping model is employed to describe the amplifiers non-linearities, the amplification factor, α, and the variance, σ_e^2, can be simplified as [320]

$$\alpha = 1 - \exp\left(-\,\mathrm{IBO}\right) + \sqrt{2\pi}\,\mathrm{IBO}\,\mathrm{Q}\left(2\,\mathrm{IBO}\right) \tag{4.50}$$

and

$$\sigma_{e_k}^2 = \sigma_u^2\left(1 - \alpha^2 - \exp\left(-\,\mathrm{IBO}\right)\right), \tag{4.51}$$

where

$$\mathrm{IBO} = \frac{A_o^2}{\sigma_u^2}, \tag{4.52}$$

denotes the input back-off factor and A_o is the power amplifier's clipping level. Note that with practical RF front-end electronics IBO belongs in the range of $2 - 10$ dB.

The influence of the ideal clipping amplifier on a $16-$QAM symbol constellation is illustrated in Fig. 4.10. In this simulation, the system experience neither the effect of fading channel nor AWGN. From this figure, it can be observed that the lower the IBO, the higher the power of the distortion term, e, is; hence, the higher the influence of the non-linearities on the symbol at the output of the amplifier is. Moreover, the mean of the symbols at the output of the amplifier is scaled with decreasing IBO.

Chapter 5

On the effects of IQI in cascaded fading channels

This chapter is devoted to the quantification and evaluation of the effect of RF IQI on wireless communications in the context of cascaded fading channels for both single-carrier and multi-carrier systems. To this end, closed form expressions are firstly derived for the outage probability over N*Nakagami$-m$ channels for the cases of ideal TX and RX, ideal TX and IQI RX, IQI TX and ideal RX, and joint TX/RX IQI. The offered expressions along with several deduced corresponding special cases are subsequently employed in the context of V2V communications to justify their importance and practical usefulness in the context of emerging communication systems.

The research results which are presented in this chapter are included in [375, 378, 382].

5.1 Introduction to cascaded fading channels

Due to the different nature of fading conditions, several statistical models have been proposed for characterizing and modeling fading envelopes under short-term, long-term, and composite fading channels. For example, the Nakagami-m and lognormal distributions have been proposed for accounting for short-term fading, also known as multipath fading, and long-term fading, also known as shadowing, respectively. Likewise, several composite fading models have been proposed for accounting for the simultaneous occurrence of multipath fading and shadowing effects (see [445–455] and references therein). In the same context, multiplicative cascaded fading models have been more recently introduced in [456–458]. The physical interpretation of these models is justified by considering received signals generated by the product of a large number of rays reflected via N statistically independent scatterers [456]. Based on this, the N*Nakagami$-m$ distribution was introduced in [457] corresponding to the product of N statistically independent, but not necessarily identically distributed Nakagami$-m$ random variables. This model is generic as it includes several special cases of more elementary cascaded fading models. For example, for the specific case of $N = 2$ and $m = 1$, it reduces to the double Rayleigh distribution, which has been shown useful in modeling fading effects in mobile-to-mobile communications [459].

5.2 Related work

In spite of the paramount importance of RF front-ends on the performance of wireless communication systems, the detrimental effects of RF impairments has been overlooked in the vast majority of reported analyses. The effect of RF impairments, modeled as independent and identically distributed (i.i.d) additive Gaussian noise, was investigated in [329, 331, 335, 460, 461]. In [366], the impact of IQI on the performance of OFDM systems was investigated. In particular, a SINR expression was evaluated, considering TX-only IQI, RX-only IQI, and joint TX/RX IQI, with equal levels of IQI at the TX and RX ends. Likewise, the effects of IQI on multi-carrier receivers was analyzed in [337, 462]; specifically, the authors in [337] analyzed the impact of the IQI on the BER performance of an OFDM based system with $M-$QAM, whereas the case of received OFDM signals subject to an I/Q imbalanced transceiver was derived in [462] along with a respective compensation algorithm.

In the context of cooperative communications, the performance of amplify-and-forward dual hop relay systems under IQI was thoroughly investigated in [350, 367, 463–466]. In more details, novel analytical expressions for the symbol error probability (SEP) over Rayleigh fading channels were derived in [350, 463, 464]. In the former, IQI was assumed only at the destination node, while upper and lower bounds for the respective SEP were reported in [463, 464] for the case of joint TX/RX IQI. Likewise, the authors in [465] derived analytic expression for the outage probability, considering independent and non-identical distribution Nakagami$-m$ fading channels, joint TX/RX IQI at the relay nodes and ideal

RF front-ends at the source and destination. Moreover, the case of dual hop opportunistic OFDM in the presence of IQI in all nodes was addressed in [367], where the outage probability was derived considering statistically independent, frequency-selective channels in all wireless links. Furthermore, the effects of IQI in the context of two way AF relaying and MIMO systems were investigated in [369, 466] and [350, 354, 358, 467], respectively. Specifically, in [466] and [369], the effects of IQI in two-way amplify-and-forward relaying systems for the case of independent, non-identically distributed Nakagami-m fading channels, were studied. Furthermore, the authors in [350] investigated the impact of IQI in single-carrier MIMO systems and proposed a base band compensation method, whereas the authors in [467] analyzed the performance degradation of both TX and RX IQI in a space division multiplexing based MIMO OFDM system, where the SER performance results were derived for the case of Rayleigh multipath fading channels. Finally, in [358], the effects of IQI in maximum ratio transmission beamforming OFDM systems were studied, while, in [354], the authors proposed a low-complexity IQI compensation method for MIMO OFDM systems.

5.3 Contribution

The technical contribution of this chapter is outlined below:

- Novel analytic expressions are derived for the outage probability in single-carrier systems over N*Nakagami$-m$ fading channels for the following three scenarios: i) IQI at the TX only; ii) IQI at the RX only; iii) joint IQI at the TX/RX.
- The above outage probability analysis is extended to a multi-carrier scenario by additionally taking into account the impact of the presence or the absence of a signal at the mirror frequency channel.
- The offered analytic results along with useful deduced special cases are readily applied in the context of V2V communication scenarios, which provides explicit justification of their overall importance and practical usefulness.
- A simple and tight lower bound is additionally proposed for the case of RX IQI in the multi-carrier scenario. To this effect, a lower bound for the outage probability is observed in the corresponding cases of RX IQI and joint TX/RX IQI.

5.4 Organization

The remainder of the chapter is organized as follows: Section 5.5 presents the single-carrier and multi-carrier system models for all possible configurations of ideal/impaired TX/RX. Section 5.6 is devoted to the derivation of the novel analytic expressions for the corresponding outage probability metrics. Section 5.7 demonstrates an application of the offered results in V2V communications over N*Nakagami-m channels. Respective numerical results and discussions are provided in section 5.8, while closing remarks are provided in Section 5.9.

5.5 System and signal model

In this section, we revisit the ideal signal model, which is, henceforth, referred to as ideal RF, as well as the realistic IQI signal models in both single-carrier and multi-carrier direct-conversion TX and RX scenarios for the case that TX and RX are equipped with a single antenna.

5.5.1 Ideal RF front-end

We assume a transmitted signal, s, transmitted over a flat wireless channel, h, with an AWGN, n. The received RF signal is passed through various processing stages, also known as the RF front-end of the RX. These stages include filtering, amplification, analog I/Q demodulation, down-conversion to base band and sampling. To this effect, the corresponding base band equivalent received signal can be expressed as

$$r_{\text{ideal}} = hs + n, \tag{5.1}$$

where h is the channel coefficient and n denotes the circularly symmetric complex AWGN. It is assumed that the transmitted signal experiences cascaded fading conditions modeled by a N*Nakagami-m process, which is composed of $N \geq 1$ independent, but not necessarily identical, Nakagami-m random variables. Based on this, the instantaneous SNR per symbol at the RX input can be expressed as

$$\gamma_{\text{ideal}} = \frac{E_s}{N_0} |h|^2 , \tag{5.2}$$

where E_s denotes the energy per transmitted symbol and N_0 is the single-sided AWGN PSD. Therefore, the corresponding average SNR can be obtained as

$$\overline{\gamma} = \frac{E_s}{N_0} \prod_{i=1}^{N} \Omega_i, \tag{5.3}$$

with Ω_i denoting the scaling parameter of the i^{th} Nakagami-m process [457].

In the case of multi-carrier systems, the corresponding base band equivalent received signal at the $k-th$ subcarrier is represented as follows:

$$r_{\text{id}}(k) = h(k)\, s(k) + n(k), \tag{5.4}$$

where $s(k)$ is the transmitted signal at the $k-th$ subcarrier, whereas $h(k)$ and $n(k)$ denote the corresponding channel coefficient and the circular symmetric complex AWGN, respectively. Hence, the corresponding instantaneous and average SNRs can be expressed as

$$\gamma_{\text{id}}(k) = \frac{E_s}{N_0} |h(k)|^2 \tag{5.5}$$

and

$$\overline{\gamma}_{\text{id}}(k) = \frac{E_s}{N_0} \prod_{i=1}^{N} \Omega_i(k), \tag{5.6}$$

respectively.

5.5.2 Single-carrier systems impaired by IQI

In this subsection, we present the signal model for single-carrier transmission in which the TX and/or the RX suffers from IQI.

5.5.2.1 TX impaired by IQI

In this scenario, it is assumed that TX experiences IQI, while the RF front-end of the RX is ideal. To this effect, it follows from (4.10) that the base band equivalent transmitted signal can be expressed as

$$s_{\text{IQI}} = K_1^t s + K_2^t s^*, \tag{5.7}$$

whereas the base band equivalent received signal is given by

$$r_{\text{IQI}}^t = h s_{\text{IQI}} + n = K_1^t h s + K_2^t h s^* + n. \tag{5.8}$$

Furthermore, the instantaneous SINR per symbol at the input of the RX can be obtained as

$$\gamma = \frac{|K_1^t|^2 |h|^2 E_s}{|K_2^t|^2 |h|^2 E_s + N_0}, \tag{5.9}$$

which after basic algebraic manipulations can be re-written as follows:

$$\gamma = \frac{1}{\frac{1}{IRR_t} + \frac{1}{|K_1^t|^2} \frac{1}{\gamma_{\text{ideal}}}}. \tag{5.10}$$

In the context of direct-conversion TX, the IQI effect can be considered as the so-called self-image problem, which is the case when the base band equivalent transmitted signal is essentially interfered by its own complex conjugate [328].

5.5.2.2 RX impaired by IQI

In this scenario, it is assumed that the RX experiences IQI, while the TX RF front-end is ideal. Based on (4.14), the base band equivalent received signal can be obtained as

$$r = K_1^r h s + K_2^r h^* s^* + K_1^r n + K_2^r n^*. \tag{5.11}$$

The corresponding instantaneous SINR per symbol at the input of the RX can be expressed as

$$\gamma = \frac{|K_1^r|^2 |h|^2 E_s}{|K_2^r|^2 |h|^2 E_s + \left(|K_1^r|^2 + |K_2^r|^2\right) N_0}, \tag{5.12}$$

which after basic algebraic manipulations can equivalently be rewritten as

$$\gamma = \frac{1}{\frac{1}{IRR_r} + \left(1 + \frac{1}{IRR_r}\right) \frac{1}{\gamma_{\text{ideal}}}}. \tag{5.13}$$

5.5.2.3 Joint TX/RX impaired by IQI

In this scenario, it is assumed that both the TX and the RX experience IQI. To this effect, and based on (4.10) and (4.14), it follows that the base band equivalent received signal can be expressed as

$$r = (\xi_{11} h + \xi_{22} h^*) s + (\xi_{12} h + \xi_{21} h^*) s^* + K_1^r n + K_2^r n^*, \tag{5.14}$$

where

$$\xi_{11} = K_1^r K_1^t, \tag{5.15}$$

$$\xi_{22} = K_2^r \left(K_2^t\right)^*, \tag{5.16}$$

$$\xi_{12} = K_1^r K_2^t \tag{5.17}$$

and

$$\xi_{21} = K_2^r \left(K_1^t\right)^*. \tag{5.18}$$

Based on (5.14), the instantaneous SINR per symbol at the input of the RX is given by

$$\gamma = \frac{|Z|^2 E_s}{|W|^2 E_s + \left(|K_1^r|^2 + |K_2^r|^2\right) N_0}, \tag{5.19}$$

with

$$|Z|^2 = |\xi_{11} h + \xi_{22} h^*|^2, \tag{5.20}$$

$$|W|^2 = |\xi_{12} h + \xi_{21} h^*|^2 = |\xi_{12}|^2 |h|^2 + |\xi_{21}|^2 |h|^2 + 2\Re\left\{\xi_{12}\xi_{21} h^2\right\}, \tag{5.21}$$

whereas

$$\frac{|\xi_{22}|^2}{|\xi_{11}|^2} = \frac{1}{\text{IRR}_r \text{IRR}_t}, \tag{5.22}$$

which practically lies in the range of $[-43, -28$ dB$]$. As a result, it can be accurately assumed that

$$|Z|^2 \approx |\xi_{11}|^2 |h|^2, \tag{5.23}$$

while due to the inequality

$$2\Re\left\{\xi_{12}\xi_{21} h^2\right\} << |\xi_{12}|^2 |h|^2 + |\xi_{21}|^2 |h|^2. \tag{5.24}$$

equation (5.21) can be accurately represented as

$$|W|^2 \approx |\xi_{12}|^2 |h|^2 + |\xi_{21}|^2 |h|^2. \tag{5.25}$$

To this effect, it follows that (5.19) can be rewritten as

$$\gamma \approx \frac{|\xi_{11}|^2}{|\xi_{12}|^2 + |\xi_{21}|^2 + \left(|K_1^r|^2 + |K_2^r|^2\right) \frac{1}{\gamma_{\text{ideal}}}}. \tag{5.26}$$

It is noted here that (5.26) is particularly accurate, since the relative error does not exceed 1%.

5.5.3 Multi-carrier systems impaired by IQI

In the case of multi-carrier transmission, we assume that multiple RF subcarriers are down-converted to the base band by means of wideband direct-conversion, where the RF spectrum is translated to the base band in a single down-conversion [321]. For notational convenience, we denote the set of channels as

$$\mathbf{S}_K = \{-K, \cdots, -1, 1, \cdots, K\} \tag{5.27}$$

and the base band equivalent IQI−free transmitted signal at the $k-$th subcarrier as $s(k)$. In addition, the parameter $\theta \in \{0, 1\}$ indicates the existence of a signal at subcarrier $-k$.

5.5.3.1 TX impaired by IQI

In this scenario, it is assumed that the RF front-end of the RX is ideal, while the TX experiences IQI. Therefore, with the aid of (4.19), it follows that the base band equivalent transmitted signal in the $k-$th subcarrier can be expressed as

$$s_{\mathrm{IQI}}(k) = K_1^t s(k) + \theta K_2^t s^*(-k). \tag{5.28}$$

Notably, (5.28) exhibits that IQI causes the transmitted base band equivalent signal at subcarrier k, $s(k)$, to be distorted by its image signal at subcarrier $-k$, $s^*(-k)$. In other words, in a multi-carrier system, the effect of IQI result in crosstalk between the mirror frequencies in the down-converted signal [299]. To this effect, the corresponding base band received signal becomes

$$r(k) = h(k)\, s_{\mathrm{IQI}}(k) + n(k), \tag{5.29}$$

which, with the aid of (5.28), can be equivalently rewritten as

$$r(k) = K_1^t h(k)\, s(k) + K_2^t h(k)\, s^*(-k) + n(k). \tag{5.30}$$

Moreover, the corresponding instantaneous SINR per symbol at the input of the RX can be obtained as

$$\gamma(k) = \frac{|K_1^t|^2 |h(k)|^2 E_s}{\theta |K_2^t|^2 |h(k)|^2 E_s + N_0}, \tag{5.31}$$

which, after carrying out basic algebraic manipulations, can be expressed as

$$\gamma(k) = \frac{1}{\theta \frac{1}{IRR_t} + \frac{1}{|K_1^t|^2} \frac{1}{\gamma_{\mathrm{id}}(k)}}. \tag{5.32}$$

5.5.3.2 RX impaired by IQI

In this scenario, it is assumed that the RF front-end of the TX is ideal, while the RX experiences IQI. Hence, by recalling once more (4.20), the base band equivalent received signal in the $k-$th subcarrier can be expressed as

$$r(k) = K_1^r h(k)\, s(k) + \theta K_2^r h^*(-k)\, s^*(-k) + K_1^r n(k) + K_2^r n^*(-k). \tag{5.33}$$

With the aid of the above expression, it is shown that IQI is the reason that the received base band equivalent signal at the $k-$th subcarrier, $s(k)$, is interfered by the image signal at subcarrier $-k$, $s^*(-k)$. The instantaneous SINR per symbol at the input of the RX can be expressed as

$$\gamma(k) = \frac{|K_1^r|^2 |h(k)|^2 E_s}{|K_2^r|^2 |h(-k)|^2 E_s + \left(|K_1^r|^2 + |K_2^r|^2\right) N_0} = \frac{\gamma_{\mathrm{id}}(k)}{\theta \frac{\gamma_{\mathrm{id}}(-k)}{IRR_r} + \left(1 + \frac{1}{IRR_r}\right)}, \tag{5.34}$$

where $\gamma_{\mathrm{id}}(k)$ is given by (5.5), and

$$\gamma_{\mathrm{id}}(-k) = \frac{|h(-k)|^2 E_s}{N_0}, \tag{5.35}$$

represents the instantaneous SNR at subcarrier $-k$ of the corresponding IQI-free system.

5.5.3.3 Joint TX/RX impaired by IQI

Finally, it is assumed that both the TX and RX experience IQI. Thus, with the aid of (8.10), and after some basic algebraic manipulations, the base band equivalent received signal at the $k-$th subcarrier can be expressed as

$$r(k) = \left(\xi_{11} h(k) + \xi_{22} h^*(-k)\right) s(k) + \left(\xi_{12} h(k) + \xi_{21} h^*(-k)\right) s^*(-k) + K_1^r n(k) + K_2^r n^*(-k), \quad (5.36)$$

which indicates that IQI renders the received base band equivalent signal at the $k-$th subcarrier, $s(k)$, subject to interference by its image signal at subcarrier $-k$, $s^*(-k)$. Therefore, the corresponding instantaneous SINR per symbol at the input of the RX can be obtained as

$$\gamma(k) = \frac{|Z_{MC}(k)|^2 E_s}{|W_{MC}(k)|^2 E_s + \left(|K_1^r|^2 + |K_2^r|^2\right) N_0}, \quad (5.37)$$

where

$$|Z_{MC}(k)|^2 = |\xi_{11} h(k) + \xi_{22} h^*(-k)|^2 \quad (5.38)$$

and

$$|W_{MC}(k)|^2 = |\xi_{12} h(k) + \xi_{21} h^*(-k)|^2. \quad (5.39)$$

Likewise, (5.38) can be accurately expressed as

$$|Z_{MC}(k)|^2 \approx |\xi_{11}|^2 |h(k)|^2. \quad (5.40)$$

In addition, it is noted that the correlation between the channel responses at the $k-$th subcarrier and its image is small, due to their large spectral separation. To this effect, it is realistic to assume them statistically independent, which satisfies the following expression:

$$E\left[\Re\left\{\xi_{12}\xi_{21}^* h(k) h^*(-k)\right\}\right] \approx 0. \quad (5.41)$$

Based on (5.41), $|W_{MC}(k)|^2$ can be tightly approximated as

$$|W_{MC}(k)|^2 \approx |\xi_{12}|^2 |h(k)|^2 + |\xi_{21}|^2 |h^*(-k)|^2. \quad (5.42)$$

Furthermore, based on (5.42), it immediately follows that (5.37) can be expressed as

$$\gamma(k) \approx \frac{|\xi_{11}|^2 \gamma_{\mathrm{id}}(k)}{\theta |\xi_{12}|^2 \gamma_{\mathrm{id}}(k) + \theta |\xi_{21}|^2 \gamma_{\mathrm{id}}(-k) + |K_1^r|^2 + |K_2^r|^2}, \quad (5.43)$$

which is a particularly accurate and simple representation. In general, it is emphasized that the nature of IQI is clearly different in the single-carrier and multi-carrier transmission cases. This is primarily because in the multi-carrier case, the image subcarrier carries an independent data symbol, while in the single-carrier case the image is the complex conjugate of the signal itself. Furthermore, the fading at mirror subcarriers is generally different, while in the single-carrier case the signal and its own conjugate experience the same fading process.

5.6 Outage probability over cascaded fading channels

It is recalled that the outage probability can be defined as the probability that the symbol error rate is greater than a certain quality of service requirement and is computed as the probability that the instantaneous SNR or SINR falls below the corresponding pre-determined threshold [468]. In what follows, we derive a novel analytical framework for the outage probability over N*Nakagami$-m$ fading channels subject to the aforementioned IQI scenarios in both single-carrier and multi-carrier systems. The offered analytic expressions are validated through extensive comparisons with respective results from computer simulations.

5.6.1 Ideal RF front-end

In the case of N*Nakagami-m fading channels, the CDF of γ_{ideal} is given by [457, Eq. (13)]

$$F_{\gamma_{\text{ideal}}}(\gamma) = \frac{1}{\prod_{i=1}^{N}\Gamma(m_i)} G_{1,N+1}^{N,1}\left(\frac{\gamma}{\overline{\gamma}}\prod_{i=1}^{N} m_i \,\middle|\, \begin{matrix} 1 \\ m_1, m_2, \cdots, m_N, 0 \end{matrix}\right), \tag{5.44}$$

where $\Gamma(\cdot)$ and $G_{s,t}^{v,w}(\cdot)$ denote the gamma function and the Meijer's G-function [274]. Based on this, the corresponding PDF of γ_{ideal} is expressed as [457, Eq. (14)], namely

$$f_{\gamma_{\text{ideal}}}(\gamma) = \frac{G_{0,N}^{N,0}\left(\frac{\gamma}{\overline{\gamma}}\prod_{i=1}^{N} m_i \,\middle|\, \begin{matrix} - \\ m_1, m_2, \ldots, m_N \end{matrix}\right)}{\gamma\prod_{i=1}^{N}\Gamma(m_i)}. \tag{5.45}$$

5.6.2 Single-carrier systems impaired by IQI

In this subsection, the outage probabilities for the three scenarios, namely IQI at TX only, IQI at RX only, and joint IQI at TX and RX, in the case of single-carrier transmission, are derived.

5.6.2.1 TX impaired by IQI

Using (5.10) and (5.44), it follows that the outage probability can be expressed as

$$\begin{aligned} P_{\text{out}} &= F_{\gamma_{\text{ideal}}}\left(\frac{1}{|K_1^t|^2\left(\frac{1}{\gamma_{th}} - \frac{1}{IRR_t}\right)}\right) \\ &= \frac{1}{\prod_{i=1}^{N}\Gamma(m_i)} G_{1,N+1}^{N,1}\left(\frac{1}{\overline{\gamma}\,|K_1^t|^2\left(\frac{1}{\gamma_{th}} - \frac{1}{IRR_t}\right)}\prod_{i=1}^{N} m_i \,\middle|\, \begin{matrix} 1 \\ m_1, m_2, \cdots, m_N, 0 \end{matrix}\right), \end{aligned} \tag{5.46}$$

with c. Moreover, γ_{th} stand for the SNR threshold, which is connected with the targeted data rate, r_{th}, by

$$\gamma_{th} = 2^{r_{th}} - 1. \tag{5.47}$$

Note that if $\gamma_{th} > IRR_t$, or equivalently $r_{th} > \log_2(IRR_t + 1)$, then $P_{\text{out}} = 1$. This indicates the importance of taking into consideration the levels of IQI, when the targeted data rate is selected.

5.6.2.2 RX impaired by IQI

With the aid of (5.13) and (5.44), the corresponding outage probability is given by

$$\begin{aligned} P_{\text{out}} &= F_{\gamma_{\text{ideal}}}\left(\frac{1 + \frac{1}{IRR_r}}{\frac{1}{\gamma_{th}} - \frac{1}{IRR_r}}\right) \\ &= \frac{1}{\prod_{i=1}^{N}\Gamma(m_i)} G_{1,N+1}^{N,1}\left(\frac{1}{\overline{\gamma}}\frac{1 + \frac{1}{IRR_r}}{\frac{1}{\gamma_{th}} - \frac{1}{IRR_r}}\prod_{i=1}^{N} m_i \,\middle|\, \begin{matrix} 1 \\ m_1, m_2, \cdots, m_N, 0 \end{matrix}\right), \end{aligned} \tag{5.48}$$

with $\gamma_{th} \leq IRR_r$. Note that if $\gamma_{th} > IRR_r$, then $P_{\text{out}} = 1$.

5.6.2.3 Joint TX/RX impaired by IQI

Using (5.26) and (5.44), the outage probability in this case is expressed as

$$\begin{aligned} P_{\text{out}} &= F_{\gamma_{\text{ideal}}}\left(\frac{|K_1^r|^2 + |K_2^r|^2}{\frac{|\xi_{11}|^2}{\gamma_{th}} - \left(|\xi_{12}|^2 + |\xi_{21}|^2\right)}\right) \\ &= \frac{1}{\prod_{i=1}^{N}\Gamma(m_i)} G_{1,N+1}^{N,1}\left(\frac{1}{\overline{\gamma}}\frac{|K_1^r|^2 + |K_2^r|^2}{\frac{|\xi_{11}|^2}{\gamma_{th}} - \left(|\xi_{12}|^2 + |\xi_{21}|^2\right)}\prod_{i=1}^{N} m_i \,\middle|\, \begin{matrix} 1 \\ m_1, m_2, \cdots, m_N, 0 \end{matrix}\right), \end{aligned} \tag{5.49}$$

with $\gamma_{th} \leq \frac{|\xi_{11}|^2}{|\xi_{12}|^2+|\xi_{21}|^2}$, otherwise $P_{\text{out}} = 1$.

5.6.3 Multi-carrier systems impaired by IQI

Similar analytic expressions can be derived for the case of multi-carrier transmission.

5.6.3.1 TX impaired by IQI

Based on the signal model in Section 5.5.3.1, and assuming a known θ, it immediately follows that

$$\begin{aligned} F_{\gamma}\left(\gamma_{th}\left|\theta\right.\right) &= F_{\gamma_{\text{ideal}}}\left(\frac{1}{\left|K_1^t\right|^2\left(\frac{1}{\gamma_{th}}-\theta\frac{1}{IRR_t}\right)}\right) \\ &= \frac{1}{\prod_{i=1}^{N}\Gamma\left(m_i\right)}G_{1,N+1}^{N,1}\left(\frac{1}{\overline{\gamma}\left|K_1^t\right|^2\left(\frac{1}{\gamma_{th}}-\frac{1}{IRR_t}\right)}\prod_{i=1}^{N}m_i\,\middle|\,\begin{matrix}1\\ m_1,m_2,\cdots,m_N,0\end{matrix}\right), \end{aligned} \tag{5.50}$$

with $\gamma_{th} \leq IRR_t$.

It is also assumed here that θ follows a Bernoulli distribution with CDF

$$P_r\left(\theta\right) = \begin{cases} q, & \theta = 1 \\ 1-q, & \theta = 0 \end{cases} \tag{5.51}$$

and $q \in [0,1]$. To this effect, the corresponding unconditional outage probability can be expressed as follows:

$$P_{\text{out}} = qF_{\gamma_{\text{ideal}}}\left(\frac{1}{\left|K_1^t\right|^2\left(\frac{1}{\gamma_{th}}-\frac{1}{IRR_t}\right)}\right) + \left(1-q\right)F_{\gamma_{\text{ideal}}}\left(\frac{\gamma_{th}}{\left|K_1^t\right|^2}\right). \tag{5.52}$$

5.6.3.2 RX impaired by IQI

Based on the signal model presented in Section 5.5.3.2, assuming a given image channel realization, SNR, $\gamma_{\text{ideal}}\left(-k\right)$, and a known θ, it follows that

$$F_{\gamma}\left(\gamma_{th}\left|\gamma_{\text{ideal}}\left(-k\right),\theta\right.\right) = F_{\gamma_{\text{ideal}}}\left(\left(\theta\frac{\gamma_{\text{ideal}}\left(-k\right)}{IRR_r}+1+\frac{1}{IRR_r}\right)\gamma_{th}\right). \tag{5.53}$$

If $\theta = 1$, the unconditional CDF can be expressed as follows

$$F_{\gamma}\left(\gamma_{th}\left|\theta=1\right.\right) = \int_0^{\infty}F_{\gamma_{\text{ideal}}}\left(\left(\frac{x}{IRR_r}+1+\frac{1}{IRR_r}\right)\gamma_{th}\right)f_{\gamma_{\text{ideal}}}\left(x\right)\mathrm{d}x. \tag{5.54}$$

By also taking into consideration (5.44) and (5.45), (5.54) can be rewritten as

$$\begin{aligned} F_{\gamma}\left(\gamma_{th}\left|\theta=1\right.\right) = \frac{1}{\left(\prod_{i=1}^{N}\Gamma\left(m_i\right)\right)^2}\int_0^{\infty}x^{-1}G_{0,N}^{N,0}\left(\frac{x}{\overline{\gamma}}\prod_{i=1}^{N}m_i\,\middle|\,\begin{matrix}-\\ m_1,m_2,\ldots,m_N\end{matrix}\right) \\ \times G_{1,N+1}^{N,1}\left(\left(\frac{x}{IRR_r}+1+\frac{1}{IRR_r}\right)\frac{\gamma_{th}}{\overline{\gamma}}\prod_{i=1}^{N}m_i\,\middle|\,\begin{matrix}1\\ m_1,m_2,\ldots,m_N,0\end{matrix}\right)\mathrm{d}x, \end{aligned} \tag{5.55}$$

which after some basic algebraic manipulations can be equivalently expressed as follows:

$$\begin{aligned} F_{\gamma}\left(\gamma_{th}\left|\theta=1\right.\right) = \frac{1}{\left(\prod_{i=1}^{N}\Gamma\left(m_i\right)\right)^2} \\ \times\int_0^{\infty}\frac{1}{y}G_{1,N+1}^{N,1}\left(y+c\,\middle|\,\begin{matrix}1\\ m_1,m_2,\ldots,m_N,0\end{matrix}\right)G_{0,N}^{N,0}\left(\frac{d}{b}y\,\middle|\,\begin{matrix}-\\ m_1,m_2,\ldots,m_N,0\end{matrix}\right)\mathrm{d}y, \end{aligned} \tag{5.56}$$

where

$$y = bx, \tag{5.57}$$

$$b = \frac{\gamma_{th}}{\overline{\gamma}} \frac{1}{IRR_r} \prod_{i=1}^{N} m_i, \tag{5.58}$$

$$c = \frac{\gamma_{th}}{\overline{\gamma}} \left(1 + \frac{1}{IRR_r}\right) \prod_{i=1}^{N} m_i \tag{5.59}$$

and

$$d = \frac{1}{\overline{\gamma}} \prod_{i=1}^{N} m_i. \tag{5.60}$$

Importantly, (5.56) can be expressed in terms of the Meijer $G-$function in [274] yielding

$$F_{\gamma}\left(\gamma_{th}\left|\theta=1\right.\right) \simeq \sum_{k=0}^{p} \frac{(-1)^k \gamma_{th}^k}{\overline{\gamma}^k k!} \left(1 + \frac{1}{IRR_r}\right)^k \left(\prod_{i=1}^{N} m_i\right)^k \times G_{N+2,N+2}^{N+1,N+1}\left(\frac{IRR_r}{\gamma_{th}} \middle| \begin{matrix} 1, k-m_1+1, k-m_2+1, \ldots, k-m_N+1, k+1 \\ m_1, m_2, \ldots, m_N, k, k+1, 0 \end{matrix}\right). \tag{5.61}$$

Likewise, when $\theta = 0$ the corresponding unconditional CDF can be readily deduced, namely

$$\begin{aligned} F_{\gamma}\left(\gamma_{th}\left|\theta=0\right.\right) &= F_{\gamma_{\text{ideal}}}\left(\left(1 + \frac{1}{IRR_r}\right)\gamma_{th}\right) \\ &= \frac{1}{\prod_{i=1}^{N}\Gamma\left(m_i\right)} G_{1,N+1}^{N,1}\left(\left(1 + \frac{1}{IRR_r}\right)\frac{\gamma_{th}}{\overline{\gamma}(k)}\prod_{i=1}^{N} m_i \middle| \begin{matrix} 1 \\ m_1, m_2, \cdots, m_N, 0 \end{matrix}\right). \end{aligned} \tag{5.62}$$

Based on the above analysis, the corresponding unconditional outage probability can be expressed as

$$\begin{aligned} P_{\text{out}} = q \sum_{k=0}^{p} \frac{(-1)^k \gamma_{th}^k}{\overline{\gamma}^k k!} \left(1 + \frac{1}{IRR_r}\right)^k \left(\prod_{i=1}^{N} m_i\right)^k \\ \times G_{N+2,N+2}^{N+1,N+1}\left(\frac{IRR_r}{\gamma_{th}} \middle| \begin{matrix} 1, k-m_1+1, k-m_2+1, \ldots, k-m_N+1, k+1 \\ m_1, m_2, \ldots, m_N, k, k+1, 0 \end{matrix}\right) \\ + (1-q)\frac{1}{\prod_{i=1}^{N}\Gamma\left(m_i\right)} G_{1,N+1}^{N,1}\left(\frac{\left(1+\frac{1}{IRR_r}\right)\gamma_{th}}{\overline{\gamma}}\prod_{i=1}^{N} m_i \middle| \begin{matrix} 1 \\ m_1, m_2, \cdots, m_N, 0 \end{matrix}\right). \end{aligned} \tag{5.63}$$

5.6.3.3 Joint TX/RX impaired by IQI

By recalling (5.43) and assuming a given $\gamma_{\text{ideal}}\left(-k\right)$ and a known θ, it immediately follows that

$$F_{\gamma}\left(\gamma_{th}\left|\gamma_{\text{ideal}}\left(-k\right),\theta\right.\right) = F_{\gamma_{\text{ideal}}}\left(\frac{\gamma_{th}\left(\theta\left|\xi_{21}\right|^2\gamma_{ideal}\left(-k\right) + \left|K_1^r\right|^2 + \left|K_2^r\right|^2\right)}{\left|\xi_{11}\right|^2 - \theta\gamma_{th}\left|\xi_{12}\right|^2}\right). \tag{5.64}$$

Likewise, in the case of $\theta = 1$, the unconditional CDF can be formulated as

$$F_{\gamma}\left(\gamma_{th}\left|\theta=1\right.\right) = \int_0^{\infty} F_{\gamma_{\text{ideal}}}\left(\frac{\gamma_{th}\left(\left|\xi_{21}\right|^2 x + \left|K_1^r\right|^2 + \left|K_2^r\right|^2\right)}{\left|\xi_{11}\right|^2 - \gamma_{th}\left|\xi_{12}\right|^2}\right) f_{\gamma_{\text{ideal}}}\left(x\right)\mathrm{d}x, \tag{5.65}$$

which with the aid of (5.44)$-$(5.45) and carrying out some basic algebraic manipulations can be equivalently expressed as

$$\begin{aligned} F_{\gamma}\left(\gamma_{th}\left|\theta=1\right.\right) = \frac{1}{\left(\prod_{i=1}^{N}\Gamma\left(m_i\right)\right)^2} \int_0^{\infty} \frac{1}{z} G_{1,N+1}^{N,1}\left(z+l \middle| \begin{matrix} 1 \\ m_1, m_2, \ldots, m_N, 0 \end{matrix}\right) \\ \times G_{0,N}^{N,0}\left(\frac{u}{g}z \middle| \begin{matrix} - \\ m_1, m_2, \ldots, m_N \end{matrix}\right)\mathrm{d}z. \end{aligned} \tag{5.66}$$

Note that in (5.66), y, g, l and u stand for

$$y = gx, \tag{5.67}$$

$$g = \frac{|\xi_{21}|^2 \gamma_{th}}{\overline{\gamma}\left(|\xi_{11}|^2 - \gamma_{th}|\xi_{12}|^2\right)} \prod_{i=1}^{N} \Gamma(m_i), \tag{5.68}$$

$$l = \frac{\left(|K_1^r|^2 + |K_2^r|^2\right)\gamma_{th}}{\overline{\gamma}\left(|\xi_{11}|^2 - \gamma_{th}|\xi_{12}|^2\right)} \prod_{i=1}^{N} \Gamma(m_i) \tag{5.69}$$

and

$$u = \frac{1}{\overline{\gamma}} \prod_{i=1}^{N} m_i. \tag{5.70}$$

It is evident that (5.56) can be also expressed in terms of the Meijer $G-$function [274], namely

$$F_\gamma(\gamma_{th}|\theta = 1) \simeq \sum_{k=0}^{p} \frac{(-1)^k \gamma_{th}^k \left(|K_1^r|^2 + |K_2^r|^2\right)^k}{k!\,\overline{\gamma}^k \left(|\xi_{11}|^2 - \gamma_{th}|\xi_{12}|^2\right)^k} \left(\prod_{i=1}^{N} \Gamma(m_i)\right)^k \times G_{N+2,N+2}^{N+1,N+1}\left(\frac{|\xi_{11}|^2 - \gamma_{th}|\xi_{12}|^2}{|\xi_{21}|^2 \gamma_{th}} \,\middle|\, \begin{matrix} 1, k - m_1 + 1, k - m_2 + 1, \ldots, k - m_N + 1, k + 1 \\ m_1, m_2, \ldots, m_N, k, k + 1, 0 \end{matrix}\right). \tag{5.71}$$

In the same context, when $\theta = 0$, the corresponding unconditional CDF can be obtained as

$$F_\gamma(\gamma_{th}|\theta = 0) = F_{\gamma_{\text{ideal}}}\left(\frac{|K_1^r|^2 + |K_2^r|^2}{|\xi_{11}|^2}\gamma_{th}\right). \tag{5.72}$$

To this effect, it immediately follows that the unconditional outage probability can be expressed as

$$P_{\text{out}} = q \sum_{k=0}^{p} \frac{(-1)^k \gamma_{th}^k \left(|K_1^r|^2 + |K_2^r|^2\right)^k}{k!\,\overline{\gamma}^k \left(|\xi_{11}|^2 - \gamma_{th}|\xi_{12}|^2\right)^k} \left(\prod_{i=1}^{N} \Gamma(m_i)\right)^k \times G_{N+2,N+2}^{N+1,N+1}\left(\frac{|\xi_{11}|^2 - \gamma_{th}|\xi_{12}|^2}{|\xi_{21}|^2 \gamma_{th}} \,\middle|\, \begin{matrix} 1, k - m_1 + 1, k - m_2 + 1, \ldots, k - m_N + 1, k + 1 \\ m_1, m_2, \ldots, m_N, k, k + 1, 0 \end{matrix}\right) + (1 - q) \frac{1}{\prod_{i=1}^{N} \Gamma(m_i)} G_{1,N+1}^{N,1}\left(\frac{|K_1^r|^2 + |K_2^r|^2}{|\xi_{11}|^2 \overline{\gamma}} \gamma_{th} \prod_{i=1}^{N} m_i \,\middle|\, \begin{matrix} 1 \\ m_1, m_2, \cdots, m_N, 0 \end{matrix}\right). \tag{5.73}$$

The offered analytic expressions can be readily computed in popular mathematical software packages such as MAPLE, MATHEMATICA and MATLAB.

5.7 Applications in vehicle-to-vehicle (V2V) communications

It is well known that V2V communications constitute a fundamental part of emerging communication systems [469, 470]. This also includes intelligent transportation systems (ITSs), which have been attracting considerable attention due to the large number of applications that they can be deployed for [471, 472]. It is recalled that the transmitted signals in V2V communication systems experience fading effects that typically differ from conventional cellular communications scenarios [473, 474]. This difference arises from the moving nature and the position of the involved TX/RX as well as the presence of reflectors/scatterers in highways and urban environments. As a result, the omnidirectional TX and RX antennas in these systems are located at relatively low elevations and thus, the corresponding wireless channel has been shown to exhibit a non-stationary behavior. As a consequence, the performance of corresponding communication systems is subject to non-negligible deteriorations in terms of throughput

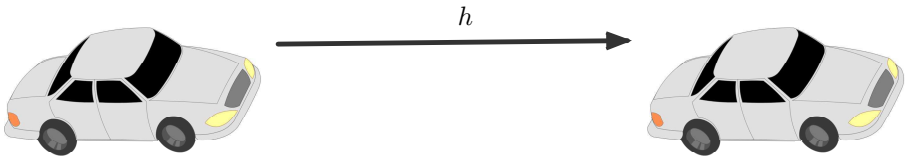

Figure 5.1 Indicative V2V Communication Scenario.

and outage probability, which becomes particularly problematic in certain communications scenarios including safety applications [475]. To this effect, wireless channels in V2V communications should be accurately characterized and modeled in order to evaluate the performance of these systems precisely and incorporate the essential techniques that are capable of ensuring the fulfillment of the corresponding application requirements, resulting to efficient and robust wireless transmission. To this end, we consider a V2V communication system, where the TX and RX are equipped with a single antenna. In this context, we evaluate the corresponding outage probability over cascaded fading channels for both single- and multi-carrier direct conversion transceivers impaired by IQI.

5.7.1 Single-carrier V2V communication system

As illustrated in 5.1, the complex fading coefficient of the considered wireless communication link is represented by h and is assumed to be the product of statistically independent, but not necessarily identically distributed N*Nakagami$-m$ RVs, namely [473]

$$h = \prod_{i=1}^{N} h_i. \tag{5.74}$$

It is recalled here that due to the nature of the surrounding environment, the position of the antennas and the mobility of both the transmitter and receiver, the double and triple Nakagami$-m$ distributions have been proven adequate to model fading in basic V2V communications [473]. In what follows, simple analytic expressions are derived for the corresponding measures for these cases which constitute special cases of the more generic N*Nakagami$-m$ fading distribution and are expressed in a simpler algebraic form.

5.7.1.1 Double Nakagami-m channel

It is recalled that the envelope PDF of double Nakagami$-m$ channels, i.e., $N = 2$, is given in [457, Eq. (6)]. Based on this and with the aid of [476, Eq. (2.3)], it immediately follows that

$$p_\gamma(\gamma) = \mathcal{A}\gamma^{\frac{m_1+m_2}{2}-1} K_{m_1-m_2}\left(\mathcal{B}\sqrt{\gamma}\right) \tag{5.75}$$

where $K_n(\cdot)$ denotes the modified Bessel function of the second kind whereas

$$\mathcal{A} = \frac{2}{\overline{\gamma}^{\frac{m_1+m_2}{2}} \prod_{i=1}^{2} \Gamma(m_i) m_i^{-\frac{m_1+m_2}{2}}}, \tag{5.76}$$

and

$$\mathcal{B} = \frac{2}{\sqrt{\overline{\gamma}}} \prod_{i=1}^{2} \sqrt{m_i}. \tag{5.77}$$

Based on (5.75), the corresponding CDF is given by

$$F_\gamma(x) = \mathcal{A} \int_0^\gamma x^{\frac{m_1+m_2}{2}-1} K_{m_1-m_2}\left(\mathcal{B}\sqrt{x}\right) \mathrm{d}x, \tag{5.78}$$

which can be expressed in closed form with the aid of [477, Eq. (1.12.2)] yielding

$$\begin{aligned} F_\gamma(\gamma) = {} & \frac{\mathcal{A}\gamma^{m_1}\Gamma(m_2-m_1)}{m_1 2^{m_1-m_2}\mathcal{B}^{m_2-m_1}} {}_1F_2\left(m_1; m_1+1, m_1-m_2+1; \frac{\mathcal{B}^2\gamma}{4}\right) \\ & + \frac{\mathcal{A}\gamma^{m_2}\Gamma(m_1-m_2)}{m_2 2^{1-m_1+m_2}\mathcal{B}^{m_2-m_1}} {}_1F_2\left(m_2; m_2+1, m_2-m_1+1; \frac{\mathcal{B}^2\gamma}{4}\right), \end{aligned} \tag{5.79}$$

where ${}_pF_q(\cdot)$ denotes the generalized hypergeometric function [477]. It is noted here that the above expression is not valid when $m_1 = m_2$ as the gamma function is by definition undefined for zero values of its argument[1]. In the same context as above, for the special case that $m_1 - m_2 \pm \frac{1}{2} \in \mathbb{N}$, the $K_n(\cdot)$ function in (5.75) can be expressed according to [274, Eq. (8.468)]. Based on this and by performing the necessary variable transformation, the SNR PDF of the double Nakagami$-m$ fading model can be alternatively expressed as

$$p_\gamma(\gamma) = \sum_{l=0}^{m_1-m_2-\frac{1}{2}} \sqrt{\frac{\pi}{2\mathcal{B}}} \frac{\mathcal{A}\left(m_1-m_2+l-\frac{1}{2}\right)!}{l!\left(m_1-m_2-l-\frac{1}{2}\right)!(2\mathcal{B})^l} \gamma^{\frac{m_1+m_2-l}{2}-\frac{5}{4}} \exp(-\mathcal{B}\sqrt{\gamma}), \tag{5.80}$$

whereas the corresponding CDF is given by

$$F_\gamma(\gamma) = \sum_{l=0}^{m_1-m_2-\frac{1}{2}} \frac{\mathcal{A}\sqrt{\pi}\Gamma\left(m_1-m_2+l+\frac{1}{2}\right)}{l!\Gamma\left(m_1-m_2-l+\frac{1}{2}\right)(2\mathcal{B})^{l+\frac{1}{2}}} \int_0^\gamma x^{\frac{m_1+m_2-l}{2}-\frac{5}{4}} \exp(-\mathcal{B}\sqrt{x})\mathrm{d}x. \tag{5.81}$$

The above integral can be expressed in closed form with the aid of [274, Eq. (8.350.1)]. As a result, by performing the necessary change of variables and substituting in (5.81) it follows that

$$F_\gamma(\gamma) = \mathcal{A}\sqrt{\pi} \sum_{l=0}^{m_1-m_2-\frac{1}{2}} \frac{\Gamma\left(m_1-m_2+l+\frac{1}{2}\right)\gamma\left(m_1-m_2+l+\frac{1}{2},\mathcal{B}\sqrt{\gamma}\right)}{l!2^{l-\frac{1}{2}}\mathcal{B}^{m_1+m_2}\Gamma\left(m_1-m_2-l+\frac{1}{2}\right)}, \tag{5.82}$$

which is also valid for the case that $m_1 - m_2 \pm \frac{1}{2} \in \mathbb{N}$.

To this effect, in the case of single-carrier V2V communication with only TX impaired with IQI, (5.46) can be straightforwardly expressed as

$$P_{\text{out}} = \frac{1}{\Gamma(m_1)\Gamma(m_2)} G_{1,3}^{2,1}\left(\frac{1}{|K_1^t|^2\left(\frac{1}{\gamma_{th}}-\frac{1}{IRR_t}\right)\overline{\gamma}}\prod_{i=1}^{2} m_i \,\middle|\, \begin{matrix} 1 \\ m_1, m_2, 0 \end{matrix}\right), \tag{5.83}$$

which with the aid of (5.79) and (5.81) can be equivalently rewritten as

$$\begin{aligned} P_{\text{out}} = & \left(\frac{1}{|K_1^t|^2\left(\frac{1}{\gamma_{th}}-\frac{1}{IRR_t}\right)}\right)^{m_1} \frac{\mathcal{A}\Gamma(m_2-m_1)}{m_1 2^{m_1-m_2}\mathcal{B}^{m_2-m_1}} \\ & \times {}_1F_2\left(m_1; m_1+1, m_1-m_2+1; \frac{1}{|K_1^t|^2\left(\frac{\mathcal{B}^2}{4}\frac{1}{\gamma_{th}}-\frac{1}{IRR_t}\right)}\right) \\ & + \left(\frac{1}{|K_1^t|^2\left(\frac{1}{\gamma_{th}}-\frac{1}{IRR_t}\right)}\right)^{m_2} \frac{\mathcal{A}\Gamma(m_1-m_2)}{m_2 2^{1-m_1+m_2}\mathcal{B}^{m_2-m_1}} \\ & \times {}_1F_2\left(m_2; m_2+1, m_2-m_1+1; \frac{\mathcal{B}^2}{4}\frac{1}{|K_1^t|^2\left(\frac{1}{\gamma_{th}}-\frac{1}{IRR_t}\right)}\right). \end{aligned} \tag{5.84}$$

Likewise, for the special case that $m_1 - m_2 \pm \frac{1}{2} \in \mathbb{N}$ it can be further simplified to

$$P_{\text{out}} = \sum_{l=0}^{m_1-m_2-\frac{1}{2}} \frac{2^{\frac{1}{2}-l}\Gamma\left(m_1-m_2+l+\frac{1}{2}\right)}{l!\mathcal{B}^{m_1+m_2}\Gamma\left(m_1-m_2-l+\frac{1}{2}\right)} \gamma\left(m_1-m_2+l+\frac{1}{2}, \frac{\mathcal{B}}{|K_1^t|\sqrt{\frac{1}{\gamma_{th}}-\frac{1}{IRR_t}}}\right), \tag{5.85}$$

with $\gamma(a,x)$ denoting the lower incomplete gamma function [477].

[1] In such cases the corresponding results can be obtained with the aid of the generic analytic expressions in Section 5.6. This is also the case in the respective considered scenarios in Section 5.8.

In the same context, in the case of only RX impaired with IQI, eq. (5.48) can be re-written as

$$P_{\text{out}} = \frac{1}{\Gamma(m_1)\Gamma(m_2)} G_{1,3}^{2,1}\left(\frac{1+\frac{1}{IRR_r}}{\left(\frac{1}{\gamma_{th}}-\frac{1}{IRR_r}\right)\overline{\gamma}} \prod_{i=1}^{2} m_i \,\middle|\, \begin{matrix} 1 \\ m_1, m_2, 0 \end{matrix} \right), \tag{5.86}$$

or alternatively as

$$\begin{aligned} P_{\text{out}} = & \frac{\mathcal{A}\Gamma(m_2-m_1)}{m_1 2^{m_1-m_2}\mathcal{B}^{m_2-m_1}} \left(\frac{1+\frac{1}{IRR_r}}{\frac{1}{\gamma_{th}}-\frac{1}{IRR_r}} \right)^{m_1} \\ & \times {}_1F_2\left(m_1; m_1+1, m_1-m_2+1; \frac{\mathcal{B}^2}{4}\frac{1+\frac{1}{IRR_r}}{\frac{1}{\gamma_{th}}-\frac{1}{IRR_r}} \right) \\ & + \frac{\mathcal{A}\Gamma(m_1-m_2)}{m_2 2^{1-m_1+m_2}\mathcal{B}^{m_2-m_1}} \left(\frac{1+\frac{1}{IRR_r}}{\frac{1}{\gamma_{th}}-\frac{1}{IRR_r}} \right)^{m_2} \\ & \times {}_1F_2\left(m_2; m_2+1, m_2-m_1+1; \frac{\mathcal{B}^2}{4}\frac{1+\frac{1}{IRR_r}}{\frac{1}{\gamma_{th}}-\frac{1}{IRR_r}} \right), \end{aligned} \tag{5.87}$$

which is also valid when $m_1 \neq m_2$. Furthermore, for the special case that $m_1 - m_2 \pm \frac{1}{2} \in \mathbb{N}$, the outage probability can be expressed as

$$P_{\text{out}} = \sum_{l=0}^{m_1-m_2-\frac{1}{2}} \frac{\mathcal{A}\sqrt{\pi}\Gamma\left(m_1-m_2+l+\frac{1}{2}\right)}{l! 2^{l-\frac{1}{2}}\mathcal{B}^{m_1+m_2}\Gamma\left(m_1-m_2-l+\frac{1}{2}\right)} \gamma\left(m_1-m_2+l+\frac{1}{2}, \mathcal{B}\sqrt{\frac{1+\frac{1}{IRR_r}}{\frac{1}{\gamma_{th}}-\frac{1}{IRR_r}}} \right). \tag{5.88}$$

Finally, in the case of joint IQI, equation (5.49) can be readily expressed as

$$P_{\text{out}} = \frac{1}{\Gamma(m_1)\Gamma(m_2)} G_{1,3}^{2,1}\left(\frac{\left(|K_1^r|^2+|K_2^r|^2\right)\gamma_{th}}{\left(\frac{|\xi_{11}|^2}{\gamma_{th}}-\left(|\xi_{12}|^2+|\xi_{21}|^2\right)\right)\overline{\gamma}} \prod_{i=1}^{2} m_i \,\middle|\, \begin{matrix} 1 \\ m_1, m_2, 0 \end{matrix} \right), \tag{5.89}$$

which with the aid of (5.79) and (5.82) can be alternatively expressed as

$$\begin{aligned} P_{\text{out}} = & \frac{\mathcal{A}\Gamma(m_2-m_1)}{m_1 2^{m_1-m_2}\mathcal{B}^{m_2-m_1}} \left(\frac{|K_1^r|^2+|K_2^r|^2}{\frac{|\xi_{11}|^2}{\gamma_{th}}-\left(|\xi_{12}|^2+|\xi_{21}|^2\right)} \right)^{m_1} \\ & \times {}_1F_2\left(m_1; m_1+1, m_1-m_2+1; \frac{\mathcal{B}^2}{4}\frac{|K_1^r|^2+|K_2^r|^2}{\frac{|\xi_{11}|^2}{\gamma_{th}}-\left(|\xi_{12}|^2+|\xi_{21}|^2\right)} \right) \\ & + \frac{\mathcal{A}\Gamma(m_1-m_2)}{m_2 2^{1-m_1+m_2}\mathcal{B}^{m_2-m_1}} \left(\frac{|K_1^r|^2+|K_2^r|^2}{\frac{|\xi_{11}|^2}{\gamma_{th}}-\left(|\xi_{12}|^2+|\xi_{21}|^2\right)} \right)^{m_2} \\ & \times {}_1F_2\left(m_2; m_2+1, m_2-m_1+1; \frac{\mathcal{B}^2}{4}\frac{|K_1^r|^2+|K_2^r|^2}{\frac{|\xi_{11}|^2}{\gamma_{th}}-\left(|\xi_{12}|^2+|\xi_{21}|^2\right)} \right), \end{aligned} \tag{5.90}$$

whereas for the case that $m_1 - m_2 \pm \frac{1}{2} \in \mathbb{N}$, it can be further simplified to

$$P_{\text{out}} = \mathcal{A}\sqrt{\pi} \sum_{l=0}^{m_1-m_2-\frac{1}{2}} \frac{\Gamma\left(m_1-m_2+l+\frac{1}{2}\right)\gamma\left(m_1-m_2+l+\frac{1}{2}, \mathcal{B}\sqrt{\frac{|K_1^r|^2+|K_2^r|^2}{\frac{|\xi_{11}|^2}{\gamma_{th}}-\left(|\xi_{12}|^2+|\xi_{21}|^2\right)}} \right)}{l! 2^{l-\frac{1}{2}}\mathcal{B}^{m_1+m_2}\Gamma\left(m_1-m_2-l+\frac{1}{2}\right)}. \tag{5.91}$$

It is recalled here that when the distance separating the involved vehicles is larger than 5m, the corresponding LoS component tends to disappear and fading becomes more severe [474]. This also includes double Rayleigh fading conditions [459, 478, 479], which constitute a special case of the double Nakagami$-m$ for $m_2 = m_1 = 1$.

5.7.1.2 Triple Nakagami-m channel

In the case of triple Nakagami$-m$ fading channels, it immediately follows from (5.44) that the CDF of γ_{id} can be obtained as

$$F_{\gamma_{\mathrm{id}}}(\gamma) = \frac{1}{\Gamma(m_1)\Gamma(m_2)\Gamma(m_3)} G_{1,4}^{3,1}\left(\frac{\gamma}{\overline{\gamma}} m_1 m_2 m_3 \,\middle|\, \begin{matrix} - \\ m_1, m_2, m_3, 0 \end{matrix}\right). \tag{5.92}$$

Therefore, in case of TX impaired by IQI, equation (5.46) can be expressed as

$$P_{\mathrm{out}} = \frac{1}{\Gamma(m_1)\Gamma(m_2)\Gamma(m_3)} G_{1,4}^{3,1}\left(\frac{m_1 m_2 m_3}{|K_1^t|^2\left(\frac{1}{\gamma_{th}} - \frac{1}{IRR_t}\right)\overline{\gamma}} \,\middle|\, \begin{matrix} - \\ m_1, m_2, m_3, 0 \end{matrix}\right), \tag{5.93}$$

whereas in the case of RX impaired by IQI, equation (5.48) can be re-written as follows

$$P_{\mathrm{out}} = \frac{1}{\Gamma(m_1)\Gamma(m_2)\Gamma(m_3)} G_{1,4}^{3,1}\left(\frac{1+\frac{1}{IRR_r}}{\left(\frac{1}{\gamma_{th}} - \frac{1}{IRR_r}\right)\overline{\gamma}} m_1 m_2 m_3 \,\middle|\, \begin{matrix} - \\ m_1, m_2, m_3, 0 \end{matrix}\right). \tag{5.94}$$

Likewise, in the case of joint TX/RX IQI and with the aid of (5.49), it immediately follows

$$P_{\mathrm{out}} = \frac{1}{\prod_{i=1}^{3}\Gamma(m_i)} G_{1,4}^{3,1}\left(\frac{|K_1^r|^2 + |K_2^r|^2}{\left(\frac{|\xi_{11}|^2}{\gamma_{th}} - \left(|\xi_{12}|^2 + |\xi_{21}|^2\right)\right)\overline{\gamma}} m_1 m_2 m_3 \,\middle|\, \begin{matrix} - \\ m_1, m_2, m_3, 0 \end{matrix}\right). \tag{5.95}$$

5.7.2 Multi-carrier V2V communication system

In this subsection, we assume that $h(k)$ and $h(-k)$ represent the base band equivalent wireless communication links complex fading coefficients of subcarriers k and $-k$, respectively, whose magnitudes $|h(k)|$ and $|h(-k)|$ follow a cascaded Nakagami$-m$ distribution. This corresponds to the case of the product of statistically independent, but not necessarily identically distributed N*Nakagami$-m$ RVs. To this effect, it immediately follows that

$$|h(k)| = \prod_{i=1}^{N} |h_i(k)|, \tag{5.96}$$

and

$$|h(-k)| = \prod_{i=1}^{N} |h_i(-k)|. \tag{5.97}$$

It is recalled that, due to the nature of the surrounding environment, $|h(k)|$ and $|h(-k)|$ can be also adequately modeled by double or triple Nakagami$-m$ processes.

5.7.2.1 Double Nakagami$-m$ channels

In the case of double Nakagami$-m$ fading channels, the SNR CDF is given by (5.79). Thus, in the case of TX impaired by IQI, (5.52) can be expressed as

$$\begin{aligned}
P_{\text{out}} =& q\Bigg\{\left(\frac{1}{|K_1^t|^2\left(\frac{1}{\gamma_{th}}-\frac{1}{IRR_t}\right)}\right)^{m_1}\frac{\mathcal{A}\Gamma(m_2-m_1)}{m_1 2^{m_1-m_2}\mathcal{B}^{m_2-m_1}}\\
&\times {}_1F_2\left(m_1;m_1+1,m_1-m_2+1;\frac{\mathcal{B}^2}{4}\frac{1}{|K_1^t|^2\left(\frac{1}{\gamma_{th}}-\frac{1}{IRR_t}\right)}\right)\\
&+\left(\frac{1}{|K_1^t|^2\left(\frac{1}{\gamma_{th}}-\frac{1}{IRR_t}\right)}\right)^{m_2}\frac{\mathcal{A}\Gamma(m_1-m_2)}{m_2 2^{1-m_1+m_2}\mathcal{B}^{m_2-m_1}}\\
&\times {}_1F_2\left(m_2;m_2+1,m_2-m_1+1;\frac{\mathcal{B}^2}{4}\frac{1}{|K_1^t|^2\left(\frac{1}{\gamma_{th}}-\frac{1}{IRR_t}\right)}\right)\Bigg\}\\
&+(1-q)\Bigg\{\left(\frac{\gamma_{th}}{|K_1^t|^2}\right)^{m_1}\frac{\mathcal{A}\Gamma(m_2-m_1)}{m_1 2^{m_1-m_2}\mathcal{B}^{m_2-m_1}}\,{}_1F_2\left(m_1;m_1+1,m_1-m_2+1;\frac{\mathcal{B}^2}{4}\frac{\gamma_{th}}{|K_1^t|^2}\right)\\
&+\left(\frac{\gamma_{th}}{|K_1^t|^2}\right)^{m_2}\frac{\mathcal{A}\Gamma(m_1-m_2)}{m_2 2^{1-m_1+m_2}\mathcal{B}^{m_2-m_1}}\,{}_1F_2\left(m_2;m_2+1,m_2-m_1+1;\frac{\mathcal{B}^2}{4}\frac{\gamma_{th}}{|K_1^t|^2}\right)\Bigg\}. \qquad (5.98)
\end{aligned}$$

Note that (5.98) is valid when $m_1 \neq m_2$. For the special case that $m_1 - m_2 \pm \frac{1}{2} \in \mathbb{N}$, the outage probability can be alternatively expressed with the aid of (5.82), which yields

$$\begin{aligned}
P_{\text{out}} =& \sum_{l=0}^{m_1-m_2-\frac{1}{2}}\frac{\mathcal{A}q\sqrt{\pi}\Gamma\left(m_1-m_2+l+\frac{1}{2}\right)}{l!2^{l-\frac{1}{2}}\mathcal{B}^{m_1+m_2}\Gamma\left(m_1-m_2-l+\frac{1}{2}\right)}\gamma\left(m_1-m_2+l+\frac{1}{2},\frac{\mathcal{B}}{|K_1^t|\sqrt{\left(\frac{1}{\gamma_{th}}-\frac{1}{IRR_t}\right)}}\right)\\
&-\sum_{l=0}^{m_1-m_2-\frac{1}{2}}\frac{\mathcal{A}(1-q)\sqrt{\pi}\Gamma\left(m_1-m_2+l+\frac{1}{2}\right)}{l!2^{l-\frac{1}{2}}\mathcal{B}^{m_1+m_2}\Gamma\left(m_1-m_2-l+\frac{1}{2}\right)}\gamma\left(m_1-m_2+l+\frac{1}{2},\frac{\mathcal{B}\sqrt{\gamma_{th}}}{|K_1^t|}\right). \qquad (5.99)
\end{aligned}$$

In the same context, in the case of only RX impaired with IQI, (5.63) can be rewritten as

$$\begin{aligned}
P_{\text{out}} =& q\sum_{k=0}^{p}\frac{(-1)^k\gamma_{th}^k}{k!\overline{\gamma}^k}\left(1+\frac{1}{IRR_r}\right)^k\left(\prod_{i=1}^{2}m_i\right)^k\\
&\times G_{4,4}^{3,3}\left(\frac{IRR_r}{\gamma_{th}}\,\middle|\,\begin{matrix}1,k-m_1+1,k-m_2+1,\ldots,k-m_N+1,k+1\\ m_1,m_2,k,k+1,0\end{matrix}\right)\\
&+(1-q)\frac{1}{\prod_{i=1}^{2}\Gamma(m_i)}G_{1,3}^{2,1}\left(\frac{\left(1+\frac{1}{IRR_r}\right)\gamma_{th}}{\overline{\gamma}}\prod_{i=1}^{2}m_i\,\middle|\,\begin{matrix}1\\ m_1,m_2,0\end{matrix}\right), \qquad (5.100)
\end{aligned}$$

whereas for the case of joint IQI, (5.73) can be expressed as

$$\begin{aligned}
P_{\text{out}} =& q\sum_{k=0}^{p}\frac{(-1)^k\gamma_{th}^k\left(|K_1^r|^2+|K_2^r|^2\right)^k}{k!\overline{\gamma}^k\left(|\xi_{11}|^2-\gamma_{th}|\xi_{12}|^2\right)^k}\left(\prod_{i=1}^{2}\Gamma(m_i)\right)^k\\
&\times G_{4,4}^{3,3}\left(\frac{|\xi_{11}|^2-\gamma_{th}|\xi_{12}|^2}{|\xi_{21}|^2\gamma_{th}}\,\middle|\,\begin{matrix}1,k-m_1+1,k-m_2+1,k+1\\ m_1,m_2,k,k+1,0\end{matrix}\right)\\
&+(1-q)\frac{1}{\prod_{i=1}^{2}\Gamma(m_i)}G_{1,3}^{2,1}\left(\frac{|K_1^r|^2+|K_2^r|^2}{|\xi_{11}|^2\overline{\gamma}}\gamma_{th}\prod_{i=1}^{2}m_i\,\middle|\,\begin{matrix}1\\ m_1,m_2,0\end{matrix}\right) \qquad (5.101)
\end{aligned}$$

It is again recalled that as the distance between the communicating vehicles becomes larger than 5m, the involved LOS component tends to disappear, which renders the corresponding fading environments more severe, including double Rayleigh fading conditions, i.e., $m_2 = m_1 = 1$.

5.7.2.2 Triple Nakagami-m channels

In case of triple Nakagami-m channels, the outage probability in the case that the TX is impaired with IQI is given by setting into (5.52) $N = 3$, namely

$$P_{\text{out}} = \frac{qG_{1,4}^{3,1}\left(\frac{1}{|K_1^t|^2\left(\frac{1}{\gamma_{th}}-\frac{1}{IRR_t}\right)\overline{\gamma}}\prod_{i=1}^{3}m_i \,\middle|\, \begin{matrix}1\\ m_1,m_2,m_3,0\end{matrix}\right)}{\prod_{i=1}^{3}\Gamma(m_i)} + \frac{(1-q)G_{1,4}^{3,1}\left(\frac{\gamma_{th}}{|K_1^t|^2\overline{\gamma}}\prod_{i=1}^{3}m_i \,\middle|\, \begin{matrix}1\\ m_1,m_2,m_3,0\end{matrix}\right)}{\prod_{i=1}^{3}\Gamma(m_i)}, \tag{5.102}$$

whereas in the case of RX impaired with IQI, (5.63) can be rewritten as

$$\begin{aligned} P_{\text{out}} = q\sum_{k=0}^{p}\frac{(-1)^k\gamma_{th}^k}{k!\overline{\gamma}^k}\left(1+\frac{1}{IRR_r}\right)^k\left(\prod_{i=1}^{3}m_i\right)^k \\ \times G_{5,5}^{4,4}\left(\frac{IRR_t}{\gamma_{th}} \,\middle|\, \begin{matrix}1,k-m_1+1,k-m_2+1,k-m_3+1,k+1\\ m_1,m_2,m_3,k,k+1,0\end{matrix}\right) \\ + (1-q)\frac{1}{\prod_{i=1}^{3}\Gamma(m_i)}G_{1,4}^{3,1}\left(\frac{\left(1+\frac{1}{IRR_r}\right)\gamma_{th}}{\overline{\gamma}}\prod_{i=1}^{3}m_i \,\middle|\, \begin{matrix}1\\ m_1,m_2,m_3,0\end{matrix}\right). \end{aligned} \tag{5.103}$$

Finally, in the case of joint TX/RX IQI, (5.73) can be expressed as

$$\begin{aligned} P_{\text{out}} = q\sum_{k=0}^{p}\frac{(-1)^k\gamma_{th}^k\left(|K_1^r|^2+|K_2^r|^2\right)^k}{k!\overline{\gamma}^k\left(|\xi_{11}|^2-\gamma_{th}|\xi_{12}|^2\right)^k}\left(\prod_{i=1}^{3}\Gamma(m_i)\right)^k \\ \times G_{5,5}^{4,4}\left(\frac{|\xi_{11}|^2-\gamma_{th}|\xi_{12}|^2}{|\xi_{21}|^2\gamma_{th}} \,\middle|\, \begin{matrix}1,k-m_1+1,k-m_2+1,k-m_3+1,k+1\\ m_1,m_2,m_3,k,k+1,0\end{matrix}\right) \\ + (1-q)\frac{1}{\prod_{i=1}^{3}\Gamma(m_i)}G_{1,4}^{3,1}\left(\frac{|K_1^r|^2+|K_2^r|^2}{|\xi_{11}|^2\overline{\gamma}}\gamma_{th}\prod_{i=1}^{3}m_i \,\middle|\, \begin{matrix}1\\ m_1,m_2,m_3,0\end{matrix}\right) \end{aligned} \tag{5.104}$$

5.8 Numerical results

In this section, we evaluate and illustrate the effects of IQI on the performance of wireless communications over cascaded Nakagami-m fading channels in terms of the corresponding outage probability. The notation $m = \{m_1, m_2, \cdots, m_N\}$ denotes up to N*Nakagami-m channels, i.e. $m = \{m_1, m_2, m_3\}$ for $N = 3$, with fading $m-$parameters of m_1, m_2, and m_3, respectively. We also consider that the SNR is normalized with respect to γ_{th}, which implies that the outage probability is evaluated as a function of $\gamma/\gamma_{\text{th}}$. Furthermore, it is important to note that, unless otherwise is stated, in the following figures, the numerical results are shown with continuous lines, while markers are employed to illustrate the simulation results.

To this end, Fig. 5.2 illustrates the outage probability versus the normalized SNR for the different considered TX/RX scenarios for the case of single-carrier communications. Specifically, we compare the outage probability between the ideal RF front-end, the RX imbalanced, the TX imbalanced and joint TX/RX imbalanced cases when the IRR = 20 dB, and $\phi = 3^o$. We consider the two cases of $\epsilon < 1$ (continuous lines), and $\epsilon > 1$ (dashed lines). Furthermore, different channels have been considered, where $m = 1$, $m = \{1, 1\}$ and $m = \{1, 1, 1, 1\}$ corresponds to the Rayleigh, double Rayleigh and N*Rayleigh with $N = 4$ channels respectively. It is shown that the performance degradation created by the IQI

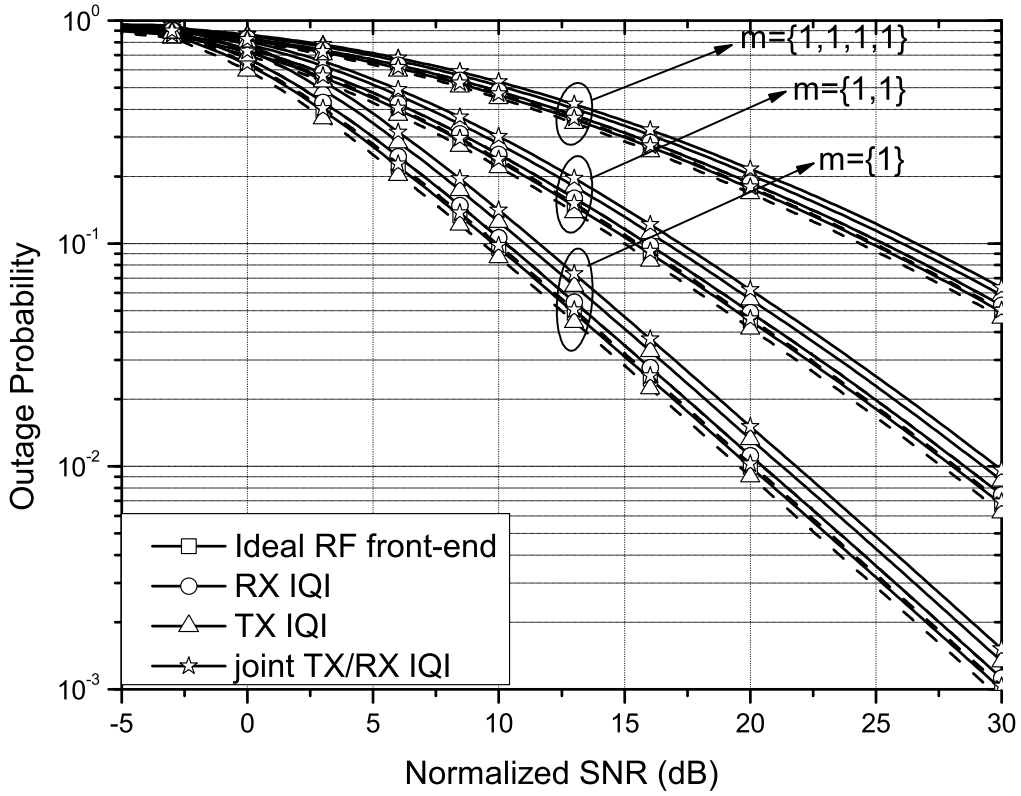

Figure 5.2 Single-carrier system P_{out} as a function of the normalized outage SNR, when IRR = 20 dB, $\phi = 3^o$, $\epsilon \simeq 0.824$ (continuous lines), and $\epsilon \simeq 1.21364$ (dashed lines).

is somewhat less severe compared to the detrimental effects of cascaded fading. For example, for the case of $\gamma/\gamma_{th} = 10$ dB, the outage probability in the case of Rayleigh fading is nearly half the outage probability value in the case of double Rayleigh fading. In addition, in the case of double Rayleigh fading channels, the assumption of ideal RF front-end results to around 20% error in the corresponding outage probability. These results highlight the importance of both accurate channel characterization and modeling as well as accounting for RF impairments, in the realistic performance analysis and design of wireless communication systems. It is also interesting to note that, when $\epsilon < 1$, the effects of TX IQI only on the outage probability degradation are more severe than the corresponding effects of RX IQI only. The underlying reason is that the SINR is higher in the case of RX IQI only than in the case of TX IQI only, since the noise is multiplied by $\left(|K_1^r|^2 + |K_2^r|^2\right)$, which for $\epsilon < 1$ does not exceed 1. Moreover, it is worth mentioning that in case of $\epsilon > 1$, the RX IQI effects are the most severe since the noise is multiplied by $\left(|K_1^r|^2 + |K_2^r|^2\right)$, which in this case is greater than 1. Interestingly, in case of $\epsilon > 1$, the TX IQI only system outperforms even the corresponding ideal RF front-end system. As can be drawn from (8.6) and (8.7), when $\epsilon > 1$, for practical levels of IQI, it follows that $|K_1^t|^2 > 1$, and $|K_2^t|^2 \to 0$. Therefore, eq. (5.9) can be tightly approximated as

$$\gamma \approx \left|K_1^t\right|^2 \gamma_{\text{ideal}} \tag{5.105}$$

which, for $\epsilon > 1$, is greater than γ_{ideal}.

Fig. 5.3 shows the effects of the IRR on the outage probability in case of single-carrier communication systems considering double Rayleigh and double Nakagami-m, with $m = \{0.5, 0.5\}$, $m = \{2, 2\}$ and $m = \{3, 3\}$ fading conditions with joint TX/RX IQI. It is evident that the outage probability decreases as the m values are increased, for a given SNR value, while, as expected, the outage probability is improved when the IRR is increased. For example, for the case of double Nakagami$-m$ conditions with $\overline{\gamma} = 10$ dB, taking an RF front-end with an IRR of 27 dB instead of 20 dB, decreases the corresponding outage probability by 30%. Notably, since the IRR of practical RF front-ends lies in the range of $20 - 40$ dB, these results highlight the importance of taking RF impairments such as the IQI into

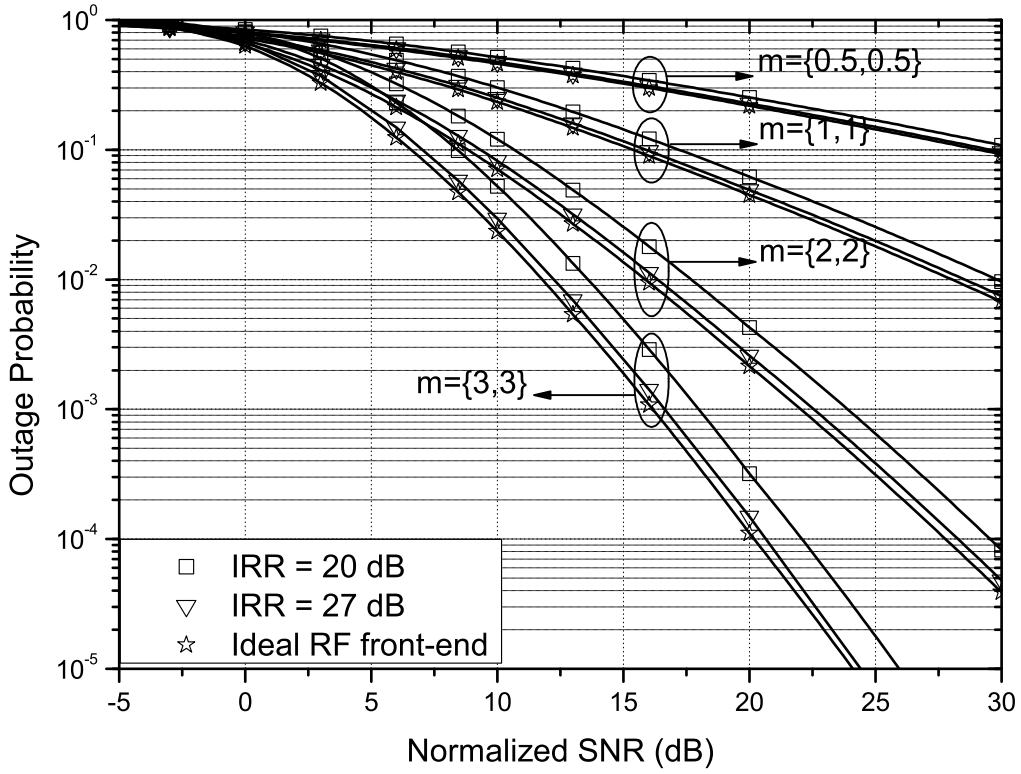

Figure 5.3 Single-carrier system P_{out} as a function of the normalized outage SNR, for different values of IRR, when $\epsilon < 1$, and $\phi = 3^o$.

consideration. Likewise, it is also shown that it is of paramount importance to take into account the effects of cascaded fading conditions, as the difference in comparison with non-multiplicative fading is about an order of magnitude in both low and high SNR regimes.

Fig. 5.4 shows the effects of the IRR on the outage probability for the different considered TX/RX scenarios assuming double Nakagami-m, with $m = \{2, 2\}$ and $m = \{3, 3\}$, fading channels. It is evident that the outage probability is lower for the case of double Nakagami-m fading with $m = \{3, 3\}$ compared to the double Nakagami-m fading with $m = \{2, 2\}$, while, as expected, the outage probability is improved when the IRR is increased. For example, for the case of double Nakagami$-m$ with $m = \{3, 3\}$ conditions with $\gamma/\gamma_{th} = 20$ dB, taking an RF front-end with an IRR of 25 dB instead of 20 dB, decreases the corresponding outage probability by 47%, in case of joint TX/RX IQI. Consequently, for realistic levels of hardware imperfections, these results highlight the detrimental effects of IQI and indicate the importance of taking RF impairments and the statistics of the channel into consideration.

Next, we consider the case of multi-carrier transmission and evaluate the effects of IQI on the outage probability in the case of signal absence and signal presence at the carrier $-k$, i.e., $q = 0$ and $q = 1$, respectively. We assume mutually uncorrelated channel gains between the carrier k and its image, $-k$. The outage probability of multi-carrier systems with $q = 0$ over N*Rayleigh channels is demonstrated in Fig. 5.5, where the impact of cascaded channels on the corresponding performance is clearly observed. Yet, it is noticed that when there is no signal in the image subcarrier, the signal carried by subcarrier k is interference-free. As a result, the performance degradation caused by the RF front-end IQI is much lower than the corresponding degradation in the single-carrier transmission scenario. In fact, when IRR = 25 dB, the outage probability is nearly the same as in the cases that the TX and/or RX are ideal. These results are expected, since the mirror-interference effects of IQI are nullified when there is no signal in subcarrier $-k$. Furthermore, we observe that as N increases, the performance degradation become more severe. For instance, for $N = 8$, the outage probability is higher than 10^{-1}, even for extreme values of normalized SNR. This finding reveals that in case of $q = 0$, the main source of outage probability degradation is the impact of the cascaded channels and not the hardware imperfections.

Fig. 5.6 depicts the outage probability versus the normalized SNR for multi-carrier systems, over

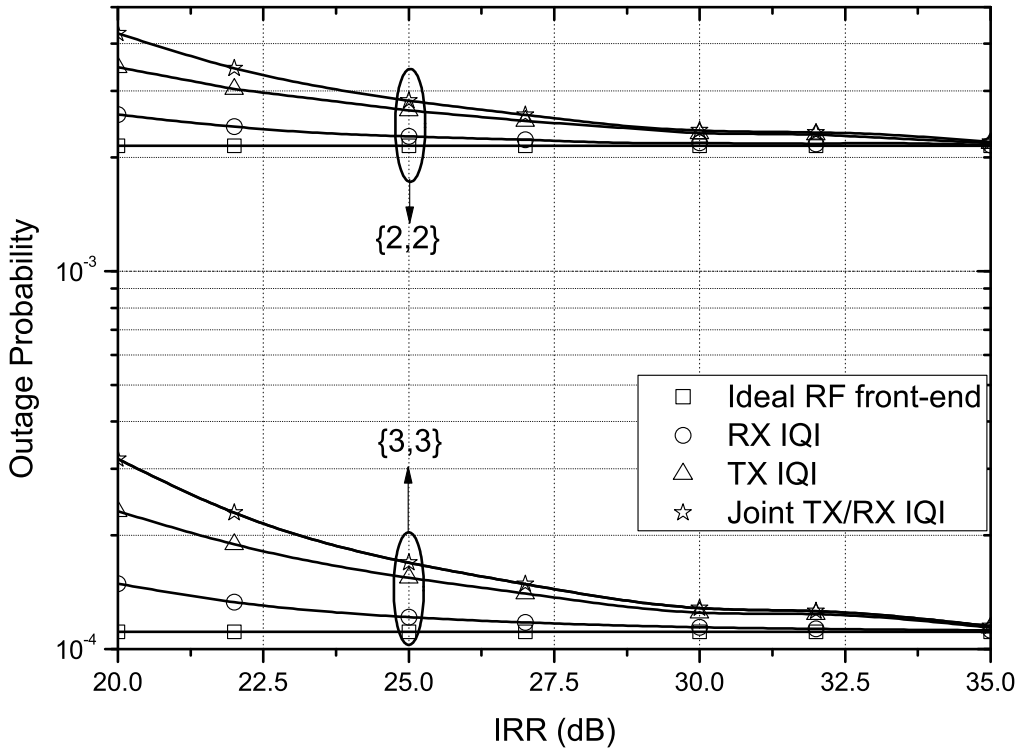

Figure 5.4 Single-carrier system P_{out} as a function of the IRR, when SNR = 20dB and $\phi = 3^o$.

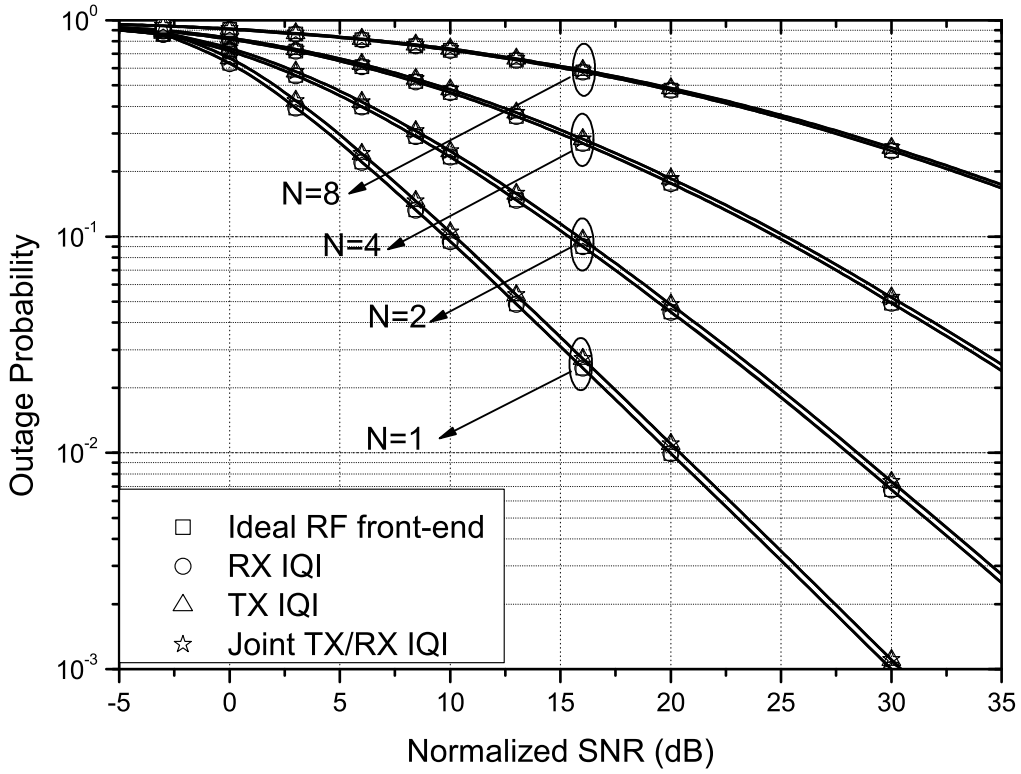

Figure 5.5 Multi-carrier system P_{out} as a function of the normalized outage SNR when $q = 0$, $IRR =$ 25 dB, $\phi = 3^o$, considering N*Rayleigh channels.

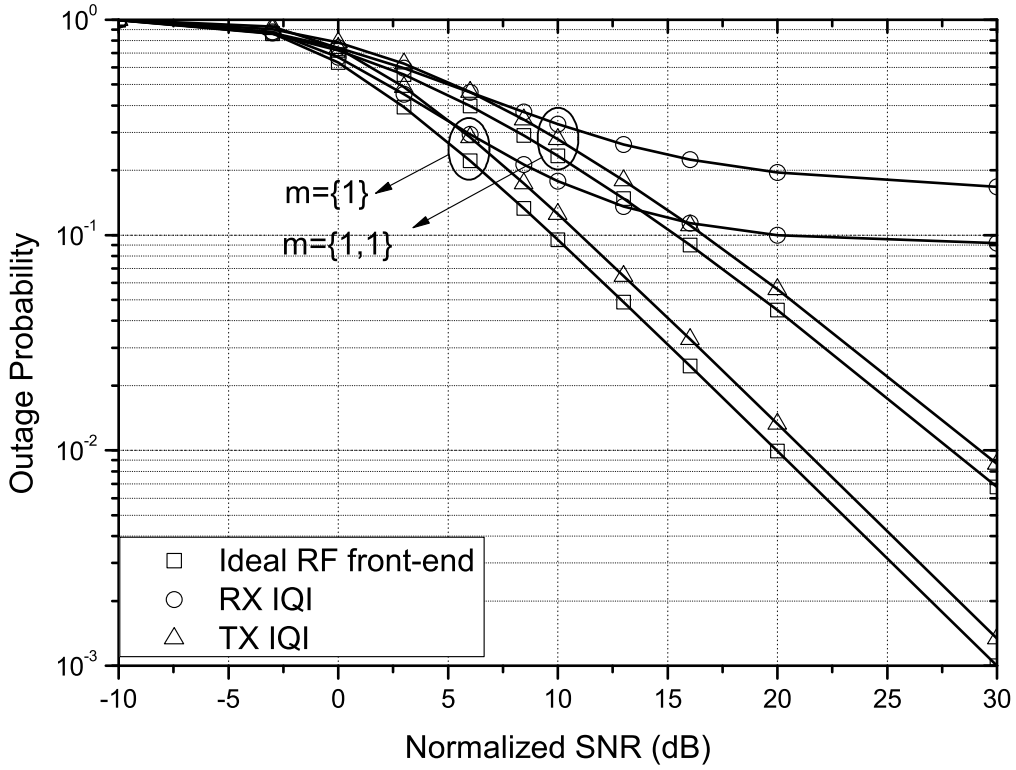

Figure 5.6 Multi-carrier system P_{out} as a function of the normalized outage SNR when $q = 1$, $IRR =$ 20 dB, $\phi = 3^o$.

both Rayleigh and double Rayleigh channels, for the case of a signal present in subcarrier $-k$, i.e. $q = 1$. In this case the IQI causes distortion of the transmitted baseband equivalent signal at the k^{th} subcarrier, $s(k)$, by its image signal at subcarrier $-k$. Furthermore, we observe a lower bound in the case of ideal TX and I/Q imbalanced RX. Intuitively, in case of TX IQI only, mirroring occurs already at TX and the total signal at subcarrier k, original and mirrored term, both travel through $h(k)$, i.e. fading does not change their ratio. However, in case of RX IQI only, mirroring occurs after wireless transmission over the multiplicative fading channel, so there can be a challenging scenario when $h(k)$ has low value (deep fade) and $h(-k)$ is strong, so the mirrored term can be very strong. Furthermore, as can be drawn from (9.44), in the high SNR regime, in the presence of signal in subcarrier $-k$, the instantaneous SINR per symbol can be accurately approximated by

$$\gamma(k) \approx \frac{\gamma_{\text{ideal}}(k)}{\gamma_{\text{ideal}}(-k)} \text{IRR}_r. \tag{5.106}$$

Furthermore, assuming $\gamma_{\text{ideal}}(k) \approx \gamma_{\text{ideal}}(-k)$, it follows that

$$\gamma(k) \approx \text{IRR}_r. \tag{5.107}$$

In other words, we observe that the maximum achievable SINR is constraint to the IRR levels, because of the effects of IQI.

To this effect, it is shown that the SINR exhibits an upper bound which in turn results to a lower bound in the corresponding outage probability performance. It is noted that the same behavior is experienced in the case of joint TX/RX IQI. Hence, it is evident that this lower bound can create detrimental effects on the performance of communication systems, which stresses the importance of the provided performance analysis and the requirement for efficient compensation techniques.

Fig. 5.7 illustrates the outage probability as a function of the normalized SNR, for different values of q, when $m = \{1, 1\}$, IRR = 20 dB, and $\phi = 3^o$, in case of ideal TX and I/Q imbalanced RX. From this figure, it is evident that, for fixed normalized SNR, as q increases, the probability of interference to the signal at the $k-$ th subcarrier, by its image signal at subcarrier $-k$ increases; consequently, the

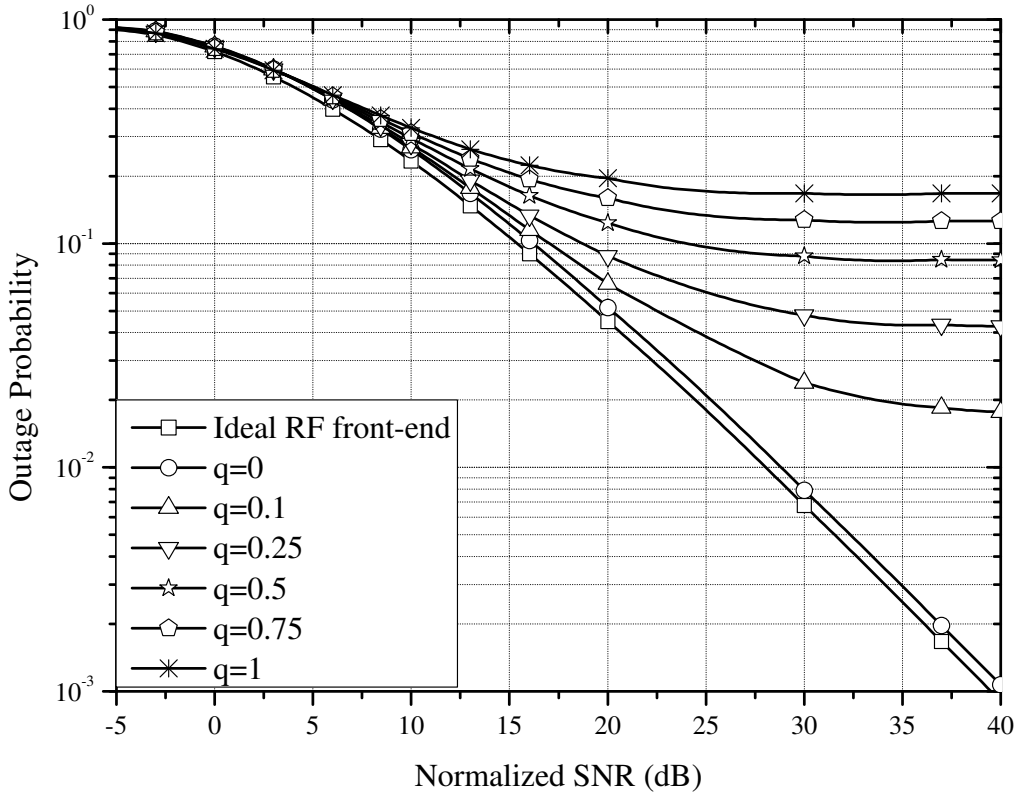

Figure 5.7 Multi-carrier system P_{out} as a function of the normalized SNR, for different values of q, when $m = \{1, 1\}$, IRR = 20 dB, and $\phi = 3^o$.

outage probability increases. For example, for normalized SNR equals 30 dB, the outage probabilities for $q = 0.5$ and $q = 1$ are respectively 8.77×10^{-2}, and 16.74×10^{-2}. This result indicates the importance of taking the effect of mirror interference uncertainty into consideration.

Finally, Fig. 5.8 compares the outage probability of multi-carrier systems over double-Rayleigh channels, when $q = 0$ and $q = 1$. It is observed that the detrimental effects of IQI on the outage probability performance are significantly increased when a signal is present in subcarrier $-k$. Specifically, in the case of $q = 1$ and RX or joint TX/RX IQI, as SNR increases, the mirror-interference increases, resulting to an outage probability lower bound. In the worst case scenario, where IRR = 20 dB, this bound is in the order of 9×10^{-1}, which may not be acceptable in practice. Meanwhile, the presence of a signal in subcarrier $-k$ creates no impact, as expected, on the performance of multi-carrier systems, when the RF front-end is considered ideal.

5.9 Conclusions

The present chapter investigated the outage probability performance of single-carrier and multi-carrier systems over cascaded Nakagami-m channels in the presence of IQI at the RF front-end. For the multi-carrier systems, we considered the case that the channel $-k$ is both occupied and unoccupied by an information signal while for each system, we considered three scenarios in our analysis corresponding to ideal TX with I/Q imbalanced RX, I/Q imbalanced TX with ideal RX, and joint I/Q imbalanced TX and RX. The ideal case was also taken into consideration for comparison and the derived analytic results were validated through extensive comparisons with respective results from computer simulations. It was shown that in single-carrier systems the performance degradation caused by IQI in one or both of the RF front-end is more significant than in multi-carrier systems when $q = 0$, while by far the most challenging case is when $q = 1$ in multi-carrier system, in particular in case of RX or joint TX/RX IQI. Furthermore, it was observed in all cases that IQI introduces significant effects that result to non-negligible outage probability degradations whereas an lower bound on the outage probability was observed in the high SNR

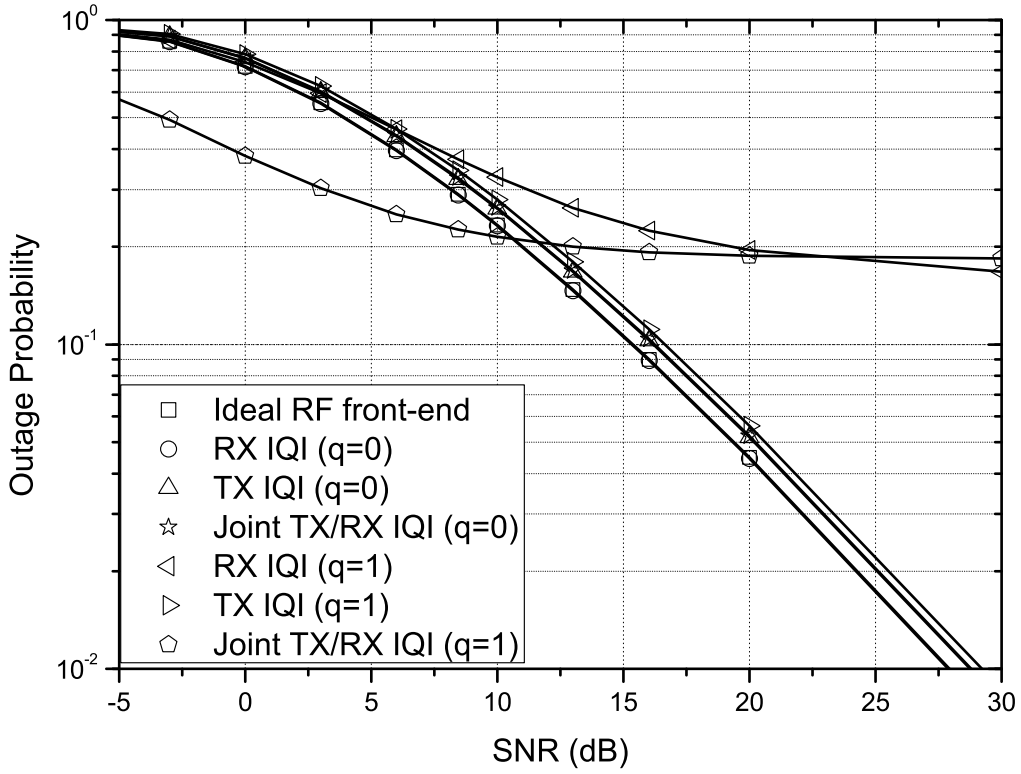

Figure 5.8 Multi-carrier system P_{out} as a function of the normalized outage SNR when $m = \{1, 1\}$, IRR = 20 dB, and $\phi = 3^o$.

regime. Additionally, it was shown that the effect of cascaded fading conditions on the outage probability performance are significant as the number of scatterers along with the involved severity of fading can increase or decrease the corresponding performance by about an order of magnitude at both low and high SNR regimes. Finally, the validity and practical usefulness of the offered results were verified by applying them in realistic wireless applications in the context of vehicle-to-vehicle communications over cascaded fading channels providing meaningful insights on the performance of such systems.

Chapter 6

Spectrum sensing in full duplex cognitive radio networks under IQI

This chapter is devoted to quantify and evaluate the effects of IQI in single- and multi-channel EDs operating in FD mode, under both cooperative and non-cooperative spectrum sensing scenarios. In this context, closed-form expressions are derived for the false alarm and detection probabilities in the general case, where partial SIS and joint TX and RX IQI, are considered. Furthermore, simplified closed form expressions for the special cases, where either the RF front-end is ideal or the SIS technique is perfect, are also presented. The presented analytical results have been verified through extensive simulations and indicate that the IQI and partial SIS can significantly affect spectrum sensing accuracy in FD-based CRNs. Specifically, if ideal RF front-end is assumed, spectrum sensing error can significantly increase, leading to a reduction in the CRN performance and negatively affect the performance of primary (PR) networks. Hence, when designing spectrum sharing algorithms for FD-based CRNs, the hardware impairments should be considered in order to improve the CRN performance, while minimizing the negative effects on PR users.

The results of the research presented in this chapter are included in [377, 378].

6.1 Introduction to spectrum sensing in full duplex cognitive radio networks

The rapid growth of wireless communications and the foreseen spectrum occupancy problems have inspired the evolution of the concept of CR [248]. As a result, CR have recently been adopted in several wireless communication standards, such as LTE [480], wireless fidelity (WiFi-IEEE 802.11), Zigbee (IEEE 802.15.4), and worldwide interoperability for microwave access (WiMAX-IEEE 802.16) [481]. In traditional CR scenarios, the transceivers operate in HD mode, i.e., at a given time interval, they can either transmit or receive/sense, but not both. However, the feasibility of enabling FD CR communications (i.e., transmit and receive/sense simultaneously over the same frequency channel) has been recently demonstrated by combining traditional and novel SIS techniques [482].

One essential functionality in the operation of CRs, whether they operate in HD or FD mode, is spectrum sensing (identifying temporarily vacant portions of spectrum). As a consequence, a great deal of effort was put in deriving optimal, sub-optimal, ad-hoc and cooperative techniques, as well as analyzing their spectrum sensing capabilities [247, 251, 251, 257, 260, 262, 483, 484]. Most of these works assumed ideal RF front-end for the CR transceivers. However, practical CR devices suffer from hardware imperfections, such as LNA non-linearities [485], local oscillator phase noise [404], and IQI [465, 466]. Particularly, IQI ultimately leads to imperfect image rejection that incurs considerable performance degradation [299, 319, 466].

6.2 Related work

In the context of CRs, several studies have shown that these imperfections restrict the spectrum sensing capabilities of HD CR systems [277–279, 360, 417, 485–488]. More specifically, in [279], the authors demonstrated the negative effects of IQI on spectrum sensing, considering both cases of single- and multi-channel SU direct-conversion RX. In [488], closed form expressions for the detection and false alarm probabilities for the Neyman-Pearson detector were presented, considering the spectrum sensing problem in single-channel OFDM CR system, under joint TX and RX IQI. On the other hand, the effects of transmit hardware imperfections in PU-SU BS cooperative FD CR systems was investigated in [489],

where the problem of interest was to find the achievable primary-cognitive rate region by studying the cognitive rate maximization problem. Nonetheless, in that work, the effects of transmit hardware impairments were approximated as a complex Gaussian process, while the effects of RX RF imperfections were neglected; as a result, the impact of RF impairments in the spectrum sensing capabilities of the CR devises was not taken into consideration. In summary, several communication protocols and mechanisms have been proposed for CRNs. However, most of them did not consider the effects of hardware impairments, which can severely degrade the CRNs performance.

6.3 Contribution

In this chapter, we study the joint impact of the RF impairments and partial SIS on the CR device's spectrum sensing capability. Specifically, the contribution of this chapter can be summarized as follows:

- Signal models that describe the joint effects of IQI and partial SIS, are presented, for single- and multi-channel EDs.
- The analytical framework to evaluate the false alarm and the detection probabilities of both single- and multi-channel EDs, which are constrained by hardware imperfections for FD-based CR systems, is derived.
- Based on the offered expressions for the false alarm and detection probabilities, the spectrum sensing capabilities of the I/Q imbalanced FD-based CRs with the ideal RF front-end FD CRs and the corresponding HD system, are compared.
- The analysis is extended in the case of cooperative sensing, where each SU has different IQI and SIS capabilities levels. Each SU independently senses each PR channel, estimates whether it is busy or idle, and reports its estimation to the other SUs. Then, each SU decides the availability of the sensed channel using the AND, the OR, or the MAJORITY rule to combine the SUs' estimations.
- Finally, to demonstrate the detrimental effects of IQI and partial SIS, several examples of false alarm/detection probabilities and ROC are demonstrated for different SIS and IQI levels.

6.4 Organization

The rest of the chapter is organized as follows. The system and signal models for both single- and multi-channel EDs, when the transceivers suffer from IQI and partial SIS, are presented in Section 6.5. The analytical framework for evaluating the false alarm and detection probabilities are provided in Section 6.6, while in Section 6.7, the analysis is extended in the case of cooperative sensing. Numerical and simulation results that verify the analysis and illustrate the detrimental effects of IQI and partial SIS, are presented in Section 6.8. Finally, Section 6.9 concludes the paper by summarizing its main contribution.

6.5 System and signal model

As demonstrated in Fig. 6.1, we consider a CRN, which consists of several PUs and the CR devices operate in FD mode. Each SU CR device is considered to be a low-cost transceiver that suffer from joint TX/RX IQI. Furthermore, it is assumed that each SU, i, has partial SIS capability, measured by the degree of SIS ($a_i \in [0, 1]$). Note that if $a_i = 0$, the SU has complete SIS capability. We assume that interference between SU links are resolved by implementing an appropriate multiple access scheme (see for example [490, 491]). Moreover, for both scenarios of single- and multi-channel EDs, for simplicity and without any loss of generality, we ignore the path loss between the SU's TX and its RX at the same node, i.e., $h_{ii} = 1$. The channel gain between the TX i and RX j at distance d_{ij} is

$$h_{ij} = C d_{i,j}^{n}, \tag{6.1}$$

where C is a frequency dependent constant and n is the path-loss exponent.

The remainder of this section is organized as follows. In Section 6.5.1, the signal model for the single-channel ED is given, while in Section 6.5.2, the signal model for the multi-channel ED is presented.

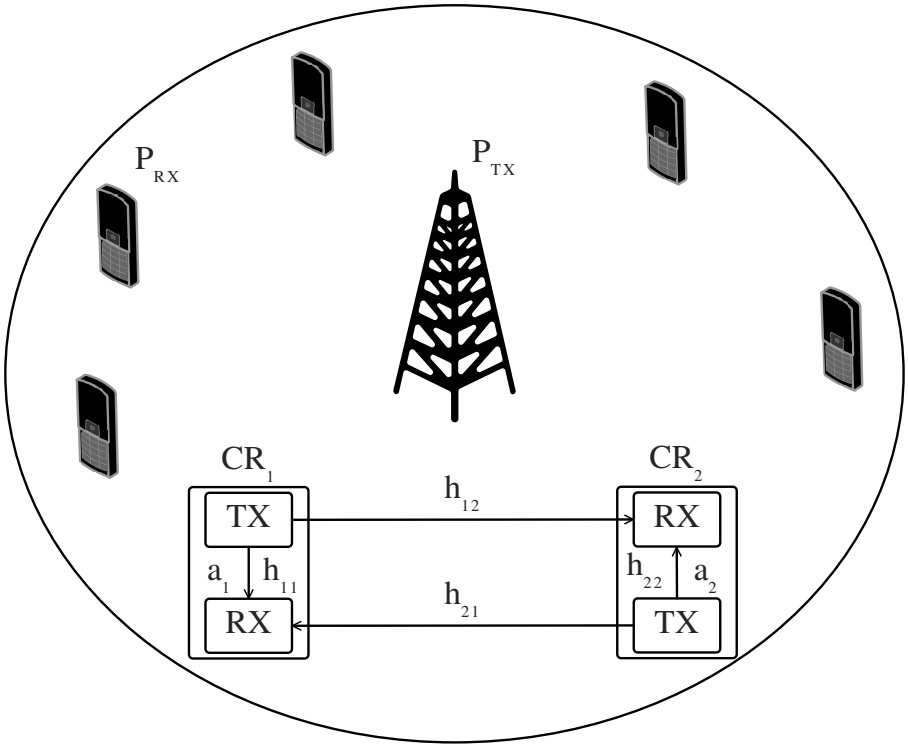

Figure 6.1 A SU link that opportunistically accesses the spectrum of a PR network.

6.5.1 Single-channel energy detector

Note that sensing only one particular frequency channel at a time is a rather limited scenario in general CR and spectrum sensing context [279]. However, for completeness, we analyze the impact of IQI and partial SIS on the spectrum sensing performance of a single-channel ED.

Two hypotheses of PU absent/present can be determined through the parameter $\theta \in \{0, 1\}$. For a given θ, the $n-$th sample of the received baseband equivalent signal for the SU i in case of single-channel EDs, can be expressed as

$$y_i(n) = \theta x_i(n) + a_i s_i(n) + w_i, \tag{6.2}$$

where $x_i(n)$, $s_i(n)$ and $w_i(n)$ are respectively the $n-$th sample of the I/Q imbalanced received PU signal by the i-th SU, the I/Q imbalanced received signal due to the SU's own transmission before applying SIS, and the I/Q imbalanced noise, given by [320]

$$x_i(n) = K_{1,i}^r x_{\mathrm{id},i}(n) + K_{2,i}^r x_{\mathrm{id},i}^*(n), \tag{6.3}$$

$$s_i(n) = \xi_{1,i} s_{\mathrm{id},i} + \xi_{2,i} s_{\mathrm{id},i}^* \tag{6.4}$$

and

$$w_i(n) = K_{1,i}^r w_{\mathrm{id},i}(n) + K_{2,i}^r w_{\mathrm{id},i}^*(n), \tag{6.5}$$

where $x_{\mathrm{id},i}(n)$, $s_{\mathrm{id},i}(n)$ and $w_{\mathrm{id},i}(n)$ are respectively the circularly symmetric complex white Gaussian (CSCWG) processes that models the received PU signal[1], the received signal due to the SU's own

[1]This is a generally accepted assumption in case of vector representation of signal, where the signals can be characterized by complex random variables. In this case, the real and imaginary part of the signal are normally distributed; hence, the complex signal can be modeled as a zero-mean complex Gaussian variable. Furthermore, since the real and imaginary part of the signal can be assumed statistically independent and have equal variance, the signals are circularly symmetric complex Gaussian. Note that this assumption was employed in several published works, such as in [279, 492] and [277].

transmission before applying SIS and the received noise, when ideal RF front-end is considered. The parameters $\xi_{1,i}$ and $\xi_{2,i}$ model the joint effect of TX/RX IQI and can be obtained as

$$\xi_{1,i} = K^r_{1,i}K^t_{1,i} + K^r_{2,i}\left(K^t_{2,i}\right)^*, \tag{6.6}$$

and

$$\xi_{2,i} = K^r_{1,i}K^t_{2,i} + \left(K^t_{1,i}\right)^* K^r_{2,i}, \tag{6.7}$$

where $K^t_{1,i}$, $K^t_{2,i}$, and $K^r_{1,i}$, $K^r_{2,i}$ stand for the TX and the RX IQI coefficients, which, according to (4.6), (4.7), (4.15) and (4.16) are given by

$$K^t_{1,i} = \frac{1+\epsilon^t_i e^{j\phi^t_i}}{2}, \quad K^t_{2,i} = \frac{1-\epsilon^t_i e^{-j\phi^t_i}}{2}, \tag{6.8}$$

$$K^r_{1,i} = \frac{1+\epsilon^r_i e^{-j\phi^r_i}}{2}, \quad K^r_{2,i} = \frac{1-\epsilon^r_i e^{j\phi^r_i}}{2}, \tag{6.9}$$

with $\epsilon^{t/r}_i$ and $\phi^{t/r}_i$ denoting the amplitude and phase imbalance at the $i-$th TX/RX. Note that the IQI coefficients are connected through the following relation

$$K^{t/r}_{1,i} = 1 - \left(K^{t/r}_{2,i}\right)^*. \tag{6.10}$$

Let IRR be the image rejection ratio that is given by

$$\mathrm{IRR}^{t/r}_i = \frac{\left|K^{t/r}_{1,i}\right|^2}{\left|K^{t/r}_{2,i}\right|^2}. \tag{6.11}$$

Note, that for practical transceivers IRR is in the range of $[20, 40$ dB] [299, 307, 314, 321, 367, 374–376, 382, 383].

By substituting (6.10) into (6.6) and (6.7), and after some algebraic manipulations, we show that

$$\xi_{1,i} = 1 - \xi^*_{2,i}. \tag{6.12}$$

It is important to note that according to (6.2)–(6.5), the received signal at the $i-$th SU, y_i, is not only interfered by the transmitted signal $s_{\mathrm{id},i}$, but it is also interfered by the signals $s^*_{\mathrm{id},i}$ and $x^*_{\mathrm{id},i}$, due to the effects of IQI. Moreover, based on the received signal model in (6.2), the sensing channel is either vacant with only channel noise or occupied by a PU signal together with the channel noise.

6.5.2 Multi-channel energy detector

In the case of multi-channel ED, we assume that $2K$ RF channels, denoted as

$$S_K = \{-K, \cdots, -1, 1, \cdots, K\}, \tag{6.13}$$

are down-converted to baseband using the wideband direct-conversion principle. This scenario was also considered in [279], where the sensitivity of wideband energy detection in HD CR systems was illustrated.

The baseband equivalent received signal model for an arbitrary channel $k \in S_K$ at the $i-$th SU is given by

$$\begin{aligned} y_{i,k}(n) = {} & \theta_k K^r_{1,i}x_{i,k}(n) + \theta_{-k}K^r_{2,i}x^*_{i,-k}(n) + \tilde{\theta}_k a_i \xi_{1,i}s_{i,k}(n) + \tilde{\theta}_{-k}a_i\xi_{2,i}s^*_{i,-k}(n) \\ & + K^r_{1,i}w_{i,k}(n) + K^r_{2,i}w^*_{i,-k}(n), \end{aligned} \tag{6.14}$$

where $x_{i,k}(n)$, $s_{i,k}(n)$ and $w_{i,k}(n)$ are zero-mean CSCWG processes with variances $\sigma^2_{x_{i,k}}$, $\sigma^2_{s_{i,k}}$ and $\sigma^2_{w_{i,k}}$, respectively, which represent the ideal received PU signal, the ideal received signal due to the SU's own transmission before applying SIS, and the received noise over channel k sampled at time instant n. The parameters $\theta_k \in \{0, 1\}$ and $\tilde{\theta}_k \in \{0, 1\}$ indicate the existence of a PU signal and a transmitted signal at channel k.

From (6.14), it is evident that the received signal at the arbitrary channel k at the $i-$th SU, $y_{i,k}$, may not only interfered by the transmitted signal at the channel k, $s_{i,k}$, but it may also interfered by the transmitted signal at channel $-k$, $s^*_{i,-k}$, due to the joint effects of IQI and partial SIS, as well as the received signal at channel $-k$, $x^*_{i,-k}$, due to the effects of IQI. The levels of interference depends on the levels of IQI and the degree of SIS, as well as the existence of PU and SU activities at channels k and $-k$.

6.6 False alarm and detection probabilities

In this section, we present closed form expressions to evaluate the false alarm and detection probabilities of hardware constrained EDs. Specifically, in Sections 6.6.1 and 6.6.2, we study the single- and multi-channel ED cases, respectively.

6.6.1 Single-channel energy detector

In the case of single-channel ED, we assume that the SU employs the classical ED, where the test statistics is evaluated according to [277] as

$$T_i = \frac{1}{N_s} \sum_{n=0}^{N_s-1} \left| y_i(n) \right|^2 . \tag{6.15}$$

In (6.15), N_s is the number of complex samples used for spectrum sensing. This test statistics are compared against a given threshold, γ, to decide whether the channel is busy or idle, i.e., if $T_i < \gamma$, the ED decides that the channel is idle, otherwise is busy.

In the propositions and special cases that follows, we evaluate the cumulative distribution function (CDF) of the test statistics for the general case, where the CR devices suffer from the joint effects of TX/RX IQI and the SIS is partial. We also consider the special cases of ideal TX and RX RF front-ends and perfect SIS.

Proposition 6.1. *The distribution of the energy test statistics conditional to θ, when the SU has partial SIS and suffers from IQI, for a sufficient large number of samples (N_s) can be well approximated by a Gaussian distribution with CDF*

$$F\left(\gamma \left| \theta \right.\right) = 1 - Q\left(\frac{\gamma - \mu_\theta}{\sqrt{\sigma_\theta^2}} \right), \tag{6.16}$$

where μ_θ and σ_θ^2 stand for the mean and variance of the test statistics, and are given by

$$\mu_\theta = \left(\left| K_{1,i}^r \right|^2 + \left| K_{2,i}^r \right|^2 \right) \left(\theta \sigma_{x_{\mathrm{id}}}^2 + \sigma_{w_{\mathrm{id}}}^2 \right) + a_i^2 \left(\left| \xi_{1,i} \right|^2 + \left| \xi_{2,i} \right|^2 \right) \sigma_{s,\mathrm{id}}^2, \tag{6.17}$$

and

$$\sigma_\theta^2 = \frac{2\theta k_r \sigma_{x_{\mathrm{id},i}}^4 + 2a_i^4 k_{t,r} \sigma_{s_{\mathrm{id},i}}^4 + 2k_r \sigma_{w_{\mathrm{id},i}}^4 + \theta k_{xw} \sigma_{x_{\mathrm{id}}}^2 \sigma_{w_{\mathrm{id}}}^2 + k_{xsw} \left(\theta \sigma_{x_{\mathrm{id}}}^2 + \sigma_{w_{\mathrm{id}}}^2 \right) a_i^2 \sigma_{s_{\mathrm{id}}}^2 - \mu_\theta^2}{N_s}, \tag{6.18}$$

where

$$k_r = \left| K_{1,i}^r \right|^4 + \left| K_{2,i}^r \right|^4 + 6 \left| K_{1,i}^r \right|^2 \left| K_{2,i}^r \right|^2 + 2\Re\{K_{1,i}^r\}^2 \Im\{K_{1,i}^r\}^2 + 2\Re\{K_{2,i}^r\}^2 \Im\{K_{2,i}^r\}^2, \tag{6.19}$$

$$k_{tr} = \left| \xi_{1,i}^r \right|^4 + \left| \xi_{2,i}^r \right|^4 + 6 \left| \xi_{1,i}^r \right|^2 \left| \xi_{2,i}^r \right|^2 + 2\Re\{\xi_{1,i}^r\}^2 \Im\{\xi_{1,i}^r\}^2 + 2\Re\{\xi_{2,i}^r\}^2 \Im\{\xi_{2,i}^r\}^2, \tag{6.20}$$

$$k_{xw} = \left(\left(2\Re\left\{ K_{1,i}^r \right\} - 1 \right)^2 + 4\Im\left\{ K_{1,i}^r \right\}^2 \right)^2 + 2 \left(\left| K_{1,i}^r \right|^2 + \left| K_{2,i}^r \right|^2 \right)^2 + 1, \tag{6.21}$$

and

$$\begin{aligned} k_{xsw} = & \left(\left(2\Re\left\{ K_{1,i}^r \right\} - 1 \right)^2 + 4\Im\left\{ K_{1,i}^r \right\}^2 \right) \left(\left(2\Re\left\{ \xi_{1,i} \right\} - 1 \right)^2 + 4\Im\left\{ \xi_{1,i} \right\}^2 \right) \\ & + 2 \left(\left| K_{1,i}^r \right|^2 + \left| K_{2,i}^r \right|^2 \right) \left(\left| \xi_{1,i} \right|^2 + \left| \xi_{2,i} \right|^2 \right) + 1. \end{aligned} \tag{6.22}$$

Proof. Please refer to the Appendix C. ■

Note that the exact distribution of the test statistics is rather complicated because of the dependency between the random variables ($\Re\{y_i\}$ and $\Im\{y_i\}$), due to the effects of IQI.

Using now the derived distribution for the test statistics, the false alarm and the detection probabilities, when the SU has partial SIS and suffers from IQI, can be computed as

$$P_{\mathrm{fa}} = P_r\left(T > \gamma \left| \theta = 0 \right. \right) = Q\left(\frac{\gamma - \mu_0}{\sqrt{\sigma_0^2}} \right) \tag{6.23}$$

and

$$P_{\mathrm{d}} = P_r\left(T > \gamma \,|\theta = 1\right) = \mathrm{Q}\left(\frac{\gamma - \mu_1}{\sqrt{\sigma_1^2}}\right). \tag{6.24}$$

For a target false alarm probability, $\tilde{P}_{\mathrm{fa}}$, the energy threshold can be evaluated using (6.23), which yields

$$\tilde{\gamma} = \sqrt{\sigma_0^2}\,\mathrm{Q}^{-1}\left(\tilde{P}_{\mathrm{fa}}\right) + \mu_0, \tag{6.25}$$

while in this case the detection probability, based on (6.24), is given by

$$\tilde{P}_{\mathrm{d}} = \mathrm{Q}\left(\frac{\sqrt{\sigma_0^2}\,\mathrm{Q}^{-1}\left(\tilde{P}_{\mathrm{fa}}\right) + \mu_0 - \mu_1}{\sqrt{\sigma_1^2}}\right). \tag{6.26}$$

6.6.1.1 Special Case 1 (Partial SIS and ideal TX/RX front-end)

In the case of partial SIS and ideal TX/RX RF front-end, $K_{1,i}^t = K_{1,i}^r = 1$, $K_{2,i}^t = K_{2,i}^r = 0$, and consequently $\xi_{1,i} = 1$ and $\xi_{2,i} = 0$. Hence, based on (6.19)–(6.22), $k_r = k_{tr} = 1$ and $k_{xw} = k_{xsw} = 4$. Substituting these values in (6.17) and (6.18), and after some algebraic manipulations, we see that the mean and the variance of the SU received signal are respectively given by

$$\mu_\theta^2 = \theta\sigma_{x_{\mathrm{id}}}^2 + a_i^2\sigma_{s,\mathrm{id}}^2 + \sigma_{w_{\mathrm{id}}}^2 \tag{6.27}$$

and

$$\sigma_\theta^2 = \frac{\mu_\theta^2}{N_s}. \tag{6.28}$$

Proposition 6.2. *In case of ideal RF front-end and partial SIS, the test statistics conditional to θ follows chi-square distribution with $2N_s$ degrees of freedom and a CDF given by*

$$F\left(x\,|\theta\right) = \frac{\gamma\left(N_s, \frac{N_s x}{2\sigma^2_{y_{i|\theta}}}\right)}{\Gamma\left(N_s\right)}, \tag{6.29}$$

where $\sigma^2_{y_{i|\theta}}$ is the variance of y_i obtained by

$$\sigma^2_{y_{i|\theta}} = E\left[\left|y_{i|\theta}\right|^2\right] = \theta\sigma^2_{x_{id}} + a_i^2\sigma^2_{s_{id}} + \sigma^2_{w_{id}}. \tag{6.30}$$

Proof. Please refer to the Appendix D. ■

6.6.1.2 Special Case 2 (Perfect SIS and ideal TX/RX front-end)

In the case of perfect SIS and ideal TX/RX SU RF front-end, $K_{1,i}^t = K_{1,i}^r = \xi_{1,i} = 1$, $K_{2,i}^t = K_{2,i}^r = \xi_{2,i} = 0$ and $a_i = 0$. Substituting these values in (6.17) and (6.18), we prove that the mean and the variance of the SU received signal are respectively given by

$$\mu_\theta^2 = \theta\sigma_{x_{\mathrm{id}}}^2 + \sigma_{w_{\mathrm{id}}}^2 \tag{6.31}$$

and

$$\sigma_\theta^2 = \frac{\mu_\theta^2}{N_s}. \tag{6.32}$$

Note that (6.31) and (6.32) coincide with [279, Eq. (3)], which refers to an ideal RF front-end HD CR system. In other words, in case of ideal RF front-end transceivers, regardless of whether the system operates in HD or FD mode with perfect SIS, the EDs achieve the same spectrum sensing capabilities.

6.6.1.3 Special Case 3 (Partial SIS and joint TX/RX IQI)

In the case of perfect SIS ($a_i = 0$) and joint TX/RX IQI, the mean and the variance of the SU received signal are respectively given by

$$\mu_\theta^2 = \left(\left|K_{1,i}^r\right|^2 + \left|K_{2,i}^r\right|^2\right)\left(\theta\sigma_{x_{\mathrm{id}}}^2 + \sigma_{w_{\mathrm{id}}}^2\right), \tag{6.33}$$

and

$$\sigma_\theta^2 = \frac{2\theta k_r \sigma_{x_{\mathrm{id},i}}^4 + 2k_r\sigma_{w_{\mathrm{id},i}}^4 + \theta k_{xw}\sigma_{x_{\mathrm{id}}}^2\sigma_{w_{\mathrm{id}}}^2 - \mu_\theta^2}{N_s}. \tag{6.34}$$

6.6.2 Multi-channel energy detector

In the case of multi-channel ED, we assume that each SU employs the classical wideband ED, which calculates the test statistics at each channel k according to

$$T_{i,k} = \frac{1}{N_s}\sum_{n=0}^{N_s-1}\left|y_{i,k}(n)\right|^2. \tag{6.35}$$

Note that $T_{i,k}$ is compared against a threshold (γ) to decide whether the channel is busy or idle.

In the proposition that follows, we evaluate the CDF of the test statistics for the general case, where the CR devices suffer from the joint effects of TX/RX IQI and the SIS is partial.

Proposition 6.3. *The distribution of the energy test statistics conditional to* $\Theta = \left\{\theta_{-k}, \theta_k, \tilde{\theta}_{-k}, \tilde{\theta}_{-k}\right\}$, *when the SU has partial SIS and suffers from IQI, for a sufficient large number of samples* (N_s), *is Gaussian with CDF*

$$F\left(\gamma\left|\Theta\right.\right) = 1 - Q\left(\frac{\gamma - \mu_\Theta}{\sqrt{\sigma_\Theta^2}}\right), \tag{6.36}$$

where μ_Θ *and* σ_Θ^2 *denote the mean and the variance of the test statistics, respectively, which are respectively obtained as*

$$\begin{aligned}\mu_\Theta = {} & \theta_k\left|K_{1,i}^r\right|^2\sigma_{x_{i,k}}^2 + \theta_{-k}\left|K_{2,i}^r\right|^2\sigma_{x_{i,-k}}^2 + \tilde{\theta}_k a_i^2\left|\xi_{1,i}\right|^2\sigma_{s_{i,k}}^2 + \tilde{\theta}_{-k}a_i^2\left|\xi_{2,i}\right|^2\sigma_{s_{i,-k}}^2 \\ & + \left|K_{1,i}^r\right|^2\sigma_{w_{i,k}}^2 + \left|K_{2,i}^r\right|^2\sigma_{w_{i,-k}}^2.\end{aligned} \tag{6.37}$$

and

$$\begin{aligned}\sigma_\Theta^2 = \frac{1}{N_s}\Big(& 2\theta_k\left|K_{1,i}^r\right|^4\sigma_{x_{i,k}}^4 + 2\theta_{-k}\left|K_{2,i}^r\right|^4\sigma_{x_{i,-k}}^4 + 2\theta_k\theta_{-k}\left(\left|K_{1,i}^r\right|^2\left|K_{2,i}^r\right|^2 + \alpha^2 + \beta^2\right)\sigma_{x_{i,k}}^2\sigma_{x_{i,-k}}^2 \\ & + 2\tilde{\theta}_k a_i^4\left|xi_{1,i}\right|^4\sigma_{s_{i,k}}^4 + 2\tilde{\theta}_{-k}a_i^4\left|\xi_{2,i}\right|^4\sigma_{s_{i,-k}}^4 + 2\tilde{\theta}_k\tilde{\theta}_{-k}a_i^4\left(\left|\xi_{1,i}\right|^2\left|\xi_{2,i}\right|^2 + \delta^2 + \zeta^2\right)\sigma_{s_{i,k}}^2\sigma_{s_{i,-k}}^2 \\ & + 2\left|K_{1,i}^r\right|^4\sigma_{w_{i,k}}^4 + 2\left|K_{2,i}^r\right|^4\sigma_{w_{i,-k}}^4 + 2\left(\left|K_{1,i}^r\right|^2\left|K_{2,i}^r\right|^2 + \alpha^2 + \beta^2\right)\sigma_{w_{i,k}}^2\sigma_{w_{i,-k}}^2 \\ & + 2a_i^2\left(\theta_k\left|K_{1,i}^r\right|^2\sigma_{x_{k,i}}^2 + \theta_{-k}\left|K_{2,i}^r\right|^2\sigma_{x_{-k,i}}^2\right)\left(\tilde{\theta}_k\left|\xi_{1,i}\right|^2\sigma_{s_{k,i}}^2 + \tilde{\theta}_{-k}\left|\xi_{2,i}\right|^2\sigma_{s_{-k,i}}^2\right) \\ & + 2\left(\theta_k\left|K_{1,i}^r\right|^2\sigma_{x_{k,i}}^2 + \theta_{-k}\left|K_{2,i}^r\right|^2\sigma_{x_{-k,i}}^2\right)\left(\left|K_{1,i}^r\right|^2\sigma_{w_{k,i}}^2 + \left|K_{2,i}^r\right|^2\sigma_{w_{-k,i}}^2\right) \\ & + 2a_i^2\left(\tilde{\theta}_k\left|\xi_{1,i}\right|^2\sigma_{s_{k,i}}^2 + \tilde{\theta}_{-k}\left|\xi_{2,i}\right|^2\sigma_{s_{-k,i}}^2\right)\left(\left|K_{1,i}^r\right|^2\sigma_{w_{k,i}}^2 + \left|K_{2,i}^r\right|^2\sigma_{w_{-k,i}}^2\right) - \mu_\Theta^2\Big).\end{aligned} \tag{6.38}$$

Note that α, β, δ *and* ζ *in* (6.38) *are as follows*

$$\alpha = \Re\{K_{1,i}^r\}\Re\{K_{2,i}^r\} + \Im\{K_{1,i}^r\}\Im\{K_{2,i}^r\}, \tag{6.39}$$

$$\beta = \Re\{K_{1,i}^r\}\Im\{K_{2,i}^r\} + \Im\{K_{1,i}^r\}\Re\{K_{2,i}^r\}, \tag{6.40}$$

$$\delta = \Re\{\xi_{1,i}\}\Re\{\xi_{2,i}\} + \Im\{\xi_{1,i}\}\Im\{\xi_{2,i}\}, \tag{6.41}$$

and

$$\zeta = \Re\{\xi_{1,i}\}\Im\{\xi_{2,i}\} + \Im\{\xi_{1,i}\}\Re\{\xi_{2,i}\}. \tag{6.42}$$

Proof. Please refer to the Appendix E. ■

Using the derived expressions for the energy test statistics distribution, the conditioned to Θ false alarm and the detection probabilities, when the SU has partial SIS and suffers from IQI, can be derived by

$$P_{fa}\left(\Theta=\{\theta_{-k},\theta_k=0,\tilde{\theta}_{-k},\tilde{\theta}_k\}\right)=Q\left(\frac{\gamma-\mu_\Theta}{\sqrt{\sigma_\Theta^2}}\right), \tag{6.43}$$

and

$$P_{d}\left(\Theta=\{\theta_{-k},\theta_k=1,\tilde{\theta}_{-k},\tilde{\theta}_k\}\right)=Q\left(\frac{\gamma-\mu_\Theta}{\sqrt{\sigma_\Theta^2}}\right). \tag{6.44}$$

Moreover, by considering that the PU existence parameter at image channel θ_{-k} and the SU existence parameters at channels $-k$ and k are Bernoulli distributed for any arbitrary channels (with success parameters p_{-k}, $\tilde{p}_{-k}$ and $\tilde{p}_k$, respectively) the false alarm and detection probabilities can respectively be expressed as

$$P_{\mathcal{FA}}=\sum_{\Theta\in\{\theta_{-k},\theta_k=0,\tilde{\theta}_{-k},\tilde{\theta}_k\}}\left(\theta_{-k}p_{-k}+(1-\theta_{-k})(1-p_{-k})\right)\left(\tilde{\theta}_{-k}\tilde{p}_{-k}+\left(1-\tilde{\theta}_{-k}\right)(1-\tilde{p}_{-k})\right)$$
$$\times\left(\tilde{\theta}_k\tilde{p}_k+\left(1-\tilde{\theta}_k\right)(1-\tilde{p}_k)\right)P_{fa}(\Theta), \tag{6.45}$$

and

$$P_{\mathcal{D}}=\sum_{\Theta\in\{\theta_{-k},\theta_k=1,\tilde{\theta}_{-k},\tilde{\theta}_k\}}\left(\theta_{-k}p_{-k}+(1-\theta_{-k})(1-p_{-k})\right)\left(\tilde{\theta}_{-k}\tilde{p}_{-k}+\left(1-\tilde{\theta}_{-k}\right)(1-\tilde{p}_{-k})\right)$$
$$\times\left(\tilde{\theta}_k\tilde{p}_k+\left(1-\tilde{\theta}_k\right)(1-\tilde{p}_k)\right)P_{d}(\Theta). \tag{6.46}$$

Note that $P_{\mathcal{FA}}$ and $P_{\mathcal{D}}$ are not only affected by the level of IQI and SIS technique's capability, but they are also affected by the uncertainty of PU signal over channels k and $-k$ and the uncertainty of the transmitted signals at k and $-k$.

6.7 Cooperative sensing

As mentioned before, the operation of a CRN should address an essential issue of identifying spectrum opportunities in order to enable an efficient spectrum utilization. Several studies have focused on this issue based on spectrum sensing in a cooperative or non-cooperative manner assuming ideal RF front-end. Non-cooperative sensing is easy to implement in practical settings and its processing overhead is small. On the other hand, cooperative spectrum sensing can provide much better sensing accuracy, which might countermeasure the joint effect of IQI and partial SIS, at the expense of extra processing and control overhead [493, 494].

In this section, we extend the analysis of Section 6.6 to investigate the performance of cooperative sensing under hardware impairments. Specifically, we consider that each one of the N_{su} SUs makes a binary decision on the PU activity, and the individual decisions are reported to the other SUs over a narrow bandwidth error-free reporting channel, i.e., common control channels (CCCs) [491, 495, 496]. Note that the existence of CCC is a characteristic of many communication protocols designed for CRNs [497, 498]. We assume that the decision rule is the OR, the AND, or the MAJORITY, i.e., the presence of primary activity is decided if at least one SU, all, or the majority of the SUs individually decides that the sensing channel is busy.

In the propositions that follow, we evaluate the false alarm and detection probabilities of the CRNs for the case in which the OR, MAJORITY or the AND rule is used, and the CR devices suffer from different levels of TX/RX IQI and the SIS.

Proposition 6.4. If the OR rule is employed, then the false alarm and the detection probabilities can respectively be obtained as

$$P_{C,\text{fa}}=1-\prod_{i=1}^{N_{\text{su}}}(1-P_{\text{fa},i}) \tag{6.47}$$

and

$$P_{C,\mathrm{d}} = 1 - \prod_{i=1}^{N_{\mathrm{su}}} \left(1 - P_{\mathrm{d},i}\right), \tag{6.48}$$

where $P_{\mathrm{fa},i}$ and $P_{\mathrm{d},i}$ ($i \in \{1, \cdots, N_{\mathrm{su}}\}$) stands for the false alarm and the detection probabilities of the i-th SU.

Proof. Please refer to the Appendix F. ■

Proposition 6.5. If the AND rule is employed, then the false alarm and detection probabilities can respectively be expressed as

$$P_{C,\mathrm{fa}} = \prod_{i=1}^{N_{\mathrm{su}}} P_{\mathrm{fa},i} \tag{6.49}$$

and

$$P_{C,\mathrm{d}} = \prod_{i=1}^{N_{\mathrm{su}}} P_{\mathrm{d},i}, \tag{6.50}$$

where $P_{\mathrm{fa},i}$ and $P_{\mathrm{d},i}$ ($i \in \{1, 2\}$ stands for the false alarm and the detection probabilities of the i-th SU.

Proof. Please refer to the Appendix G. ■

Proposition 6.6. If the MAJORITY rule is employed, then the false alarm and detection probabilities can be respectively expressed as

$$P_{C,\mathrm{fa}} = \sum_{i=1}^{\mathrm{card}(\mathcal{D})} U\left(\sum_{l=1}^{N_{\mathrm{su}}} d_{l,k} - \left\lceil \frac{N_{\mathrm{su}}}{2} \right\rceil\right) \prod_{j=1}^{N_{\mathrm{su}}} \left(U\left(-d_{j,k}\right)\left(1 - P_{\mathrm{fa},j}\right) + U\left(d_{j,k} - 1\right) P_{\mathrm{fa},j}\right). \tag{6.51}$$

and

$$P_{C,\mathrm{d}} = \sum_{i=1}^{\mathrm{card}(\mathcal{D})} U\left(\sum_{l=1}^{N_{\mathrm{su}}} d_{l,k} - \left\lceil \frac{N_{\mathrm{su}}}{2} \right\rceil\right) \prod_{j=1}^{N_{\mathrm{su}}} \left(U\left(-d_{j,k}\right)\left(1 - P_{\mathrm{d},j}\right) + U\left(d_{j,k} - 1\right) P_{\mathrm{d},j}\right). \tag{6.52}$$

where $P_{\mathrm{fa},i}$ and $P_{\mathrm{d},i}$ represent the false alarm and the detection probabilities of the i-th SU, whereas $\lceil \cdot \rceil$ stand for the ceil function. Moreover,

$$\mathcal{D} = \left[d_1, d_2, \cdots, d_{N_{\mathrm{su}}}\right], \tag{6.53}$$

denotes the SUs' decision set, where $d_i = 0$ and $d_i = 1$, $i = 1, \cdots, N_{\mathrm{su}}$, stand respectively for the absence or presence of PU activity at the sensing channel.

Proof. Please refer to the Appendix H. ■

6.8 Numerical and simulation Results

In this section, we demonstrate the effects of IQI on the spectrum sensing performance of EDs by illustrating numerical and simulation results for different IQI and SIS levels. In sections 6.8.1 and 6.8.2, the joint impact of IQI and partial SIS on single- and multi-channel ED are respectively illustrated. In section 6.8.3, we demonstrate their impact in cooperative sensing systems. Finally, it should be noted that each of the reported figures contains both analytical and simulation results, which are represented by lines and discrete marks, respectively.

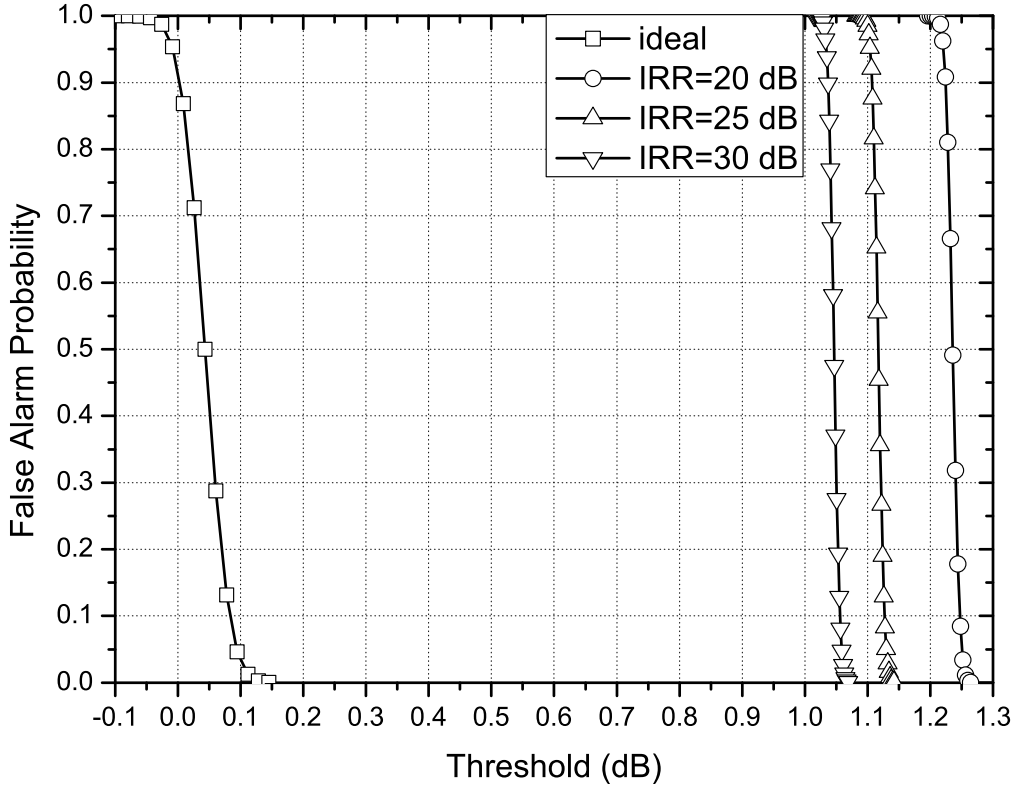

Figure 6.2 The false alarm probability as a function of the energy threshold for different values of IRR and $a_1 = a_2 = 0.01$.

6.8.1 Single-channel energy detector

In the case of single-channel ED, we consider the following insightful scenario. The SNR of the received ideal signal at the SU i, $i \in \{1, 2\}$, due to the PU activity is -15 dB, while before applying a SIS technique, the self-interference to noise ratio (INR), due to the transmission of the SU i is set to 20 dB. We assume that both TX and RX suffer from the same level of IQI and the degree of SIS is set to 0.01 (i.e., 40 dB). Furthermore, the ED is assumed to use $N_s = 8 \times 10^3$ samples.

In Fig. 6.2, the false alarm probability is plotted against the energy detection threshold, for different values of IRR. It becomes evident from this figure that the analytical results are identical with simulation results; thus, verifying the the presented analytical framework. Moreover, it is observed that as IRR decreases, the self-interference due to IQI increases; consequently, to achieve a target false alarm probability, the energy threshold should be increased. For instance, if the target false alarm probability equals 0.1, then in the case of ideal RF front-end, the energy threshold should be set to 0.085 dB. However, when a non-ideal CR device with IRR = 25 dB is considered, it should be shifted by about 0.96 dB and be set to 1.05 dB. This may not seem to be a significant shift, yet, if the effects of IQI is not taken into consideration, the false alarm probability of the system will be equal to 1. This observation indicates the importance of the derived expressions, as well as the need of taking into consideration the levels of IQI and SIS, when the energy detection threshold is selected.

Fig. 6.3 illustrates the impact of IQI in the detection performance of the FD CR devices. Specifically, the detection probability is plotted against the energy threshold for different levels of IQI. We observe that as IRR decreases, the interference, due to IQI and partial SIS, increases, and consequently, for a given energy threshold, the detection probability increases. For example, for $\gamma = 1.05$ dB and considering ideal RF front-end, the detection probability is about 0.2. On the other hand, in case of I/Q imbalanced RF front-end with IRR = 25 dB and for the same energy threshold, the detection probability equals to 1. Additionally, if the target false alarm probability is set to 0.1, then in case of ideal RF front-end the corresponding detection probability equals to 1, whereas in case of non-ideal RF front-end with IRR = 20 dB, the energy threshold should be set to 1.257 dB, and the corresponding detection

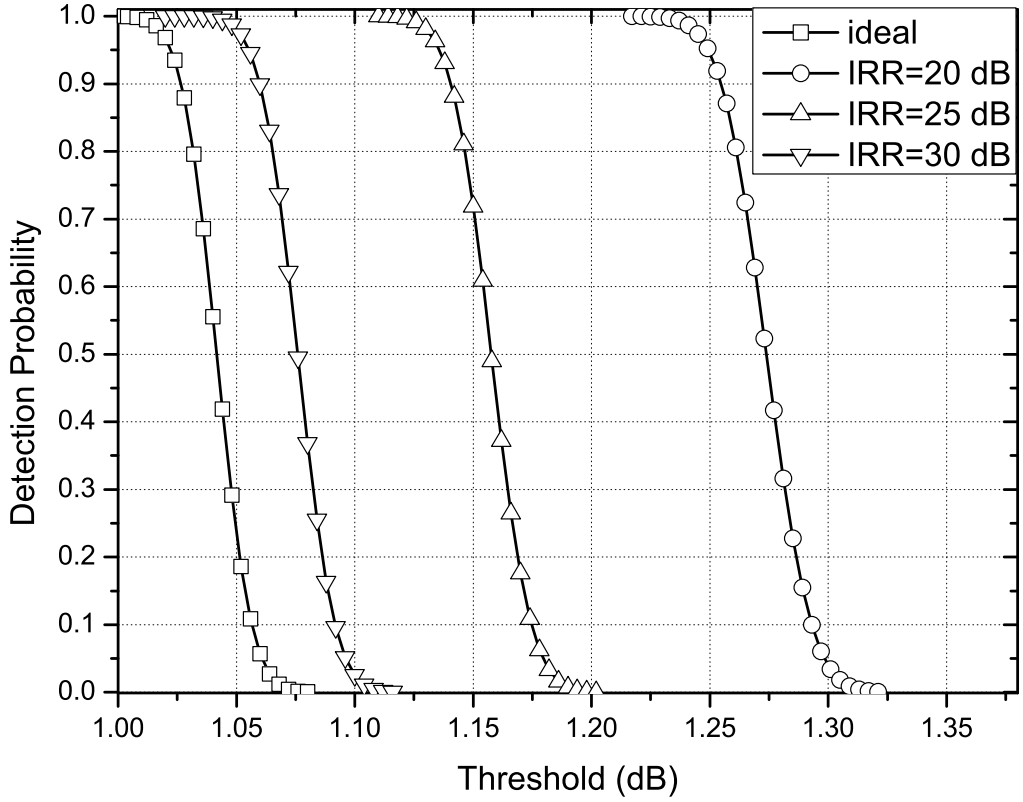

Figure 6.3 The detection probability as a function of the energy threshold for different values of IRR and $a_1 = a_2 = 0.01$.

probability is 0.87. This example indicates that the spectrum sensing capabilities of the FD CR ED are constrained due to IQI.

In Fig. 6.4, the false alarm probability is illustrated as a function of the energy detection threshold for different IRR and a values. Note that the curve referred as "ideal, $a = 0$" corresponds to special case 2, while the curves referred as "ideal, $a = 0.005$" and "ideal, $a = 0.01$" correspond to special case 1. Moreover, the curves referred as "IRR = 20 dB, $a = 0$" correspond to special case 3. It becomes evident from this figure that the analytical results presented at the special cases in Section 6.6 are identical with simulation results; thus, verifying the the presented analytical framework. Additionally, we observe that for a given IRR, as a increases the false alarm probability increases. For example, for energy threshold equal 0.99 dB, IRR = 20 dB and $a = 0$, the false alarm probability is about 0.1. However, if a increases to 0.01, the false alarm probability becomes 1. This indicates the importance of taking into consideration the impact of partial SIS, when selecting the energy threshold. Finally, by comparing the spectrum sensing performance affected by IQI and partial SIS, it becomes apparent that the impact of IQI to the spectrum sensing performance is more detrimental than the impact of partial SIS.

6.8.2 Multi-channel energy detector

In case of multi-channel ED, it is assumed that there are 8 channels and the second channel is sensed ($k = 2$). The signal and the total guard band bandwidths are assumed to be 9 MHz and 125 kHz, respectively. The noise variance for all channels is assumed to be equal to 1. Unless otherwise is stated, the SNR of the received ideal signal at the SU i, $i \in \{1, 2\}$ at $k = 2$, due to the PU activity is -15 dB, whereas the INR of the PU mirror-channel ($k = -2$) is 15 dB. We also consider that before applying any SIS technique, the INR due to the transmission of the SU i is set to 20 dB for both $k = 2$ and $k = -2$ channels. To determine the PU channel status, the ED is assumed to use $N_s = 8 \times 10^3$ samples.

In Fig. 6.5, the joint impact of IQI and partial SIS in the false alarm probability is demonstrated. Specifically, the false alarm probability against the INR caused by the activity at the image PU channel

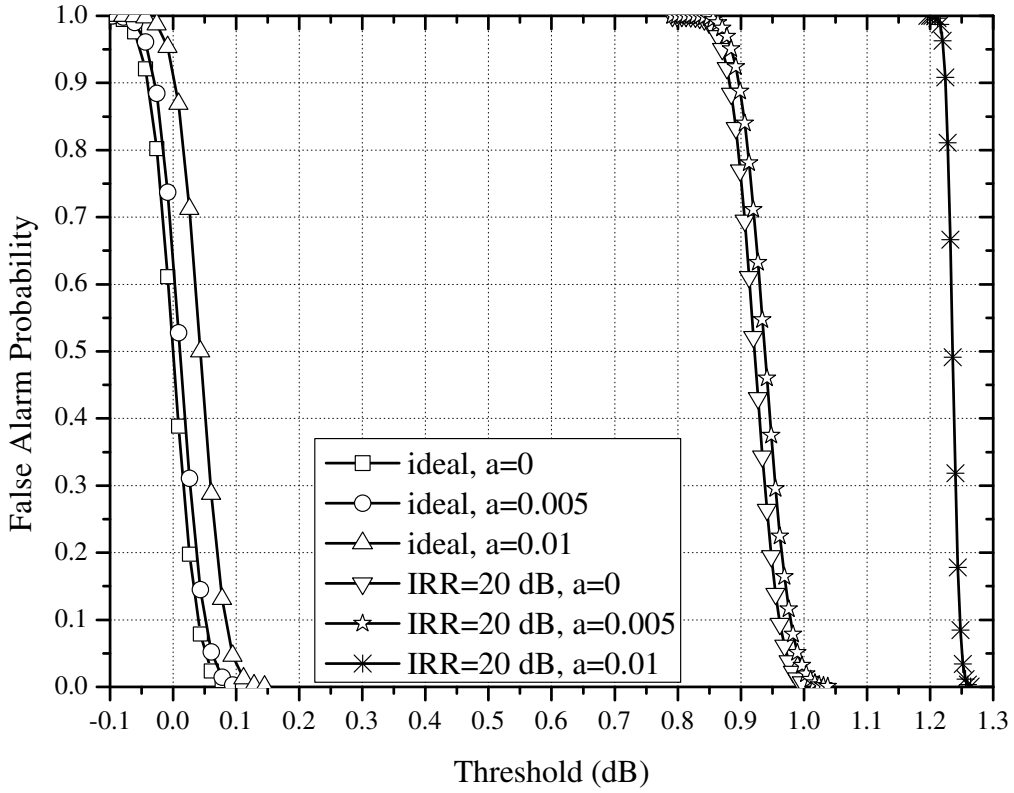

Figure 6.4 The false alarm probability as a function of the energy threshold for different values of IRR and a values.

for different values of IRR and levels of SIS, is presented in this figure, for the worst case scenario in which $\theta_{-k} = \tilde{\theta}_{-k} = \tilde{\theta}_k = 1$. Note that the energy detection threshold is set to 1.14 dB, i.e., $\gamma \approx 1.14$ dB. Furthermore, as a benchmark, we consider the ideal RF front-end case with perfect SIS and $\gamma \approx 1.14$ dB, where the false alarm probability is practically set to zero. As expected, for fixed IRR and a, as the INR from the image PU signal increases, the interference from the mirror channels increases, which consequently increases the false alarm probability. Moreover, for given a and INR from the image PU signal value, as IRR increases, the leakage from the image PU channel decreases; resulting in decreasing the false alarm alarm probability. For given IRR and INR from the image PU signal values, as a increases, the leakage from the transmitted channels k and $-k$ increases, which increases the false alarm probability. For example, for INR = 6 dB and IRR = 20 dB, the increase of a from 0.005 to 0.01 leads to about 145% increase of the false alarm probability.

In Figs. 6.6 and 6.7, the joint impact of IQI and partial SIS in the detection probability is demonstrated. Specifically, in Fig. 6.6, the detection probability is plotted against the SNR for different interference channel occupancy sets,

$$\Theta_I = [\theta_{-k}, \tilde{\theta}_k, \tilde{\theta}_{-k}], \tag{6.54}$$

when the energy detection threshold is $\gamma \approx 1.14$ dB, the level of SIS is set to -40 dB, IRR = 20 dB, $\phi = 3^o$ and the INR caused by the activity at the image PU channel is 10 dB. For each interference channel occupancy set, the corresponding false alarm probabilities are reported in the legend. As benchmarks, the detection probability of an ideal RF front-end transceiver with $a = 0$ and $a = 0.01$ are also illustrated. As expected, for a given Θ_I, as SNR increases, the detection probability increases. Furthermore, it is observed that for a given SNR, the detection probability increases as the interference increases. However, this comes with an inevitable price of increased false alarm probability and hence a dramatic decrease in the ability to identify vacant spectrum. For example, for SNR $= -20$ dB and $\Theta_I = [1, 0, 1]$, the detection and false alarm probabilities are respectively 0.5638 and 0.0146, whereas for the same SNR and $\Theta_I = [1, 1, 1]$, the detection and false alarm probabilities are 0.34902 and 0.1264, respectively. In addition, since the leakage to the sensed channel k from the transmitted signal at the channel $-k$ is

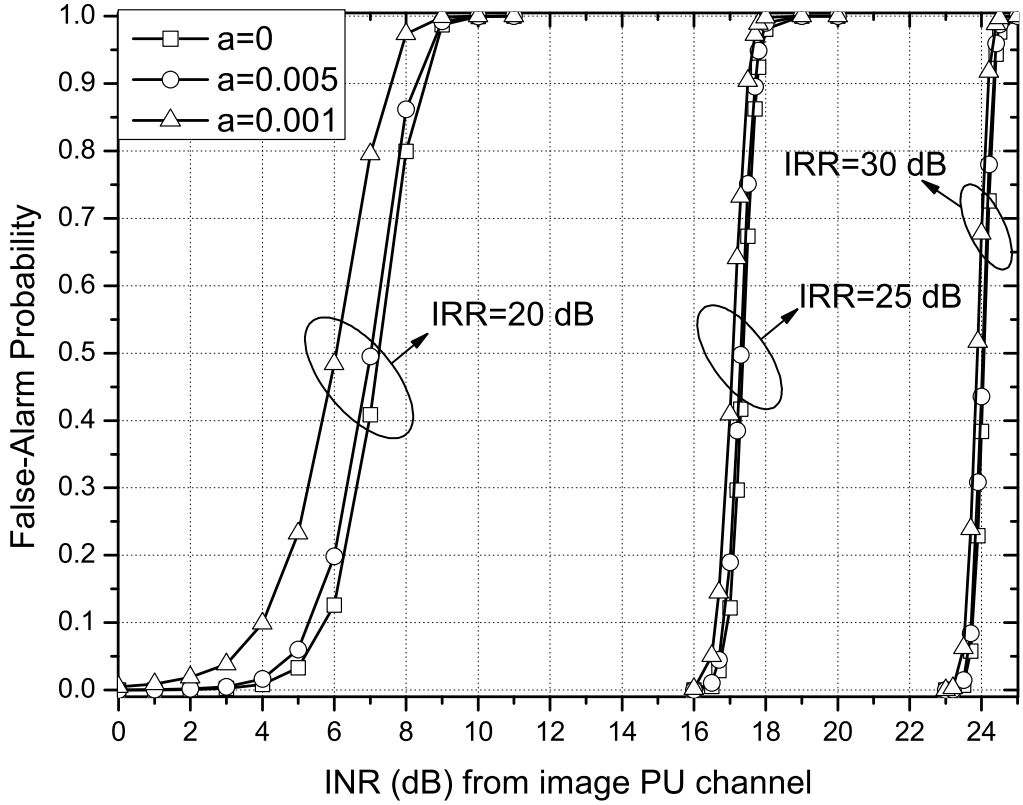

Figure 6.5 The false alarm probability as a function of the INR caused by the activity at the image PU channel for different values of IRR and levels of SIS, when $\theta_{-k} = \tilde{\theta}_{-k} = \tilde{\theta}_k = 1$.

about -20 dB due to IQI, and -40 dB due to the employed SIS technique, the signal leakage to channel k from the signal transmitted at channel $-k$ due to the joint effect of IQI and SIS is about -60 dB. Consequently, the leakage from signal transmitted at channel $-k$ do not significantly affect the spectrum sensing capabilities of the multi-channel ED.

In Fig. 6.7, the detection probability as a function of SNR for different values of $p = p_{-k} = \tilde{p}_{-k} = \tilde{p}_k$, when the energy detection threshold is $\gamma \approx 1.14$ dB, the level of SIS is set to -40 dB, IRR = 20 dB, $\phi = 3^o$, the INR caused by the activity at the image PU channel is set to 10 dB, while the INR due to the transmission of the SU at both channels k and $-k$ is set to 20 dB. For each interference channel occupancy set, the corresponding false alarm probabilities are reported in the legend. It is observed that as p increases, the probability of channel leakage from the received signal at channel k and the transmitted signals at k and $-k$ channel increases, and therefore the detection probability also increases. However, this comes at the expense of increasing the false alarm probability. Furthermore, for SNR values in the range of $[-14, -10$ dB] and a given p, the detection probability remains constant. This can be explained using Fig. 6.6, where the contributions of the channel occupancy sets $\Theta_I = [0, 1, 0]$ and $\Theta_I = [0, 1, 1]$ are observed after the -10 dB, whereas the contributions of the remaining channel occupancy sets are observed after -14 dB. Therefore, for SNR values in the range of $[-14, -10$ dB] and a given p, the detection probability remains constant.

In Fig. 6.8, ROC are presented for different values of IRR, when $p_{-k} = \tilde{p}_{-k} = \tilde{p}_k = 0.5$, $a = 0.01$, the SNR is set to -15 dB, the INR caused by the activity at the image PU channel is set to 10 dB, while the INR, due to the transmission of the SU at both channels k and $-k$, is set to 20 dB. Again the detrimental effects of IQI and partial SIS on the CR ED's spectrum sensing capabilities are observed. For example, for $P_{\text{fa}} = 0.1$ and IRR = 25 dB, the detection probability cannot exceed 0.6. However, in case of ideal RF front-end and perfect SIS, for the same P_{fa}, the detection probability is about 0.9. In other words, the joint effects of IQI and imperfect SIS result to a degradation of the order of 50%. Furthermore, it is evident that as IRR increases, the leakage from the image channels is constrained, and hence the spectrum sensing capability of the ED is improved.

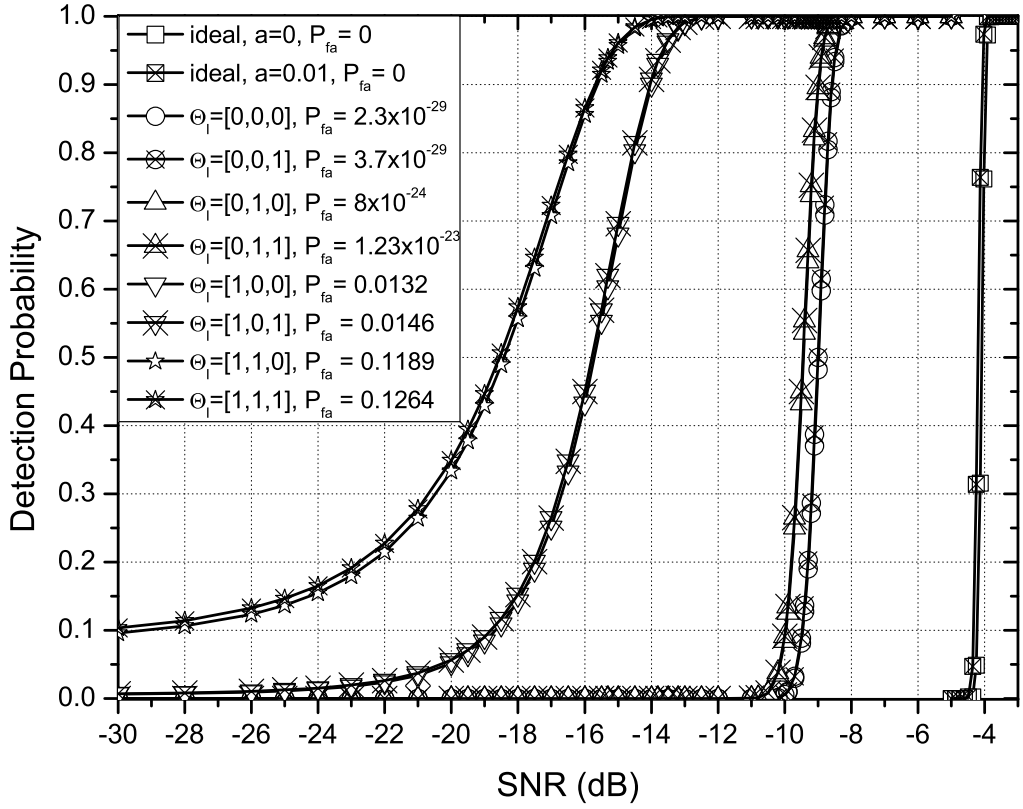

Figure 6.6 The detection probability as a function of the SNR for different $\Theta_I = [\theta_{-k}, \tilde{\theta}_k, \tilde{\theta}_{-k}]$, when IRR = 20 dB and $a = 0.01$.

6.8.3 Cooperative sensing

In the case of cooperative spectrum sensing, we consider that each one of the two SUs employs a multi-channel ED that down-converts 8 channels ($K = 8$) and senses the second one ($k = 2$). Note that in the case, where only two SUs are involved, the MAJORITY rule coincides with the AND rule. The SNR of the received ideal signal at the SU i, $i \in \{1, 2\}$ at $k = 2$, due to the PU activity is -15 dB, whereas the INR of the PU mirror-channel ($k = -2$) is 15 dB. We also consider that before applying a SIS technique, the INR due to the transmission of the SU i is set to 20 dB in both $k = 2$ and $k = -2$ channels, $p_{-k} = \tilde{p}_{-k} = \tilde{p}_k = 0.5$, and $a = 0.01$. Again, the ED of each SU is assumed to use $N_s = 8 \times 10^3$ samples.

The ROCs corresponding to this scenario are plotted in Fig. 6.9, considering that the SUs employ the AND or OR rule. As benchmarks, we also present the ideal case ROC, i.e., $IRR \to \infty$ and $a = 0$, and the ideal and non-ideal ROC, when the SUs do not use cooperative sensing. It is observed that the joint effects of IQI and partial SIS constrain the spectrum sensing capabilities for both cases of non-cooperative and cooperative sensing. For instance, for $P_{\text{fa}} = 0.1$, the detection probabilities in case of ideal RF front-end and perfect SIS in case of individual sensing, cooperative sensing using AND rule and cooperative sensing using OR rule are respectively 0.94, 0.98 and 0.99. In case of non-ideal RF front-end and partial SIS for $P_{\text{fa}} = 0.1$, the corresponding probabilities are 0.58, 0.68 and 0.75. In other words, for $P_{\text{fa}} = 0.1$, the spectrum sensing capability of the ED that uses the AND (OR) rule is reduced by 44.12% (32%), due to the effects of IQI and partial SIS. Furthermore, we observe that both the presented cooperative sensing schemes outperform the corresponding individual sensing scheme. However, the joint effects of IQI and partial SIS are so detrimental even with the use of cooperative sensing, the performance of non-ideal cooperative sensing is worse than that of the individual sensing CR system with ideal RF front-end and perfect SIS. Moreover, in case of ideal RF front-end and perfect SIS, we observe that in terms of spectrum sensing performance, systems that employ the OR rule outperforms those that employ the AND rule, irrespective of the false alarm probability range. In case of IRR = 25 dB and $a = 0.01$,

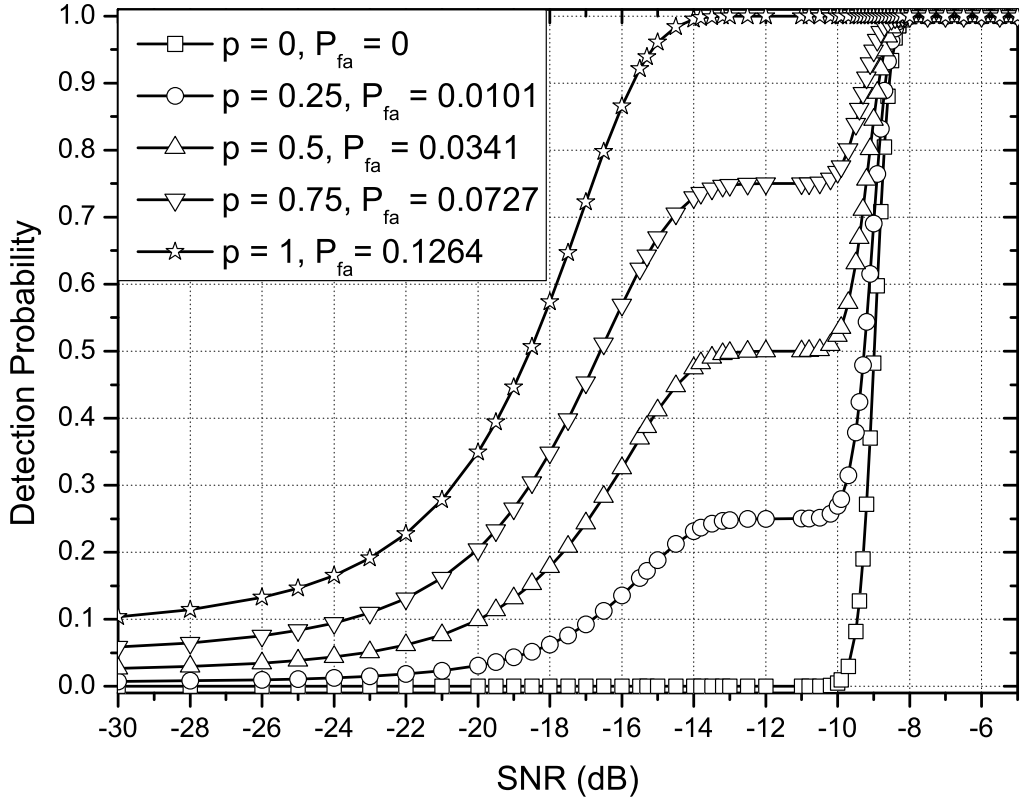

Figure 6.7 The detection probability as a function of the SNR for different values of $p = p_{-k} = \tilde{p}_{-k} = \tilde{p}_k$, when IRR = 20 dB and $a = 0.01$.

the OR rule outperforms the AND rule for $P_{\text{fa}} \in [0, 0.16941]$, whereas the AND rule outperforms the OR rule for $P_{\text{fa}} \in (0.16941, 1]$.

In Fig. 6.10, ROCs are demonstrated for different values of N_{su}, considering that the SUs employ the AND, the MAJORITY or the OR rule, and the SUs' RXs have the same IRR, which equals 30 dB. As expected, for a fixed decision rule, as N_{su} increases, the spectrum sensing capability of the EDs is improved. Moreover, it is observed that for fixed N_{su}, in the low false alarm regime, systems that employ the OR rule outperform those that employ the MAJORITY and the AND rules. However, as the requirement for low false alarm probability is relaxed, the AND rule outperforms both the MAJORITY and the OR rules. This indicates the importance of taking into consideration the N_{su}, the IQI levels, and the targeted false alarm probability, in order to select the decision rule that maximizes the spectrum sensing performance of the ED.

6.9 Conclusions

This paper investigated the spectrum sensing performance of opportunistic spectrum access (OSA) FD CR system in both single- and multi- channel EDs, when the SUs' devices employ SIS techniques and suffer from joint TX/RX IQI. We derived closed form expressions for the false alarm and detection probabilities under realistic scenarios of non-perfect SIS and transceivers' RF front-end impairments, as well as for the theoretical scenarios of ideal RF front-end and/or perfect SIS. Our results illustrated the degrading joint effects of IQI and partial SIS on the ED spectrum sensing performance, which results in significant losses in spectrum utilization. Specifically, in the case of single-channel ED, we observed that the negligence of IQI and partial SIS can lead to a wrong choice of the energy threshold, which may results in a dramatic increase of the false alarm probability, while at the same time the detection probability might significantly decrease. Moreover, in the case of multi-channel EDs, partial SIS and IQI cause self-interference and mirror interference that appreciably restrict the ED's capabilities. Hence, when designing FD CR devices, whether a single- or multi-channel ED is employed, IQI and partial SIS

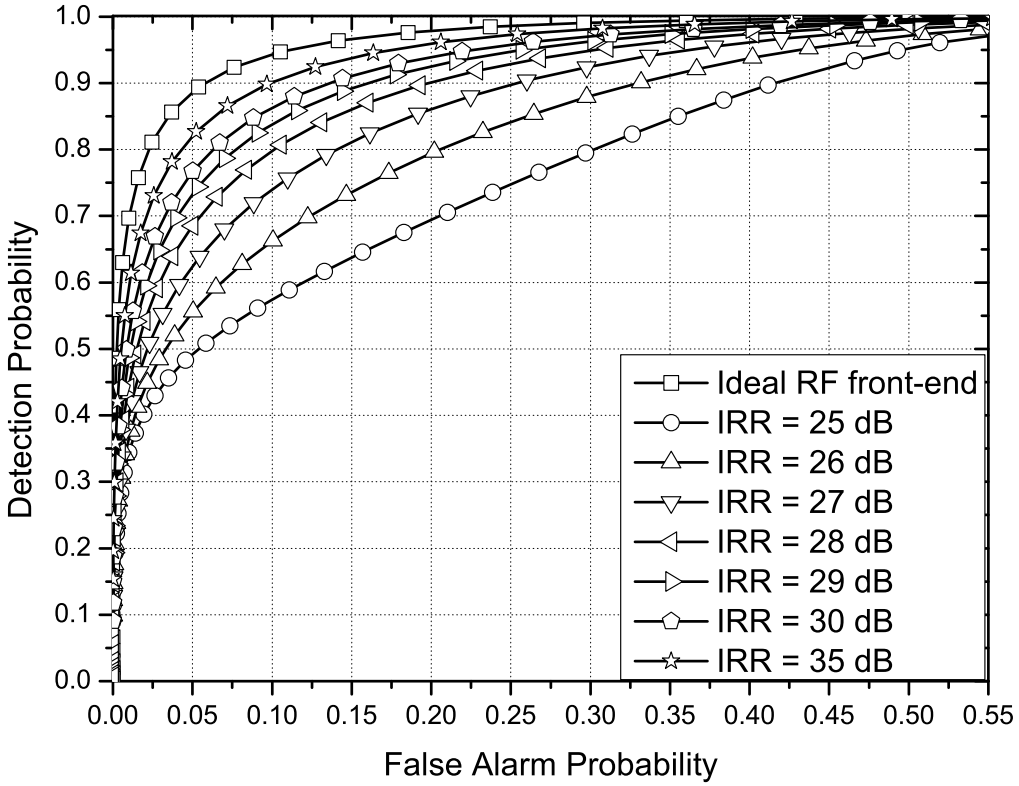

Figure 6.8 ROC for different values of IRR, when $p_{-k} = \tilde{p}_{-k} = \tilde{p}_k = 0.5$, $a = 0.01$, SNR $= -15$ dB and INR caused by the activity at the image PU channel is equal to 10 dB.

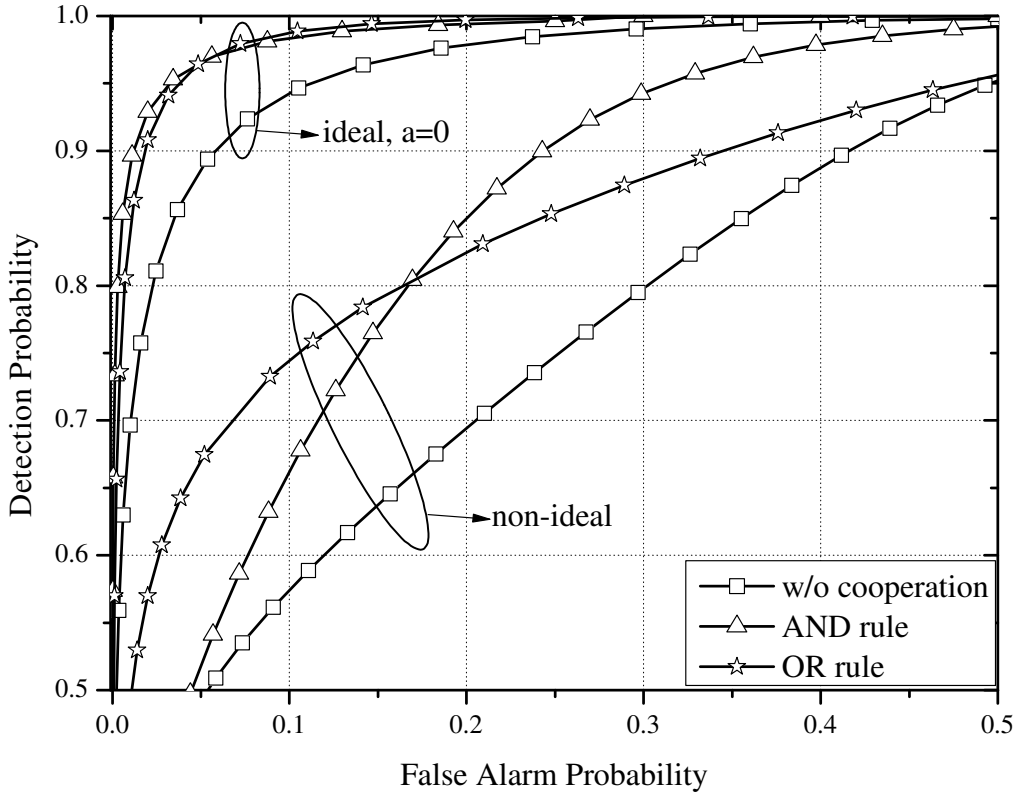

Figure 6.9 ROC for different decision rules, when $p = p_{-k} = \tilde{p}_{-k} = \tilde{p}_k = 0.5$, IRR $= 25$ dB and $a = 0.01$.

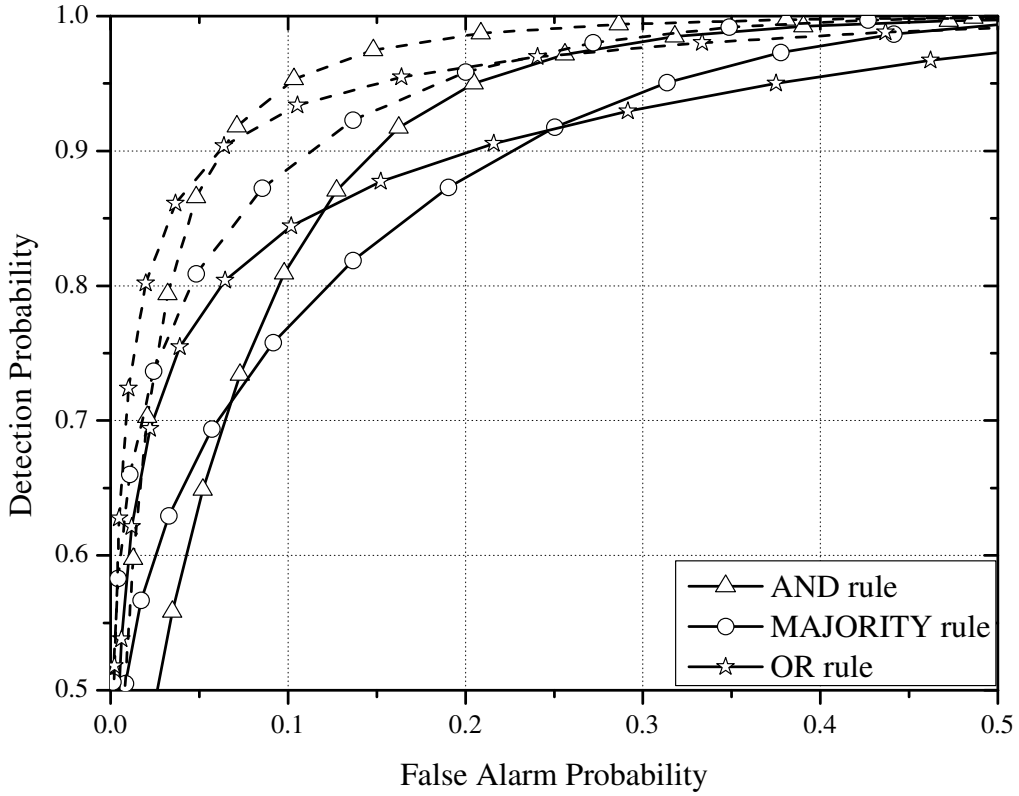

Figure 6.10 ROC for different decision rules, when $p = p_{-k} = \tilde{p}_{-k} = \tilde{p}_k = 0.5$, IRR = 30 dB, $a = 0.01$ and $N_{\text{su}} = 3$ (continuous lines) or $N_{\text{su}} = 5$ (dashed lines).

should be carefully taken into consideration. Finally, we extended the analysis in case of cooperative sensing to observe that even with the use of cooperative schemes, it is impossible to fully compensate for the joint effects of IQI and partial SIS.

Chapter 7

Spectrum sensing under hardware constraints

In this chapter, the joint effect of several RF impairments on energy detection based spectrum sensing for CR systems in multi-channel environments are investigated. In particular, novel closed form expressions for the evaluation of the detection and false alarm probabilities, assuming Rayleigh fading, are provided. Furthermore, the analysis is extended to the case of CR networks with cooperative sensing, where the secondary users suffer from different levels of RF imperfections, considering both scenarios of error free and imperfect reporting channel. Numerical and simulation results demonstrate the accuracy of the analysis as well as the detrimental effects of RF imperfections on the spectrum sensing performance, which bring significant losses in the spectrum utilization.

The research results of this chapter are included in [277, 278].

7.1 Introduction to spectrum sensing using direct conversion receivers

The rapid growth of wireless communications and the foreseen spectrum occupancy problems, due to the exponentially increasing consumer demands on mobile traffic and data, motivated the evolution of the concept of CR [248]. CR systems require intelligent reconfigurable wireless devices, capable of sensing the conditions of the surrounding RF environment and modifying their transmission parameters accordingly, in order to achieve the best overall performance, without interfering with other users [264]. One fundamental task in CR is spectrum sensing, i.e., the identification of temporarily vacant portions of spectrum, over wide ranges of spectrum resources and determine the available spectrum holes on its own. Spectrum sensing allows the exploitation of the under-utilized spectrum, which is considered to be an essential element in the operation of CRs. Therefore, great amount of effort has been put to derive optimal, suboptimal, ad-hoc, and cooperative solutions to the spectrum sensing problem (see for example [251, 257, 260–263, 265–267, 483, 484, 499–501]). However, the majority of these works ignore the imperfections associated with the RF front-end. Such imperfections, which are encountered in the widely deployed low-cost DCR RXs, include IQI [279], LNA nonlinearities [485], and phase noise [417].

7.2 Related work

The effects of RF imperfections in general were studied in several works [144, 320, 331, 355, 360, 367, 414, 416, 417, 461, 464–466, 486–488, 502–505]. However, only recently, the impact of RF imperfections in the spectrum sensing capabilities of CR was investigated [279, 360, 417, 486–488, 504, 505]. In particular, the importance of improved front-end linearity and sensitivity was illustrated in [504] and [505], while the impacts of RF impairments in DCRs on single-channel energy and/or cyclostationary based sensing were discussed in [486] and [487]. Furthermore, in [488] the authors presented closed form expressions for the detection and false alarm probabilities for the Neyman-Pearson detector, considering the spectrum sensing problem in single-channel OFDM CR RX, under the joint effect of transmitter and receiver IQI. On the other hand, multi-channel sensing under IQI was reported in [360], where a three-level hypothesis blind detector was introduced. Moreover, the impact of RF IQI on ED for both single-channel and multi-channel DCRs was investigated in [279], where it was shown that the false alarm probability in a multi-channel environment increases significantly, compared to the ideal RF RX case. Additionally, in [417], the authors analyzed the effect of phase noise on ED, considering a multi-channel DCR and AWGN channels, whereas in [145], the impact of third-order non-linearities on the detection and false alarm probabilities for classical and cyclostationary EDs considering imperfect LNA, was investigated.

7.3 Contribution

In this chapter, the impact on the multi-channel energy-based spectrum sensing mechanism of the joint effect of several RF impairments, such as LNA non-linearities, phase noise and IQI is investigated. After assuming flat-fading Rayleigh channels and complex Gaussian PU transmitted signals[1], and proving that, for a given channel realization, the joint effects of RF impairments can be modeled as a complex Gaussian process, we derive closed form expressions for the probabilities of false alarm and detection. Based on these expressions, the impact of RF impairments on ED is investigated. Specifically, the contribution of this chapter can be summarized as follows:

- We, first, derive analytical closed form expressions for the false alarm and detection probabilities for an ideal RF front-end ED detector, assuming flat fading Rayleigh channels and complex Gaussian transmitted signals. This is the first time that such expressions are presented in the open technical literature, under these assumptions. For instance, in [258, 260, 266, 506, 507], the authors assumed deterministic PU signal.

- Next, a signal model that describes the joint effect of all RF impairments is presented. Based on this model, it is proven that, for a given channel realization, the joint effects of RF impairments can be modeled as a complex Gaussian process [465], which is tractable model to algebraic manipulations.

- Analytical closed form expressions are provided for the evaluation of false alarm and detection probabilities of multi-channel EDs constrained by RF impairments, under Rayleigh fading. Based on this framework, the joint effect of RF impairments on energy-based spectrum sensing performance are investigated.

- Finally, we address an analytical study for the detection capabilities of cooperative spectrum sensing scenarios considering both cases of ideal EDs and multi-channel EDs constrained by RF impairments.

7.4 Organization

The remainder of the chapter is organized as follows. The system and signal model for both ideal and hardware impaired RF front-ends are described in Section 7.5. The analytical framework for evaluating the false alarm and detection probabilities, when both ideal sensing or RF imperfections are considered, are provided in Section 7.6. Moreover, analytical closed form expression for deriving the false alarm and detection probabilities, when a cooperative spectrum sensing with decision fusion system is considered, are provided in Section 7.7. Numerical and simulation results that illustrate the detrimental effects of RF impairments in spectrum sensing are presented in Section 7.8. Finally, Section 7.9 concludes the chapter by summarizing our main findings.

7.5 System and signal model

In this section, we briefly present the ideal signal model, which is referred to as ideal RF front-end in what follows. Build upon that, we demonstrate the practical signal model, where the RX is considered to suffer from RF imperfections, such as LNA nonlinearities, phase noise and IQI. Note that it is assumed that K RF channels are down-converted to baseband using the wideband direct-conversion principle, which is referred to as multi-channel down-conversion [307].

7.5.1 Ideal RF front-end

The two hypothesis, namely absence/presence of PU signal, is denoted with parameter $\theta_k \in \{0, 1\}$. Suppose the n-th sample of the PU signal, $s(n)$, is conveyed over a flat-fading wireless channel, with channel gain, $h(n)$, and additive noise $w(n)$. The received wide band RF signal is passed through various RF front-end stages, including filtering, amplification, analog I/Q demodulation (down-conversion) to

[1] This is a valid assumption that has been employed in [278, 279, 417].

base band and sampling. The wide band channel after sampling is assumed to have a bandwidth of W and contain K channels, each having bandwidth

$$W_{ch} = W_{sb} + W_{gb}, \tag{7.1}$$

where W_{sb} and W_{gb} are the signal band and total guard band bandwidth within this channel, respectively. Additionally, it is assumed that the sampling is performed, with rate W. Note, that the rate of the signal is reduced by a factor of

$$L = \frac{W}{W_{sb}} \geq K, \tag{7.2}$$

where for simplicity we assume $L \in \mathbb{Z}$.

Under the ideal RF front-end assumption, after the selection filter, the $n-$th sample of the base band equivalent received signal vector for the $k-$ th channel ($k \in S = \{-K/2, \ldots, -1, 1 \ldots, K/2\}$) can be expressed as

$$r_k(n) = \Re\{r_k(n)\} + j\Im\{r_k(n)\} = \theta_k h_k(n) s_k(n) + w_k(n), \tag{7.3}$$

where h_k, s_k and w_k are zero-mean CSCWG processes with variances σ_h^2, σ_s^2 and σ_w^2, respectively. Furthermore,

$$\Re\{r_k(n)\} = \theta_k \Re\{h_k(n)\}\Re\{s_k(n)\} - \theta_k \Im\{h_k(n)\}\Im\{s_k(n)\} + \Re\{w_k(n)\} \tag{7.4}$$

and

$$\Im\{r_k(n)\} = \theta_k \Im\{h_k(n)\}\Re\{s_k(n)\} + \theta_k \Re\{h_k(n)\}\Im\{s_k(n)\} + \Im\{w_k(n)\}. \tag{7.5}$$

7.5.2 Non-ideal RF front-end

In the case of non-ideal RF front-end, the n-th sample of the impaired base band equivalent received signal vector for the $k-$ th channel is given by [279] and [320]

$$r_k(n) = \Re\{r_k(n)\} + j\Im\{r_k(n)\} = \xi_k(n)\theta_k h_k(n) s_k(n) + \eta_k(n) + w_k(n), \tag{7.6}$$

with

$$\Re\{r_k(n)\} = \theta_k \Re\{h_k(n)\xi_k\}\Re\{s_k(n)\} - \theta_k \Im\{h_k(n)\xi_k\}\Im\{s_k(n)\} + \Re\{\eta_k(n) + w_k(n)\} \tag{7.7}$$

and

$$\Im\{r_k(n)\} = \theta_k \Im\{h_k(n)\xi_k\}\Re\{s_k(n)\} - \theta_k \Re\{h_k(n)\xi_k\}\Im\{s_k(n)\} + \Im\{\eta_k(n) + w_k(n)\}, \tag{7.8}$$

where ξ_k denotes the amplitude and phase rotation due to phase noise caused by common phase error (CPE), LNA nonlinearities and IQI, and is given by [320, Eq. (7.7)]

$$\xi_k = \gamma_0 K_1 \alpha, \tag{7.9}$$

with γ_0, K_1 and α be constant phase noise, IQI and LNA nonlinearities parameters that stand for the amplitude and phase distortion, respectively, while η_k denotes the distortion noise from impairments in the RX, and specifically due to phase noise caused by ICI, IQI and non-linear distortion noise, and is given by [320, Eq. (7.8)]

$$\eta_k(n) = K_1(\gamma_o e_k(n) + \psi_k(n)) + K_2\left(\gamma_o^*\left(\alpha\theta_{-k} h_{-k}^*(n) s_{-k}^*(n) + e_{-k}^*(n)\right)\right) + K_2 \psi_{-k}^*(n), \tag{7.10}$$

where K_2 is an IQI coefficient, whereas ψ_k, ψ_{-k} and e_k, e_{-k} represent the additive distortion noises to the channel k and $-k$, due to phase noise and LNA nonlinearities. After denoting as

$$\Theta_k = \{\theta_{k-1}, \theta_{k+1}\} \tag{7.11}$$

and

$$H_k = \{h_{k-1}, h_{k+1}\}, \tag{7.12}$$

this distortion noise term can be modeled as

$$\eta_k \sim \mathcal{CN}\left(0, \sigma^2_{\eta_k}\right), \tag{7.13}$$

with

$$\sigma^2_{\eta_k} = |\gamma_0|^2 \Big(|K_1|^2 \sigma^2_{e,k} + |K_2|^2 \sigma^2_{e,-k} \Big) + |K_1|^2 \sigma^2_{\psi|H_k,\Theta_k} + |K_2|^2 \sigma^2_{\psi|H_{-k},\Theta_{-k}} + |\gamma_0|^2 |K_2|^2 |\alpha|^2 \theta_{-k} |h_{-k}|^2 \sigma^2_s. \tag{7.14}$$

It should be noted that this model has been supported and validated by many theoretical investigations and measurements [325, 329, 416, 461, 465, 502, 503, 508].

Next, we describe how the various parameters in (7.9), (7.10) and (7.14) stem from the imperfections associated with the RF front-end.

7.5.2.1 LNA Nonlinearities

The parameters α and e_k represent the nonlinearity parameters, which model the amplitude/phase distortion and the nonlinear distortion noise, respectively. According to Bussgang's theorem [436], e_k is a zero-mean Gaussian error term with variance $\sigma^2_{e_k}$. Considering an ideal clipping power amplifier, the amplification factor α and the variance $\sigma^2_{e_k}$, are respectively given by (4.50) and (4.51).

Furthermore, if a polynomial model is employed to describe the effects of nonlinearities, the amplification factor α and the variance $\sigma^2_{e_k}$, are respectively given by (4.46) and (4.47).

7.5.2.2 IQI

The RX IQI coefficients, which for notation convenience are represented as K_1 and K_2, can be respectively obtained as (4.15) and (4.16).

7.5.2.3 Phase noise

The parameter, γ_0, stands for CPE, which is equal for all channels, whereas ψ_k represents the ICI from all other neighboring channels due to spectral regrowth caused by phase noise. Notice that, since the typical 3 dB bandwidth values for the oscillator process is in the order of few tens or hundreds of Hz, with rapidly fading spectrum after this point (approximately 10 dB/decade), for channel bandwidth that is typical few tens or hundreds KHz, the only effective interference is due to leakage from successive neighbors only [417]. Consequently, the ICI term can be approximated as [417]

$$\psi_k(n) \approx \theta_{k-1}\gamma(n) h_{k-1}(n) s_{k-1}(n) + \theta_{k+1}\gamma(n) h_{k+1}(n) s_{k+1}(n), \tag{7.15}$$

with $\gamma(n) = \exp(j\phi(n))$ and $\phi(n)$ being a discrete Brownian error process, i.e.,

$$\phi(n) = \sum_{m=1}^{n} \phi(m-1) + \epsilon(n), \tag{7.16}$$

where $\epsilon(n)$ is a zero-mean real Gaussian variable with variance

$$\sigma^2_\epsilon = \frac{4\pi\beta}{W} \tag{7.17}$$

and β being the 3 dB bandwidth of the LO process.

The interference term ψ_k in (7.10) might have zero or non-zero contribution depending on the existence of PU signals in the successive neighboring channels. In general, this term is typically non-white and strictly speaking cannot be modeled by a Gaussian process. However, for practical 3 dB bandwidth of the oscillator process, the influence of the regarded impairments can all be modeled as a zero-mean Gaussian process with $\sigma^2_{\psi_k|\{H_k,\Theta_k\}}$ given by

$$\sigma^2_{\psi|\{H_k,\Theta_k\}} = \theta_{k-1} A_{k-1} |h_{k-1}(n)|^2 \sigma^2_s + \theta_{k+1} A_{k+1} |h_{k+1}(n)|^2 \sigma^2_s, \tag{7.18}$$

where

$$A_{k-1} = \frac{|I(f_{k-1} - f_k + f_{\text{cut-off}}) - I(f_{k-1} - f_k - f_{\text{cut-off}})|}{2\pi f_{\text{cut-off}}}, \tag{7.19}$$

$$A_{k+1} = \frac{|I(f_{k+1} - f_k + f_{\text{cut-off}}) - I(f_{k+1} - f_k - f_{\text{cut-off}})|}{2\pi f_{\text{cut-off}}}, \tag{7.20}$$

and f_k is the centered normalized frequency of the $k-$th channel, i.e.,

$$f_k = \text{sgn}(k)\frac{2|k|-1}{2K} \tag{7.21}$$

and $f_{\text{cut-off}}$ is the normalized cut-off frequency of the $k-$th channel, which can be obtained by

$$f_{\text{cut-off}} = \frac{W_{sb}}{2W}. \tag{7.22}$$

Furthermore,

$$\begin{aligned} I(f) = {} & (f_{\text{cut-off}} - f)\tan^{-1}(\delta \tan(\pi(f_{\text{cut-off}} - f))) + (f_{\text{cut-off}} + f)\tan^{-1}(\delta \tan(-\pi(f_{\text{cut-off}} + f))) \\ & - \frac{1}{\delta}\left((f_{\text{cut-off}} + f)\cot(\pi(f_{\text{cut-off}} + f)) - (f_{\text{cut-off}} - f)\cot(\pi(f_{\text{cut-off}} - f))\right) \\ & + \frac{1}{\pi\delta}\left(\log(|sin(\pi(f_{\text{cut-off}} + f))|) + \log(|sin(\pi(f_{\text{cut-off}} - f))|)\right), \end{aligned} \tag{7.23}$$

with

$$\delta = \frac{\exp(-2\pi\beta/W) + 1}{\exp(-2\pi\beta/W) - 1}. \tag{7.24}$$

Due to (7.19) and (7.20), it follows that $A_{k-1} = A_{k+1}$.

7.5.2.4 Joint effect of RF impairments

Here, we explain the joint impact of RF imperfections in the spectra of the down-converted received signal. Comparing‘(7.6) with (7.3), we observe that the RF imperfections result in not only amplitude/phase distortion, but also neighbor and mirror interference, as demonstrated intuitively in Fig. 7.1.

According to (7.9) and (7.14), LNA nonlinearities cause amplitude/phase distortion and an additive nonlinear distortion noise, whereas, based on (7.18), phase noise causes interference to the received base band signal at the $k-$th channel, due to the received base band signals at the neighbor channels $k-1$ and $k+1$.

Moreover, based on (7.14), the joint effects of phase noise and IQI, described by the terms $|K_1|^2\sigma^2_{\psi|H_k,\Theta_k}$, $|K_2|^2\sigma^2_{\psi|H_{-k},\Theta_{-k}}$ and $|\gamma_0|^2|K_2|^2|\alpha|^2\theta_{-k}|h_{-k}|^2\sigma_s^2$, result in interference to the signal at the $k-$th ($k \in \{-\frac{K}{2}+1, \cdots, \frac{K}{2}+1\}$) channel by the signals at the channels $-k-1$, $-k$, $-k+1$, $k-1$ and $k+1$. Note that if $k = -\frac{K}{2}$ or $k = \frac{K}{2}$, then phase noise and IQI cause interference to the signal at the $k-$th channel due to the signals at the channels $-k$, $-k+1$ and $k-1$. Consequently, in this case, the terms that refer to the signals at the channels $-k-1$ and $k+1$ should be omitted.

Furthermore, the joint effects of LNA nonlinearties and IQI are described by the first term and the last terms in (7.14), i.e., $|K_1|^2\sigma^2_{e,k} + |K_2|^2\sigma^2_{e,-k}$ and $|\gamma_0|^2|K_2|^2|\alpha|^2\theta_{-k}|h_{-k}|^2\sigma_s^2$, respectively, and result in additive distortion noises and mirror channel interference. Finally, the amplitude and phase distortion caused by the joint effects of all RF imperfections are modeled by the parameter ξ described in (7.9).

Fig. 7.1 clearly demonstrates that LNA nonlinearities, IQI and phase noise results in an amplitude and phase distortion, as well as interference to channel k from the channels $-k-1$, $-k$, $-k+1$, $k-1$ and $k+1$, plus a distortion noise. If channel k is busy, the received signal's energy at channel k is increased, due to the interference of the neighbor and mirror channels, hence, the ED decision will more accurate. However, if channel k is idle, the received signal's energy at channel k, due to the interference and the noise, may be greater than the decision threshold, and the ED will wrongly decides that the channel is busy. Consequently, this interference plays an important role in the spectrum sensing capabilities; therefore, it should be quantified and taken into consideration when selecting the energy statistics threshold.

According to (7.9), the amplitude and phase distortion, due to the joint effect of RF impairments, is a constant variable, while, based on (7.10) and (7.15), since s_{-k-1}, s_{-k}, s_{-k+1}, s_{k-1}, s_{k+1}, e_k and e_{-k} are independent zero-mean complex Gaussian RVs, for a given channel realization, η_k is also a zero-mean complex Gaussian RV.

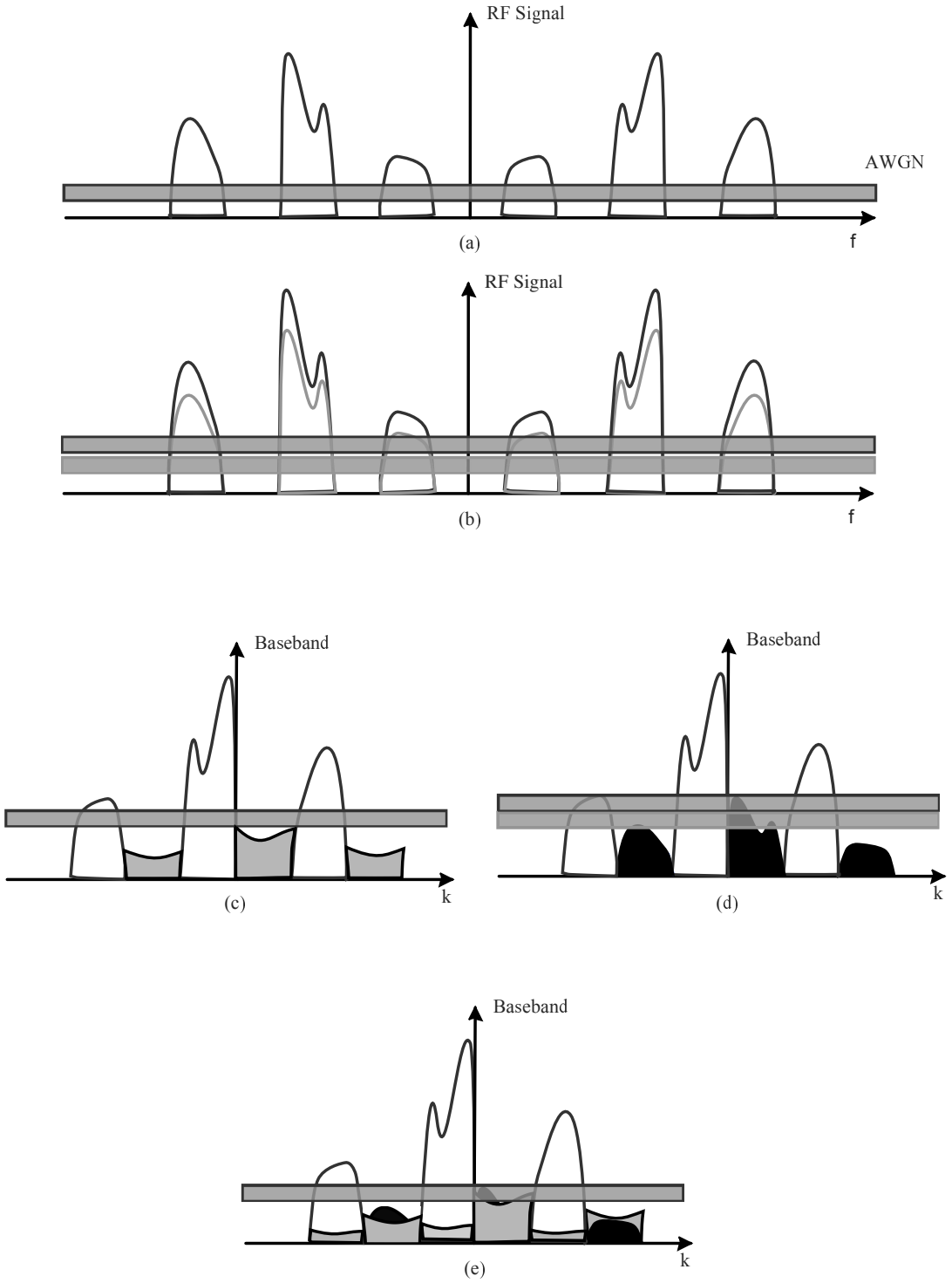

Figure 7.1 Spectra of the received signal: (a) before LNA (passband RF signal), (b) after LNA (passband RF signal), (c) after down-conversion (baseband signal), when local oscillator's phase noise is considered to be the only RF imperfection, (d) after down-conversion (baseband signal), when IQI is considered to be the only RF imperfection, (e) after down-conversion (baseband signal), the joint effect of LNA nonlinearities, phase noise and IQI.

7.6 False alarm and detection probabilities for channel detection

In the classical ED, the energy of the received signals is used to determine whether a channel is idle or busy. Based on the signal model described in Section 7.5, the ED calculates the test statistics for the $k-$th channel as

$$T_k = \frac{1}{N_s}\sum_{m=0}^{N_s-1}\left|r_k\left(n\right)\right|^2 = \frac{1}{N_s}\sum_{m=0}^{N_s-1}\Re\left\{r_k\left(n\right)\right\}^2 + \Im\left\{r_k\left(n\right)\right\}^2, \tag{7.25}$$

where N_s is the number of complex samples used for sensing the $k-$th channel. This test statistic is compared against a threshold, $\gamma_{th}\left(k\right)$, to yield the sensing decision, i.e., the ED decides that channel k is busy, if $T_k > \gamma_{th}\left(k\right)$, or idle, otherwise.

The remainder of this section is organized as follows. In Section 7.6.1, the detection and false alarm probabilities for the ideal RF front-end scenario are evaluated, while in Section 7.6.2, the detection and false alarm probabilities for the non-ideal RF front-end scenario are derived.

7.6.1 Ideal RF front-end

Based on the signal model presented in Section 7.5.1 and taking into consideration that

$$\sigma^2 = E\left[\Re\left\{r_k\right\}^2\right] = E\left[\Im\left\{r_k\right\}^2\right] = \theta_k\left(\Re\left\{h_k\right\}^2 + \Im\left\{h_k\right\}^2\right)\frac{\sigma_s^2}{2} + \frac{\sigma_w^2}{2}, \tag{7.26}$$

and

$$E\left[\Re\left\{r_k\right\}\Im\left\{r_k\right\}\right] = 0, \tag{7.27}$$

for a given channel realization h_k and channel occupation θ_k, the received energy follows chi-square distribution with $2N_s$ degrees of freedom (DoF) and CDF given by

$$F_{T_k}\left(x\left|h_k,\theta_k\right.\right) = \frac{\gamma\left(N_s, \frac{N_s x}{2\sigma^2}\right)}{\Gamma\left(N_s\right)}. \tag{7.28}$$

The following theorem returns a closed form expression for the CDF of the test statistics assuming that the channel is busy.

Theorem 7.1. *The CDF of the energy statistics assuming an ideal RF front end and a busy channel can be evaluated by*

$$F_{T_k}\left(x\left|\theta_k=1\right.\right) = 1 - \exp\left(\frac{\sigma_w^2}{\sigma_h^2\sigma_s^2}\right)\sum_{k=0}^{N_s-1}\frac{1}{k!}\left(\frac{N_s x}{\sigma_h^2\sigma_s^2}\right)^k\Gamma\left(-k+1, \frac{\sigma_w^2}{\sigma_h^2\sigma_s^2}, \frac{N_s x}{\sigma_h^2\sigma_s^2}, 1\right). \tag{7.29}$$

Proof. Please refer to the Appendix I. ■

Based on the above analysis, the false alarm probability for the ideal RX can be obtained by

$$\mathcal{P}_{fa}(\gamma) = P_r\left(T_k > \gamma\left|\theta_k=0\right.\right) = \frac{\Gamma\left(N_s, \frac{N_s\gamma}{\sigma_w^2}\right)}{\Gamma\left(N_s\right)}, \tag{7.30}$$

while the probability of detection can be calculated as

$$\mathcal{P}_d(\gamma) = P_r\left(T_k > \gamma\left|\theta_k=1\right.\right) = \exp\left(\frac{\sigma_w^2}{\sigma_h^2\sigma_s^2}\right)\sum_{k=0}^{N_s-1}\frac{1}{k!}\left(\frac{N_s\gamma}{\sigma_h^2\sigma_s^2}\right)^k\Gamma\left(-k+1, \frac{\sigma_w^2}{\sigma_h^2\sigma_s^2}, \frac{N_s\gamma}{\sigma_h^2\sigma_s^2}, 1\right). \tag{7.31}$$

From (7.30) and (7.31), we observe that, in the case of ideal RF front-end, the false alarm and detection probabilities depend on the number of samples, the noise variance and the channel variance. As a result, the ED should know these parameters to set the sensing threshold in order to achieve the required false alarm or detection probability.

7.6.2 Non-Ideal RF front-end

Based on the signal model presented in Section 7.5.2, and assuming given channel realization and channel occupancy vectors

$$H = \{H_{-k}, h_{-k}, h_k, H_k\} \tag{7.32}$$

and

$$\Theta = \{\Theta_{-k}, \theta_{-k}, \theta_k, \Theta_k\}, \tag{7.33}$$

respectively, it holds that

$$\sigma^2 = E\left[\Re\{r_k\}^2\right] = E\left[\Im\{r_k\}^2\right] = \theta_k\left(\Re\{h_k\}^2 + \Im\{h_k\}^2\right)\left(\Re\{\xi_k\}^2 + \Im\{\xi_k\}^2\right)\frac{\sigma_s^2}{2} + \frac{\sigma_w^2 + \sigma_{\eta_k}^2}{2}, \tag{7.34}$$

and $\Re\{r_k\}$, $\Im\{r_k\}$ are uncorrelated random variables, i.e.,

$$E\left[\Re\{r_k\}\Im\{r_k\}\right] = 0. \tag{7.35}$$

Thus, the received energy, given by (3.9), follows chi-square distribution with $2N_s$ DoF and CDF given by

$$F_{T_k}(x\,|H, \Theta) = \frac{\gamma\left(N_s, \frac{N_s x}{2\sigma^2}\right)}{\Gamma(N_s)}, \tag{7.36}$$

where σ^2 can be expressed, after taking into account (7.14), (7.18) and (7.34), as

$$\begin{aligned}\sigma^2 = {} & \theta_k \mathcal{A}_1 |h_k|^2 + \theta_{k-1}\mathcal{A}_2 |h_{k-1}|^2 + \theta_{k+1}\mathcal{A}_2 |h_{k+1}|^2 + \theta_{-k+1}\mathcal{A}_3 |h_{-k+1}|^2 \\ & + \theta_{-k-1}\mathcal{A}_3 |h_{-k-1}|^2 + \theta_{-k}\mathcal{A}_4 |h_{-k}|^2 + \mathcal{A}_5.\end{aligned} \tag{7.37}$$

In (7.37),

$$\mathcal{A}_1 = |\xi_k|^2 \frac{\sigma_s^2}{2}, \tag{7.38}$$

$$\mathcal{A}_2 = |K_1|^2 A_{k-1}\frac{\sigma_s^2}{2}, \tag{7.39}$$

$$\mathcal{A}_3 = |K_2|^2 A_{-k+1}\frac{\sigma_s^2}{2}, \tag{7.40}$$

$$\mathcal{A}_4 = |\gamma_0|^2 |K_2|^2 |a|^2 \frac{\sigma_s^2}{2} \tag{7.41}$$

and

$$\mathcal{A}_5 = \frac{\sigma_w^2}{2} + \frac{|\gamma_0|^2}{2}\left(|K_1|^2 \sigma_{e,k}^2 + |K_2|^2 \sigma_{e,-k}^2\right) \tag{7.42}$$

model the amplitude distortion due to the joint effects of RF impairments, the interference from the $k-1$ and $k+1$ channels, the interference from the $-k-1$ and $-k+1$ channels due to phase noise, the mirror interference due to IQI, and the distortion noise due to the joint effects of RF impairments, respectively.

The following theorems return closed form expressions for the CDF of the energy test statistics for a given channel occupancy vector, when at least one channel of $\{-k-1, -k, -k+1, k-1, k, k+1\}$ is busy and when all channels are idle.

Theorem 7.2. *The CDF of the energy statistics assuming a non-ideal RF front end and an arbitrary channel occupancy vector Θ that is different than the all idle vector, can be evaluated by*

$$\begin{aligned}
F_{T_k}(x\,|\Theta) &= \sum_{i=2}^{3} U(m_i-2)\, w_{1,i} w_{2,i} \mathcal{A}_i \exp\left(-\frac{\mathcal{A}_5}{\mathcal{A}_i}\right) + \sum_{i=1}^{4} U(m_i-2)\, w_{1,i} \mathcal{A}_i (\mathcal{A}_5+\mathcal{A}_i) \exp\left(-\frac{\mathcal{A}_5}{\mathcal{A}_i}\right) \\
&+ \sum_{i=1}^{4} U(m_i-1)\left(U(1-m_i) - \mathcal{A}_5 U(m_i-2)\right) w_{1,i} \mathcal{A}_i \exp\left(-\frac{\mathcal{A}_5}{\mathcal{A}_i}\right) \\
&- \sum_{i=2}^{3}\sum_{k=0}^{N_s-1} U(m_i-2)\,\frac{1}{k!}\frac{w_{1,i}w_{2,i}}{\mathcal{A}_i^{k-1}}\left(\frac{N_s x}{2}\right)^k \Gamma\left(-k+1, \frac{\mathcal{A}_5}{\mathcal{A}_i}, \frac{N_s x}{2\mathcal{A}_i}, 1\right) \\
&- \sum_{i=1}^{4}\sum_{k=0}^{N_s-1} U(m_i-1)\left(U(1-m_i) - \mathcal{A}_5 U(m_i-2)\right)\frac{1}{k!}\frac{w_{1,i}}{\mathcal{A}_i^{k-1}}\left(\frac{N_s x}{2}\right)^k \Gamma\left(-k+1, \frac{\mathcal{A}_5}{\mathcal{A}_i}, \frac{N_s x}{2\mathcal{A}_i}, 1\right) \\
&- \sum_{i=1}^{4}\sum_{k=0}^{N_s-1} U(m_i-2)\,\frac{1}{k!}\frac{w_{1,i}}{\mathcal{A}_i^{k-1}}\left(\frac{N_s x}{2}\right)^k \Gamma\left(-k+2, \frac{\mathcal{A}_5}{\mathcal{A}_i}, \frac{N_s x}{2\mathcal{A}_i}, 1\right). \qquad (7.43)
\end{aligned}$$

where $w_{1,i}$ and $w_{2,i}$ are given by

$$w_{1,i} = \frac{\exp\left(\frac{\mathcal{A}_5}{\mathcal{A}_i}\right)}{\Gamma(m_i)\left(\prod_{j=1}^{4}\mathcal{A}_j^{m_j}\right)} \prod_{j=1, j\neq i}^{4}\left(\frac{1}{\mathcal{A}_j} - \frac{1}{\mathcal{A}_i}\right)^{-m_j}, \qquad (7.44)$$

and

$$w_{2,i} = \sum_{j=1, j\neq i} m_j \left(\frac{1}{\mathcal{A}_j} - \frac{1}{\mathcal{A}_i}\right)^{-1}, \qquad (7.45)$$

respectively.

Proof. Please refer to the Appendix J. ■

Theorem 7.3. *The CDF of the energy statistics assuming a non-ideal RF front-end and that the channel occupancy vector*

$$\Theta = \tilde{\Theta}_{2,0} = [0,0,0,0,0,0], \qquad (7.46)$$

can be obtained as

$$F_{T_k}\left(x \,\middle|\, \tilde{\Theta}_{2,0}\right) = \frac{\gamma\left(N_s, \frac{N_s x}{2\mathcal{A}_5}\right)}{\Gamma(N_s)}. \qquad (7.47)$$

Proof. Please refer to the Appendix K. ■

Based on the above analysis, the detection probability of the ED with RF impairments can be obtained as

$$\mathcal{P}_D = \sum_{i=1}^{\mathrm{card}\left(\tilde{\Theta}_1\right)} P_r\left(\tilde{\Theta}_1\right)\left(1 - F_{T_k}\left(\gamma^{\mathrm{ni}} \,\middle|\, \tilde{\Theta}_1\right)\right), \qquad (7.48)$$

where $\Pr(\Theta)$ denotes the probability of the given channel occupancy Θ, and $\tilde{\Theta}_1$ is the set defined as

$$\tilde{\Theta}_1 = [\theta_k = 1, \theta_{k-1}, \theta_{k+1}, \theta_{-k+1}, \theta_{-k-1}, \theta_{-k}]. \qquad (7.49)$$

Similarly, the probability of false alarm can be expressed as

$$\mathcal{P}_{FA} = \sum_{i=1}^{\mathrm{card}\left(\tilde{\Theta}_{2,c}\right)} P_r\left(\tilde{\Theta}_2\right)\left(1 - F_{T_k}\left(\gamma^{\mathrm{ni}} \,\middle|\, \tilde{\Theta}_{2,c}\right)\right) + P_r\left(\tilde{\Theta}_{2,0}\right)\frac{\Gamma\left(N_s, \frac{N_s \gamma^{\mathrm{ni}}}{2\mathcal{A}_5}\right)}{\Gamma(N_s)}, \qquad (7.50)$$

where $\tilde{\Theta}_{2,c}$ is the set defined as

$$\tilde{\Theta}_{2,c} = \tilde{\Theta}_2 - \tilde{\Theta}_{2,0}, \tag{7.51}$$

and $\tilde{\Theta}_2$ is the set defined as

$$\tilde{\Theta}_2 = [\theta_k = 0, \theta_{k-1}, \theta_{k+1}, \theta_{-k+1}, \theta_{-k-1}, \theta_{-k}]\,. \tag{7.52}$$

Note that (7.50) applies even when the channel K or $-K$ is sensed. However, in this case $\tilde{\Theta}_1 = [\theta_k = 1, \theta_{k-1}, \theta_{k+1} = 0, \theta_{-k+1}, \theta_{-k-1} = 0, \theta_{-k}]$ and $\tilde{\Theta}_2 = [\theta_k = 0, \theta_{k-1}, \theta_{k+1} = 0, \theta_{-k+1}, \theta_{-k-1} = 0, \theta_{-k}]$.

According to (7.48) and (7.50), in the case of non-ideal RF front-end, the detection and false alarm probabilities depend not only on the number of samples, the variance of the sensing channel and the noise variance, but also on the level of RF front-end imperfections and the probability of the neighbor and mirror channels occupancy. Therefore, since the sensing threshold is set in order to achieve a required detection or false alarm probability, the ED should have knowledge of these parameters.

7.7 Cooperative spectrum sensing with decision fusion

In this section, we consider a cooperative spectrum sensing scheme, in which each SU makes a binary decision on the channel occupancy, namely '0' or '1' for the absence or presence of PU activity, respectively, and the one-bit individual decisions are forwarded to a fusion center (FC) over a narrow band reporting channel [258, 260, 266]. The sensing channels (the channels between the PU and the SUs) are considered identical and independent, due to their different distances from the PU [258, 259, 267]. Moreover, we assume that the decision device of the FC is implemented with the k_{SU}-out-of-n_{SU} rule, which implies that if there are k_{SU} or more SUs that individually decide that the channel is busy, the FC decides that the channel is occupied. Note that when $k_{\mathrm{su}} = 1$, $k_{\mathrm{su}} = n_{\mathrm{su}}$ or $k_{\mathrm{su}} = \lceil n/2 \rceil$, the k_{su}-out-of-n_{su} rule is simplified to the OR, AND and MAJORITY rule, respectively.

7.7.1 Ideal RF front-end

Here, we derive closed form expression for the false alarm and detection probabilities, assuming that the RF front-ends of the SUs are ideal, considering both scenarios of error free and imperfect reporting channels.

7.7.1.1 Reporting channels without errors

If the channel between the SUs and the FC is error free, the false alarm probability ($\mathcal{P}_{C,fa}$) and the detection probability ($\mathcal{P}_{C,d}$) are given by [260, Eq. (17)]

$$\mathcal{P}_{C,fa} = \sum_{i=k_{\mathrm{su}}}^{n_{\mathrm{su}}} \binom{n_{\mathrm{su}}}{i} (\mathcal{P}_{fa})^i (1-\mathcal{P}_{fa})^{n_{\mathrm{su}}-i} \tag{7.53}$$

and

$$\mathcal{P}_{C,d} = \sum_{i=k_{\mathrm{su}}}^{n_{\mathrm{su}}} \binom{n_{\mathrm{su}}}{i} (\mathcal{P}_{d})^i (1-\mathcal{P}_{d})^{n_{\mathrm{su}}-i}\,. \tag{7.54}$$

Taking into consideration (7.30), (7.31) and (7.29) and after some basic algebraic manipulations, (7.53) and (7.54) can be expressed as

$$\mathcal{P}_{C,fa} = \sum_{i=k_{\mathrm{su}}}^{n_{\mathrm{su}}} \binom{n_{\mathrm{su}}}{i} \left(\frac{\Gamma\left(N_s, \frac{N_s\gamma}{\sigma_w^2}\right)}{\Gamma(N_s)} \right)^i \left(\frac{\gamma\left(N_s, \frac{N_s\gamma}{\sigma_w^2}\right)}{\Gamma(N_s)} \right)^{n-i}, \tag{7.55}$$

and

$$\begin{aligned}\mathcal{P}_{C,d} = \sum_{i=k_{\mathrm{su}}}^{n_{\mathrm{su}}} \binom{n_{\mathrm{su}}}{i} &\left(\exp\left(\frac{\sigma_w^2}{\sigma_h^2\sigma_s^2}\right) \sum_{k=0}^{N_s-1} \frac{1}{k!} \left(\frac{N_s\gamma}{\sigma_h^2\sigma_s^2}\right)^k \Gamma\left(-k+1, \frac{\sigma_w^2}{\sigma_h^2\sigma_s^2}, \frac{N_s\gamma}{\sigma_h^2\sigma_s^2}, 1\right) \right)^i \\ &\times \left(1 - \exp\left(\frac{\sigma_w^2}{\sigma_h^2\sigma_s^2}\right) \sum_{k=0}^{N_s-1} \frac{1}{k!} \left(\frac{N_s\gamma}{\sigma_h^2\sigma_s^2}\right)^k \Gamma\left(-k+1, \frac{\sigma_w^2}{\sigma_h^2\sigma_s^2}, \frac{N_s\gamma}{\sigma_h^2\sigma_s^2}, 1\right) \right)^{n_{\mathrm{su}}-i}.\end{aligned} \tag{7.56}$$

From (7.55) and (7.56), we observe that the false alarm and detection probabilities, in the case of cooperative spectrum sensing, when the SU's EDs are considered ideal, and the reporting channels are assumed to be error free, depends on the number of SU (n_{su}), the decision rule that is employed by the FC, the number of samples (N_s), the noise and the sensing channel variances.

7.7.1.2 Reporting channels with errors

If the reporting channel is imperfect, error occur on the detection of the transmitted, by the SU, bits. In this case, the false alarm and the detection probabilities can be derived by [260, Eq. (18)]

$$\mathcal{P}_{C,\mathcal{X}} = \sum_{i=k_{\text{su}}}^{n_{\text{su}}} \left(\begin{array}{c} n \\ i \end{array} \right) \left(\mathcal{P}_{\mathcal{X},e}\right)^{i} \left(1-\mathcal{P}_{\mathcal{X},e}\right)^{n_{\text{su}}-i}, \tag{7.57}$$

where

$$\mathcal{P}_{\mathcal{X},e} = \mathcal{P}_{\mathcal{X}}\left(1-P_e\right) + \left(1-\mathcal{P}_{\mathcal{X}}\right)P_e, \tag{7.58}$$

is the equivalent false alarm ('$\mathcal{X}$ = fa') or detection ('$\mathcal{X} = d$') probability and P_e is the cross-over probability of the reporting channel, which is equal to the BER of the channel. Considering BPSK, ideal RF front-end in the FC and Rayleigh fading, the BER can be expressed as

$$P_e = \frac{1}{2}\left(1-\sqrt{\frac{\gamma_r}{1+\gamma_r}}\right), \tag{7.59}$$

with γ_r be the signal to noise ratio (SNR) of the link between the SUs and the FC.

Notice that since $\mathcal{P}_{\mathcal{X}} \in [0,1]$, $\mathcal{P}_{\mathcal{X},e}$ is bounded in $[P_e, 1-P_e]$. Consequently, according to (7.57), $\mathcal{P}_{C,\mathcal{X}} \in \left[\mathcal{P}^{-}_{C,\mathcal{X}}, \mathcal{P}^{+}_{C,\mathcal{X}}\right]$, where

$$\mathcal{P}^{-}_{C,\mathcal{X}} = \sum_{i=k_{\text{su}}}^{n_{\text{su}}} \left(\begin{array}{c} n_{\text{su}} \\ i \end{array} \right) \left(P_e\right)^{i} \left(1-P_e\right)^{n_{\text{su}}-i} \tag{7.60}$$

and

$$\mathcal{P}^{+}_{C,\mathcal{X}} = \sum_{i=k_{\text{su}}}^{n_{\text{su}}} \left(\begin{array}{c} n_{\text{su}} \\ i \end{array} \right) \left(1-P_e\right)^{i} \left(P_e\right)^{n_{\text{su}}-i}. \tag{7.61}$$

7.7.2 Non-ideal RF front-end

In this section, we consider that the RXs front-end of the SUs suffer from different level RF imperfections.

7.7.2.1 Reporting channels without errors

Here, we assume that the reporting channel is error free and that the SU j sends $d_{j,k} = 0$ or $d_{j,k} = 1$ to the FC to report absence or presence of PU activity at the channel k.

If the sensing channel k is idle ($\theta_k = 0$), then the probability that the $j-$th SU reports that the channel is busy ($d_{j,k} = 1$), can be expressed as $\mathcal{P}_{fa,j}$, while the probability that the $j-$th SU reports that the channel is idle ($d_{j,k} = 0$), is given by $(1-\mathcal{P}_{fa,j})$. Therefore, since each SU decides individually whether there is PU activity in the channel k, the probability that the n_{su} SUs report a given decision set

$$\mathcal{D} = \left[d_{1,k}, d_{2,k}, \cdots, d_{n_{\text{su}},k}\right], \tag{7.62}$$

if $\theta_k = 0$, can be written as

$$\mathcal{P}_{fa}(\mathcal{D}) = \prod_{j=1}^{n_{\text{su}}} \left(U\left(-d_{j,k}\right)\left(1-\mathcal{P}_{fa,j}\right) + U\left(d_{j,k}-1\right)\mathcal{P}_{fa,j}\right). \tag{7.63}$$

Furthermore, based on the k_{su}-out-of-n_{su} rule, the FC decides that the $k-$th channel is busy, if the k_{su} out of the n_{su} SUs reports "1". Consequently, for a given decision set, the false alarm probability at the FC can be evaluated by

$$\mathcal{P}_{C,FA|\mathcal{D}} = U\left(\sum_{l=1}^{n_{\text{su}}} d_{l,k} - k_{\text{su}}\right) \prod_{j=1}^{n_{\text{su}}} \left(U\left(-d_{j,k}\right)\left(1-\mathcal{P}_{fa,j}\right) + U\left(d_{j,k}-1\right)\mathcal{P}_{fa,j}\right). \tag{7.64}$$

Hence, for any possible $\mathcal{D}$, the false alarm probability at the FC, using k_{su}-out-of-n_{su} rule, can be obtained as

$$\mathcal{P}_{C,FA} = \sum_{i=1}^{\text{card}(\mathcal{D})} U\left(\sum_{l=1}^{n_{\text{su}}} d_{l,k} - k_{\text{su}}\right) \prod_{j=1}^{n_{\text{su}}} \left(U\left(-d_{j,k}\right)\left(1-\mathcal{P}_{fa,j}\right) + U\left(d_{j,k}-1\right)\mathcal{P}_{fa,j}\right). \tag{7.65}$$

Similarly, the detection probability at the FC, using k_{su}-out-of-n_{su} rule, can be expressed as

$$\mathcal{P}_{C,D} = \sum_{i=1}^{\text{card}(\mathcal{D})} U\left(\sum_{l=1}^{n_{\text{su}}} d_{l,k} - k_{\text{su}}\right) \prod_{j=1}^{n_{\text{su}}} \left(U\left(-d_{j,k}\right)\left(1-\mathcal{P}_{d,j}\right) + U\left(d_{j,k}-1\right)\mathcal{P}_{d,j}\right). \tag{7.66}$$

From (7.65) and (7.66), it is evident that in the case of non-ideal RF front-ends, the false alarm and detection probabilities depend not only on the number of samples (N_s), the variances of the sensing channels (σ_h^2), the noise variance (σ_w^2), and the decision rule, but also on the level of RF front-end imperfections of each SU's ED, the variances of the neighbor and mirror channels, and the probability of the neighbor and mirror channels occupancy.

Note that if the FC uses the OR rule, (7.65) and (7.66) can be respectively simplified to

$$\mathcal{P}_{\text{OR},FA} = 1 - \prod_{i=1}^{n_{\text{su}}} \left(1-\mathcal{P}_{fa,i}\right), \tag{7.67}$$

and

$$\mathcal{P}_{\text{OR},D} = 1 - \prod_{i=1}^{n_{\text{su}}} \left(1-\mathcal{P}_{d,i}\right), \tag{7.68}$$

while, if the FC uses the AND rule, (7.65) and (7.66) can be respectively simplified to

$$\mathcal{P}_{\text{AND},FA} = \prod_{i=1}^{n_{\text{su}}} \mathcal{P}_{fa,i}, \tag{7.69}$$

and

$$\mathcal{P}_{\text{AND},D} = \prod_{i=1}^{n_{\text{su}}} \mathcal{P}_{d,i}. \tag{7.70}$$

In the special case, where all the SUs suffer from the same level of RF impairments, the false alarm probability ($\mathcal{P}_{C,fa}$) and the detection probability ($\mathcal{P}_{C,d}$) are given by

$$\mathcal{P}_{C,FA} = \sum_{i=k_{\text{su}}}^{n_{\text{su}}} \left(\begin{array}{c} n_{\text{su}} \\ i \end{array}\right) \left(\mathcal{P}_{FA}\right)^i \left(1-\mathcal{P}_{FA}\right)^{n_{\text{su}}-i}, \tag{7.71}$$

and

$$\mathcal{P}_{C,D} = \sum_{i=k_{\text{su}}}^{n_{\text{su}}} \left(\begin{array}{c} n_{\text{su}} \\ i \end{array}\right) \left(\mathcal{P}_{D}\right)^i \left(1-\mathcal{P}_{D}\right)^{n_{\text{su}}-i}, \tag{7.72}$$

where $\mathcal{P}_{FA}$ and $\mathcal{P}_D$ are given by (7.50) and (7.48), respectively.

7.7.2.2 Reporting channels with errors

Next, we consider the case of imperfect reporting channel. In this scenario, the false alarm and the detection probabilities can be obtained as

$$\mathcal{P}_{C,\mathcal{X}} = \sum_{i=1}^{\text{card}(\mathcal{D})} U\left(\sum_{l=1}^{n_{\text{su}}} d_{l,k} - k_{\text{su}}\right) \prod_{j=1}^{n_{\text{su}}} \left(U\left(-d_{j,k}\right)\left(1-\mathcal{P}_{\mathcal{X},e,j}\right) + U\left(d_{j,k}-1\right)\mathcal{P}_{\mathcal{X},e,j}\right), \tag{7.73}$$

where $\mathcal{P}_{\mathcal{X},e,j}$ can be expressed as

$$\mathcal{P}_{\mathcal{X},e,j} = \mathcal{P}_{\mathcal{X},j}\left(1-P_{e,j}\right) + \left(1-\mathcal{P}_{\mathcal{X},j}\right)P_{e,j}, \tag{7.74}$$

with $\mathcal{P}_{\mathcal{X},j}$ denoting the equivalent false alarm ('$\mathcal{X}$ = FA') or detection ('$\mathcal{X}$ = D') probability of the $j-$th SU and $P_{e,j}$ being the cross-over probability of the reporting channel connecting the $j-$th SU with the FC. Notice that since $\mathcal{P}_{\mathcal{X},j} \in [0,1]$, based on (7.74), $\mathcal{P}_{\mathcal{X},e,j}$ is bound by $P_{e,j}$ and $1-P_{e,j}$.

In the special case, where all the SUs suffer from the same level of RF impairments, (7.73) can be expressed as [260, Eq. (18)]

$$\mathcal{P}_{C,\mathcal{X}} = \sum_{i=k_{\text{su}}}^{n_{\text{su}}} \binom{n_{\text{su}}}{i} \left(\mathcal{P}_{\mathcal{X},e}\right)^{i} \left(1-\mathcal{P}_{\mathcal{X},e}\right)^{n_{\text{su}}-i}. \tag{7.75}$$

7.8 Numerical and simulation results

In this section, we investigate the effects of RF impairments on the spectrum sensing performance of EDs by illustrating analytical and Monte-Carlo simulation results for different RF imperfection levels. In particular, we consider the following insightful scenario. It is assumed that the wideband signal is consisted of $K = 8$ channels and the second channel is sensed (i.e., $k = 2$). The signal and the total guard band bandwidths are assumed to be $W_{sb} = 1$ MHz and $W_{gb} = 125$ KHz, respectively, while the sampling rate is chosen to be equal to the bandwidth of wireless signal as $W = 9$ MHz. Moreover, the channel occupancy process is assumed to be Bernoulli distributed with probability, $q = 1/2$, and independent across channels, while the signal variance is equal for all channels. The number of samples is set to 5 ($N_s = 5$), while it is assumed that $\sigma_h^2 = \sigma_w^2 = 1$. In addition, for simplicity and without loss of generality, we consider an ideal clipping power amplifier. In the following figures, the numerical results are shown with continuous lines, while markers are employed to illustrate the simulation results. Moreover, the performance of the classical ED with ideal RF front-end is used as a benchmark.

Figs. 7.2 and 7.3 demonstrate the impact of LNA non-linearities on the performance of the classical ED, assuming different SNR values. Specifically, in Fig. 7.2, false alarm probabilities are plotted against threshold for different SNR and IBO values, considering $\beta = 100$ Hz, IRR = 25 dB and phase imbalance equal to $\phi = 3^o$. It becomes evident from this figure that the analytical results are identical with simulation results; thus, verifying the presented analytical framework. Additionally, it is observed that for a fixed IBO value, as SNR increases, the interference for the neighbor and mirror channels increases; hence, the false alarm probability increases. On the contrary, as IBO increases, for a given SNR value, the effects of LNA non-linearities are constrained; therefore the false alarm probability decreases. Moreover, this figure indicates that the levels of RF impairments should be taken into consideration, when selecting the energy threshold, in order to achieve a false alarm probability requirement.

In Fig. 7.3, ROCs are plotted for different SNR and IBO values, considering $\beta = 100$ Hz, IRR = 25 dB and $\phi = 3^o$. We observe that for low SNR values, LNA non-linearities do not affect the ED performance. However, as SNR increases, the distortion noise caused due to the imperfection of the amplifier increases; as a result, LNA non-linearities become to have more adverse effects on the spectrum capabilities of the classical ED, significantly reducing its performance for low IBO values. Furthermore, as IBO increases, the effects of LNA non-linearities become constrained and therefore the performance of the non-ideal ED tends to the performance of the ideal ED.

Fig. 7.4 illustrates the impact of phase noise on the performance of the classical ED, assuming various SNR values, when IRR = 25 dB, $\phi = 3^o$ and IBO = 6 dB. We observe that for practical levels of IQI and phase noise, the signal leakage from channels $-k+1$ and $-k-1$ to channel $-k$ due to phase noise is small. Note that the signal leakage to channel k from the channel $-k-1$ and $-k+1$ due to the joint effect of phase noise and IQI is in the range of $[-70$ dB, -50 dB$]$. Consequently, in the low SNR regime,

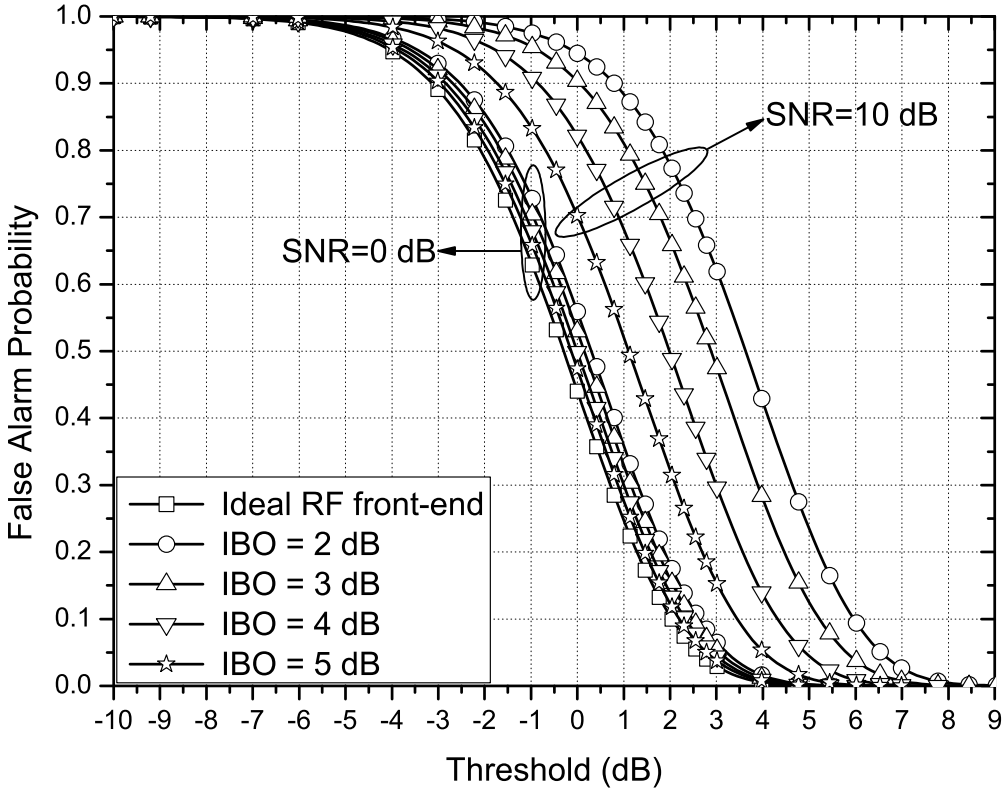

Figure 7.2 False alarm probability vs Threshold for different values of IBO and SNRs, when IRR = 25 dB and $\beta = 100$ Hz.

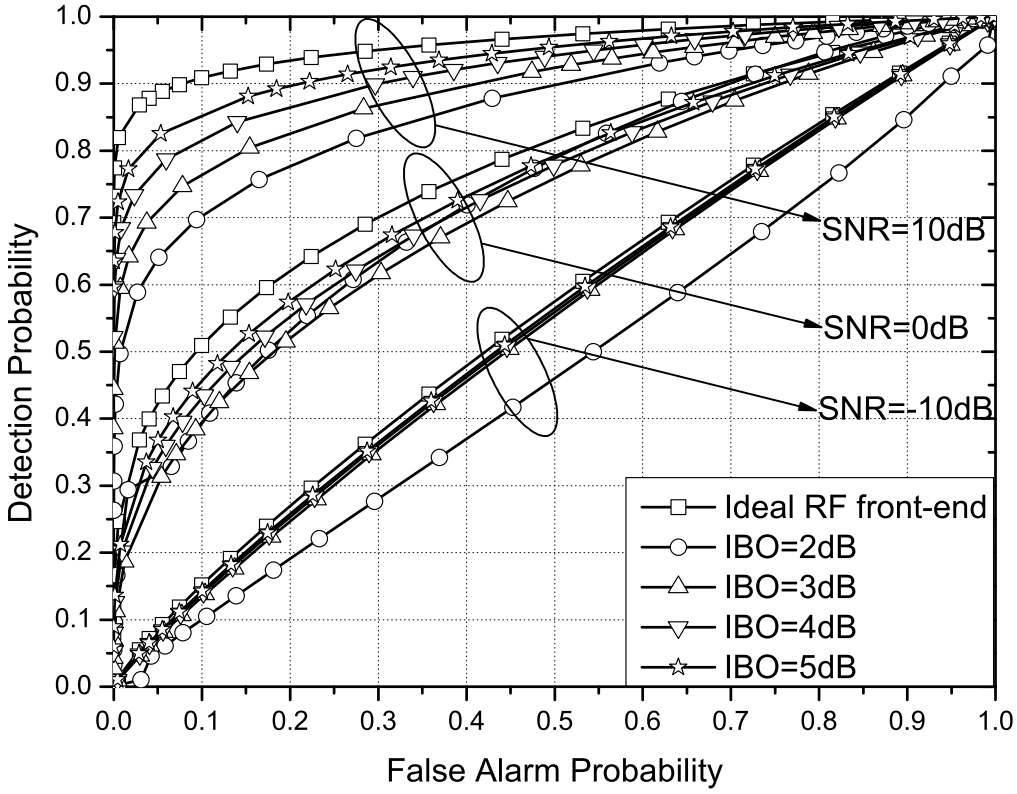

Figure 7.3 ROC for different values of IBO and SNRs, when IRR = 25 dB and $\beta = 100$ Hz.

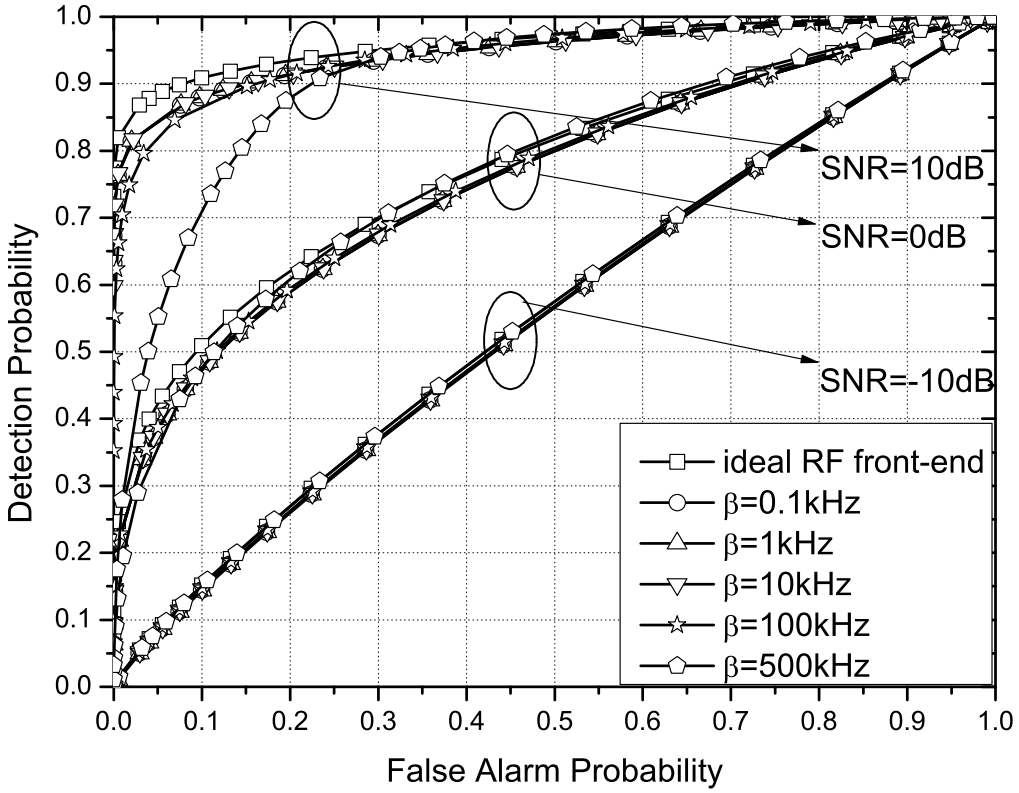

Figure 7.4 ROCs for different values of β and SNRs, when IBO = 6 dB and IRR = 25 dB.

the leakage from the channels $-k-1$ and $-k+1$ do not affect the spectrum sensing capabilities. In other words, at low SNR values, phase noise do not affect the spectrum sensing capability of the classical ED compared with the ideal RF front-end ED. On the other hand, as SNR increases, phase noise has more severe effect on the spectrum sensing capabilities of the classical ED, significantly reducing the ED performance for high β values.

The effect of IQI on the spectrum sensing performance of ED are presented at Fig. 7.5. In particular, in this figure, ROCs are plotted assuming various SNRs, when the IBO = 6 dB and $\beta = 100Hz$. Again, the analytical results coincide with the simulation, verifying the derived expressions. At low SNRs, it is observed that there is no significant performance degradation due to IQI. Nonetheless, as SNR increases, the interference of the mirror channels increases. As a result, IQI notably affects the spectrum sensing performance. Additionally, for a fixed SNR, it is evident that as IRR increases, the signal leakage of the mirror channels, due to IQI, decreases; hence, the performance of the non-ideal ED tends to become identical to the one of the ideal ED. Finally, when compared with the spectrum sensing performance affected by LNA nonlinearities, as depicted in Fig. 7.3, it becomes apparent that the impact of LNA nonlinearity to the spectrum sensing performance is more detrimental than the impact of IQI.

The effect of RF impairments in cooperative sensing, when the reporting channel is considered error free, is illustrated in Fig. 7.6. In this figure, ROCs for ideal (continuous lines) and non-ideal (dashed lines) RF front-end SUs are presented, considering a CR network composed of $n_{\text{su}} = 5$ SUs, and a single FC, which uses the OR or AND rule to decide whether the sensing channel is idle or busy. The EDs of the SUs are assumed identical with IBO = 3 dB, IRR = 20 dB, and $\beta = 100$ Hz. Again it is shown that the analytical results are identical with simulation results; thus, verifying the presented analytical framework. Moreover, it is observed that as the FC decision rule becomes more strict, the performance of the CR network improves; consequently the OR rule outperforms the AND rule. When a given decision rule is applied, it becomes evident from the figure that the RF imperfections cause severe degradation of the sensing capabilities of the CR network. For instance, if the OR rule is employed and false alarm probability is equal to 14%, the RF impairments results in about 31% degradation compared with the ideal RF front-end scenario. This result indicates that it is important to take into consideration the hardware constraints of the low-cost spectrum sensing SUs. Furthermore, this figure

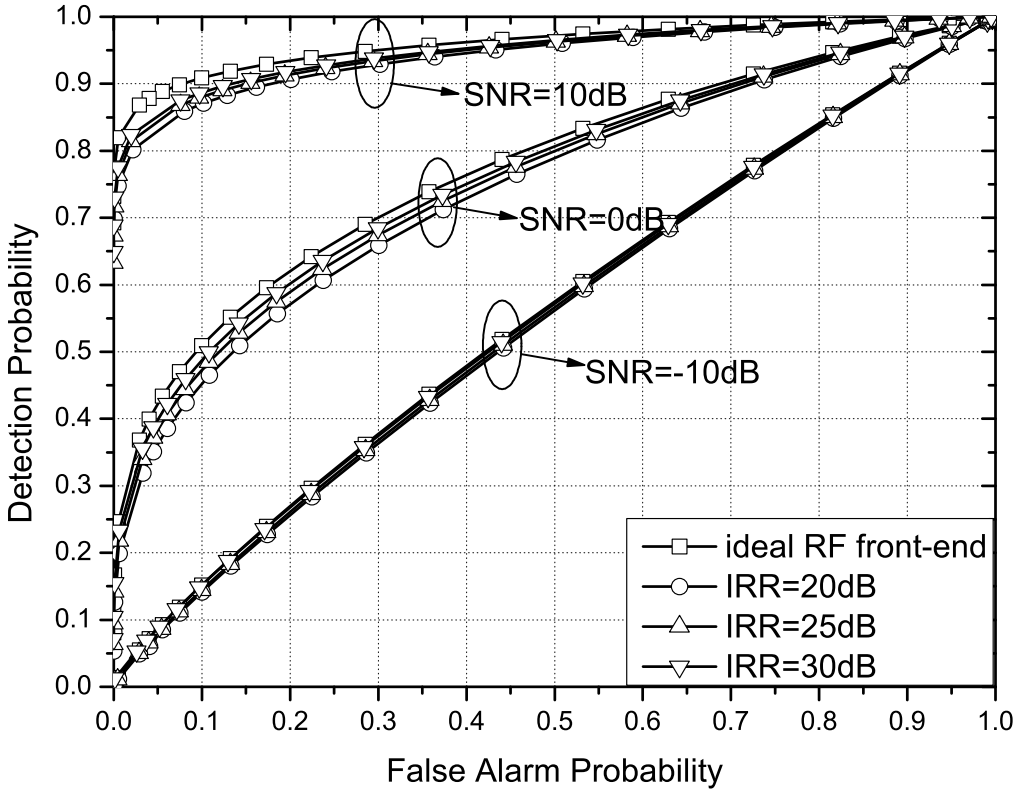

Figure 7.5 ROCs for different values of IRR and SNRs, when IBO = 6 dB and $\beta = 100$ Hz.

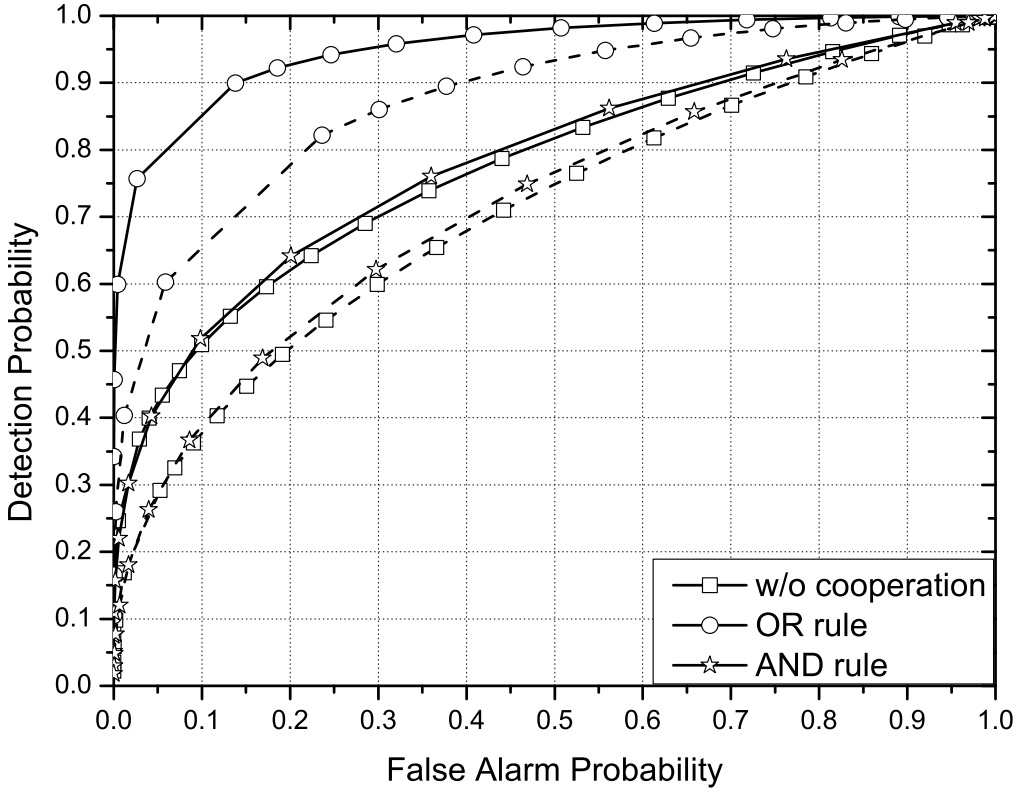

Figure 7.6 ROCs for ideal (continuous line) and non-ideal (dashed lines) RF front-end, when $n_{\text{su}} = 5$.

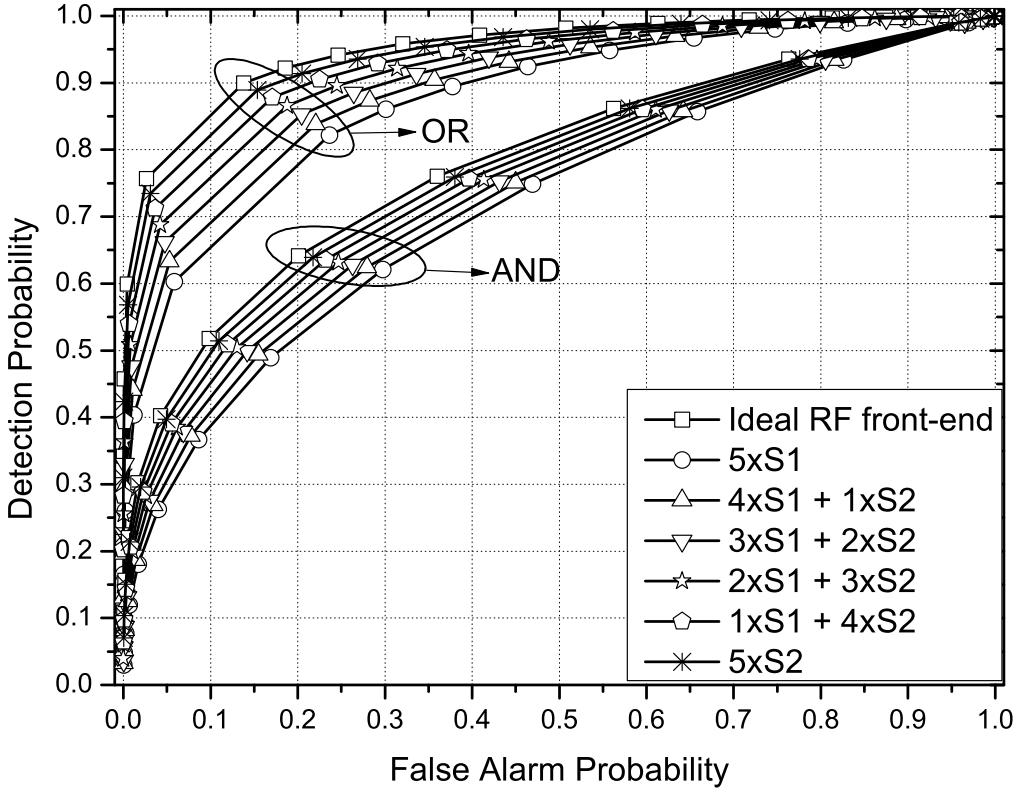

Figure 7.7 ROCs for ideal and non-ideal RF front-end, when the CR network is equipped with 5 SUs under different levels of RF imperfections. S_1 and S_2 stands for SUs with IBO = 3 dB and IRR = 20 dB, and IBO = 6 dB and IRR = 30 dB, respectively.

reveals that cooperative spectrum sensing can be used as a countermeasure to deal with the effects of RF imperfections.

In Fig. 7.7, ROCs are illustrated for a CR network composed of $n_{\text{su}} = 5$, which suffer from different levels of RF imperfections, and a single FC that employs either the AND or the OR rule to decide whether the sensing channel is idle or busy. In this scenario, we consider two types of SUs, namely S_1 and S_2. The RF front-end specifications of S_1 are IBO = 3 dB, IRR = 20 dB and β = 100 Hz, whereas the specifications of S_2 are IBO = 6 dB, IRR = 30 dB and β = 100 Hz. In other words, the CR network, in this scenario, includes both SUs of almost the worst (S_1) and almost optimal (S_2) RF front-end quality. As benchmarks, the ROCs of a CR network equipped with classical ED sensor nodes in which the RF front-end is considered to be ideal, and CR networks that uses only S_1 or only S_2 sensor nodes are presented. In this figure, we observe the detrimental effects of the RF imperfections of the ED sensor nodes to the sensing capabilities of the CR network. Furthermore, it is demonstrated that as the numbers of S_1 and S_2 SUs are respectively decreasing and increasing, the ED performance of the FC tends to become identical to the case when all the SUs are considered to be ideal. This was expected since S_2 SUs have higher quality RF front-end characteristics than the other set of SUs. Finally, we observe that the OR rule outperforms the AND rule for any number of S_1 and S_2.

7.9 Conclusions

We studied the performance of multi-channel spectrum sensing, when the RF front-end is impaired by hardware imperfections. In particular, assuming Rayleigh fading, we provided the analytical framework for evaluating the detection and false alarm probabilities of EDs when LNA nonlinearities, IQI and phase noise are taken into account. Next, we extended our study to the case of a CR network, in which the SUs suffer from different levels of RF impairments, taking into consideration both scenarios of error free and imperfect reporting channels. Our results illustrated the degrading effects of RF imperfections on

the ED spectrum sensing performance, which bring significant losses in the utilization of the spectrum. Among others, LNA non-linearities were shown to have the most detrimental effect on the spectrum sensing performance. Furthermore, we observed that in cooperative spectrum sensing, the sensing capabilities of the CR system are significantly influenced by the different levels of RF imperfections of the SUs. Therefore, RF impairments should be seriously taken into consideration when designing direct conversion CR RXs.

Chapter 8

Optimal power allocation for OFDMA systems under IQI

This chapter studies the PA problem in an ODFMA system, when the served UEs suffer from different levels of IQI. Additionally, we present a novel low-complexity solution with directly calculated PA policies, given the Lagrange multiplier, which mitigates the impact of IQI and achieves fairness in terms of capacity for the served UEs, by maximizing the minimum achievable capacity of the UEs. The effectiveness of the offered solution is validated through reliable simulation results, which reveal that it can drastically increase the minimum achievable UEs' capacity.

The research results of this chapter are included in [379].

8.1 Related work and contribution

Various approaches have been proposed so far to eliminate, compensate, and mitigate the effects of IQI using baseband signal processing techniques at the RX (see [299, 319, 341, 343, 351, 352, 356, 357, 359, 363, 365, 371, 385, 509], and references therein). For example, in [371], the authors presented an IQI mitigation method for OFDMA systems, in which each subcarrier is processed jointly with its counterpart at the image subcarrier. All previously mentioned works deal with IQI at the RX by employing digital signal processing. However, in wireless systems, where low-cost, energy efficiency, low-complexity, and compactness of the RXs are key design requirements, the extra processes in the RX may be prohibitive. Inspired by this, in the present work, we investigate the PA problem for OFDMA wireless systems, when the served UEs suffer from different levels of IQI. To mitigate the impact of IQI, we propose a novel low-complexity solution with directly calculated PA policies, given the Lagrange multiplier, that maximizes the minimum UEs' achievable capacity, with respect to the BS transmitted power. The proposed PA solution outperforms the conventional one, which does not take into consideration the IQI levels of the served UEs, while, at the same time, fairness in terms of capacity of the served UEs is achieved. The effectiveness of the offered solution is validated through simulations, which reveal that it can significantly increase the minimum achievable UEs' capacity.

8.2 Organization

The reminder of this chapter is organized as follows. The system and the signal model of both the ideal and the IQI impaired RF front-ends are presented in Section 8.3. The optimization problem is formulated in Section 8.4. In the same section, the proposed PA scheme, which takes into account the level of IQI of each UE, is provided. Simulation results that demonstrate the effectiveness of the proposed PA scheme in comparison with the conventional PA scheme, are presented in Section 8.5. Finally, Section 8.6 concludes the chapter by summarizing the main findings.

8.3 System and signal model

In this section, we revisit the ideal signal model, as well as the realistic IQI signal models in multi-carrier direct-conversion RX scenario in an OFDMA system.

8.3.1 Ideal RF front-end

We assume OFDMA transmission, where a transmitted signal at subcarrier k for the UE i, $s_i(k)$, conveyed over a wireless channel, $h_i(k)$, with an AWGN, $n_i(k)$. The received RF signal is passed through various processing stages, also known as the RF front-end of the RX. These stages include filtering, amplification, analog I/Q demodulation, down-conversion to base band and sampling. To this end, the corresponding base band equivalent received signal can be expressed as

$$r_{\mathrm{id},i}(k) = h_i(k)s_i(k) + n_i(k). \tag{8.1}$$

Note that $h_i(k)$ is given by

$$h_i(k) = \frac{g_i(k)}{D_i^n}, \tag{8.2}$$

where $g_i(k)$ is a complex Gaussian RV, n represents the path loss exponent and

$$D_i = \frac{d_i}{d_0}, \tag{8.3}$$

with d_i and d_0 be the distance between the BS ans the $i-$th UE, and the reference distance, respectively. Based on this, the instantaneous SNR per symbol at the RX input of the $i-th$ UE can be given by,

$$\gamma_{\mathrm{id},i}(k) = \frac{P_s(k)}{N_0}\left|h_i(k)\right|^2, \tag{8.4}$$

where, $P_s(k)$, denotes the power per transmitted symbol at subcarrier k and N_0 is the single-sided AWGN PSD.

8.3.2 IQI model for OFDMA systems

Based on (4.14), the time-domain base band representation of the IQI impaired signal at the $i-$th UE can be obtained as

$$g_i^{\mathrm{no}} = K_{1,i}g_i + K_{2,i}g_i^*, \tag{8.5}$$

where g_i denotes the base band IQI−free signal at the $i-$th UE and g_i^* raised due to the involved IQI effects. Furthermore, according to (4.15) and (4.16), the RX IQI coefficients, $K_{1,i}$ and $K_{2,i}$, can be expressed as

$$K_{1,i} = \frac{1}{2}\left(1 + \epsilon_i e^{-j\phi_i}\right) \tag{8.6}$$

and

$$K_{2,i} = \frac{1}{2}\left(1 - \epsilon_i e^{j\phi_i}\right), \tag{8.7}$$

where ϵ_i and ϕ_i account for the RX amplitude and phase mismatch, of the $i-$th UE, respectively. It is also noted that the IQI parameters are algebraically linked to each other as

$$K_{2,i} = 1 - \left(K_{1,i}\right)^*. \tag{8.8}$$

The RX IQI coefficients are associated with the corresponding IRR though

$$\mathrm{IRR}_i = \frac{\left|K_{1,i}\right|^2}{\left|K_{2,i}\right|^2}. \tag{8.9}$$

It is recalled here that for practical analog RF front-end electronics, the value of IRR is typically in the range of 20 dB − 40 dB [299, 307, 314, 320, 510]. Furthermore, the second term, $K_{2,i}g_{\mathrm{id},i}^*$, is due to the associated imbalances and in multi-carrier transmission it denotes the image *aliasing* effect, which results to crosstalk between the mirror-frequencies in the down-converted signal. This is because, in general, complex conjugate in time domain corresponds to complex conjugate and mirroring in the frequency domain. Therefore, the spectrum of the imbalance signal at the k-th subcarrier becomes

$$G_{IQI,i}\left(k\right) = K_{1,i}G_i\left(k\right) + K_{2,i}G_i^*\left(-k\right), \tag{8.10}$$

where $G_i\left(k\right)$ and $G_i\left(-k\right)$ denote the spectrum of the IQI free signal at the k and $-k$ subcarriers, respectively.

8.3.3 OFDMA systems impaired by IQI

In the case of multi-user transmission, we assume that multiple RF subcarriers are down-converted to the baseband by means of wideband direct-conversion, where the RF spectrum is translated to the baseband in a single down-conversion [321]. Note that the wideband conversion is the most general scenario in multi-carrier wireless systems [279]. For notational convenience, we denote the set of subcarriers/UEs as

$$\mathcal{K} = \{-K, \cdots, -1, 1, \cdots, K\}. \tag{8.11}$$

Without loss of generality, it is assumed that the signal carried by the $k-$th subcarrier is intended for the $k-$th UE, a signal carried by the mirror subcarrier, $-k$, is intended for UE $-k$. Moreover, since the BS is usually a high-complexity device, the RF front-end of the TX is considered ideal, while the RX experiences IQI. Hence, by using (8.10), the baseband equivalent received signal in the $k-$th subcarrier can be represented as

$$r_k(k) = K_{1,k} h_k(k) s_k(k) + K_{2,k} h_k^*(-k) s_{-k}^*(-k) + K_{1,k} n_k(k) + K_{2,k} n_k^*(-k), \tag{8.12}$$

while the baseband equivalent received signal in the $-k$-th subcarrier can be expressed as

$$r_{-k}(-k) = K_{1,-k} h_{-k}(-k) s_{-k}(-k) + K_{2,-k} h_{-k}^*(k) s_k^*(k) + K_{1,-k} n_{-k}(-k) + K_{2,-k} n_{-k}^*(k). \tag{8.13}$$

With the aid of (8.13), it is shown that IQI is the reason that the received baseband equivalent signal intended for the $k-$th UE, $s_k(k)$, is interfered by the image signal intended for UE $-k$, $s_{-k}^*(-k)$. The instantaneous SINR per symbol at the input of the RX of the $k-$th UE at subcarrier k can be expressed as

$$\gamma_k(k) = \frac{|K_{1,k}|^2 |h_k(k)|^2 P_s(k)}{|K_{2,k}|^2 |h_k(-k)|^2 P_s(-k) + \left(|K_{1,k}|^2 + |K_{2,k}|^2\right) N_0}, \tag{8.14}$$

or equivalently

$$\gamma_k(k) = \frac{|h_i(k)|^2 P_s(k)}{\frac{|h_i(-k)|^2}{\mathrm{IRR}_k} P_s(-k) + \left(1 + \frac{1}{\mathrm{IRR}_i}\right) N_0}. \tag{8.15}$$

Similarly, the instantaneous SINR per symbol at the input of the RX of the $-k$-th UE can be obtained by interchanging k with $-k$ and vise versa in (9.44). Consequently, the achievable rates at UE k, with $k \in \mathcal{K}$, can be obtained as

$$R_k(k) = \log_2(1 + \gamma_k(k)). \tag{8.16}$$

8.4 Problem formulation & proposed PA scheme

In this section, we first define the PA optimization problem, and then, we present a novel solution. We consider that the optimization is performed by the BS, which has full CSI[1] as well as the served UEs IQI levels, i.e., their IRR values. As we are interested in increasing the achievable capacity of each UE, we aim to maximize the minimum capacity with respect to the transmitted power. The corresponding optimization problem can be written as

$$\begin{aligned} \max_{\mathbf{P}} \quad & \min_{k \in \mathcal{K}} R_k \\ \text{s.t.} \quad & \mathrm{C1}: \sum_{k \in \mathcal{K}} P_s(k) \leq P_{\max}, \end{aligned} \tag{8.17}$$

where

$$\mathbf{P} = [P_s(-K), \cdots, P_s(-1), P_s(1), \cdots, P_s(K)], \tag{8.18}$$

[1]Note that a low complexity method that can be used by each UE in order to estimate its channel in the presence of IQI was presented in [349]. Moreover, if the channel reciprocity property is valid, i.e. uplink and downlink occurs within a coherence block, the BS can perform the channel estimation process [511–513].

and $P_{\max}$ stands for the maximum allowable transmitted power. The optimization problem in (8.17) corresponds is identical to the problem of minimum SINR maximization, and, thus, it can be rewritten as

$$\begin{aligned} \underset{\mathbf{P}}{\mathbf{max}} \quad & \min_{k\in\mathcal{K}} \gamma_k \\ \mathbf{s.t.} \quad & \mathrm{C1}: \sum_{k\in\mathcal{K}} P_s(k) \leq P_{\max}, \end{aligned} \tag{8.19}$$

The objective function in (8.19) is not a purely analytical expression. However, by using the epigraph representation of the optimization problem in (8.17), it can be equivalently expressed as

$$\begin{aligned} \underset{\mathbf{P}}{\mathbf{max}} \quad & \mathcal{R} \\ \mathbf{s.t.} \quad & \mathrm{C}_1: \sum_{k\in\mathcal{K}} P_s(k) \leq P_{\max}, \\ & \mathrm{C}_2: \gamma_k \geq \mathcal{R}, \forall k \in \mathcal{K}. \end{aligned} \tag{8.20}$$

In the above, C_2 represents the hypograph of the original optimization problem in (8.17), with $\mathcal{R}$ being an extra auxiliary variables.

Notice that the optimization problem in (8.20) is non-convex. However, it can be easily transformed into a convex one by replacing $P_s(k)$ with $\exp(x(k))$ and $\mathcal{R}$ with $\exp(y)$ and by following similar steps as in [514]. After some mathematical manipulations, this problem can be finally expressed as

$$\begin{aligned} \underset{\mathbf{P}}{\mathbf{max}} \quad & y \\ \mathbf{s.t.} \quad & \mathrm{C}_1: \sum_{k\in\mathcal{K}} exp\left(x(k)\right) \leq P_{\max}, \\ & \mathrm{C}_2: \ln\left(\frac{\left|h_k\left(-k\right)\right|^2}{\mathrm{IRR}_k}\exp\left(x(-k)-x(k)\right)+\left(1+\frac{1}{\mathrm{IRR}_k}\right)N_0\exp(-x(k))\right) \\ & \quad + y - \ln\left(\left|h_k\left(k\right)\right|^2\right) \leq 0, \forall k \in \mathcal{K}. \end{aligned} \tag{8.21}$$

Apparently, the constraint C_1 is convex as a summation of convex functions. Next, to prove the convexity of C_2, we use (9.44), and rewrite C_2 as

$$\frac{\left|h_k\left(k\right)\right|^2 P_s(k)}{\frac{\left|h_k(-k)\right|^2}{\mathrm{IRR}_k}P_s(-k)+\left(1+\frac{1}{\mathrm{IRR}_k}\right)N_0} \geq \mathcal{R}. \tag{8.22}$$

Note that the left side of (8.22) corresponds to the SINR and it is not convex.

By replacing $P_s(k)$ with $\exp(x(k))$ and $\mathcal{R}$ with $\exp(y)$, (8.22) can be expressed as

$$\frac{\left|h_k\left(k\right)\right|^2 \exp(x(k))}{\frac{\left|h_k(-k)\right|^2}{\mathrm{IRR}_k}\exp(x(-k))+\left(1+\frac{1}{\mathrm{IRR}_k}\right)N_0} \geq \exp(y), \tag{8.23}$$

or

$$\frac{1}{\exp(y)} \geq \frac{\left|h_k\left(-k\right)\right|^2 \exp(x(-k)) + \left(1+\mathrm{IRR}_k\right)N_0}{\mathrm{IRR}_k\left|h_k\left(k\right)\right|^2\exp(x(k))}, \tag{8.24}$$

which can equivalently be written as

$$\frac{\frac{\left|h_k(-k)\right|^2}{\mathrm{IRR}_k}\exp(x(-k)-x(k))+\left(1+\frac{1}{\mathrm{IRR}_k}\right)N_0\exp(-x(k))}{\left|h_k\left(k\right)\right|^2} \leq \frac{1}{\exp(y)}. \tag{8.25}$$

By taking the natural logarithm, $\ln(\cdot)$, to both sides, (8.25) can be transformed to

$$f \leq 0, \tag{8.26}$$

where

$$f = \ln\left(\frac{|h_k(-k)|^2}{\mathrm{IRR}_k}\exp\left(x(-k)-x(k)\right)+\left(1+\frac{1}{\mathrm{IRR}_k}\right)N_0\exp(-x(k)\right)+y-\ln\left(|h_k(k)|^2\right). \quad (8.27)$$

In order to prove that (8.26) is convex, we need to prove that the eigenvalues of the Hessian matrix of f are non-negative [515]. According to [515], the Hessian matrix of f can be obtained as

$$\mathcal{H}_f = \begin{bmatrix} \frac{\partial^2 f}{\partial^2 x(k)} & \frac{\partial^2 f}{\partial x(k)\partial x(-k)} & \frac{\partial^2 f}{\partial x(k)\partial y} \\ \frac{\partial^2 f}{\partial x(-k)\partial x(k)} & \frac{\partial^2 f}{\partial^2 x(-k)} & \frac{\partial^2 f}{\partial x(-k)\partial y} \\ \frac{\partial^2 f}{\partial y\partial x(k)} & \frac{\partial y}{\partial^2 x(-k)} & \frac{\partial^2 f}{\partial^2 y} \end{bmatrix} \quad (8.28)$$

where

$$\begin{aligned}\frac{\partial^2 f}{\partial^2 x(k)} &= \frac{\partial^2 f}{\partial x(k)\partial x(-k)} = \frac{\partial^2 f}{\partial x(k)\partial y} = \frac{\partial^2 f}{\partial x(-k)\partial x(k)} = \frac{\partial^2 f}{\partial x(-k)\partial y} \\ &= \frac{\partial^2 f}{\partial x(-k)\partial y} = \frac{\partial^2 f}{\partial y\partial x(k)} = \frac{\partial y}{\partial^2 x(-k)} = \frac{\partial^2 f}{\partial^2 y} = 0, \end{aligned} \quad (8.29)$$

and

$$\frac{\partial^2 f}{\partial^2 x(-k)} = \frac{|h_k(-k)|^2\left(1+\mathrm{IRR}_k\right)N_0\exp(x(-k))}{\left(\left(1+\mathrm{IRR}_k\right)N_0+|h_k(-k)|^2\exp(x(-k))\right)^2}. \quad (8.30)$$

Therefore, the eigenvalues of $\mathcal{H}_f$ can be derived as

$$\phi_1 = \frac{|h_k(-k)|^2\left(1+\mathrm{IRR}_k\right)N_0\exp(x(-k))}{\left(\left(1+\mathrm{IRR}_k\right)N_0+|h_k(-k)|^2\exp(x(-k))\right)^2} \geq 0, \quad \phi_2 = 0, \quad \phi_3 = 0, \quad (8.31)$$

which are non-negative. This proves that the constraint C_2 is convex. In other words, the optimization problem can be solved by using convex optimization and specifically dual decomposition. Consequently, it can be solved by using the dual decomposition method [515]. For this reason, the Lagrangian of (8.21) is needed, which can be obtained as [515, Ch. 5]

$$\begin{aligned} L = y - \lambda\left(\sum_{k\in\mathcal{K}}\exp\left(x(k)\right)-P_{\max}\right) - \sum_{k\in\mathcal{K}}\mu_k\left(\ln\left(\frac{|h_k(-k)|^2}{\mathrm{IRR}_k}\exp\left(x(-k)-x(k)\right)\right.\right. \\ \left.\left.+\left(1+\frac{1}{\mathrm{IRR}_k}\right)N_0\exp(-x(k))\right)+y-\ln\left(|h_k(k)|^2\right)\right), \end{aligned} \quad (8.32)$$

where $\lambda \geq 0$ and $\mu_k \geq 0$ are the Lagrange multipliers (LMs).

Finally, for fixed LMs, by solving the Karush-Kuhn-Tucker conditions, i.e.,

$$\frac{\partial L}{\partial x(k)} = \frac{\partial L}{\partial x(-k)} = 0, \quad (8.33)$$

and after some mathematical manipulations, we get the optimal solutions $\tilde{x}(k)$ and $\tilde{x}(-k)$, which are respectively given by

$$\tilde{x}(k) = \ln\left(-\frac{\xi_k}{2}+\frac{\mu_{-k}-\mu_k}{2\lambda}+\sqrt{\frac{\xi_k^2}{4}+\frac{\left(\mu_{-k}-\mu_k\right)^2}{4\lambda^2}+\frac{\xi_k}{2\lambda}(\mu_{-k}+\mu_k)}\right). \quad (8.34)$$

or equivalently the $P_s(k)$ and $P_s(-k)$, which can be obtained as

$$\tilde{P}_s(k) = -\frac{\xi_k}{2}+\frac{\mu_{-k}-\mu_k}{2\lambda}+\sqrt{\frac{\xi_k^2}{4}+\frac{\left(\mu_{-k}-\mu_k\right)^2}{4\lambda^2}+\frac{\xi_k}{2\lambda}(\mu_{-k}+\mu_k)}. \quad (8.35)$$

and

$$\tilde{x}(-k) = \ln\left(-\frac{\xi_{-k}}{2} + \frac{\mu_k - \mu_{-k}}{2\lambda} + \sqrt{\frac{\xi_{-k}^2}{4} + \frac{(\mu_k - \mu_{-k})^2}{4\lambda^2} + \frac{\xi_{-k}}{2\lambda}(\mu_k + \mu_{-k})}\right). \tag{8.36}$$

or equivalently the $P_s(k)$ and $P_s(-k)$, which can be respectively obtained as

$$\tilde{P}_s(k) = -\frac{\xi_k}{2} + \frac{\mu_{-k} - \mu_k}{2\lambda} + \sqrt{\frac{\xi_k^2}{4} + \frac{(\mu_{-k} - \mu_k)^2}{4\lambda^2} + \frac{\xi_k}{2\lambda}(\mu_{-k} + \mu_k)}. \tag{8.37}$$

and

$$\tilde{P}_s(-k) = -\frac{\xi_{-k}}{2} + \frac{\mu_k - \mu_{-k}}{2\lambda} + \sqrt{\frac{\xi_{-k}^2}{4} + \frac{(\mu_k - \mu_{-k})^2}{4\lambda^2} + \frac{\xi_{-k}}{2\lambda}(\mu_k + \mu_{-k})}. \tag{8.38}$$

where the coefficients ξ_k and ξ_{-k} are given by

$$\xi_k = \frac{\mathrm{IRR}_k + 1}{|h_{-k}(k)|^2} N_0. \tag{8.39}$$

$$\xi_{-k} = \frac{\mathrm{IRR}_{-k} + 1}{|h_k(k)|^2} N_0. \tag{8.40}$$

For given LMs, (8.35) and (8.38) are low-complexity directly calculated PA optimization solution, given the Lagrange multiplier, that can be calculated in parallel. Interestingly, it takes into consideration the RXs non-ideal characteristics and guarantees fairness in terms of UE achievable capacity. Additionally, we point out that, according to (8.35), the power allocated to the $k-$th UE is dependent from the RF characteristics and the channels of all the $2K$ UEs that are served via the LMs, λ and μ_k. Note that for $K_{1,k} = 1$ and $K_{2,k} = 0$ ($k \in \{-K, \cdots, -1, 1, \cdots, K\}$), the proposed optimization solution is simplified to the PA for an ideal RF front-end scheme. This PA is used by the BS that is unaware of the UEs' RF imperfections, and to what follows, we refer to as "classical PA" [515]. The constants λ and μ_k can be easily estimated, in polynomial time, by an iterative algorithm such as subgradient method [516–518].

Proposition 8.1. *The minimum achievable capacity is maximized when the inequality constraint in* (8.17) *is satisfied with equality.*

Proof. Please refer to Appendix L. ■

This proposition indicates that the system should always use the total transmit power in order to maximize the minimum achievable capacity of the $2K$ UEs.

Proposition 8.2. *At the optimal, the k and $-k$ UEs will have the same achievable capacity.*

Proof. Please refer to Appendix M. ■

Proposition 8.2 claims that at the optimal solution, the k and $-k$ UEs have the same achievable capacity.

8.5 Numerical results & discussion

In this section, we demonstrate the efficiency of the proposed PA scheme by presenting simulation results. In particular, we consider that a BS serves $2K$ UEs. Each UE suffers from different levels of IQI. Furthermore, it is important to note that, unless otherwise is stated, in the following figures, we consider that $n = 3$, $\phi_k = 3^o$, $\epsilon_k < 1$ and $D_k = 1$ for $k \in \mathcal{K}$. Finally, without loss of generality, we assume that $P_{\max} = 1$.

Fig. 8.1 illustrates the detrimental effects of IQI on the achievable capacity of each UE and the efficiency of the proposed PA scheme. We observe that for low $\frac{P_{\max}}{N_0}$ values, IQI does not affect the

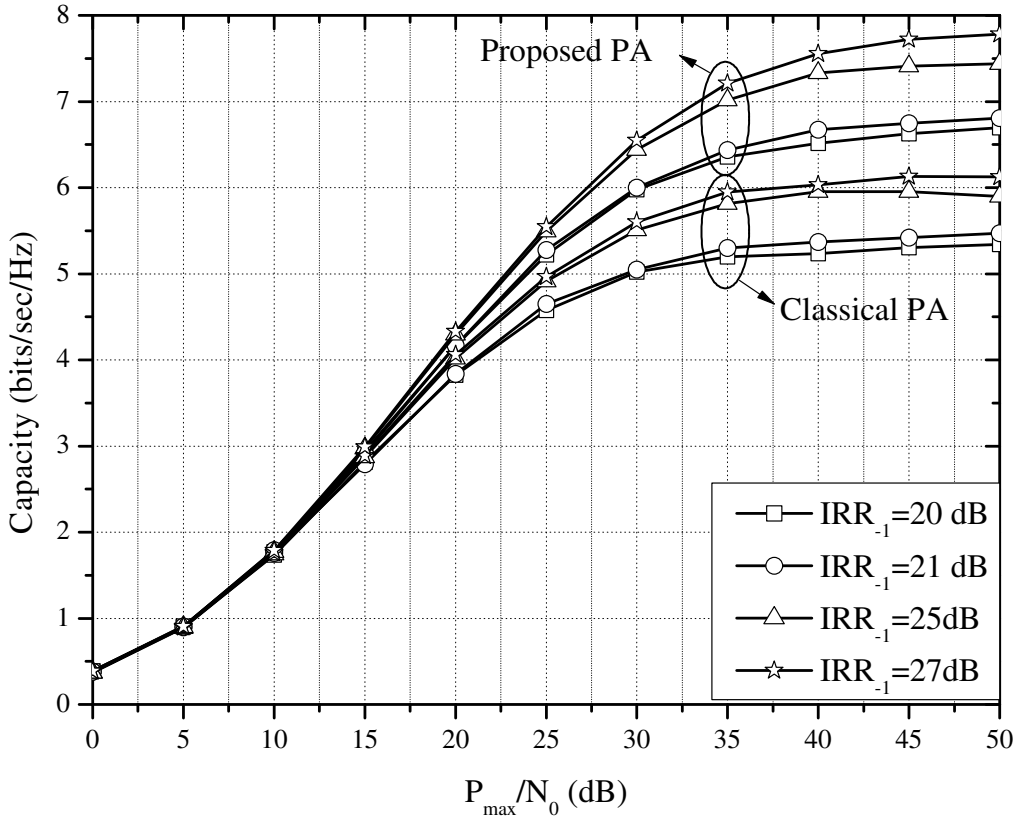

Figure 8.1 Capacity as a function of $\frac{P_{\max}}{N_0}$ for different levels of IRR_{-1}, when $\mathrm{IRR}_1 = 20$ dB and $K = 1$.

UEs capacity performance. However, as $\frac{P_{\max}}{N_0}$ increases, the impact of IQI has adverse effects on its UEs achievable capacity. Furthermore, it is evident that the proposed PA scheme can mitigate the performance degradation, due to IQI and positively contribute to the increase of the UEs achievable capacity. For example, for $\frac{P_{\max}}{N_0} = 35$ dB, $\mathrm{IRR}_1 = \mathrm{IRR}_{-1} = 20$ dB, the use of the proposed PA scheme increases the average achievable rate about 22.3%. This indicates the importance of taking into consideration the effects of the UEs IQI, when designing a PA scheme.

In Fig. 8.2, the UEs capacity as a function of the IRR_1, for different values of IRR_2 and $\frac{P_{\max}}{N_0} = 30$ dB for both classical and the proposed PA schemes, is plotted. From this figure, it is evident that the proposed PA scheme outperforms the classical one for all the IRR values. Moreover, it is observed that, for a given IRR_{-1}, as IRR_1 increases, the signal leakage of the mirror subcarrier decreases; hence, the performance of the proposed PA scheme tends to these of the conventional scheme. For example, for $\mathrm{IRR}_{-1} = 30$ dB, for $\mathrm{IRR}_1 = 20$ dB, the use of the proposed PA scheme increases the average achievable rate about 18%, whereas for $\mathrm{IRR}_1 = 30$ dB and the same IRR_1, the increase of the average achievable rate is about 5.6%.

In Fig. 8.3, the average achievable capacity of each UE of the proposed PA scheme as a function of $\frac{P_{\max}}{N_0}$ for different values of K is depicted, when $\mathrm{IRR}_k = 20$ dB, with $k \in \mathcal{K}$. Again, it is observed that the proposed PA scheme outperforms the classical PA scheme for any value of K and in all the $\frac{P_{\max}}{N_0}$ regime. Furthermore, from this figure, it is evident that as K increases, the effects of IQI become more detrimental. For instance, for $K = 2$, in the high $\frac{P_{\max}}{N_0}$ regime, each UE capacity is limited to 4.21 bits/sec/Hz, while for $K = 3$, it is constrained to 3.63 bits/sec/Hz. Additionally, we observe that as K increases, the effectiveness of the proposed PA scheme increases. For example, for $\frac{P_{\max}}{N_0} = 40$ dB, the use of the proposed PA scheme results to 24.47%, 33.79% and 41.36% increase of the average UE capacity for $K = 1$, $K = 2$ and $K = 3$, respectively.

In Fig. 8.4, the average achievable capacity of each UE as a function of $\frac{P_{\max}}{N_0}$ for different values of D_1, when $K = 1$, $D_{-1} = 1$, and $\mathrm{IRR}_1 = \mathrm{IRR}_{-1} = 20$ dB, is plotted. From this figure, it is evident that the proposed PA scheme outperforms the classical PA scheme for any value of D_1 and in all the transmitted

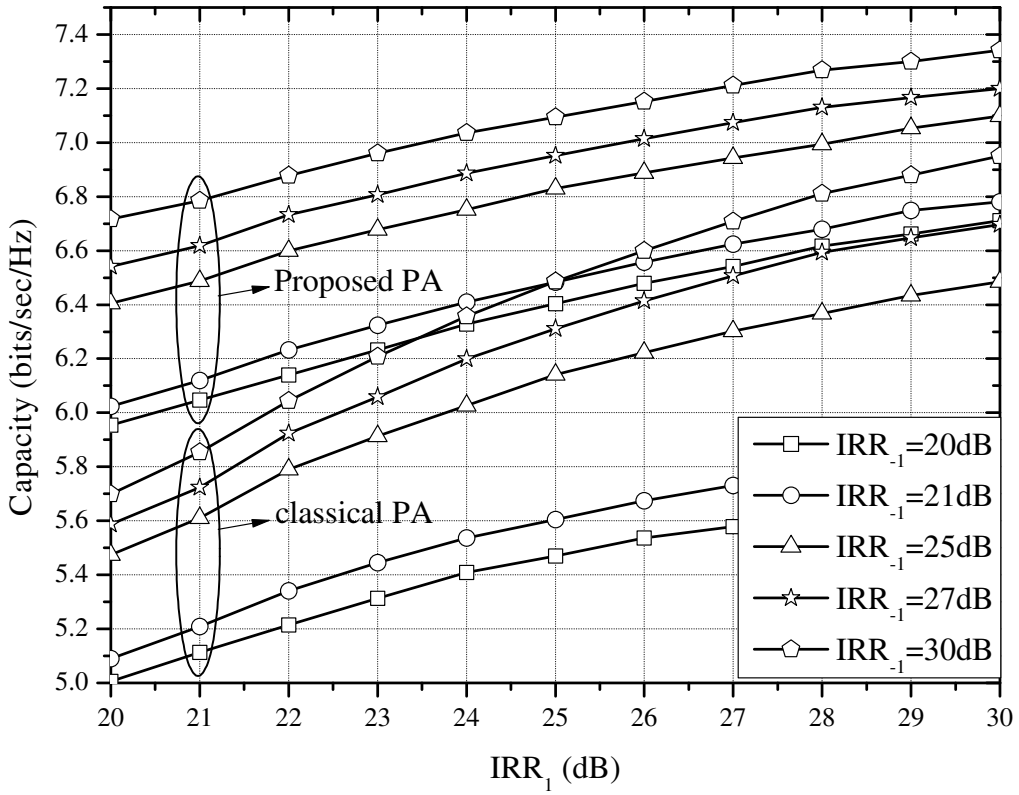

Figure 8.2 Capacity as a function of IRR_1 for different levels of IRR_{-1}, $\frac{P_{\max}}{N_0} = 30$ dB and $K = 1$.

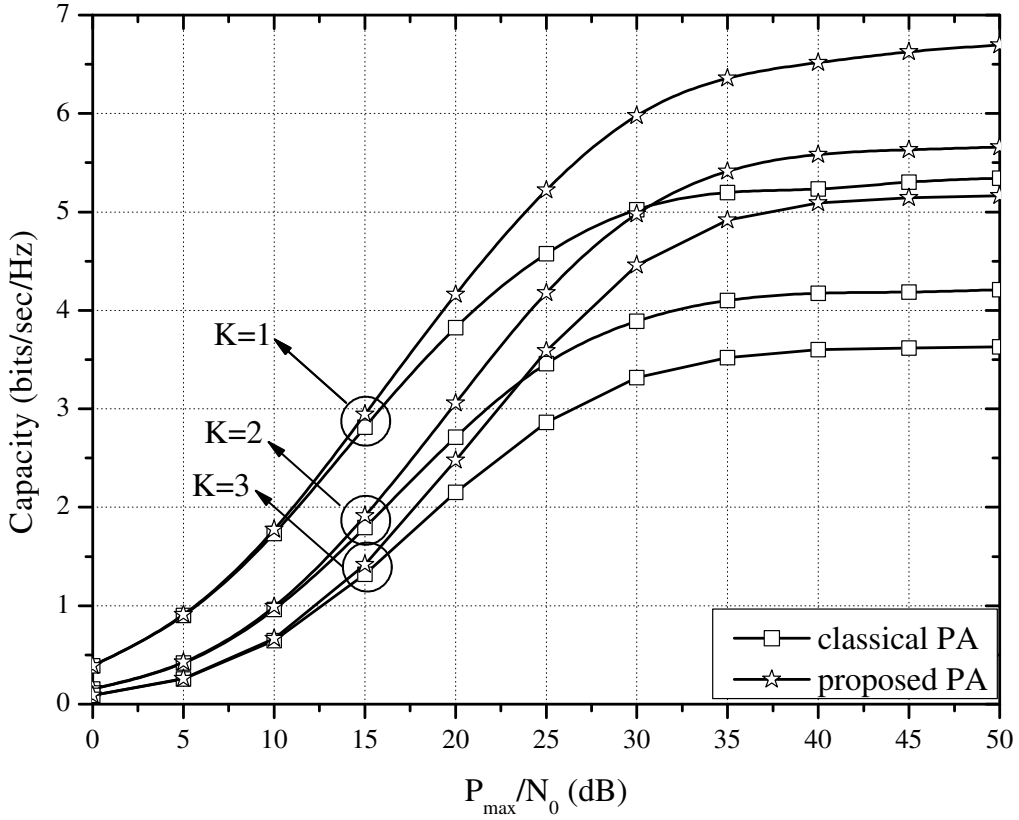

Figure 8.3 Capacity as a function of $\frac{P_{\max}}{N_0}$ for $\mathrm{IRR}_k = 20$ dB ($k \in \mathcal{K}$) and different values of K.

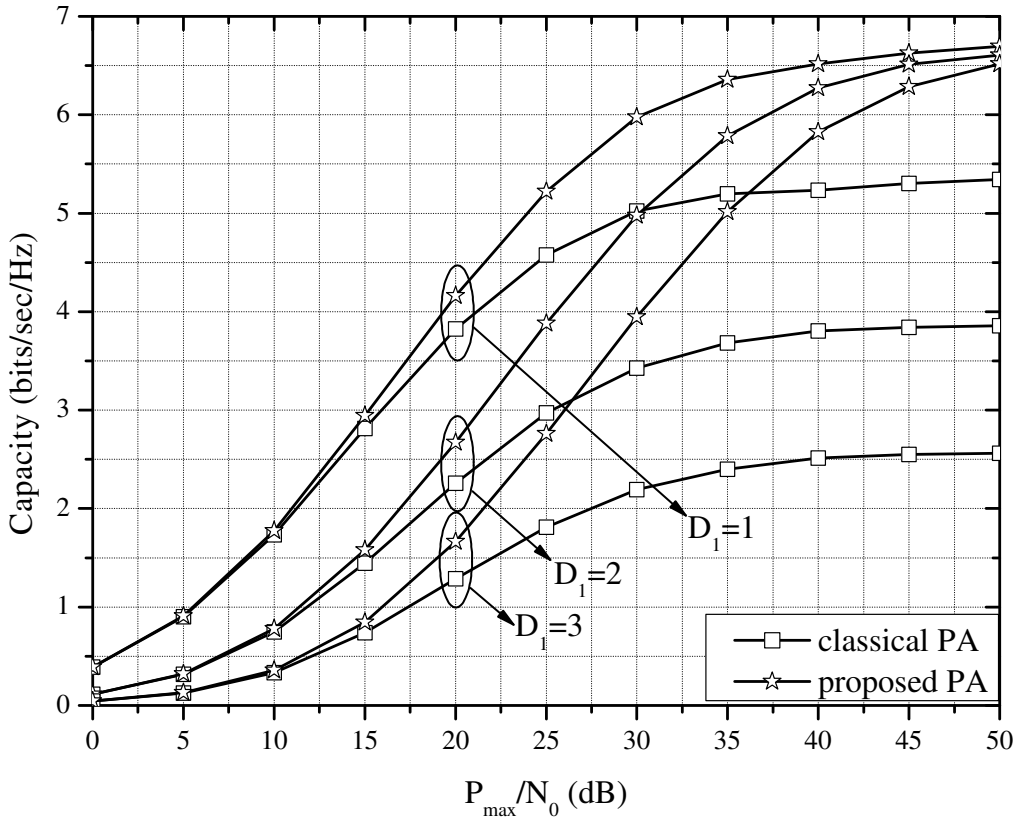

Figure 8.4 Capacity as a function of $\frac{P_{\max}}{N_0}$ for $\text{IRR}_1 = \text{IRR}_{-1} = 20$ dB, $K = 1$, $D_{-1} = 1$ and different values of D_1.

SNR region. Also, for fixed $\frac{P_{\max}}{N_0}$, as D_1 increases, the impact of IQI in the average achievable capacity become more severe, when the classical PA is employed. For example, for $\frac{P_{\max}}{N_0} = 40$ dB and $D_1 = 1$, each UE's capacity equals 6.5 bits/sec/Hz, whereas, for the same $\frac{P_{\max}}{N_0}$ value and $D_1 = 3$, each UE's capacity is 2.5 bits/sec/Hz. Moreover, we observe that as D_1 increases the effectiveness of the proposed PA scheme increases. For instance, for $\frac{P_{\max}}{N_0} = 40$ dB, the use of the proposed PA scheme results to 24.5%, 64.9% and 131.7% increase of the average UE's capacity for $D_1 = 1$, $D_1 = 2$ and $D_1 = 3$, respectively. This reveals that the proposed PA scheme provides even larger gain as compared to classic PA, when the UEs have different channel qualities.

8.6 Conclusions

In this chapter, the minimum achievable rate of UEs that suffers from IQI was maximized, with respect to the BS transmitted power. In particular, we presented a novel low-complexity solution with directly calculated PA policies, given the Lagrange multiplier, which by taking into account the impact of IQI, achieves fairness in terms of capacity for the served UEs. The proposed PA scheme has the same computational complexity as the conventional one. However, as it was demonstrated, through computer simulations, the proposed PA scheme leads to a notable increase of the UEs achievable rate, compared to the conventional PA scheme, especially, when the UEs have different channel qualities.

Chapter 9

I/Q imbalance self-interference coordination

This chapter presents a novel low-complexity scheme, which improves the performance of single-antenna multi-carrier communication systems, suffering from IQI at the RX. We refer to the proposed scheme as *I/Q-imbalance self-interference coordination (IQSC)*. IQSC does not only mitigate the detrimental effects of IQI, but, through appropriate signal processing, also coordinates the self-interference terms produced by IQI in order to achieve second-order frequency diversity. However, these benefits come at the expense of a reduction in transmission rate. More specifically, IQSC is a simple transmit diversity scheme that improves the signal quality at the RX, by elementary signal processing operations across symmetric (mirror) pairs of subcarriers. Thereby, the proposed transmission protocol has a similar complexity as Alamouti's STBC scheme and does not require extra transmit power nor any feedback. To evaluate the performance of IQSC, closed form expressions for the resulting outage probability and symbol error rate are derived. Interestingly, IQSC outperforms not only existing IQI compensation schemes, but also the ideal system without IQI for the same spectral efficiency and practical target error rates, while it achieves almost the same performance as ideal (i.e., IQI-free) equal-rate repetition coding (RC). Our findings reveal that IQSC is a promising low-complexity technique for significantly increasing the reliability of low-cost devices that suffer from high levels of IQI.

The research results of this chapter are included in [314].

9.1 Related work

The effect of RF imperfections, in genera,l was studied in several works [278, 320, 331, 417, 486, 487, 502, 503, 519], while performance degradation due to IQI in particular was investigated in [279, 350, 355, 358, 366, 367, 382, 461, 464–466, 520–522]. For instance, the authors in [366] derived an exact expression for the SINR in OFDM systems impaired by IQI, assuming that the channel of each subcarrier and its image are uncorrelated. In [520], the performance of OFDM systems employing M-QAM was studied in the presence of IQI in terms of the error vector magnitude, which is a modulation quality measure used to evaluate the effects of imperfections in digital communication systems. In [355], the impact of IQI caused by a low pass filter mismatch was illustrated and the importance of IQI compensation was highlighted. Furthermore, the authors of [367, 464–466] analyzed the performance of relaying systems in the presence of IQI. The impact of IQI in cognitive radio systems was analyzed in [278, 279, 486], where it was shown that, in a multi-channel environment, IQI increases the false alarm probability significantly and considerably limits the spectrum sensing capabilities of EDs compared to the ideal RF RX case.

Various approaches have been proposed so far to eliminate, compensate, and mitigate the effects of IQI using base band signal processing techniques (see, for example [64, 299, 319, 327, 339, 341, 347, 351, 353, 356, 365, 462, 521, 523], and references therein). For example, in [353], the authors proposed a number of pilot designs for channel estimation in OFDM systems in the presence of I/Q mismatches at both the TX and the RX. Moreover, estimation-based system-level algorithms, including least square equalization, adaptive equalization, and post-fast Fourier transform least square, were proposed in [462] to compensate the distortions caused by IQI. Furthermore, blind (non-data-aided) digital signal processing-based compensation of IQI for wideband multi-carrier systems was studied in [299, 319, 341, 351]. Specifically, in [341] a digital compensation method was proposed for MIMO systems employing STBC, which is based on the algebraic properties of the received signal combined with a suitable pilot structure, while interference cancellation-based and blind source separation-based compensation methods, were presented in [319].

All previously mentioned works deal with IQI as a source of impairment that should be compensated. In contrast to this approach, IQI at the TX may also be seen as a source of diversity, due to the TX-

induced mirror-frequency interference. This diversity can be fully exploited via joint ML detection of the signals received in the mirror subcarriers, or partially exploited by other sub-optimal nonlinear detection techniques such as SIC, as was demonstrated experimentally for OFDM in [524], and later confirmed in [525]. Still, when weighed against the implementation complexity of nonlinear RXs, the small achievable SNR improvement may prove to be too expensive [300]. Moreover, as pointed out in several prior works including [524], RX IQI is detrimental for the outage and error performance of wireless communication systems, regardless of the detector that is used. The reason for this is that RX IQI affects both the received signal and the noise; hence, it is commonly believed that RX IQI should be compensated [299, 319, 341, 350, 351, 356, 367, 374, 378, 382]. However, to the best of the author's knowledge, no solution has been proposed so far that achieves a diversity gain in the presence of RX IQI.

9.2 Motivation and contribution

From an implementation point of view, DCA is a promising approach to realize low-cost highly integrated wireless equipment. Although DCRs avoid the main drawbacks of other RX architectures, the insufficient image rejection due to IQI is a major concern. For instance, in the case of using a non-zero intermediate frequency (IF), the image signal can be up to $50-100$ dB stronger than the desired one [319]. Thus, in such situations, the $20-40$ dB attenuation provided by the quadrature down-conversion alone is clearly insufficient. Furthermore, with wideband modulated communication waveforms and high-order symbol alphabets, IQI has a tremendous impact on the demodulated signal quality and can severely degrade the RX performance, if not taken properly into account. Notice also that, although the distortion caused by IQI resembles to some extent ordinary ISI, it cannot be properly mitigated using ordinary equalization techniques due to its special structure [341].

In this chapter, we propose a novel low-complexity technique, which we refer to as *(IQSC)*, which significantly increases the performance of single-antenna multi-carrier communication systems suffering from IQI at the RX, by coordinating the self-interference caused by IQI. In contrast to the IQI compensation approach, IQSC does not only eliminate the effects of IQI, but, through signal processing, also coordinates the self-interference terms produced by IQI to achieve frequency diversity, which we refer to as *mirror-frequency diversity (MFD)*. In other words, IQSC is a low-complexity transmit diversity scheme, which improves the signal quality at the RX by simple signal processing operations across symmetric subcarrier pairs. IQSC achieves a diversity order of two, i.e., the same diversity order as maximal-ratio combining (MRC) with two RX antennas or Alamouti's STBC with two TX antennas [526]. Notably, by applying IQSC in DCA systems, the IQI is not only compensated but is no longer harmful for the system's performance. Furthermore, the proposed transmission protocol requires neither extra transmit power nor any feedback from the RX to the TX, while its computational complexity is similar to that of Alamouti's STBC scheme. However, the exploitation of the extra DoF offered by IQI to achieve two-fold transmit diversity comes at the expense of a reduction in transmission rate. In particular, the encoding process at the TX requires two consecutive time intervals (or time-slots) for transmission of each data block. Finally, an alternative IQSC *(A-IQSC)* technique is also presented, which achieves similar outage and error performance as IQSC, with the same computational complexity and rate.

To confirm the effectiveness of the proposed method, we derive closed form expressions for the outage probability and the SER of IQSC, and compare its performance (with respect to these two metrics) with two baseline systems; namely an ideal system without IQI, called *ideal RF front-end*, and a system with uncompensated IQI in the RF front-end, called *IQI RF front-end*, which correspond to the best case and the conventional transmission scenarios, respectively. Our results demonstrate the superior reliability (which comes at the expense of sacrificing throughput) of IQSC compared to the baseline systems. Surprisingly, in medium-to-high SNRs, the proposed scheme outperforms both baseline schemes in terms of error performance even for the same spectral efficiency. As another means to assess its error performance fairly, we also compare IQSC with RC and the frequency-time block code (FTBC) proposed in [527], which both have the same rate as IQSC. Again, we observe that IQSC outperforms both RC and FTBC with uncompensated IQI, referred to as *IQI RF front-end with RC* and *FTBC*, respectively, while it has a similar performance as the *ideal RF front-end with RC* and *FTBC*, i.e., RC and FTBC without IQI in the RF front-end.

9.3 Organization

The remainder of this chapter is organized as follows. The equivalent complex baseband signal representation of a multi-carrier communication system with IQI at the RX is presented in Section 9.4. In Section 9.5, the proposed IQSC encoding at the TX and the associated combining at the RX, as well as an alternative IQI coordination scheme, namely A-IQSC, are presented in detail. A performance analysis of IQSC in terms of outage probability and SER is provided in Section 9.6. A point-to-point comparison of IQSC with a system employing RC, under the same bandwidth and power constraints, is given at the end of the same section. In Section 9.7, we verify our theoretical analysis by computer simulations, confirming that IQSC is a robust technique for multi-carrier transmission under IQI. In Section 9.8.1, the main merits and drawbacks of IQSC are outlined, followed by some discussion regarding the new concept of MFD. Finally, Section 9.8.2 concludes the chater by summarizing the main findings.

9.4 System and signal model

We start this section by considering the base band signal model of a system without IQI, which will be referred to as the ideal RF front-end. Having this as a reference, we present the practical IQI signal model of multi-carrier DCRs, assuming a single antenna at both the TX and the RX, perfect channel estimation at the RX, and no CSI at the TX.

9.4.1 Ideal RF front-end

We consider a multi-carrier system with $2K$ RF subcarriers and assume down-conversion to base band using the wide band direct-conversion principle. For notational convenience, we denote the set of these subcarriers as

$$\{-K, \cdots, -1, 1 \cdots, K\} = \{k\}_{k=-K}^{K}, \tag{9.1}$$

and the set of data symbols loaded to them as

$$S_K = \{s(-K), \ldots, s(-1), s(1), \ldots, s(K)\} = \{s(k)\}_{k=-K}^{K}. \tag{9.2}$$

We further assume flat fading on each subcarrier, and that the RF front-ends of both the TX and the RX are perfect, i.e., no IQI is present in the system.

The received signal is passed through various front-end stages, including filtering, amplification, analog I/Q demodulation (down-conversion), and sampling. The baseband equivalent received signal in subcarrier k is

$$r_{\mathrm{id}}(k) = h(k)s(k) + n(k), \tag{9.3}$$

where fading gain $h(k)$ is modeled as a zero-mean complex Gaussian process of unit variance, and $n(k)$ represents circularly symmetric AWGN with PSD N_0.

9.4.2 RX with IQI in the RF front-end

In this section, we explore the effect of I/Q mismatch on the overall link quality, assuming that the RF front-end of the TX is perfect, while the RX suffers from IQI.[1] We also assume that transmitted signals $s(k)$ and $s(-k)$, carried by subcarriers k and $-k$, are associated with channel gains $h(k)$ and $h(-k)$, respectively, which are mutually independent RVs.

According to (4.20), the base band equivalent received signal on subcarrier k is given by

$$r(k) = K_1 r_{\mathrm{id}}(k) + K_2 r_{\mathrm{id}}^{*}(-k), \tag{9.4}$$

with $r_{\mathrm{id}}(-k)$ being the base band equivalent received signal for perfect I/Q balance on subcarrier $-k$. Note that for notational convenience, the superscript r has been neglected from the RX IQI coefficients. Substituting (9.3) into (9.4), we obtain

$$r(k) = K_1 h(k)s(k) + i(k) + w(k), \tag{9.5}$$

[1] This might correspond to a downlink scenario, where the low-cost DCA user equipment (UE) suffers from IQI.

Table 9.1 The IQSC encoding and transmission protocol.

Subcarrier index	$-K$	$\cdots$	$-k$	$\cdots$	-1	1	$\cdots$	k	$\cdots$	K
Intended data set	$s(-K)$	$\cdots$	$s(-k)$	$\cdots$	$s(-1)$	$s(1)$	$\cdots$	$s(k)$	$\cdots$	$s(K)$
1st time interval	$s^*(-K)$	$\cdots$	$s^*(-k)$	$\cdots$	$s^*(-1)$	$s(1)$	$\cdots$	$s(k)$	$\cdots$	$s(K)$
2nd time interval	$s(K)$	$\cdots$	$s(k)$	$\cdots$	$s(1)$	$-s^*(-1)$	$\cdots$	$-s^*(-k)$	$\cdots$	$-s^*(-K)$

where the interference and composite noise terms, namely $i(k)$ and $w(k)$, are given by

$$i(k) = K_2 h^*(-k)s^*(-k), \tag{9.6}$$
$$w(k) = K_1 n(k) + K_2 n^*(-k). \tag{9.7}$$

Here, $w(k)$ is a zero-mean complex Gaussian process with variance

$$\sigma_w^2 = \left(|K_1|^2 + |K_2|^2\right) N_0. \tag{9.8}$$

9.5 The proposed IQSC transceiver design

In this section, we present IQSC, a novel low-complexity scheme for increasing the performance of single-antenna multi-carrier communication systems suffering from IQI at the RX. The proposed architecture has two main components:

a) the IQSC encoding scheme at the TX, and

b) the combining scheme at the RX.

9.5.1 The IQSC encoding scheme

Transmission is organized in two time intervals. As shown in Table 9.1, given the data set S_K, the following sequences of symbols are transmitted during the first and second time intervals, respectively,

$$\mathrm{T}_1(S_K) = \left(s^*(-K), \ldots, s^*(-k), \ldots, s^*(-1), s(1), \ldots, s(k), \ldots, s(K)\right), \tag{9.9}$$
$$\mathrm{T}_2(S_K) = \left(s(K), \ldots, s(k), \ldots, s(1), -s^*(-1), \ldots, -s^*(-k), \ldots, -s^*(-K)\right). \tag{9.10}$$

Assuming that the channels for subcarriers k and $-k$ remain constant over two consecutive time intervals,[2] the received signal in the first time interval on subcarrier k becomes

$$\begin{aligned} x_1(k) &= K_1 h(k)s(k) + K_2 \left(h(-k)s^*(-k)\right)^* + K_1 n_1(k) + K_2 n_1^*(-k) \\ &= a_1 s(k) + a_2 s(-k) + w_1(k), \end{aligned} \tag{9.11}$$

where a_1 and a_2 are newly introduced channel-related parameters given by

$$a_1 = K_1 h(k) \quad \text{and} \quad a_2 = K_2 h^*(-k), \tag{9.12}$$

and the composite noise term $w_1(k)$ in the first time interval on subcarrier k is given by

$$w_1(k) = K_1 n_1(k) + K_2 n_1^*(-k). \tag{9.13}$$

Similarly, the received signal in the second time interval on subcarrier k is

$$\begin{aligned} x_2(k) &= K_1 h(k) \left(-s^*(-k)\right) + K_2 \left(h(-k)s(k)\right)^* + K_1 n_2(k) + K_2 n_2^*(-k) \\ &= -a_1 s^*(-k) + a_2 s^*(k) + w_2(k), \end{aligned} \tag{9.14}$$

[2] Practical systems are usually designed such that this assumptions holds in order to facilitate channel estimation and tracking. For channel estimation, the technique proposed in [524] could be applied.

with the composite noise term $w_2(k)$ in the second time interval on subcarrier k being

$$w_2(k) = K_1 n_2(k) + K_2 n_2^*(-k). \tag{9.15}$$

The received signals in the first and second time intervals on subcarrier $-k$ are

$$\begin{aligned} x_3(-k) &= K_1 h(-k) s^*(-k) + K_2 \left(h(k)s(k)\right)^* + K_1 n_1(-k) + K_2 n_1^*(k) \\ &= a_3 s^*(-k) + a_4 s^*(k) + w_1(-k), \end{aligned} \tag{9.16}$$

and

$$\begin{aligned} x_4(-k) &= K_1 h(-k) s(k) + K_2 \left(-h(k)s^*(-k)\right)^* + K_1 n_2(-k) + K_2 n_2^*(k) \\ &= a_3 s(k) - a_4 s(-k) + w_2(-k), \end{aligned} \tag{9.17}$$

respectively, where the channel-related parameters a_3 and a_4 are given by

$$a_3 = K_1 h(-k) \quad \text{and} \quad a_4 = K_2 h^*(k), \tag{9.18}$$

and $w_1(-k)$ and $w_2(-k)$ are the composite noise terms in the first and second time intervals on subcarrier $-k$, calculated from (9.13) and (9.15), respectively.

From (9.11), (9.14), (9.16), and (9.17), we observe that the received signals on subcarriers k and $-k$ are interfered by the received signals on subcarriers $-k$ and k, respectively.

9.5.2 The IQSC combining scheme

The IQSC combiner uses the four received signals in the first and second time interval on subcarriers k and $-k$ to form the following two signals

$$y(k) = a_1^* x_1(k) + a_2 x_2^*(k) + a_3^* x_4(-k) + a_4 x_3^*(-k), \tag{9.19}$$

$$y(-k) = -a_1 x_2^*(k) + a_2^* x_1(k) + a_3 x_3^*(-k) - a_4^* x_4(-k), \tag{9.20}$$

which are subsequently used for decoding. Substituting (9.11), (9.14), (9.16), and (9.17) into (9.19) and (9.20), we obtain

$$y(k) = \sum_{i=1}^{4} |a_i|^2 s(k) + z(k), \tag{9.21}$$

$$y(-k) = \sum_{i=1}^{4} |a_i|^2 s(-k) + z(-k), \tag{9.22}$$

where

$$\sum_{i=1}^{4} |a_i|^2 = \left(|K_1|^2 + |K_2|^2\right)\left(|h(k)|^2 + |h(-k)|^2\right) \tag{9.23}$$

is the gain achieved by IQSC, and

$$z(k) = a_1^* w_1(k) + a_2 w_2^*(k) + a_3^* w_2(-k) + a_4 w_1^*(-k), \tag{9.24}$$

$$z(-k) = -a_1 w_2^*(k) + a_2^* w_1(k) + a_3 w_1^*(-k) - a_4^* w_2(-k), \tag{9.25}$$

represent the noise components at the output of the combiner, which both have variance

$$\sigma_z^2 = \left(|K_1|^2 + |K_2|^2\right)^2 \left(|h(k)|^2 + |h(-k)|^2\right) N_0. \tag{9.26}$$

The combined signals in (9.21) and (9.22) are not only IQI free, but, at the same time, they reveal that the diversity order achieved by IQSC is equal to those of MRC with two antennas at the RX and Alamouti's STBC with two antennas at the TX [526].

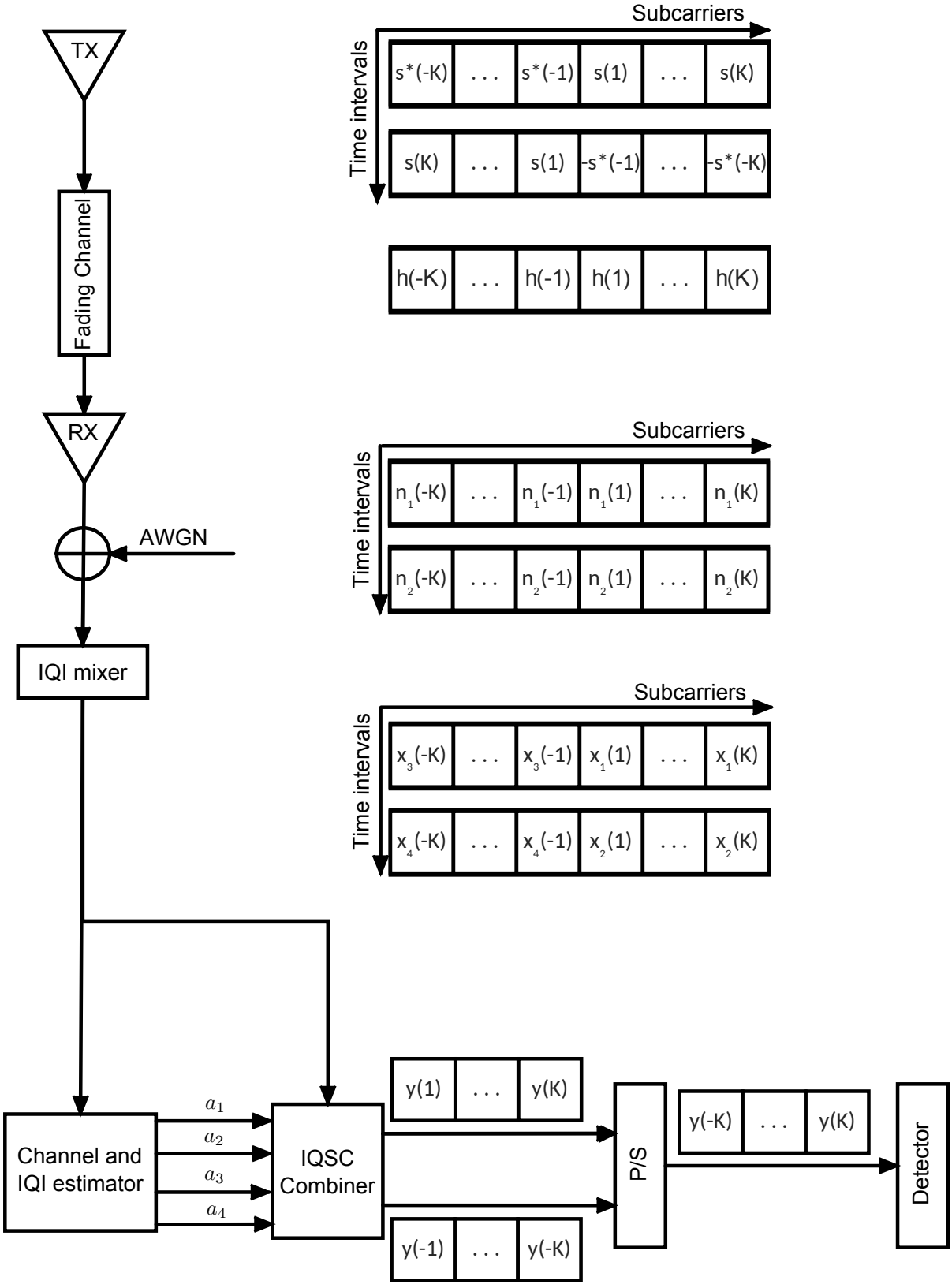

Figure 9.1 Block diagram of the proposed IQSC scheme with RX IQI. In this block diagram, P/S stands for the parallel-to-serial converter.

9.5.3 An alternative mirror-frequency diversity scheme

Next, we present an alternative low-complexity transmit diversity scheme, i.e., A-IQSC, which is also applicable when the fading channel is constant only over a single time interval. Like IQSC, A-IQSC requires neither extra transmit power nor feedback. In fact, A-IQSC has the same properties, complexity, and rate as IQSC, since it uses two mirror subcarriers to transmit the same signal.

Particularly, given the intended data set $\tilde{S}_K$,

$$\tilde{S}_K = \{s(1), \cdots, s(K)\} = \{s(k)\}_{k=1}^{K}, \tag{9.27}$$

the following sequence of symbols is transmitted in one time interval

$$\mathrm{T}(\tilde{S}_K) = \left(s^*(K), \ldots, s^*(k), \ldots, s^*(1), s(1), \ldots, s(k), \ldots, s(K)\right). \tag{9.28}$$

Then, the received signal at subcarriers k and $-k$ are

$$\begin{aligned} x(k) &= K_1 h(k) s(k) + K_2 \left(h(-k) s^*(k)\right)^* + K_1 n(k) + K_2 n^*(-k) \\ &= \alpha s(k) + w(k), \end{aligned} \tag{9.29}$$

and

$$\begin{aligned} x(-k) &= K_1 h(-k) s^*(k) + K_2 \left(h(k) s(k)\right)^* + K_1 n(-k) + K_2 n^*(k) \\ &= \beta s^*(k) + w(-k), \end{aligned} \tag{9.30}$$

respectively, where the new channel-related parameters are now given by

$$\alpha = a_1 + a_2 = K_1 h(k) + K_2 h^*(-k) \tag{9.31}$$

and

$$\beta = a_3 + a_4 = K_1 h(-k) + K_2 h^*(k). \tag{9.32}$$

The combiner, by using the received signals on subcarriers k and $-k$, forms the following signal that is sent to the detector

$$y(k) = \alpha^* x(k) + \beta x^*(-k). \tag{9.33}$$

By substituting (9.29) and (9.30) into (9.33), we obtain

$$y(k) = \left(|\alpha|^2 + |\beta|^2\right) s(k) + z_c(k), \tag{9.34}$$

where

$$z_c(k) = \alpha^* w(k) + \beta w^*(-k) \tag{9.35}$$

is the noise component at the output of the combiner and has variance

$$\sigma_{z_c}^2 = \left(|K_1|^2 + |K_2|^2\right)^2 \left(|h(k)|^2 + |h(-k)|^2\right) N_0. \tag{9.36}$$

Notice that the resulting combined signal in (9.34) is IQI free. Furthermore, according to (9.31) and (9.32), and after some basic algebraic manipulations, we obtain

$$|\alpha|^2 + |\beta|^2 = \left(|K_1|^2 + |K_2|^2\right) \left(|h(k)|^2 + |h(-k)|^2\right) + 4\mathrm{Re}\{K_1 K_2^* h(k) h(-k)\}. \tag{9.37}$$

For practical values of ϕ, i.e., $\phi < 5^o$ [367], according to (4.15) and (4.16) , K_1 and K_2 can be approximated as $K_1 \approx \Re\{K_1\}$ and $K_2 \approx \Re\{K_2\}$, which based on (4.17) are connected through

$$\Re\{K_1\} + \Re\{K_2^*\} \approx 1, \tag{9.38}$$

or equivalently

$$\frac{\Re\{K_2^*\}}{\Re\{K_1\}} \approx \frac{1}{\Re\{K_1\}} - 1. \tag{9.39}$$

Moreover, for practical values of IRR, i.e., 20 dB $\leq$ IRR $\leq$ 40 dB [299, 307, 318, 321], we have $\frac{1}{10} \leq |\frac{\Re\{K_2^*\}}{\Re\{K_1\}}| \leq \frac{1}{100}$. By substituting these values into (9.39), we obtain $\frac{10}{11} \leq \Re\{K_1\} \leq \frac{100}{101}$. Hence, as IRR increases, $K_1 \to 1$ and consequently

$$K_1 K_2^* = K_1 - K_1^2 \to 0. \tag{9.40}$$

Furthermore, except for few central subcarriers, the correlation between subcarrier k and its image subcarrier $-k$ is small due to their large spectral separation, hence, they can be assumed to be independent, i.e.,

$$E\left\{4\Re\{K_1 K_2^* h(k)h(-k)\}\right\} = 0. \tag{9.41}$$

Therefore, the second term on the right-hand side of (9.37) can be neglected, and (9.37) can be approximated as [367]

$$|\alpha|^2 + |\beta|^2 \approx \left(|K_1|^2 + |K_2|^2\right)\left(|h(k)|^2 + |h(-k)|^2\right), \tag{9.42}$$

which is identical to the combined channel gain for IQSC in (9.23). Since IQSC and A-IQSC also exhibit the same noise variance (see (9.26) and (9.36)), we expect A-IQSC to achieve a similar performance as IQSC.

9.6 Performance analysis

In this section, we investigate the effects of IQI on the system performance considering the cases of 1) ideal RF front-end, 2) uncompensated IQI at the RX (i.e., IQI RF front-end), 3) compensated IQI using IQSC, and 4) compensated IQI using A-IQSC. Thereby, perfect CSI and IQI parameter knowledge is assumed at the RX.[3] In Section 9.6.1, we give the respective instantaneous SINR expressions, and then, in Section 9.6.2, we use these expressions to evaluate the end-to-end outage probability, i.e., the probability that the SINR falls below a given threshold. In Section 9.6.3, we derive closed form expressions for the SER.

9.6.1 Signal-to-interference-plus-noise ratio

9.6.1.1 Ideal RF front-end

In case of an ideal RF front-end, the instantaneous SINR is given by

$$\gamma_{\mathrm{id}}(k) = |h(k)|^2 \frac{E_s}{N_0}, \tag{9.43}$$

where E_s is the average energy of the transmitted symbol.

9.6.1.2 IQI RF front-end

When IQI impairs the RX, then, based on (9.5) and (9.7), the instantaneous SINR per symbol on subcarrier k is given by

$$\gamma(k) = \frac{|K_1|^2|h(k)|^2 E_s}{|K_2|^2|h(-k)|^2 E_s + \left(|K_1|^2 + |K_2|^2\right) N_0} = \frac{\gamma_{\mathrm{id}}(k)}{\frac{\gamma_{\mathrm{id}}(-k)}{\mathrm{IRR}} + \left(1 + \frac{1}{\mathrm{IRR}}\right)}. \tag{9.44}$$

We assume that the correlation between subcarrier k and its image $-k$ is small due to their large spectral separation. Hence, $\gamma_{\mathrm{id}}(k)$ and $\gamma_{\mathrm{id}}(-k)$ can be assumed statistically independent. In general, $\gamma_{\mathrm{id}}(k)$ and $\gamma_{\mathrm{id}}(-k)$ are correlated RVs with the correlation coefficient given by

$$\rho = \mathrm{E}\{\gamma_{\mathrm{id}}(k)\gamma_{\mathrm{id}}^*(-k)\}. \tag{9.45}$$

When subcarriers k and $-k$ are close to each other, then the correlation may be significant. To simplify the analysis, we assume that $\rho = 0$, which is an accurate assumption except for few central subcarriers [366, 367, 465]. Note that this assumption is valid for several practical wireless communication systems, such as LTE, high performance radio local area network (HIPERLAN), and WLAN, since the central subcarriers are not used in those systems [269, 528–530].

[3] The case of imperfect CSI due to IQI and outdated estimation will not be investigated in this chapter. However, the performance results presented here can be considered as upper bounds for the case of imperfect CSI.

9.6.1.3 IQSC

Assuming equal transmit power for the IQSC scheme and the IQI RF front-end scenario, then, based on (9.21), (9.22), and (9.26), the instantaneous SNR is given by

$$\begin{aligned}\gamma_{\mathrm{IQSC}}(k) &= \left(|h(k)|^2 + |h(-k)|^2\right)\frac{E_s}{2N_0} \\ &= \frac{1}{2}\left(\gamma_{\mathrm{id}}(k) + \gamma_{\mathrm{id}}(-k)\right). \end{aligned} \tag{9.46}$$

9.6.1.4 A-IQSC

Assuming that the total transmit power of both subcarriers in A-IQSC is identical to that of the IQI RF front-end scenario, then, based on (9.34), (9.36), and (9.42), for practical IQI levels, the instantaneous SNR can be approximated by (9.46).

9.6.2 Outage probability analysis

9.6.2.1 Ideal RF front-end

Assuming that the channel amplitude $|h(k)|$ follows a Rayleigh distribution, the instantaneous SNR $\gamma_{\mathrm{id}}(k)$ given by (9.43) is an exponential distributed RV. Hence, the end-to-end outage probability is given by

$$P_{\mathrm{out}}\left(\gamma_{\mathrm{th}}\right) = 1 - e^{-\frac{\gamma_{\mathrm{th}}}{\overline{\gamma}_{\mathrm{id}}}}, \tag{9.47}$$

where

$$\overline{\gamma}_{\mathrm{id}} = \frac{E_s}{N_0} \tag{9.48}$$

and

$$\gamma_{\mathrm{th}} = 2^R - 1, \tag{9.49}$$

is the SNR threshold with R being the transmission rate.

9.6.2.2 IQI RF front-end

Taking into account (9.44), using $x = \gamma_{\mathrm{id}}(k)$ and $y = \gamma_{\mathrm{id}}(-k)$, and exploiting the independence between the exponentially distributed RVs x and y, we obtain for the outage probability [367, 531]

$$P_{\mathrm{out}}\left(\gamma_{\mathrm{th}}\right) = \int_0^{\infty} F_x\left(x < \frac{\gamma_{\mathrm{th}}}{\mathrm{IRR}}y + \gamma_{\mathrm{th}}\left(1 + \frac{1}{\mathrm{IRR}}\right)\right) f_y(y)dy, \tag{9.50}$$

where $F_x(x < X)$ and $f_y(y)$ are the CDF of x and the PDF of y, respectively. Therefore, (9.50) can be equivalently rewritten as

$$P_{\mathrm{out}}\left(\gamma_{\mathrm{th}}\right) = \int_0^{\infty}\left(1 - \exp\left(-\left(\frac{\gamma_{\mathrm{th}}}{\mathrm{IRR}\overline{\gamma}_{\mathrm{id}}}y + \frac{\gamma_{\mathrm{th}}}{\overline{\gamma}_{\mathrm{id}}}\left(1 + \frac{1}{\mathrm{IRR}}\right)\right)\right)\right)\exp\left(-\frac{y}{\overline{\gamma}_{\mathrm{id}}}\right)dy, \tag{9.51}$$

By evaluating the integral in (9.51), we get

$$P_{\mathrm{out}}\left(\gamma_{\mathrm{th}}\right) = 1 - \frac{e^{-\frac{\gamma_{\mathrm{th}}}{\overline{\gamma}_{\mathrm{id}}}\left(1+\frac{1}{\mathrm{IRR}}\right)}}{1 + \frac{\gamma_{\mathrm{th}}}{\mathrm{IRR}}}, \tag{9.52}$$

which depends in the IQI via the IRR. Note that, in the high-SNR regime ($\overline{\gamma}_{\mathrm{id}} \to \infty$), the outage probability approaches

$$P_{\mathrm{out}}\left(\gamma_{\mathrm{th}}\right) \doteq 1 - \frac{1}{1 + \frac{\gamma_{\mathrm{th}}}{\mathrm{IRR}}}. \tag{9.53}$$

Furthermore, notice that in case of an ideal RF front-end, i.e., IRR $\to \infty$, (9.52) simplifies to (9.47), while the lower bound of the outage probability at the high SNR regime tends to zero.

9.6.2.3 IQSC

In the proposed scheme, the effective SNR, γ_{IQSC}, is the sum of the instantaneous SNRs on subcarriers k and $-k$, which follow exponential distributions. Therefore, γ_{IQSC} is a chi-square distributed RV with mean $\overline{\gamma}_{\mathrm{IQSC}}$ and the PDF is given by

$$f_{\gamma_{\mathrm{IQSC}}}(\gamma) = \frac{\gamma}{\overline{\gamma}^2_{\mathrm{IQSC}}} e^{-\frac{\gamma}{\overline{\gamma}_{\mathrm{IQSC}}}}. \tag{9.54}$$

Hence, the outage probability is obtained as

$$P_{\mathrm{out}}\left(\tilde{\gamma}_{\mathrm{th}}\right) = 1 - \frac{\overline{\gamma}_{\mathrm{IQSC}} + \tilde{\gamma}_{\mathrm{th}}}{\overline{\gamma}_{\mathrm{IQSC}}} e^{-\frac{\tilde{\gamma}_{\mathrm{th}}}{\overline{\gamma}_{\mathrm{IQSC}}}}, \tag{9.55}$$

where $\overline{\gamma}_{\mathrm{IQSC}} = \overline{\gamma}_{\mathrm{id}}$, and $\tilde{\gamma}_{th}$ is the SNR threshold. Since, IQSC requires two time slots to transmit one data set S_K, $\tilde{\gamma}_{th}$ and R are connected via

$$\tilde{\gamma}_{\mathrm{th}} = 2^{2R} - 1. \tag{9.56}$$

Interestingly, when IQSC is employed, the outage performance is independent of the levels of IQI at the RX, i.e., it is not a function of IRR.

9.6.2.4 A-IQSC

In A-IQSC and for practical IQI levels, according to (9.42), the effective SNR is approximately equal to γ_{IQSC}. Hence, the outage probability of A-IQSC is approximately equal to that of IQSC.

9.6.3 Symbol error rate analysis

For slow flat fading, the SER can be derived by averaging the conditional error probability in AWGN, $P_s(e|\gamma)$, over the fading distribution. Mathematically, the SER can be evaluated as

$$P_s(e) = \int_0^\infty P_s(e|\gamma) f_\gamma(\gamma) d\gamma, \tag{9.57}$$

where $f_\gamma(\gamma)$ is the PDF of the end-to-end SNR. For several Gray bit-mapped constellations employed in practical systems, $P_s(e|\gamma)$ is of the form

$$P_s(e|\gamma) = A \operatorname{erfc}\left(\sqrt{B\gamma}\right), \tag{9.58}$$

where A and B are modulation dependent constants. For example, for binary phase-shift keying (BPSK) $A = 0.5$ and $B = 1$, while for QPSK $A = 1$ and $B = 0.5$. In the case of square/rectangular M-QAM, $P_s(e|\gamma)$ can be written as a finite weighted sum of erfc $\left(\sqrt{B\gamma}\right)$ [532].

9.6.3.1 Ideal RF front-end

The instantaneous SNR follows an exponential distribution with PDF

$$f_{\gamma_{\mathrm{id}}}(\gamma) = \frac{1}{\overline{\gamma}_{\mathrm{id}}} e^{-\frac{\gamma}{\overline{\gamma}_{\mathrm{id}}}}. \tag{9.59}$$

Substituting (9.58) and (9.59) into (9.57), and carrying out the integration, we get

$$P_s(e) = \frac{A}{1 + B\overline{\gamma}_{\mathrm{id}} + \sqrt{B\overline{\gamma}_{\mathrm{id}} + (B\overline{\gamma}_{\mathrm{id}})^2}}. \tag{9.60}$$

9.6.3.2 IQI RF front-end

In case of uncompensated IQI, the SER is given by [340]

$$P_s(e) = \frac{1}{M} \sum_{m=1}^{M} P_s(e_m), \tag{9.61}$$

where M is the modulation order and

$$P_s(e_m) = \frac{M-1}{M} - \frac{2(\sqrt{M}-1)}{M\sqrt{1+\phi_m^2}} - \frac{4(M-1)^2}{\pi M\sqrt{1+\phi_m^2}} \arctan\left(\frac{1}{1+\phi_m^2}\right) \tag{9.62}$$

with

$$\phi_m^2 = \frac{2(M-1)}{3E_s\mathrm{IRR}}\left(|i_m|^2 + (\mathrm{IRR}+1)\,N_0\right). \tag{9.63}$$

In (9.63), i_m denotes the m-th complex-valued symbol of the modulation alphabet. From (9.62) and (9.63), we observe that for uncompensated IQI, the SER depends on the levels of the IQI via IRR.

9.6.3.3 IQSC

By substituting (9.54) and (9.58) into (9.57) and carrying out the integration, we get after some basic algebraic manipulations

$$P_s(e) = A\frac{-3\sqrt{B} - 2\overline{\gamma}_{\mathrm{IQSC}}\sqrt{B^3} + 2(B+1)\sqrt{B+\frac{1}{\overline{\gamma}_{\mathrm{IQSC}}}}}{2\overline{\gamma}_{\mathrm{IQSC}}\sqrt{\left(B+\frac{1}{\overline{\gamma}_{\mathrm{IQSC}}}\right)^3}}. \tag{9.64}$$

From (9.64), we observe that by employing IQSC, the error performance of a receiver with IQI becomes independent of the IQI level.

9.6.3.4 A-IQSC

For practical values of IRR, based on (9.42), the SER can be straightforwardly approximated by (9.64).

9.6.4 Comparison with equal-rate repetition coding (RC)

In this section, we compare the performance of the proposed IQSC with RC across subcarriers, where the same signal is sent from the TX to the RX twice using subcarriers k and $-k$. We make this comparison in order to demonstrate the efficiency of IQSC compared to a scheme having the same rate. Besides, since IQSC and RC assume the same form in the absence of IQI, we expect then to achieve similar performance in this case.

Assuming a system with RX IQI, the received signals on subcarriers k and $-k$ are

$$x(k) = K_1 h(k)s(k) + K_2 h^*(-k)s^*(k) + w(k), \tag{9.65}$$

and

$$x(-k) = K_1 h(-k)s(k) + K_2 h^*(k)s^*(k) + w(-k), \tag{9.66}$$

respectively, where we set $s(k) = s(-k)$ due to the RC. In (9.65) and (9.66), $w\,(k)$ and $w\,(-k)$ are given by (9.7).

After combining the received signal using MRC, the overall signal can be written as

$$\begin{aligned} y_{\mathrm{RC}}(k) &= h^*(k)x(k) + h^*(-k)x(-k) \\ &= K_1\left(|h(k)|^2 + |h(-k)|^2\right)s(k) + i_{\mathrm{RC}}(k) + z_{\mathrm{RC}}(k), \end{aligned} \tag{9.67}$$

where $i_{\mathrm{RC}}(k)$ and $z_{\mathrm{RC}}(k)$ are the self-interference and noise terms, respectively, given by

$$i_{\mathrm{RC}}(k) = 2K_2 h^*(k)h^*(-k)s^*(k), \tag{9.68}$$

$$z_{\mathrm{RC}}(k) = K_1 h^*(k)n(k) + K_2 h^*(k)n^*(-k) + K_1 h^*(-k)n(-k) + K_2 h^*(k)n^*(k). \tag{9.69}$$

Under perfect I/Q matching, i.e., $K_1 = 1$ and $K_2 = 0$, the model in (9.67) reduces to

$$y_{\mathrm{RC}}(k) = \left(|h_1(k)|^2 + |h_2(k)|^2\right)s(k) + w(k). \tag{9.70}$$

In this case, since (9.70) is similar to (9.21), the outage probability can be written as in (9.55), and the SER is given by (9.64), i.e., in the absence of IQI, IQSC and RC achieve indeed the same performance.

Based on (9.67)-(9.69), the instantaneous SINR can be expressed as

$$\gamma_{\mathrm{RC}}(k) = \frac{S_{\mathrm{RC}}}{I_{\mathrm{RC}} + N_{\mathrm{RC}}}, \tag{9.71}$$

where S_{RC}, I_{RC}, and N_{RC} are the signal, interference, and noise power components, respectively, and are given by

$$S_{\mathrm{RC}} = |K_1|^2 \left(|h(k)|^2 + |h(-k)|^2\right)^2 E_s, \tag{9.72}$$

$$I_{\mathrm{RC}} = 4|K_2|^2 |h(k)|^2 |h(-k)|^2 E_s, \tag{9.73}$$

$$N_{\mathrm{RC}} = \left(|K_1|^2 + |K_2|^2\right) \left(|h(k)|^2 + |h(-k)|^2\right) N_0. \tag{9.74}$$

Note that, in the high SNR regime, i.e., $N_0 \to 0$, the instantaneous SINR can be obtained as

$$\begin{aligned} \gamma_{\mathrm{RC}}(k) &\triangleq \frac{\left(|h(k)|^2 + |h(-k)|^2\right)^2}{|h(k)|^2 |h(-k)|^2} \frac{\mathrm{IRR}}{4} \\ &= \left(\frac{|h(k)|^2}{|h(-k)|^2} + \frac{|h(-k)|^2}{|h(k)|^2} + 2\right) \frac{\mathrm{IRR}}{4}. \end{aligned} \tag{9.75}$$

Considering (9.71) and (9.75), the effect of IQI on RC is fundamentally different from the effect of IQI on ordinary single time-slot (i.e., full-rate) systems. The interference term is not only affected by $h(-k)$ but also by $h(k)$. Unlike IQSC, although RC has the same rate, its SINR is upper bounded due to the IQI even for $N_0 \to 0$, as described by (9.75). Hence, in the presence of IQI, IQSC achieves a better performance than RC.

9.7 Numerical and simulation results

In this section, the performance of the schemes proposed in Section 9.5 is illustrated in terms of outage and error probabilities for linearly modulated signals. In all cases, we validate the theoretical results (indicated with lines in the plots) with Monte-Carlo simulations (indicated with markers in the plots) so as to verify the accuracy of the closed form expressions derived in Section 9.6. Exceptions to the rule are the A-IQSC, RC, and FTBC [527] schemes, where we (abusively) use lines with markers to plot simulation results. We compare the performance of the two proposed IQI coordination schemes (i.e., IQSC and A-IQSC) to that of the IQI RF front-end and the ideal RF front-end systems. The following assumptions are made for all schemes: a) equal total transmit power, b) uncorrelated channel gains for a subcarrier and its image, c) equal average signal power on each subcarrier, and d) perfect CSI and IQI parameter knowledge.

The outage probability versus the SNR for the IQSC, IQI RF front-end, and ideal RF front-end systems is shown in Figs. 9.2 and 9.3 for transmission rates of 1 bit/sec/Hz and 2 bit/sec/Hz, respectively, and IRR values of $20, 25, 30$, and 35 dB. We observe that the simulation results confirm the analytical expressions over the entire SNR range for all IQI levels. Interestingly, IQSC achieves a lower outage probability than the ideal RF front-end for practical availability requirements, and the corresponding gain increases for increasing SNR because of the achieved diversity. Indicatively, for transmission rates equal to $R = 1$ bit/sec/Hz and $R = 2$ bit/sec/Hz, IQSC outperforms the ideal RF front-end for SNR values greater than 4 dB and outage probabilities lower than 0.08, respectively.

In Fig. 9.4, the outage probability is plotted as a function of transmission rate, R, for the IQSC, IQI RF front-end, and ideal RF front-end systems for an SNR of 35 dB and IRR values of $20, 25, 30$, and 35 dB. It can be observed that, for practical values of R, IQSC significantly outperforms the ideal RF front-end. For example, for $R = 2$ bit/s/Hz and IRR = 20 dB, the outage probability of IQSC is 99% and 98.8% lower than those of the IQI RF front-end and the ideal RF front-end systems, respectively, while for $R = 4$ bit/s/Hz the corresponding values are 97.7% and 34.9%.

To further illustrate the effect of IQI on the error performance, in Fig. 9.5, the average SER is plotted for QPSK and different values of IRR. It can be observed that, without IQI compensation, the lower the IRR, the larger the average SER becomes. Furthermore, as expected, the performance of IQSC is not affected by the values of the IQI parameters. This finding indicates that, for low-cost devices, IQSC

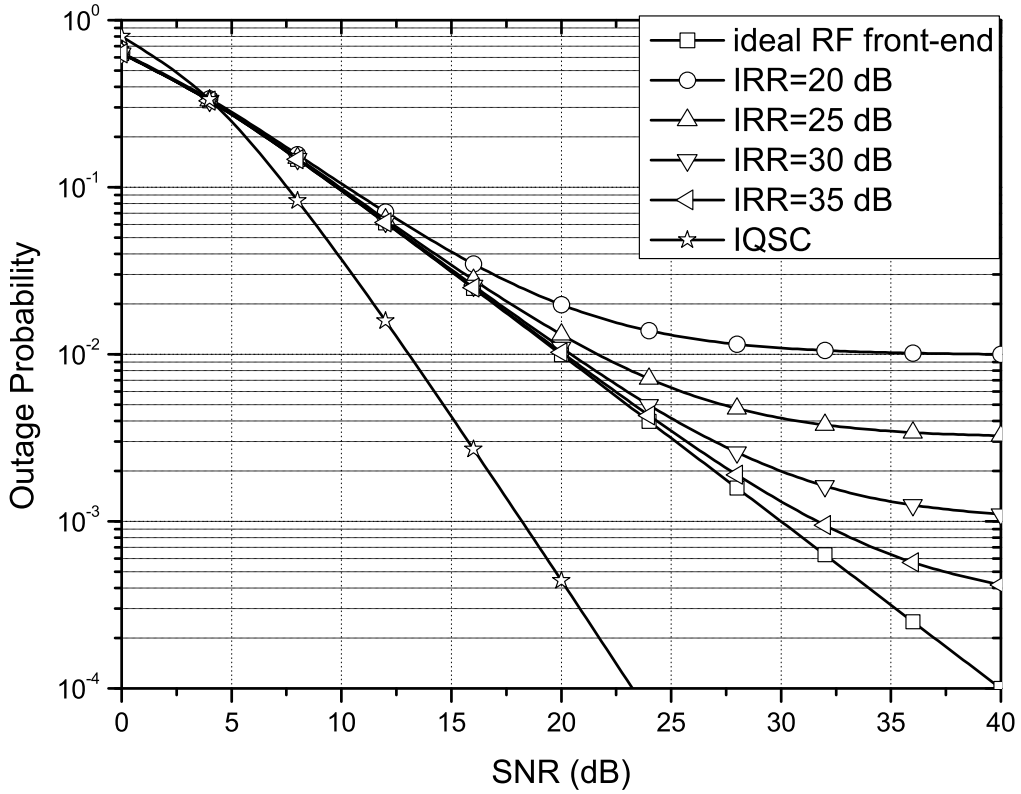

Figure 9.2 Outage probability versus SNR for transmission rate 1 bit/s/Hz and different IQI levels.

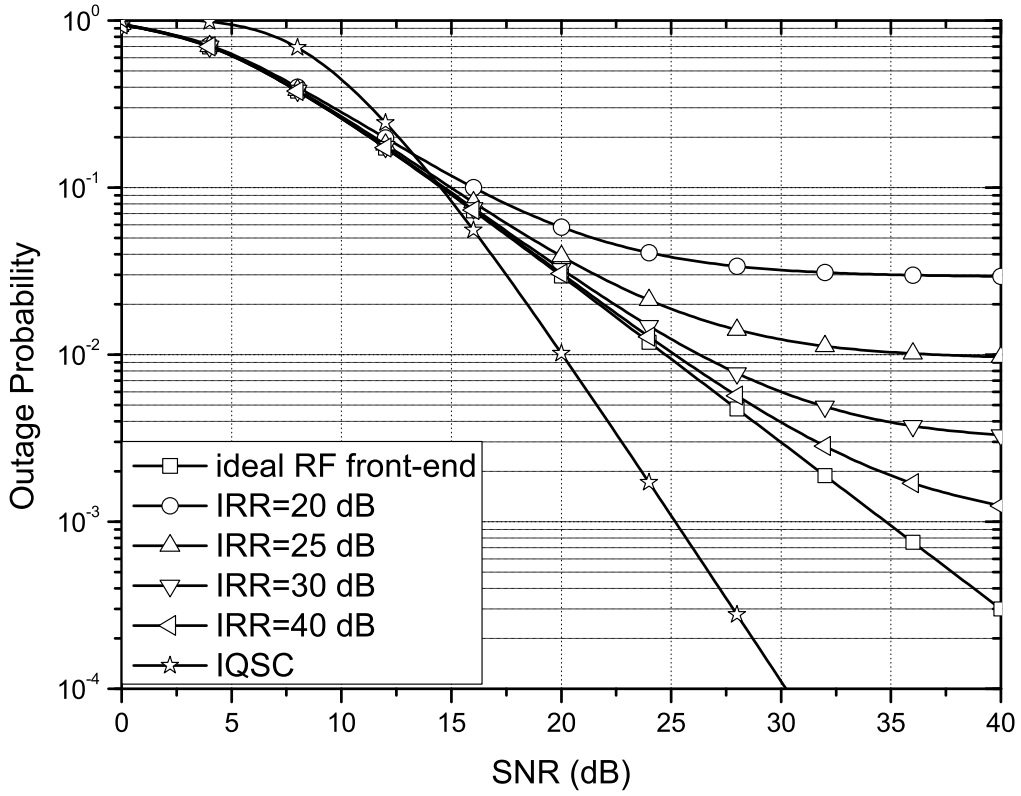

Figure 9.3 Outage probability versus SNR for transmission rate 2 bit/s/Hz and different IQI levels.

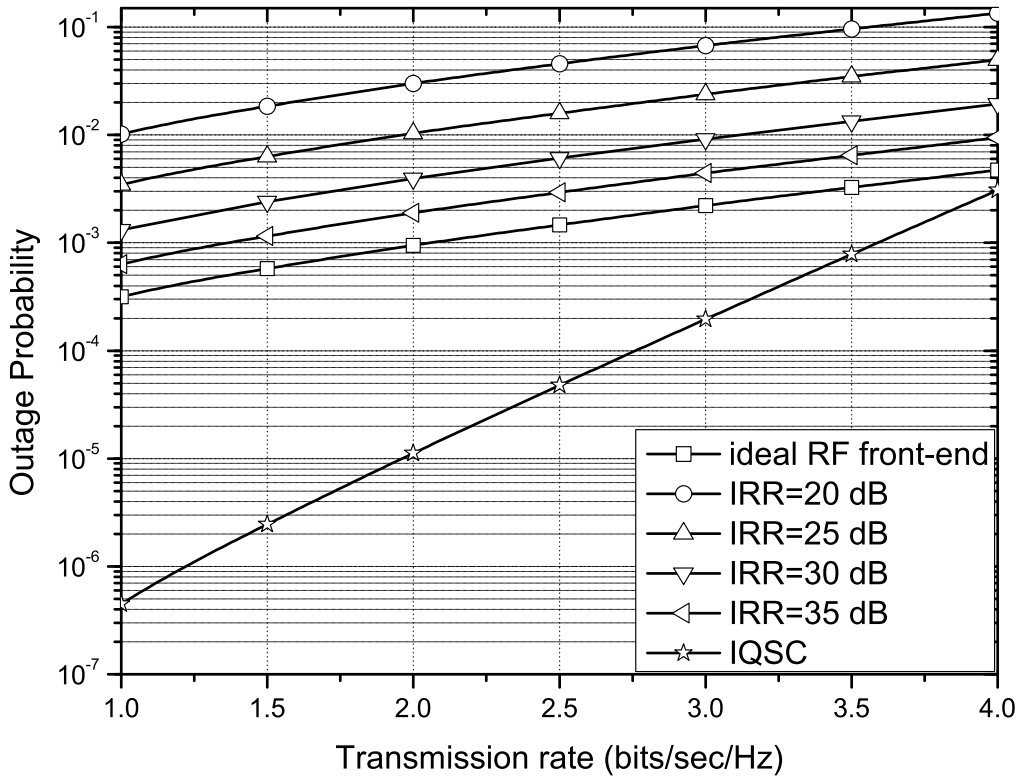

Figure 9.4 Outage probability versus transmission rate for SNR equal to 35 dB and different IQI levels.

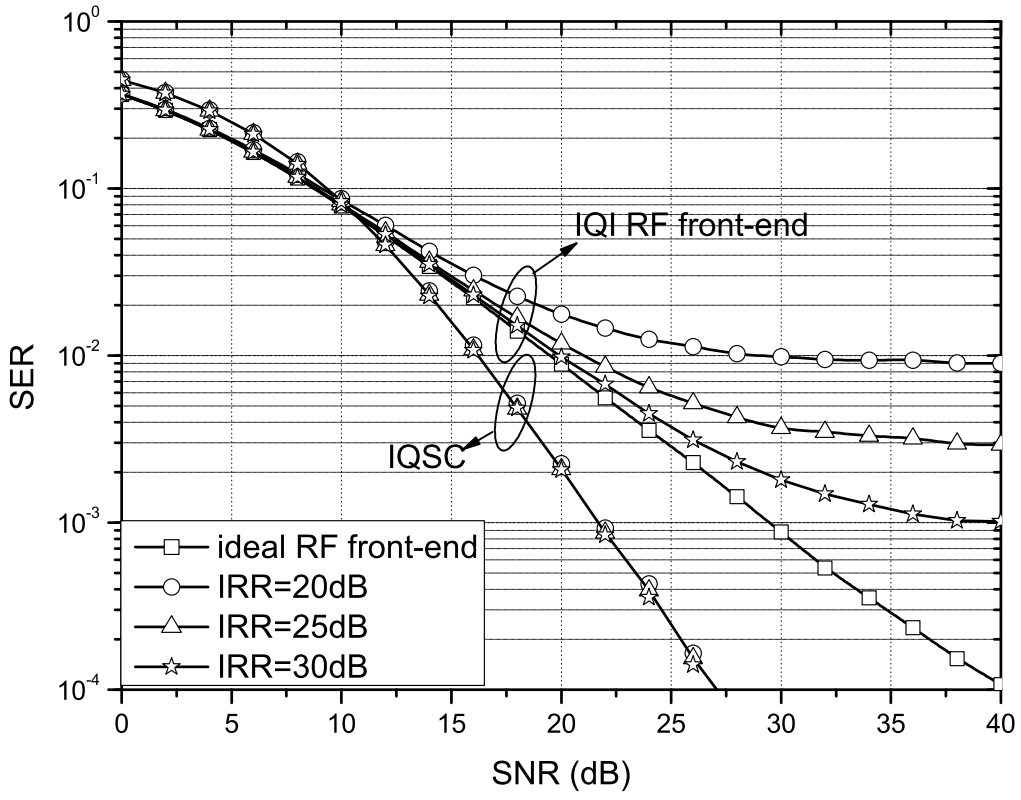

Figure 9.5 SER versus SNR for different values of IRR and QPSK.

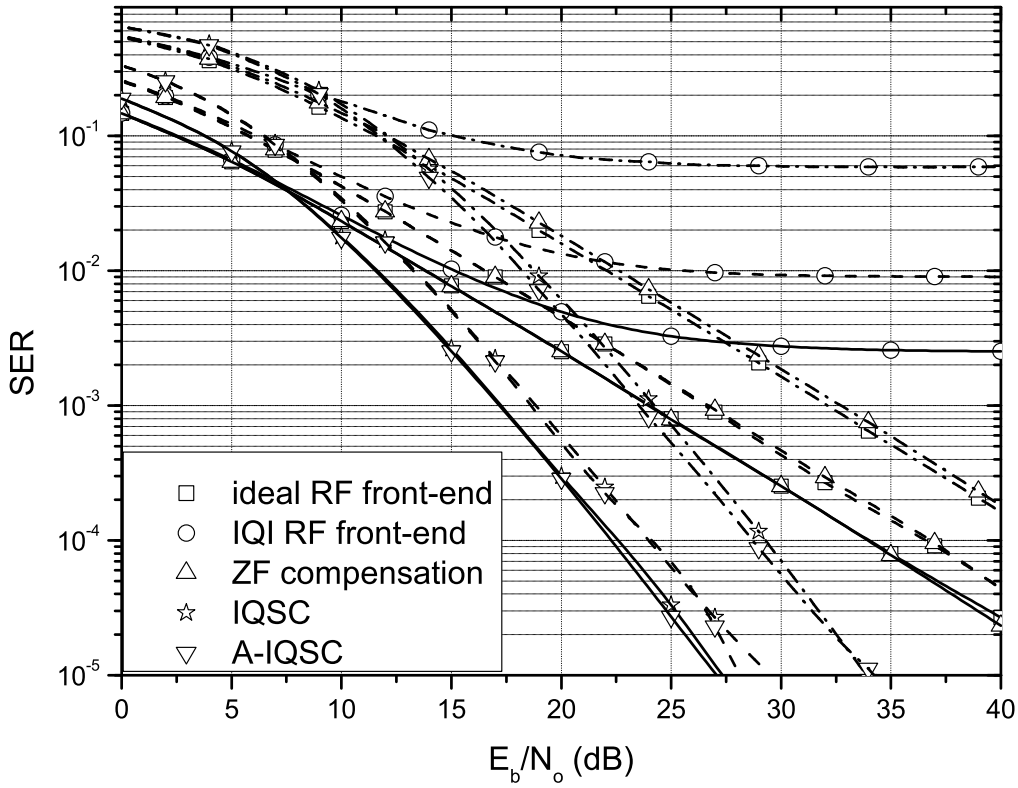

Figure 9.6 SER versus SNR per bit for IRR = 20 dB, $\phi = 5^o$, and BPSK (solid), QPSK (dashed), and 16-QAM (dash-dotted).

can achieve a significant diversity gain without the use of additional antennas by coordinating the IQI effect through appropriate block coding and signal processing.

To demonstrate the efficiency of IQSC for different modulations schemes [125, 354, 533–535], the SER versus the SNR per bit is plotted in Fig. 9.6 for BPSK, QPSK, and 16-QAM, and IRR = 20 dB assuming the following five systems: i) ideal RF front-end, ii) IQI RF front-end, iii) compensated IQI with ZF [346, 354, 536], iv) IQSC, and v) A-IQSC. As expected, the error performance of ZF is very close to the case of the ideal RF front-end. This indicates that the latter scheme can be used as a benchmark for the evaluation of the IQSC performance. Besides, as expected, IQSC and A-IQSC achieve almost the same SER. Interestingly, at a SER of 10^{-3}, which is a practical requirement in several wireless communication standards [537–539], the gain achieved by the proposed schemes with QPSK is about 5 dB compared to the ideal RF front-end with BPSK[4]. For the IQI RF front-end with BPSK, an error floor is observed at an SER of 2.5×10^{-3}, and the degradation caused by IQI on the average SER increases as the average SNR per bit gets larger. In the high SNR regime, a SER lower bound is observed. For example, for 16-QAM, the SER floor is 5×10^{-2}, which may not be acceptable in practice. Similarly, at a SER of 10^{-4}, the SNR gain of IQSC with 16-QAM is more than 15 dB compared to the ideal RF front-end with QPSK. Clearly, due to the MFD gain in (9.46), IQSC achieves a better performance when compared to the ideal RF front-end. For the same SNR and transmission rate, systems employing IQSC can be far more reliable than single-input single-output (SISO) systems with ideal RF front-end, while they need less transmission energy to meet the same (practical) SER target. In other words, IQSC systems can overcome the rate reduction by utilizing higher order modulation schemes.

In Fig. 9.7, we illustrate the effect of IQI on the average SER of $16-$QAM, when RC and FTBC [527] are used. We compare IQSC and A-IQSC with RC and FTBC for the cases of an ideal RF front-end and an IQI RF front-end. Both RC and FTBC have the same rate as IQSC and A-IQSC. The IQI RF front-end with RC, as expected from (9.75), suffers from an error floor in the high-SNR regime. For the considered case, the SER floor is 5×10^{-3}, which might not be acceptable in practice. Furthermore,the IQI RF front-end with FTBC, also exhibits an error floor in the high-SNR regime. For example, for

[4]Notice that, for both schemes, the transmission rate is the same.

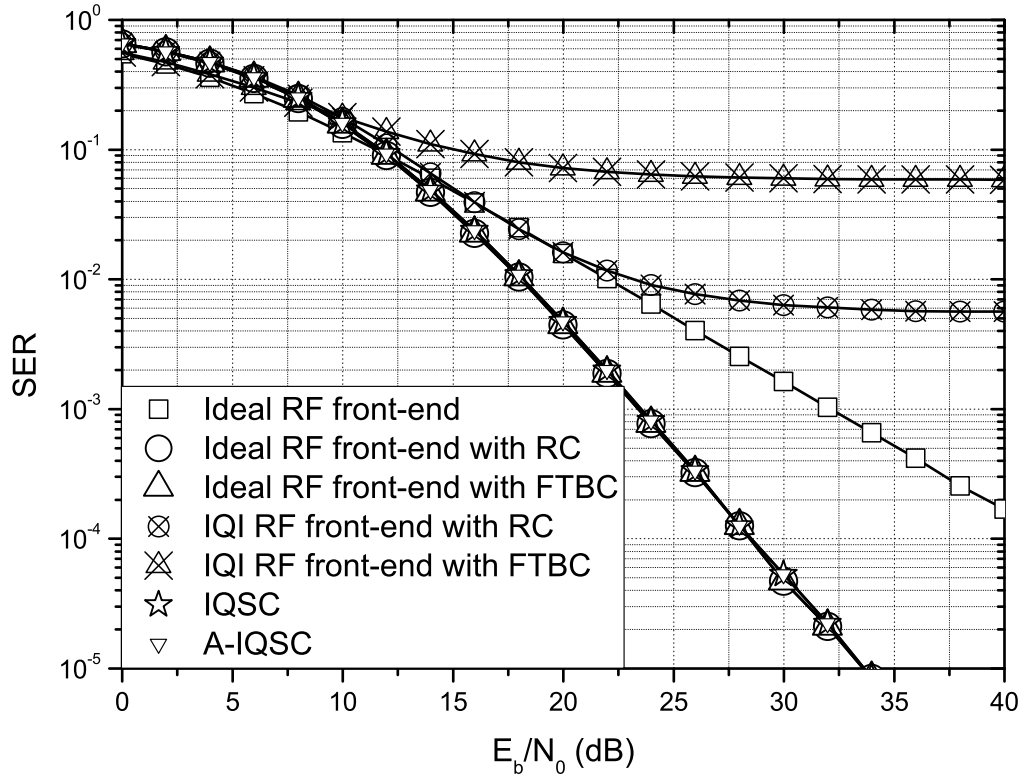

Figure 9.7 Comparison of IQSC with RC and FTBC for IRR = 20 dB, $\phi = 5^o$, and 16-QAM.

16−QAM, the SER floor is 5.9×10^{-2}, which again might not be acceptable in practice. On the other hand, due to the achieved MFD, IQSC and A-IQSC achieve a better performance than the IQI RF front-end with RC and FTBC, while they have a similar performance as the ideal RF front-end with RC and FTBC.

9.8 Discussion and conclusion

In this section, we summarize the advantages and disadvantages of the two proposed IQSC schemes and discuss the new concept of MFD, highlighting the main findings.

9.8.1 Merits and drawbacks of IQSC

The proposed IQSC schemes are low-complexity countermeasures against any level of IQI, enabling their use in practical low-cost communication devices with unavoidable RF imperfections. IQSC and A-IQSC require neither extra transmit power nor any feedback from the RX, and their computational complexity is similar to Alamouti's STBC scheme [526]. Moreover, the proposed IQSC schemes (original and alternative) achieve second-order diversity without the use of extra antennas, which renders them far more reliable and power efficient than conventional SISO systems (with or without IQI compensation). Therefore, IQSC may find application in wireless systems, where low-cost, energy efficiency, low-complexity, and compactness of the communication devices are key design requirements. Notable examples are relaying systems and wireless sensors networks, where single-antenna nodes are physically limited in size, and have to operate without battery replacement for a long period of time [5, 286, 287, 540–542].

In summary, both IQSC schemes have the following merits:

- They coordinate IQI in order to achieve two-fold diversity with a single antenna at TX and RX;
- They are energy and/or bandwidth efficient compared to conventional SISO;
- They do not require any type of feedback from the RX;

- They are low-complexity schemes (their complexity is similar to that of Alamouti's STBC scheme);
- They provide interoperability and compatibility with existing wireless standards;
- They support high-order modulation schemes avoiding an error floor in the SER due to IQI;
- Their outage and SER performances are independent of the severity of the IQI.

The above reasons –and especially the last one– may allow the relaxation of hardware requirements and design specifications for future low-cost DCA communication devices.

The main drawback of the IQSC schemes is that they reduce the transmission rate by 50%. However, our results clearly demonstrate that uncompensated IQI severely degrades the error rate of conventional wireless communication systems especially for high constellation orders. Therefore, for high-order modulation schemes, performance may become unacceptable. On the other hand, when (A-)IQSC is employed, there is no such constraint. Hence, systems using (A-)IQSC can overcome the half-rate limitation by employing higher-order modulation schemes. As mentioned above, an obvious application of (A-) IQSC is the provision of diversity for low-cost remote units, which unavoidably suffer from RF imperfections, and have to operate without battery replacement for a long time.

9.8.2 Conclusions

Two novel low-complexity techniques, namely IQSC and A-IQSC, were presented for significantly increasing the performance of single-antenna multi-carrier communication systems suffering from IQI. It was shown that the proposed schemes cannot only compensate the effects of IQI but they can even be beneficial for the system's performance due to the achieved MFD. In particular, IQSC (both original and alternative) outperforms the systems with uncompensated IQI at the RX, and the ideal RF front-end without IQI, when the same modulation order is employed. Moreover, it shows better performance compared to equal-rate repetition coding with uncompensated IQI, and the same performance as equal-rate RC with ideal RF front-end. Our results indicate that IQSC can be a promising technique for use in a variety of applications involving DCA low-cost devices.

Part IV

Conclusion

Chapter 10

Conclusions and future work

This chapter summons up the conclusions drawn from each part of this research, while it also presents some possible extensions.

10.1 Conclusions

The first part of this thesis studied various types of interference and presented network- and device-side interference management solutions, which are utilized in 5G wireless systems, as well as interference suppression approaches for FD devices.

More specifically, Chapter 3 investigated the influence of CCI, caused by multiple PUs, and fading on the spectrum sensing capability of a classical ED. By evaluating the false alarm and detection probabilities, the impact of CCI and fading on spectrum sensing was quantified. Likewise, the offered expressions can be used in order to select the optimum combination of the energy detection threshold and the sensing duration in order to maximize the performance of the ED. The results revealed the detrimental effect of CCI on spectrum sensing, as well as the importance of taking into consideration the fading statistics, especially in the medium to high SNR regime. Furthermore, it is observed that the spectrum sensing performance is constrained, as the probability of interference from neighbor PUs increases. Therefore, when selecting the operational energy detection threshold, we should not only take into consideration the PU that is located in the same cell with the SU, but also the wireless environment, i.e., the interference from neighboring PUs, as well as the fading characteristics of the PUs-SU links.

In the second part of the dissertation, the impact of hardware imperfections on the wireless link quality was examined. Moreover, two approaches were presented that aim at confronting and coordinating the impact of IQI.

In particular, in Chapter 5, the effect of IQI on wireless communications, in the context of cascaded fading channels, for both single- and multi-carrier systems, was quantified by evaluating the outage probability. For multi-carrier systems, the cases that the mirror channel may or may not be occupied by an information signal were considered. Moreover, three scenarios were investigated, namely ideal TX with I/Q imbalanced RX, I/Q imbalanced TX with ideal RX, and joint I/Q imbalanced TX and RX. The ideal case was also taken into consideration for comparison and the derived analytic results were validated through extensive comparisons with respective results from computer simulations. The results revealed that the IQI introduces detrimental effects that result to non-negligible degradation in the quality of the wireless link, whereas a lower bound on the outage probability was observed in the high SNR regime. Additionally, it was shown that the effect of cascaded fading conditions on the outage probability performance are significant as the number of scatterers along with the involved severity of fading can increase or decrease the corresponding performance by about an order of magnitude at both low and high SNR regimes. Finally, the validity and practical usefulness of the offered results were verified by applying them in realistic wireless applications in the context of V2V communications over cascaded fading channels providing meaningful insights on the performance of such systems.

Chapter 6 investigated the spectrum sensing performance of OSA FD CR system in both single- and multi- channel EDs, when the SUs' devices employ imperfect SIS techniques and suffer from joint TX/RX IQI. By deriving closed form expressions for the false alarm and detection probabilities under realistic scenarios of non-perfect SIS and transceivers' RF front-end impairments, the impact of imperfect SIS and IQI was quantified. The results demonstrated the degrading joint effects of IQI and partial SIS on the ED spectrum sensing performance, which results in significant losses in spectrum utilization. Specifically, in the case of single-channel ED, we observed that the negligence of IQI and partial SIS can lead to a wrong choice of the energy detection threshold, which may results in a dramatic increase of the false alarm probability, while at the same time the detection probability might significantly decrease. Additionally,

in the case of multi-channel EDs, partial SIS and IQI cause self-interference and mirror interference that appreciably restrict the ED's capabilities. Therefore, it is important to take into consideration the joint impact of IQI and partial SIS in the design and deployment of FD CR devices.

In Chapter 7, the performance of multi-channel spectrum sensing, when the RF front-end is impaired by hardware imperfections was examined. In particular, assuming Rayleigh fading, we provided the analytical framework for evaluating the detection and false alarm probabilities of EDs, when LNA nonlinearities, IQI and phase noise are taken into account. Next, we extended our study to the case of a CRN, in which the SUs suffer from different levels of RF impairments, taking into consideration both scenarios of error free and imperfect reporting channels. The results illustrated the degrading effects of RF imperfections on the ED spectrum sensing performance, which bring significant losses in the utilization of the spectrum. Among others, LNA non-linearities were shown to have the most detrimental effect on the spectrum sensing performance. Furthermore, we observed that in cooperative spectrum sensing, the sensing capabilities of the CR system are significantly influenced by the different levels of RF imperfections of the SUs. Therefore, RF impairments should be seriously taken into consideration when designing direct conversion CR RXs.

In Chapter 8, the PA problem for OFDMA wireless systems, when the served UEs suffer from different levels of IQI, was investigated. By taking into consideration the levels of IQI of the served UEs, a novel low-complexity solution with directly calculated PA policies, given the LMs, that maximizes the minimum UEs' achievable capacity, with respect to the BS transmitted power, was proposed. To evaluate the performance of the proposed PA scheme, the conventional PA scheme was used as a benchmark. The results illustrated that the proposed PA scheme leads to a notable increase of the UEs achievable rate, compared to the conventional PA scheme, especially, when the UEs have different channel qualities.

Finally, in Chapter 9, two novel low-complexity techniques, namely IQSC and A-IQSC, were presented, which achieve significantly performance enhance of the quality of the wireless link in single-antenna multi-carrier communication systems suffering from IQI. It was shown that the proposed schemes cannot only compensate the effects of IQI, but they can even be beneficial for the system's performance due to the achieved MFD. In particular, IQSC (both original and alternative) outperforms the systems with uncompensated IQI at the RX, and the ideal RF front-end without IQI, when the same modulation order is employed. Moreover, it shows better performance compared to equal-rate repetition coding with uncompensated IQI, and the same performance as equal-rate RC with ideal RF front-end. Our results indicate that IQSC can be a promising technique for use in a variety of applications involving DCA low-cost devices.

10.2 Future extensions

The research topics that this thesis covers have multiple possible extensions, some of which are summarized here.

Regarding interference management solutions, the research included in this dissertation has focused on the evaluation of the impact of Nakagami-m fading and CCI, which is caused by multiple PUs, on the performance of classical EDs, as well as the presentation of the analytical framework for the appropriate assignment of the energy detection threshold and the spectrum sensing duration. The selection of classical EDs was motivated by their low-complexity, which classifies them as attractive candidates for modern wireless systems. A possible extension of this analysis would be to investigate the impact of multiple PUs and/or fading in other types of spectrum sensing mechanisms, such as matched filter detection and feature detection [505], as well as to propose interference aware spectrum sensing solutions, which by taking into consideration the wireless environment, can maximize their capabilities [543]. Additionally, the presented analysis can straightforwardly be applied in the case of cooperative sensing with FC, which uses the M-out-of-N rule, is employed.

Another possible extension of this work could be the optimization of the spectrum sensing and the transmission duration of the SUs. In particular, by increasing the spectrum sensing duration, the spectrum capability of a SU increases, i.e., the false alarm probability decreases, while the detection probability increases; however, at the same time, since the total duration of spectrum sensing and transmission is constant, the transmission duration decreases. Therefore, it is important to study the problem of minimizing the spectrum sensing duration, while maintaining the false alarm and detection probabilities within tolerable limits. Finally, in this work, it was assumed that the noise variance was known. However, in practice, only an estimation of the noise variance is known. Consequently, this

work can be extended in the case in which a noise estimation is used, and the problem of the (so-called) SNR-wall [268, 544–546] can be investigated in the presence of CCI and fading.

Regarding the quantification of the influence of hardware imperfections on the performance of wireless systems, the analytical approach presented in Chapter 5 provides closed form expressions for the evaluation of the impact of IQI on the outage probability of SISO wireless systems. An extension of this work is the analytical extraction of the outage probability of MIMO and relaying wireless systems, in the presence of $N*$Nakagami-m fading channels and IQI. This extension is straightforward for single-input multiple-output (SIMO) or multiple-input single-output (MISO) systems that use the selection combine (SC) protocol, as well as for opportunistic DF relaying systems, since their outage probabilities are exclusively connected with the outage probability of each individual channel. However, in the cases of more sophisticated MIMO and/or relaying systems, the nature of IQI may render impossible the derivation of exact closed form expressions for the outage probabilities. In these cases, approximations and/or upper and lower bounds need to be derived.

Another possible extension of this work could be the investigation of the impact of other hardware imperfections, such as phase noise and amplifiers nonlinearities, on the outage probability of the wireless systems, in the presence of $N*$Nakagami-m fading. Excluding the case of multi-carrier communications, when the TX and/or RX suffer from phase noise, the methodology presented in Chapter 5 can be used in order to derive closed form expressions for the outage probabilities. In the case of multi-carrier communications, in which the transceivers suffer from IQI, the distribution of the sum of $N*$Nakagami-m need to be derived. Note that this is a difficult problem that has not yet been addressed. Moreover, an interesting problem would be the quantification of the influence of residual RF impairments in the presence of $N*$Nakagami-m channels. Finally, the impact of hardware imperfections on the performance of wireless optical communications that employ multi-carrier transmission schemes, needs to be evaluated [547–549].

Regarding the influence of hardware imperfections on the spectrum sensing capability of the classical ED, the research included in this dissertation has focused on the evaluation of the joint effect of IQI, phase noise and LNA nonlinearities, as well as Rayleigh fading, on the false alarm and detection probability. A possible extension of this analysis would be to design hardware aware spectrum sensing approaches that aim to improve the capability of the spectrum sensing device, by taking into consideration the possible interference from neighboring and mirror channels, as well as the LNA nonlinearities level of distortion. For example, a possible approach might be to order the sensing channels based on their received powers (or their occupancy probabilities) in decreasing order, and first to sense the channel with the highest power (or occupancy probability). If the ED decides that this channel is busy, then it can subtract its impact from the channels that it affects. The same procedure will be applied in the next channel with the highest power (occupancy probability), and will continued to be applied, until the last ordered channel will be sensed.

Regarding the PA problem for OFDMA systems, in which the UEs suffer from different levels of IQI, a PA strategy, which, by taking into consideration the level of IQI of each UE, as well as the instantaneous channel gains, can achieve significantly improvements in each UE's capacity, and fairness between the served UEs, was illustrated in Chapter 8. In this work, it was assumed that the BS has full CSI knowledge, as well as it is aware of the level of IQI, i.e., the IRR, of each served UE. In practice, the BS can achieve instantaneous full CSI, if the reciprocity property is valid (see [511–513] and references therein), or delayed CSI through a feedback channel. Moreover, each UE would feed back to the BS a quantified version of its IRR. As a result, the investigation of the impact of delay CSI and partial knowledge of the UEs' IRR parameters by the BS on the UE's capacity, would be a zestful extension of the PA problem. Furthermore, in this work, it was assumed that the channel allocation is fixed. By relaxing this assumption, a strategy that takes into account the instantaneous channel gains, as well as the level of IQI of each UE, and allocates both power and channels, is expected to further improve the performance of the wireless system.

Another possible extension is the study of PA schemes in OFDMA systems, which aim at maximizing the overall system performance, considering that the served UEs suffer from different levels of IQI. Such a PA policy would result in maximizing the capacity of an arbitrary UE k at a certain time-slot i, by minimizing, or even eliminating, the received power at the UE that uses the mirror subcarrier, $-k$. Consequently, this PA strategy cannot guarantee fairness between different UEs. Finally, a PA scheme that, instead of using instantaneous CSI knowledge, it employs the statistical channel characteristics, can significantly reduce the feedback overhead, or the complexity of the BS, since the latter does not need to perform channel estimation. However, dynamic PA schemes, like the one presented in Chapter 8, generally outperform the corresponding fixed PA schemes.

Regarding the IQSC, the proposed schemes, presented in Chapter 9, even though they outperform both the systems with uncompensated IQI at the RX, and the ideal RF front-end without IQI, they sacrifice data rate for MFD. Hence, a possible extension of this work is to propose more sophisticated schemes, which can achieve MFD without the rate losses, or with lower rate losses, even if the diversity order is constrained. Finally, the basic ideal of IQSC can be extended in the case of MIMO systems. In these cases, a careful design of both the precoder and combiner is required, in order to take into account the impact of IQI in systems with multiple antennas.

Appendices

Appendix A

Proof of Theorem 3.1

Since $|h_i|$ is a Nakagami-m distributed random variable (RV), the variance of the received signal, given by (3.13), is a sum of squared Nakagami-m RV with PDF given by [276]

$$f_{\sigma^2}(y) = \sum_{i=1}^{L} \sum_{k=1}^{a_i} \Xi(i,k) \frac{(y-c)^{k-1}}{b_i^k (k-1)!} \exp\left(-\frac{y-c}{b_i}\right), \tag{A.1}$$

with $y \in [c, \infty)$. Hence, the unconditional CDF of the energy test statistic, T, can be expressed as

$$F_T(x|\Theta) = \int_c^{\infty} f_{\sigma^2}(y)\, dy - \sum_{n=0}^{N_s-1} \frac{1}{n!} \left(\frac{N_s x}{2}\right)^n \int_c^{\infty} y^{-n} \exp\left(-\frac{N_s x}{2y}\right) f_{\sigma^2}(y)\, dy. \tag{A.2}$$

Since $y \in [c, \infty)$,

$$\int_c^{\infty} f_{\sigma^2}(y)\, dy = 1. \tag{A.3}$$

Additionally, by substituting (A.1) into (A.2) and after some mathematical manipulations, (A.2) yields

$$F_T(x|\Theta) = 1 - \sum_{n=0}^{N_s-1} \sum_{i=1}^{L} \sum_{k=1}^{a_i} \frac{\Xi(i,k)}{b_i^k (k-1)! n!} \left(\frac{N_s x}{2}\right)^n \int_c^{\infty} y^{-n} (y-c)^{k-1} \exp\left(-\frac{y-c}{b_i} - \frac{N_s x}{2y}\right) dy. \tag{A.4}$$

Since k is an integer and $k \geq 1$, by using the binomial expansion in $(y-c)^{k-1}$, (A.4) can equivalently be written as

$$F_T(x|\Theta) = 1 - \sum_{n=0}^{N_s-1} \sum_{i=1}^{L} \sum_{k=1}^{a_i} \sum_{j=0}^{k-1} \frac{\Xi(i,k)}{n! b_i^k (k-1)!} \binom{k-1}{j} \left(\frac{N_s x}{2}\right)^n (-c)^{k-1-j} \exp\left(\frac{c}{b_i}\right) \times \int_c^{\infty} y^{-n+j} \exp\left(-\frac{N_s x}{2y} - \frac{y}{b_i}\right) dy. \tag{A.5}$$

Finally, by setting

$$z = \frac{y}{b_i} \tag{A.6}$$

into (A.5) and using [275, Eq. (6.2)], (A.5) yields (3.16). This concludes the proof.

Appendix B

Approximation for extended incomplete gamma function calculation

Theorem B.1. *The extended incomplete Gamma function can be approximated as*

$$\Gamma(a,x,b,1) \approx \sum_{n=0}^{N} \frac{(-b)^n}{n!}\Gamma(a-n,x), \tag{B.1}$$

with an approximation error upper-bounded by

$$\epsilon(a,x,b,N) = \exp(b)\,\Gamma(a-N-1,x)\,\frac{\gamma(N+1,b)}{\Gamma(N+1)}. \tag{B.2}$$

Proof. The series expansion of the extended incomplete Gamma function can be expanded in terms of the incomplete Gamma function as [275, Eq. (6.54)]

$$\Gamma(a,x,b,1) = \sum_{n=0}^{\infty} \frac{(-b)^n}{n!}\Gamma(a-n,x). \tag{B.3}$$

By denoting

$$f(a,x,b,n) = \frac{b^n}{n!}\Gamma(a-n,x), \tag{B.4}$$

the extended incomplete gamma function can be rewritten as

$$\Gamma(a,x,b,1) = \sum_{n=0}^{\infty} (-1)^n f(a,x,b,n). \tag{B.5}$$

Moreover, according to [275, Eq. (3.84)], the auxiliary function $f(a,x,b,n)$ is equivalent to

$$f(a,x,b,n) = \frac{b^n}{n!}\frac{E_{n-a+1}(x)}{x^{n-a}}, \tag{B.6}$$

where $E_n(x)$ is the exponential integral function, which is defined in [550, Eq. (5.1.4)]. By taking into consideration the property [550, Eq. (5.1.17)], it follows that for given parameters a, $x > 0$ and n,

$$\Gamma(a-n,x) \geq \Gamma(a-n-1,x), \tag{B.7}$$

and, hence, for a given $b > 0$,

$$\lim_{n\to\infty} f(a,x,b,n) = 0. \tag{B.8}$$

Thus, the extended incomplete gamma function can be approximated by (B.1).

The approximation error is given by

$$e(a,x,b,N) = \sum_{n=N+1}^{\infty} (-1)^n f(a,x,b,n), \tag{B.9}$$

which can be upper-bounded, according to (B.7) and (B.8), as

$$e(a,x,b,N) \leq \sum_{n=N+1}^{\infty} f(a,x,b,n) \leq \Gamma(a-N-1,x) \sum_{n=N+1}^{\infty} \frac{b^n}{n!}. \tag{B.10}$$

Hence, using [274, Eq. (1.211/1)] and [274, Eq. (8.352/2)], the upper bound on the approximation error given by (B.2) is derived. ■

Appendix C

Proof of Proposition 6.1

Since N_s is sufficiently large, the central limit theorem [436] can be applied. In this case, the test statistics follows a Gaussian distribution with mean and variance that can respectively be obtained as

$$\mu_\theta = E\left[T_i\,|\theta\right] = \frac{1}{N_s} E\left[\sum_{n=0}^{N_s-1} |y_i(n)|^2\right] = E\left[|y_i(n)|^2\right], \tag{C.1}$$

and

$$\sigma_\theta^2 = \mathrm{Var}\left[T_i\,|\theta\right] = \frac{1}{N_s}\left(E\left[|y_i|^4\right] - \mu_\theta^2\right), \tag{C.2}$$

Taking into consideration that x_i, s_i and w_i are uncorrelated random variables, (C.1) can be rewritten as

$$\mu_\theta = \theta E\left[|x_i|^2\right] + a_i^2 E\left[|s_i|^2\right] + E\left[|w_i|^2\right]. \tag{C.3}$$

Moreover, since $x_{id,i}$, $s_{id,i}$ and $w_{id,i}$ are zero-mean CSCWG processes with uncorrelated real and imaginary parts with variances

$$\sigma_{x_{id,i}}^2 = \left[|x_{\mathrm{id},i}|^2\right], \tag{C.4}$$

$$\sigma_{s_{id,i}}^2 = E\left[|s_{\mathrm{id},i}|^2\right] \tag{C.5}$$

and

$$\sigma_{w_{id,i}}^2 = \left[|w_{\mathrm{id},i}|^2\right], \tag{C.6}$$

respectively, the terms x_i, s_i and w_i in (6.3)–(6.5), are random uncorellated processes with variances that are given by

$$E\left[|x_i|^2\right] = \left(\left|K_{1,i}^r\right|^2 + \left|K_{2,i}^r\right|^2\right)\sigma_{x_{id,i}}^2, \tag{C.7}$$

$$E\left[|s_i|^2\right] = \left(|\xi_{1,i}|^2 + |\xi_{2,i}|^2\right)\sigma_{s_{id,i}}^2, \tag{C.8}$$

and

$$E\left[|w_i|^2\right] = \left(\left|K_{1,i}^r\right|^2 + \left|K_{2,i}^r\right|^2\right)\sigma_{w_{id,i}}^2, \tag{C.9}$$

respectively. Substituting (C.7)–(C.9) into (C.3) and after some algebraic manipulations, we get (6.17).

Nevertheless, to derive the variance of the test statistics, we need to evaluate $E\left[|y_i|^4\right]$, which can be obtained using (6.2) as follows

$$\begin{aligned} E\left[|y_i|^4\right] = {} & \theta E\left[|x_i|^4\right] + a_i^4 E\left[|s_i|^4\right] + E\left[|w_i|^4\right] + 2a_i^2\theta E\left[|x_i|^2\right] E\left[|s_i|^2\right] + 2\theta E\left[|x_i|^2\right] E\left[|w_i|^2\right] \\ & + 2a_i^2 E\left[|s_i|^2\right] E\left[|w_i|^2\right] + 4E\left[\left(\Re\left\{\theta a_i x_i s_i^* + \theta x_i w_i^* + a_i s_i w_i^*\right\}\right)^2\right], \end{aligned} \tag{C.10}$$

where, according to (6.3)–(6.5), $E\left[|x_i|^4\right]$, $E\left[|s_i|^4\right]$, $E\left[|w_i|^4\right]$ and $E\left[\left(\Re\left\{\theta a_i x_i s_i^* + \theta x_i w_i^* + a_i s_i w_i^*\right\}\right)^2\right]$ can be expressed as

$$E\left[|x_i|^4\right] = 2k_r\sigma_{x_{\mathrm{id},i}}^4, \tag{C.11}$$

$$E\left[|s_i|^4\right] = 2k_{t,r}\sigma_{s_{\mathrm{id},i}}^4, \tag{C.12}$$

$$E\left[|w_i|^4\right] = 2k_r\sigma_{w_{\mathrm{id},i}}^4, \tag{C.13}$$

and

$$\begin{aligned} E\left[\left(\Re\left\{\theta a_i x_i s_i^* + \theta x_i w_i^* + a_i s_i w_i^*\right\}\right)^2\right] = {} & \theta a_i^2 E\left[\Re\{x_i\}^2\right] E\left[\Re\{s_i\}^2\right] + a_i^2\theta E\left[\Im\{x_i\}^2\right] E\left[\Im\{s_i\}^2\right] \\ & + \theta E\left[\Re\{x_i\}^2\right] E\left[\Re\{w_i\}^2\right] + \theta E\left[\Im\{x_i\}^2\right] E\left[\Im\{w_i\}^2\right] \\ & + a_i^2 E\left[\Re\{s_i\}^2\right] E\left[\Re\{w_i\}^2\right] + a_i^2 E\left[\Im\{s_i\}^2\right] E\left[\Im\{w_i\}^2\right]. \end{aligned} \tag{C.14}$$

Next, we derive $E\left[\Re\{x_i\}^2\right]$, $E\left[\Re\{s_i\}^2\right]$, $E\left[\Re\{w_i\}^2\right]$, $E\left[\Im\{x_i\}^2\right]$, $E\left[\Im\{s_i\}^2\right]$ and $E\left[\Im\{w_i\}^2\right]$. By using (6.10), (6.12) and the fact that

$$E\left[\Re\{x_{\mathrm{id},i}\}^2\right] = E\left[\Im\{x_{\mathrm{id},i}\}^2\right] = \frac{\sigma_{x_{\mathrm{id}}}^2}{2}, \tag{C.15}$$

$$E\left[\Re\{s_{\mathrm{id},i}\}^2\right] = E\left[\Im\{s_{\mathrm{id},i}\}^2\right] = \frac{\sigma_{s_{\mathrm{id}}}^2}{2} \tag{C.16}$$

and

$$E\left[\Re\{w_{\mathrm{id},i}\}^2\right] = E\left[\Im\{w_{\mathrm{id},i}\}^2\right] = \frac{\sigma_{w_{\mathrm{id}}}^2}{2}, \tag{C.17}$$

we get

$$E\left[\Re\{x_i\}^2\right] = \frac{\sigma_{x_{\mathrm{id}}}^2}{2}, \tag{C.18}$$

$$E\left[\Re\{s_i\}^2\right] = \frac{\sigma_{s_{\mathrm{id}}}^2}{2}, \tag{C.19}$$

$$E\left[\Re\{w_i\}^2\right] = \frac{\sigma_{w_{\mathrm{id}}}^2}{2}, \tag{C.20}$$

$$E\left[\Im\{x_i\}^2\right] = \left(\left(2\Re\left\{K_{1,i}^r\right\} - 1\right)^2 + 4\Im\left\{K_{1,i}^r\right\}^2\right)\frac{\sigma_{x_{\mathrm{id}}}^2}{2}, \tag{C.21}$$

$$E\left[\Im\{s_i\}^2\right] = \left(\left(2\Re\left\{\xi_{1,i}\right\} - 1\right)^2 + 4\Im\left\{\xi_{1,i}\right\}^2\right)\frac{\sigma_{s_{\mathrm{id}}}^2}{2}, \tag{C.22}$$

and

$$E\left[\Im\{w_i\}^2\right] = \left(\left(2\Re\left\{K_{1,i}^r\right\} - 1\right)^2 + 4\Im\left\{K_{1,i}^r\right\}^2\right)\frac{\sigma_{w_{\mathrm{id}}}^2}{2}. \tag{C.23}$$

Substituting (C.18)–(C.23) into (C.14) and then into (C.10) and (C.2), we get (6.18). This concludes the proof.

Appendix D

Proof of Proposition 6.2

In case of ideal RF front-end, since $K_{1,i}^t = K_{1,i}^r = 1$ and $K_{2,i}^t = K_{2,i}^r = 0$, the base band received signal at the $i-$th SU can be expressed as

$$y_{i|\theta} = \theta x_{\mathrm{id},i} + a s_{\mathrm{id},i} + w_{id,i}. \tag{D.1}$$

Furthermore, since

$$x_{id,i} \sim \mathcal{CN}\left(0, \sigma^2_{x_{id,i}}\right), \tag{D.2}$$

$$s_{id,i} \sim \mathcal{CN}\left(0, \sigma^2_{s_{id,i}}\right) \tag{D.3}$$

and

$$w_{id,i} \sim \mathcal{CN}\left(0, \sigma^2_{w_{id,i}}\right), \tag{D.4}$$

$y_i(n)$ follows zero-mean complex Gaussian random distributed with variance given by (6.30). Additionally, since T_i is the sum of zero-mean Gaussian processes, it follows chi-square distribution with $2N_s$ DoF and a CDF shown in (6.29). This concludes the proof.

Appendix E

Proof of Proposition 6.3

Since N_s is sufficiently large, using the central limit theorem [436], the test statistics follow Gaussian distribution with the following mean and variance

$$\mu_\Theta = E\left[T_i\left|\Theta\right.\right] = \frac{1}{N_s} E\left[\sum_{n=0}^{N_s-1} \left|y_{i,k}(n)\right|^2\right] = E\left[\left|y_{i,k}(n)\right|^2\right], \tag{E.1}$$

and

$$\sigma_\theta^2 = \mathrm{Var}\left[T_i\left|\Theta\right.\right] = \frac{1}{N_s}\left(E\left[\left|y_{i,k}\right|^4\right] - \mu_\Theta^2\right). \tag{E.2}$$

Taking into consideration that $x_{i,k}$, $x_{i,-k}$, $s_{i,k}$, $s_{i,-k}$ and $w_{i,k}$, $w_{i,-k}$ are uncorrelated RVs, (E.1) yields to (6.37).

Moreover, based on (E.2), to evaluate the variance of the test statistics, we need to derive $E\left[\left|y_{i,k}\right|^4\right]$, which can be expressed as

$$\begin{aligned} E\left[\left|y_{i,k}\right|^4\right] &= E\left[\left(x_{IQI} + a_i s_{IQI} + w_{IQI}\right)^4\right] \\ &= E\big[\left|x_{IQI}\right|^4\big] + a_i^4 E\big[\left|s_{IQI}\right|^4\big] + E\big[\left|w_{IQI}\right|^4\big] + 4E\Big[\left(\Re\left\{a_i x_{IQI} s_{IQI}^* + x_{IQI} w_{IQI}^* + a_i s_{IQI} w_{IQI}^*\right\}\right)^2\Big] \end{aligned} \tag{E.3}$$

where

$$x_{IQI} = \theta_k K_{1,i}^r x_{i,k}(n) + \theta_{-k} K_{2,i}^r x_{i,-k}^*(n), \tag{E.4}$$

$$s_{IQI} = \tilde{\theta}_k a_i \xi_{1,i} s_{i,k}(n) + \tilde{\theta}_{-k} a_i \xi_{2,i} s_{i,-k}^*(n), \tag{E.5}$$

and

$$w_{IQI} = K_{1,i}^r w_{i,k}(n) + K_{2,i}^r w_{i,-k}^*(n). \tag{E.6}$$

Therefore,

$$E\left[\left|x_{IQI}\right|^4\right] = 2\theta_k \left|K_{1,i}^r\right|^4 \sigma_{x_{i,k}}^4 + 2\theta_{-k}\left|K_{2,i}^r\right|^4 \sigma_{x_{i,-k}}^4 + 2\theta_k\theta_{-k}\Big(\left|K_{1,i}^r\right|^2\left|K_{2,i}^r\right|^2 + \alpha^2 + \beta^2\Big)\sigma_{x_{i,k}}^2\sigma_{x_{i,-k}}^2, \tag{E.7}$$

$$E\left[\left|s_{IQI}\right|^4\right] = 2\tilde{\theta}_k \left|xi_{1,i}\right|^4 \sigma_{s_{i,k}}^4 + 2\tilde{\theta}_{-k}\left|\xi_{2,i}\right|^4 \sigma_{s_{i,-k}}^4 + 2\tilde{\theta}_k\tilde{\theta}_{-k}\left(\left|\xi_{1,i}\right|^2\left|\xi_{2,i}\right|^2 + \delta^2 + \zeta^2\right)\sigma_{s_{i,k}}^2\sigma_{s_{i,-k}}^2, \tag{E.8}$$

and

$$E\left[\left|w_{IQI}\right|^4\right] = 2\left|K_{1,i}^r\right|^4 \sigma_{w_{i,k}}^4 + 2\left|K_{2,i}^r\right|^4 \sigma_{w_{i,-k}}^4 + 2\left(\left|K_{1,i}^r\right|^2\left|K_{2,i}^r\right|^2 + \alpha^2 + \beta^2\right)\sigma_{w_{i,k}}^2\sigma_{w_{i,-k}}^2. \tag{E.9}$$

Furthermore, we can easily prove that x_{IQI}, s_{IQI} and w_{IQI} are zero-mean uncorrelated RVs. Consequently, $E\left[\left(\Re\left\{a_i x_{IQI} s_{IQI}^* + x_{IQI} w_{IQI}^* + a_i s_{IQI} w_{IQI}^*\right\}\right)^2\right]$ can be expressed as

$$\begin{aligned} E\Big[\Big(\Re\left\{a_i x_{IQI} s_{IQI}^* + x_{IQI} w_{IQI}^* + a_i s_{IQI} w_{IQI}^*\right\}\Big)^2\Big] \\ = a_i^2 E\left[\left(\Re\{x_{IQI}\}\right)^2\right] E\left[\left(\Re\{s_{IQI}\}\right)^2\right] + a_i^2 E\left[\left(\Im\{x_{IQI}\}\right)^2\right] E\left[\left(\Im\{s_{IQI}\}\right)^2\right] \\ + E\left[\left(\Re\{x_{IQI}\}\right)^2\right] E\left[\left(\Re\{w_{IQI}\}\right)^2\right] + E\left[\left(\Im\{x_{IQI}\}\right)^2\right] E\left[\left(\Im\{w_{IQI}\}\right)^2\right] \\ + a_i^2 E\left[\left(\Re\{s_{IQI}\}\right)^2\right] E\left[\left(\Re\{w_{IQI}\}\right)^2\right] + a_i^2 E\left[\left(\Im\{s_{IQI}\}\right)^2\right] E\left[\left(\Im\{w_{IQI}\}\right)^2\right]. \end{aligned} \tag{E.10}$$

Additionally, since $\Re\{x_{i,k}\}$, $\Im\{x_{i,k}\}$, $\Re\{x_{i,-k}\}$, $\Im\{x_{i,-k}\}$, $\Re\{s_{i,k}\}$, $\Im\{s_{i,k}\}$, $\Re\{s_{i,-k}\}$, $\Im\{s_{i,-k}\}$, $\Re\{w_{i,k}\}$, $\Im\{w_{i,k}\}$, $\Re\{w_{i,-k}\}$ and $\Im\{w_{i,-k}\}$ are uncorrelated RVs, we show that

$$E\left[\left(\Re\{x_{IQI}\}\right)^2\right] = E\left[\left(\Im\{x_{IQI}\}\right)^2\right] = \theta_k \left|K_{1,i}^r\right|^2 \frac{\sigma_{x_{k,i}}}{2} + \theta_{-k} \left|K_{2,i}^r\right|^2 \frac{\sigma_{x_{-k,i}}}{2}, \tag{E.11}$$

$$E\left[\left(\Re\{s_{IQI}\}\right)^2\right] = E\left[\left(\Im\{s_{IQI}\}\right)^2\right] = \tilde{\theta}_k \left|\xi_{1,i}\right|^2 \frac{\sigma_{s_{k,i}}}{2} + \tilde{\theta}_{-k} \left|\xi_{2,i}\right|^2 \frac{\sigma_{s_{-k,i}}}{2}, \tag{E.12}$$

and

$$E\left[\left(\Re\{w_{IQI}\}\right)^2\right] = E\left[\left(\Im\{w_{IQI}\}\right)^2\right] \left|K_{1,i}^r\right|^2 \frac{\sigma_{w_{k,i}}}{2} + \left|K_{2,i}^r\right|^2 \frac{\sigma_{w_{-k,i}}}{2}. \tag{E.13}$$

By substituting (E.11)–(E.13) into (E.10), and then by substituting this result and (E.7)–(E.9) into (E.2), we get (6.38). This concludes the proof.

Appendix F

Proof of Proposition 6.4

When the OR rule is employed, the false alarm probability can be expressed as

$$P_{C,\mathrm{fa}} = P_r\left(\{T_1 > \gamma_1\} \cup \{T_2 > \gamma_2\} \cup \cdots \cup \{T_{N_{\mathrm{su}}} > \gamma_{N_{\mathrm{su}}}\} \,|\theta = 0\right) \tag{F.1}$$

or equivalently as

$$P_{C,\mathrm{fa}} = 1 - P_r\left(\{T_1 < \gamma_1\} \cup \{T_2 < \gamma_2\} \cup \cdots \cup \{T_{N_{\mathrm{su}}} < \gamma_{N_{\mathrm{su}}}\} \,|\theta = 0\right). \tag{F.2}$$

In (F.2), T_i and γ_i ($i \in \{1, 2, \cdots, N_{\mathrm{su}}\}$) stand for the energy statistics and energy threshold of the $i-$th SU. Since the N_{su} SUs decides independently whether the sensing channel is occupied, (F.2) yields (6.47). Similarly, we can prove (6.48). This concludes the proof.

Appendix G

Proof of Proposition 6.5

When the AND rule is employed, the false alarm probability can be obtained as

$$P_{C,\mathrm{fa}} = P_r\left(\{T_1 > \gamma_1\} \cap \{T_2 > \gamma_2 \cap \cdots \cap \{T_{N_{\mathrm{su}}} > \gamma_{N_{\mathrm{su}}}\} \,|\theta = 0\right). \tag{G.1}$$

In (G.1), T_i and γ_i ($i \in \{1, \cdots, N_{\mathrm{su}}\}$) stand for the energy statistics and energy threshold of the $i-$th SU. Since the SUs independently decide whether the sensing channel is occupied, Eq. (G.1) can be re-written as (6.49). Similarly, we can prove that the detection probability is given by (6.50). This concludes the proof.

Appendix H

Proof of Proposition 6.6

If the sensing channel is idle ($\theta = 0$), then the probability that the SU j reports that the channel is busy ($d_j = 1$), can be expressed as $P_{fa,j}$, while the probability that the SU j reports that the channel is idle ($d_j = 0$), is given by $(1 - P_{\text{fa},j})$. Therefore, since each SU decides individually whether there is PU activity in the sensing channel, the probability that $\left\lceil \frac{N_{\text{su}}}{2} \right\rceil$ SUs report a fixed decision set

$$\mathcal{D} = [d_1, d_2, \cdots, d_{N_{\text{su}}}], \tag{H.1}$$

if $\theta_k = 0$, can be obtained as

$$P_{\text{fa}}(\mathcal{D}) = \prod_{j=1}^{N_{\text{su}}} \left(U\left(-d_j\right)\left(1 - P_{\text{fa},j}\right) + U\left(d_j - 1\right) P_{\text{fa},j} \right). \tag{H.2}$$

Furthermore, based on the MAJORITY rule, the sensing channel is considered busy, if at least $\left\lceil \frac{N_{\text{su}}}{2} \right\rceil$ SUs reports "1". Consequently, for a given decision set $\mathcal{D}$, the false alarm probability can be evaluated as

$$P_{C,\text{FA}|\mathcal{D}} = U\left(\sum_{l=1}^{N_{\text{su}}} d_l - k_{\text{su}} \right) \prod_{j=1}^{n_{\text{su}}} \left(U\left(-d_j\right)\left(1 - P_{\text{fa},j}\right) + U\left(d_j - 1\right) P_{\text{fa},j} \right). \tag{H.3}$$

Hence, for any possible $\mathcal{D}$, the false alarm probability, using the MAJORITY rule, can be obtained by (6.51). Similarly, we can prove that the detection probability is given by (6.52). This concludes the proof.

Appendix I

Proof of Theorem 7.1

Since $h_k \sim \mathcal{CN}\left(0, \sigma_h^2\right)$, it follows that the parameter σ^2 follows exponential distribution with PDF given by

$$f_{\sigma^2}\left(x \,|\theta_k = 1\right) = \frac{2\exp\left(\frac{\sigma_w^2}{\sigma_s^2\sigma_h^2}\right)}{\sigma_s^2\sigma_h^2}\exp\left(-\frac{2x}{\sigma_s^2\sigma_h^2}\right), \tag{I.1}$$

with $x \in \left[\frac{\sigma_w^2}{2}, \infty\right)$. Hence, the unconditional CDF can be expressed as

$$F_{T_k}\left(x \,|\theta_k = 1\right) = \frac{1}{\Gamma\left(N_s\right)}\frac{2\exp\left(\frac{\sigma_w^2}{\sigma_s^2\sigma_h^2}\right)}{\sigma_s^2\sigma_h^2}\int_{\frac{\sigma_w^2}{2}}^{\infty}\gamma\left(N_s, \frac{N_s x}{2y}\right)\exp\left(-\frac{2y}{\sigma_h^2\sigma_s^2}\right)dy, \tag{I.2}$$

which is equivalent to

$$\begin{aligned} F_{T_k}\left(x \,|\theta_k = 1\right) = {} & \frac{1}{\Gamma\left(N_s\right)}\frac{2\exp\left(\frac{\sigma_w^2}{\sigma_s^2\sigma_h^2}\right)}{\sigma_s^2\sigma_h^2}\int_{\frac{\sigma_w^2}{2}}^{\infty}\Gamma\left(N_s\right)\exp\left(-\frac{2y}{\sigma_h^2\sigma_s^2}\right)dy \\ & - \frac{1}{\Gamma\left(N_s\right)}\frac{2\exp\left(\frac{\sigma_w^2}{\sigma_s^2\sigma_h^2}\right)}{\sigma_s^2\sigma_h^2}\int_{\frac{\sigma_w^2}{2}}^{\infty}\Gamma\left(N_s, \frac{N_s x}{2y}\right)\exp\left(-\frac{2y}{\sigma_h^2\sigma_s^2}\right)dy, \end{aligned} \tag{I.3}$$

or

$$F_{T_k}\left(x \,|\theta_k = 1\right) = 1 - \frac{1}{\Gamma\left(N_s\right)}\frac{2\exp\left(\frac{\sigma_w^2}{\sigma_s^2\sigma_h^2}\right)}{\sigma_s^2\sigma_h^2}\int_{\frac{\sigma_w^2}{2}}^{\infty}\Gamma\left(N_s, \frac{N_s x}{2y}\right)\exp\left(-\frac{2y}{\sigma_h^2\sigma_s^2}\right)dy. \tag{I.4}$$

Since N_s is a positive integer, the upper incomplete Gamma function can be written as a finite sum [274, Eq. (8.352/2)],

$$\Gamma\left(N_s, \frac{N_s x}{2y}\right) = \sum_{k=0}^{N_s-1}\frac{(N_s-1)!}{k!}\left(\frac{N_s x}{2y}\right)^k\exp\left(-\frac{N_s x}{2y}\right). \tag{I.5}$$

Substituting (I.5) into (I.4), yields

$$F_{T_k}\left(x \,|\theta_k = 1\right) = 1 - \frac{2\exp\left(\frac{\sigma_w^2}{\sigma_s^2\sigma_h^2}\right)}{\sigma_s^2\sigma_h^2}\sum_{k=0}^{N_s-1}\int_{\frac{\sigma_w^2}{2}}^{\infty}\frac{1}{k!}\left(\frac{N_s x}{2y}\right)^k\exp\left(-\frac{N_s x}{2y} - \frac{2y}{\sigma_h^2\sigma_s^2}\right)dy. \tag{I.6}$$

After some algebraic manipulations and using [275, Eq. (6.2)], (I.6) can be written as in (7.29). This concludes the proof.

Appendix J

Proof of Theorem 7.2

According to [276] and after some basic algebraic manipulations, its PDF can be expressed as

$$f_{\sigma^2}(x\,|\Theta) = \sum_{i=2}^{3} U(m_i-2)\, w_{1,i} w_{2,i} \exp\left(-\frac{x}{\mathcal{A}_i}\right) + \sum_{i=1}^{4} U(m_i-1)\, U(m_i-2)\, w_{1,i} x \exp\left(-\frac{x}{\mathcal{A}_i}\right) + \sum_{i=1}^{4} U(m_i-1)\left(U(1-m_i) - \mathcal{A}_5 U(m_i-2)\right) w_{1,i} \exp\left(-\frac{x}{\mathcal{A}_i}\right), \tag{J.1}$$

where $x \in [\mathcal{A}_5, \infty)$, $w_{1,i}$ and $w_{2,i}$ are respectively defined by (7.44) and (7.45), whereas

$$m = [\theta_k, \theta_{k-1} + \theta_{k+1}, \theta_{-k+1} + \theta_{-k-1}, \theta_{-k}]\,. \tag{J.2}$$

Based on the above, the CDF of the received energy, in case of non-ideal RF front-end, unconditioned with respect to Θ, can be expressed as

$$F_{T_k}(x\,|\Theta) = \sum_{i=2}^{3} U(m_i-2)\, w_{1,i} w_{2,i} \mathcal{I}_{1,i} + \sum_{i=1}^{4} U(m_i-1)\left(U(1-m_i) - \mathcal{A}_5 U(m_i-2)\right) w_{1,i} \mathcal{I}_{1,i} + \sum_{i=1}^{4} U(m_i-1)\, U(m_i-2)\, w_{1,i} \mathcal{I}_{2,i}, \tag{J.3}$$

with

$$\mathcal{I}_{1,i} = \frac{1}{\Gamma(N_s)} \int_{\mathcal{A}_5}^{\infty} \exp\left(-\frac{y}{\mathcal{A}_i}\right) \gamma\left(N_s, \frac{N_s x}{2y}\right) dy, \tag{J.4}$$

and

$$\mathcal{I}_{2,i} = \frac{1}{\Gamma(N_s)} \int_{\mathcal{A}_5}^{\infty} y \exp\left(-\frac{y}{\mathcal{A}_i}\right) \gamma\left(N_s, \frac{N_s x}{2y}\right) dy. \tag{J.5}$$

Eqs. (J.4) and (J.5), after some basic algebraic manipulations, can be respectively written as

$$\begin{aligned}\mathcal{I}_{1,i} &= \frac{1}{\Gamma(N_s)} \int_{\mathcal{A}_5}^{\infty} \exp\left(-\frac{y}{\mathcal{A}_i}\right) \left(\Gamma(N_s) - \Gamma\left(N_s, \frac{N_s x}{2y}\right)\right) dy \\ &= \int_{\mathcal{A}_5}^{\infty} \exp\left(-\frac{y}{\mathcal{A}_i}\right) dy - \frac{1}{\Gamma(N_s)} \int_{\mathcal{A}_5}^{\infty} \exp\left(-\frac{y}{\mathcal{A}_i}\right) \Gamma\left(N_s, \frac{N_s x}{2y}\right) dy\end{aligned} \tag{J.6}$$

and

$$\begin{aligned}\mathcal{I}_{2,i} &= \frac{1}{\Gamma(N_s)} \int_{\mathcal{A}_5}^{\infty} y \exp\left(-\frac{y}{\mathcal{A}_i}\right) \left(\Gamma(N_s) - \Gamma\left(N_s, \frac{N_s x}{2y}\right)\right) dy \\ &= \int_{\mathcal{A}_5}^{\infty} y \exp\left(-\frac{y}{\mathcal{A}_i}\right) dy - \frac{1}{\Gamma(N_s)} \int_{\mathcal{A}_5}^{\infty} y \exp\left(-\frac{y}{\mathcal{A}_i}\right) \Gamma\left(N_s, \frac{N_s x}{2y}\right) dy.\end{aligned} \tag{J.7}$$

Moreover, by using [274, Eq. (8.352/2)] and [275, Eq. (6.2)], (J.6) and (J.7) can be rewritten as

$$\mathcal{I}_{1,i} = \mathcal{A}_i \exp\left(-\frac{\mathcal{A}_5}{\mathcal{A}_i}\right) - \sum_{k=0}^{N_s-1} \frac{(N_s-1)!}{k!} \left(\frac{N_s x}{2}\right)^k \frac{1}{\mathcal{A}_i^{k+1}} \frac{\Gamma\left(-k+1, \frac{\mathcal{A}_5}{\mathcal{A}_i}, \frac{N_s x}{2\mathcal{A}_i}, 1\right)}{\Gamma(N_s)}, \tag{J.8}$$

and

$$\mathcal{I}_{2,i}=\mathcal{A}_i\left(\mathcal{A}_5+\mathcal{A}_i\right)\exp\left(-\frac{\mathcal{A}_5}{\mathcal{A}_i}\right)-\sum_{k=0}^{N_s-1}\frac{(N_s-1)!}{k!}\left(\frac{N_s x}{2}\right)^k\frac{1}{\mathcal{A}_i^{k+1}}\frac{\Gamma\left(-k+2,\frac{\mathcal{A}_5}{\mathcal{A}_i},\frac{N_s x}{2\mathcal{A}_i},1\right)}{\Gamma\left(N_s\right)}. \tag{J.9}$$

Hence, taking into consideration (J.8), (J.9) and since

$$U\left(m_i-1\right)U\left(m_i-2\right)=U\left(m_i-2\right), \tag{J.10}$$

Eq. (J.3) results in (7.43). This concludes the proof.

Appendix K

Proof of Theorem 7.3

If the channel occupancy vector Θ is the all idle vector, i.e.,

$$\Theta = \tilde{\Theta}_{2,0} = [0, 0, 0, 0, 0, 0], \tag{K.1}$$

then, in accordance to (7.37), the signal variance can be expressed as

$$\sigma^2_{\tilde{\Theta}_{2,0}} = \mathcal{A}_5. \tag{K.2}$$

According to (7.36), since $\sigma^2_{\tilde{\Theta}_{2,0}}$ is independent of H, the CDF of the energy statistics, assuming an non-ideal RF front-end, when all the channels of $\{-k-1, -k, -k+1, k-1, k, k+1\}$ are idle, can be obtained by (7.47). This concludes the proof.

Appendix L

Proof of Proposition 8.1

Proposition 8.1 can be proven by following the same steps as Corollary 1 in [466]. Specifically, let

$$\mathbf{P}^{'} = \left\{ P_s^{'}(-K), \cdots, P_s^{'}(-1), P_s^{'}(1), \cdots, P_s^{'}(K) \right\} \tag{L.1}$$

be an optimal solution for the optimization problem presented in (8.17). Then, it is possible to find a feasible solution

$$\begin{aligned} \mathbf{P}_{\text{opt}} &= \left\{ P_s^{\text{opt}}(-K), \cdots, P_s^{\text{opt}}(-1), P_s^{\text{opt}}(1), \cdots, P_s^{\text{opt}}(K) \right\} \\ &= \eta \mathbf{P}^{'} = \left\{ \eta P_s^{'}(-K), \cdots, \eta P_s^{'}(-1), \eta P_s^{'}(1), \cdots, \eta P_s^{'}(K) \right\} \end{aligned} \tag{L.2}$$

with

$$\eta = \frac{P_{\max}}{\sum_{k \in \mathcal{K}} P_s^{'}(k)} > 1, \tag{L.3}$$

such that the power constraint is satisfied with equality. Consequently, the corresponding signal to interference plus noise ratio (SINR) at the $k-$th US can be obtained as

$$\begin{aligned} \gamma_k \left(\eta P_s^{'}(k), \eta P_s^{'}(-k) \right) &= \frac{|K_{1,k}|^2 |h_k(k)|^2 P_s^{\text{opt}}(k)}{|K_{2,k}|^2 |h_k(-k)|^2 P_s^{\text{opt}}(-k) + \left(|K_{1,k}|^2 + |K_{2,k}|^2 \right) N_0} \\ &= \frac{|K_{1,k}|^2 |h_k(k)|^2 P_s^{'}(k)}{|K_{2,k}|^2 |h_k(-k)|^2 P_s^{'}(-k) + \left(|K_{1,k}|^2 + |K_{2,k}|^2 \right) \frac{N_0}{\eta}} \\ &> \gamma_k \left(P_s^{'}(k), P_s^{'}(-k) \right). \end{aligned} \tag{L.4}$$

From (L.4), it is evident that the SINR of UE k is improved. Consequently, the achievable capacity of the k-th UE is increased, which contradicts the assumption that $\mathbf{P'}$ is an optimal solution. Hence, the achievable capacity of the $k-$th UE is maximized, when the inequality constraint in (8.17) is satisfied with equality.

Appendix M

Proof of Proposition 8.2

Proposition 8.2 can be proven by following the same steps as Corollary 2 in [466]. In particular, we assume that there exists an optimal solution

$$\mathbf{P} = \{P_s(-K), \cdots, P_s(-k), \cdots, P_s(-1), P_s(1), \cdots, P_s(k), \cdots, P_s(K)\} \tag{M.1}$$

such that

$$R_k\left(P_s(k), P_s(-k)\right) > R_{-k}\left(P_s(k), P_s(-k)\right). \tag{M.2}$$

Based on Proposition 8.1, we have that

$$\sum_{k\in\mathcal{K}} P_s(k) = P_{\max}. \tag{M.3}$$

Moreover, we observe that as $P_s(k)$ decreases, R_k decreases, while R_{-k} increases. Thus, it is possible to find a feasible solution

$$\mathbf{P}_{\text{opt}}^{'} = \{P_s(-K), \cdots, P_s(-k), \cdots, P_s(-1), P_s(1), \cdots, \tau P_s(k), \cdots, P_s(K)\}, \tag{M.4}$$

with $\tau < 1$, which satisfies that

$$R_k\left(\tau P_s(k), P_s(-k)\right) = R_{-k}\left(P_s(k), P_s(-k)\right). \tag{M.5}$$

and

$$R_k\left(\tau P_s(k), P_s(-k)\right) < R_k\left(P_s(k), P_s(-k)\right). \tag{M.6}$$

Consequently, replacing $P_s(k)$ with $\tau P_s(k)$ will result in the same value of the worst achievable capacity. Therefore, $\mathbf{P}_{\text{opt}}^{'}$ is an optimal solution. However, since $\tau < 1$,

$$P_s(-K) + \cdots + P_s(-k) + \cdots + P_s(-1) + P_s(1) + \cdots + \tau P_s(k) + \cdots + P_s(K) < P_{\max}. \tag{M.7}$$

This contradicts the conclusion made in the Proposition 8.1 that the worst achievable capacity is minimized when the inequality constraint in (8.17) is satisfied with equality.

Bibliography

[1] T. Nakamura, S. Nagata, A. Benjebbour, Y. Kishiyama, T. Hai, S. Xiaodong, Y. Ning, and L. Nan, "Trends in small cell enhancements in LTE advanced," *IEEE Commun. Mag.*, vol. 51, no. 2, pp. 98–105, Feb. 2013.

[2] S. Chen and J. Zhao, "The requirements, challenges, and technologies for 5G of terrestrial mobile telecommunication," *IEEE Commun. Mag.*, vol. 52, no. 5, pp. 36–43, May 2014.

[3] A. Osseiran, F. Boccardi, V. Braun, K. Kusume, P. Marsch, M. Maternia, O. Queseth, M. Schellmann, H. Schotten, H. Taoka, H. Tullberg, M. A. Uusitalo, B. Timus, and M. Fallgren, "Scenarios for 5G mobile and wireless communications: the vision of the METIS project," *IEEE Commun. Mag.*, vol. 52, no. 5, pp. 26–35, May 2014.

[4] F. Boccardi, R. W. Heath, A. Lozano, T. L. Marzetta, and P. Popovski, "Five disruptive technology directions for 5G," *IEEE Commun. Mag.*, vol. 52, no. 2, pp. 74–80, Feb. 2014.

[5] P. K. Agyapong, M. Iwamura, D. Staehle, W. Kiess, and A. Benjebbour, "Design considerations for a 5G network architecture," *IEEE Commun. Mag.*, vol. 52, no. 11, pp. 65–75, Nov. 2014.

[6] E. Hossain, M. Rasti, H. Tabassum, and A. Abdelnasser, "Evolution toward 5G multi-tier cellular wireless networks: An interference management perspective," *IEEE Wireless Commun.*, vol. 21, no. 3, pp. 118–127, Jun. 2014.

[7] L. Sanguinetti, A. L. Moustakas, and M. Debbah, "Interference management in 5G reverse TDD HetNets with wireless backhaul: A large system analysis," *IEEE J. Sel. Areas Commun.*, vol. 33, no. 6, pp. 1187–1200, Jun. 2015.

[8] S. P. Thompson, *The life of Lord Kelvin*, ser. AMS Chelsea Publishing Series. AMS (American Mathematical Society) Chelsea Pub., 2005, vol. 2.

[9] B. Saltzberg, "Intersymbol interference error bounds with application to ideal bandlimited signaling," *IEEE Trans. Inf. Theory*, vol. 14, no. 4, pp. 563–568, Jul. 1968.

[10] P. McLane, "A residual intersymbol interference error bound for truncated-state viterbi detectors," *IEEE Trans. Inf. Theory*, vol. 26, no. 5, pp. 548–553, Sep. 1980.

[11] G. Forney, "Maximum-likelihood sequence estimation of digital sequences in the presence of intersymbol interference," *IEEE Trans. Inf. Theory*, vol. 18, no. 3, pp. 363–378, May 1972.

[12] H. Kobayashi, "Coding schemes for reduction of intersymbol interference in data transmission systems," *IBM J. Res. Dev.*, vol. 14, no. 4, pp. 343–353, Jul. 1970.

[13] J. Hu, T. M. Duman, M. F. Erden, and A. Kavcic, "Achievable information rates for channels with insertions, deletions, and intersymbol interference with i.i.d. inputs," *IEEE Trans. Commun.*, vol. 58, no. 4, pp. 1102–1111, Apr. 2010.

[14] F. Lim, A. Kavcic, and M. Fossorier, "List decoding techniques for intersymbol interference channels using ordered statistics," *IEEE J. Sel. Areas Commun.*, vol. 28, no. 2, pp. 241–251, Feb. 2010.

[15] Y. Chen, P. Njeim, T. Cheng, B. J. Belzer, and K. Sivakumar, "Iterative soft decision feedback Zig-Zag equalizer for 2D intersymbol interference channels," *IEEE J. Sel. Areas Commun.*, vol. 28, no. 2, pp. 167–180, Feb. 2010.

[16] W. Huleihel and N. Merhav, "Universal decoding for gaussian intersymbol interference channels," *IEEE Trans. Inf. Theory*, vol. 61, no. 4, pp. 1606–1618, Apr. 2015.

[17] J. Cordaro and T. Wagner, "Intersymbol interference on a continuous-time gaussian channel," *IEEE Trans. Inf. Theory*, vol. 16, no. 4, pp. 422–429, Jul. 1970.

[18] K. Yao and L. Milstein, "On ML bit detection of binary signals with intersymbol interference in Gaussian noise," *IEEE Trans. Commun.*, vol. 23, no. 9, pp. 971–976, Sep. 1975.

[19] N. Bershad and P. Vena, "Eliminating intersymbol interference-A state-space approach," *IEEE Trans. Inf. Theory*, vol. 18, no. 2, pp. 275–281, Mar. 1972.

[20] R. Lugannani, "Intersymbol interference and probability of error in digital systems," *IEEE Trans. Inf. Theory*, vol. 15, no. 6, pp. 682–688, Nov. 1969.

[21] O. Shimbo, M. Celebiler, and R. Fang, "Performance analysis of DPSK systems in both thermal noise and intersymbol interference," *IEEE T. Commun. Techn.*, vol. 19, no. 6, pp. 1179–1188, Dec. 1971.

[22] C. E. Shannon *et al.*, "Two-way communication channels," in *4th Berkeley Symp. Math. Stat. Prob*, vol. 1. Berkeley, Calif.: University of California Press, Jun. 1961, pp. 611–644.

[23] V. K. Garg and J. E. Wilkes, *Wireless and personal communications systems*. Prentice-Hall, Inc., 1996.

[24] J. D. Gibson, *Mobile communications handbook*. CRC press, 2012.

[25] G. L. Stüber, *Principles of mobile communication*. Springer Science & Business Media, 2011.

[26] C. E. Shannon, "A mathematical theory of communication," *The Bell System Technical Journal*, vol. 27, no. 3, pp. 379–423, Jul. 1948.

[27] M. Dohler, R. W. Heath, A. Lozano, C. B. Papadias, and R. A. Valenzuela, "Is the PHY layer dead?" *IEEE Commun. Mag.*, vol. 49, no. 4, pp. 159–165, Apr. 2011.

[28] Z. Hadzi-Velkov, N. Zlatanov, and G. K. Karagiannidis, "On the second order statistics of the multihop Rayleigh fading channel," *IEEE Trans. Commun.*, vol. 57, no. 6, pp. 1815–1823, Jun. 2009.

[29] G. K. Karagiannidis, "On the symbol error probability of general order rectangular QAM in Nakagami-m fading," *IEEE Commun. Lett.*, vol. 10, no. 11, pp. 745–747, November 2006.

[30] D. A. Zogas and G. K. Karagiannidis, "Infinite-series representations associated with the bivariate Rician distribution and their applications," *IEEE Trans. Commun.*, vol. 53, no. 11, pp. 1790–1794, Nov. 2005.

[31] H. A. Suraweera, T. A. Tsiftsis, G. K. Karagiannidis, and A. Nallanathan, "Effect of feedback delay on amplify-and-forward relay networks with beamforming," *IEEE Trans. Veh. Technol.*, vol. 60, no. 3, pp. 1265–1271, Mar. 2011.

[32] D. S. Karas, A.-A. A. Boulogeorgos, and G. K. Karagiannidis, "Physical layer security with uncertainty on the location of the eavesdropper," *IEEE Wireless Commun. Lett.*, vol. 5, no. 5, pp. 540–543, Oct. 2016.

[33] Y. Liu, G. Pan, H. Zhang, and M. Song, "On the capacity comparison between MIMO-NOMA and MIMO-OMA," *IEEE Access*, vol. 4, pp. 2123–2129, 2016.

[34] J. F. Morrison, "A new broadcast-transmitter circuit design for frequency modulation," *Proc. IRE*, vol. 28, no. 10, pp. 444–449, Oct. 1940.

[35] W. A. Edson, "Noise in oscillators," *Proc. IRE*, vol. 48, no. 8, pp. 1454–1466, Aug. 1960.

[36] B. E. Love, "Intermodulation effects in FM and PM systems," *Transactions of the American Institute of Electrical Engineers, Part I: Communication and Electronics*, vol. 79, no. 3, pp. 245–248, Jul. 1960.

[37] F. Casadevall and J. J. Olmos, "On the behavior of the LINC transmitter," in *IEEE 40th Vehicular Technology Conference*. Orlando, FL: IEEE, May 1990, pp. 29–34.

[38] R. Howald, S. Kesler, and M. Kam, "BER performance of M-QAM using OFDM with RF carrier phase noise," in *Proceedings of the Thirtieth Southeastern Symposium on System Theory*. Morgantown, WV: IEEE, Mar. 1998, pp. 419–423.

[39] R. L. Howald, S. Kesler, and M. Kam, "BER performance analysis of OFDM-QAM in phase noise," in *IEEE International Symposium on Information Theory*. Cambridge, MA: IEEE, Aug. 1998, pp. 256–256.

[40] J. Nielsen, S. Lai, and C. Bedard, "Effect of transceiver generated phase noise on transmission and reception of CDMA signals," in *IEEE Vehicular Technology Conference (VTC)*, vol. 2. Ottawa, CA: IEEE, May 1998, pp. 1618–1621.

[41] P. Baudin and F. Belveze, "Impact of RF impairments on a DS-CDMA receiver," *IEEE Trans. Commun.*, vol. 52, no. 1, pp. 31–36, Jan. 2004.

[42] L. Angrisani and R. Colella, "Detection and evaluation of I/Q impairments in RF digital transmitters," *IEE Proceedings - Science, Measurement and Technology*, vol. 151, no. 1, pp. 39–45, Jan. 2004.

[43] J. C. Pedro, N. B. Carvalho, and P. M. Lavrador, "Modeling nonlinear behavior of band-pass memoryless and dynamic systems," in *IEEE MTT-S International Microwave Symposium Digest*, vol. 3. Philadelphia, PA, US: IEEE, Jun. 2003, pp. 2133–2136.

[44] S. Woo, D. Lee, K. Kim, Y. Hur, C.-H. Lee, and J. Laskar, "Combined effects of RF impairments in the future IEEE 802. 11n WLAN systems," in *IEEE 61st Vehicular Technology Conference*, vol. 2. Stockholm, SE: IEEE, May 2005, pp. 1346–1349.

[45] R. Salmond, J. f. Bousquet, and S. Magierowski, "RF hardware modeling of a direct conversion receiver using SDMA," in *IEEE Vehicular Technology Conference*. Montreal, CA: IEEE, Sep. 2006, pp. 1–6.

[46] T. C. W. Schenk and E. R. Fledderus, "RF impairments in high-rate wireless systems-understanding the impact of TX/RX-asymmetry," in *3rd International Symposium on Communications, Control and Signal Processing (ISCCSP)*. St Julians, MT: IEEE, Mar. 2008, pp. 117–122.

[47] S. A. Bassam, M. Helaoui, S. Boumaiza, and F. M. Ghannouchi, "Experimental study of the effects of RF front-end imperfection on MIMO transmitter performance," in *IEEE MTT-S International Microwave Symposium Digest*. Atlanta, GA, US: IEEE, Jun. 2008, pp. 1187–1190.

[48] S. Woo, H. Yu, J. Lee, C.-H. Lee, and J. Laskar, "Effects of RF impairments in transmitter for the future beyond-3G communications systems," in *IEEE International Symposium on Circuits and Systems*. Island of Kos, GR: IEEE, May 2006, pp. 5668–5671.

[49] G. Fettweis, M. Lohning, D. Petrovic, M. Windisch, P. Zillmann, and W. Rave, "Dirty RF: a new paradigm," in *IEEE 16th International Symposium on Personal, Indoor and Mobile Radio Communications*, vol. 4. Berlin, DE: IEEE, Sep. 2005, pp. 2347–2355.

[50] U. H. Rizvi, G. J. M. Janssen, and J. H. Weber, "Impact of RF circuit imperfections on multi-carrier and single-carrier based transmissions at 60 GHz," in *IEEE Radio and Wireless Symposium*. Orlando, FL: IEEE, Jan. 2008, pp. 691–694.

[51] S. Mikroulis, S. Karabetsos, E. Pikasis, and A. A. Nassiopoulos, "Performance evaluation of a radio over fiber (ROF) system subject to the transmitter's limitations for application in broadband networks," *IEEE Trans. Consum. Electron.*, vol. 54, no. 2, pp. 437–443, May 2008.

[52] Y. Gao, T. Kreul, and T. Kaiser, "A simplified RF model to investigate impacts of RF impairments on OFDM," in *18th International OFDM Workshop (InOWo)*. Essen, DE: IEEE, Aug. 2014, pp. 1–6.

[53] X. Zhang, M. Matthaiou, M. Coldrey, and E. Bjornson, "Impact of residual transmit RF impairments on training-based MIMO systems," *IEEE Trans. Commun.*, vol. 63, no. 8, pp. 2899–2911, Aug. 2015.

[54] A. Tarighat and A. H. Sayed, "MIMO OFDM receivers for systems with IQ imbalances," *IEEE Trans. Signal Process.*, vol. 53, no. 9, pp. 3583–3596, Sep. 2005.

[55] M. Lucente, T. Rossi, A. Jebril, M. Ruggieri, S. Pulitano, A. Iera, A. Molinaro, C. Sacchi, and L. Zuliani, "Experimental missions in W-band: A small LEO satellite approach," *IEEE Syst. J.*, vol. 2, no. 1, pp. 90–103, Mar. 2008.

[56] P. Angeletti, S. D'Addio, E. Colzi, and M. Aloisio, "Modeling of complex telecommunication satellite payloads," in *IEEE MTT-S International Microwave Symposium Digest (MTT)*. Boston, MA: IEEE, Jun. 2009, pp. 1597–1600.

[57] K. Guo, D. Guo, Y. Huang, X. Wang, and B. Zhang, "Performance analysis of a dual-hop satellite relay network with hardware impairments," in *25th Wireless and Optical Communication Conference (WOCC)*. Chengdu, CN: IEEE, May 2016, pp. 1–5.

[58] E. Cetin, I. Kale, and R. C. S. Morling, "Analysis and compensation of rf impairments for next generation multimode GNSS receivers," in *IEEE International Symposium on Circuits and Systems*. New Orleans, LA: IEEE, May 2007, pp. 1729–1732.

[59] D. Valente, E. Cianca, S. Mukherjee, T. Rossi, M. Ruggieri, and R. Prasad, "Comparison of UWB approaches applied to EHF satellite communications," in *IEEE Aerospace Conference*. Big Sky, MT: IEEE, Mar. 2012, pp. 1–6.

[60] E. Colzi, P. Angeletti, M. Aloisio, S. D'Addio, R. O. Balague, and E. Casini, "Characterization of TWTA nonlinearity by means of a time-domain correlation method," in *10th International Workshop on Signal Processing for Space Communications*. Rhodes Island, GR: IEEE, Oct. 2008, pp. 1–5.

[61] S. Park, I. Cha, and K. Chang, "Link-level performance of satellite DMB system a considering frequency timing synchronization error and HPA non-linearity," in *IEEE Workshop on Signal Processing Systems Design and Implementation*. Athens, GR: IEEE, Nov. 2005, pp. 7–12.

[62] S. Narayanan, "Application of volterra series to intermodulation distortion analysis of transistor feedback amplifiers," *IEEE T. Circuits. Syst.*, vol. 17, no. 4, pp. 518–527, Nov. 1970.

[63] L. D. Clercq, M. Peeters, S. Schelstraete, and T. Pollet, "Mitigation of radio interference in xDSL transmission," *IEEE Commun. Mag.*, vol. 38, no. 3, pp. 168–173, Mar. 2000.

[64] P. Rykaczewski, D. Pienkowski, R. Circa, and B. Steinke, "Signal path optimization in software-defined radio systems," *IEEE Trans. Microw. Theory Tech.*, vol. 53, no. 3, pp. 1056–1064, Mar. 2005.

[65] M. J. Bruno, L. Citta, and J. E. Cousseau, "A 6 Watt linear RF power amplifier for WiMAX base station," in *Argentine School of Micro-Nanoelectronics, Technology and Applications (EAMTA)*. Buenos Aires, AR: IEEE, Sep. 2008, pp. 134–139.

[66] E. Cetin, I. Kale, and R. C. S. Morling, "Living and dealing with RF impairments in communication transceivers," in *IEEE International Symposium on Circuits and Systems*. New Orleans, LA: IEEE, May 2007, pp. 21–24.

[67] P. M. Cabral, L. Cabria, J. A. Garcia, and J. C. Pedro, "Polar transmitter architecture used in a software defined radio context," in *IEEE International Microwave Workshop Series on RF Front-ends for Software Defined and Cognitive Radio Solutions (IMWS)*. Aveiro, PT: IEEE, Feb. 2010, pp. 1–4.

[68] E. S. Erdogan and S. Ozev, "Detailed characterization of transceiver parameters through loop-back-based BiST," *IEEE Trans. Very Large Scale Integr. VLSI Syst.*, vol. 18, no. 6, pp. 901–911, Jun. 2010.

[69] N. B. Carvalho, J. C. Pedro, and J. P. Martins, "A corrected microwave multisine waveform generator," *IEEE Trans. Microwave Theory Tech.*, vol. 54, no. 6, pp. 2659–2664, Jun. 2006.

[70] M. Valkama, L. Anttila, and M. Renfors, "Some radio implementation challenges in 3G-LTE context," in *IEEE 8th Workshop on Signal Processing Advances in Wireless Communications*. Helsinki, FI: IEEE, Jun. 2007, pp. 1–5.

[71] G. Hueber, Y. Zou, K. Dufrene, R. Stuhlberger, and M. Valkama, "Smart front-end signal processing for advanced wireless receivers," *IEEE J. Sel. Top. Signal Process.*, vol. 3, no. 3, pp. 472–487, Jun. 2009.

[72] Z. Zhu, H. Leung, and X. Huang, "Challenges in reconfigurable radio transceivers and application of nonlinear signal processing for RF impairment mitigation," *IEEE Circuits Syst. Mag.*, vol. 13, no. 1, pp. 44–65, Firstquarter 2013.

[73] G. Hueber and R. B. Staszewski, *RF Impairment Compensation for Future Radio Systems*. Wiley-IEEE Press, 2011, ch. 15, pp. 451–496.

[74] E. Dahlman, G. Mildh, S. Parkvall, J. Peisa, J. Sachs, and Y. Selén, "5G radio access," *Ericsson review*, vol. 6, pp. 2–7, Jun. 2014.

[75] E. Hossain and M. Hasan, "5G cellular: key enabling technologies and research challenges," *IEEE Instrumentation Measurement Magazine*, vol. 18, no. 3, pp. 11–21, Jun. 2015.

[76] N. Lee and R. W. H. Jr, "Advanced interference management technique: potentials and limitations," *IEEE Wireless Commun.*, vol. 23, no. 3, pp. 30–38, Jun. 2016.

[77] M. O. Hasna, M. S. Alouini, A. Bastami, and E. S. Ebbini, "Performance analysis of cellular mobile systems with successive co-channel interference cancellation," *IEEE Trans. Wireless Commun.*, vol. 2, no. 1, pp. 29–40, Jan. 2003.

[78] X. Ge, H. Cheng, M. Guizani, and T. Han, "5G wireless backhaul networks: challenges and research advances," *IEEE Network*, vol. 28, no. 6, pp. 6–11, Nov. 2014.

[79] X. Ge, S. Tu, G. Mao, C. X. Wang, and T. Han, "5G ultra-dense cellular networks," *IEEE Wireless Commun.*, vol. 23, no. 1, pp. 72–79, Feb. 2016.

[80] W. Tong and Z. Peiying, "5G: A technology vision," *WinWin*, no. 19, pp. 17–21, Mar. 2014.

[81] B. Soret, K. I. Pedersen, N. T. K. Jorgensen, and V. Fernandez-Lopez, "Interference coordination for dense wireless networks," *IEEE Commun. Mag.*, vol. 53, no. 1, pp. 102–109, Jan. 2015.

[82] S. F. Yunas, M. Valkama, and J. Niemela, "Spectral and energy efficiency of ultra-dense networks under different deployment strategies," *IEEE Commun. Mag.*, vol. 53, no. 1, pp. 90–100, Jan. 2015.

[83] C. X. Wang, F. Haider, X. Gao, X. H. You, Y. Yang, D. Yuan, H. M. Aggoune, H. Haas, S. Fletcher, and E. Hepsaydir, "Cellular architecture and key technologies for 5G wireless communication networks," *IEEE Commun. Mag.*, vol. 52, no. 2, pp. 122–130, Feb. 2014.

[84] D. Lopez-Perez, M. Ding, H. Claussen, and A. H. Jafari, "Towards 1 Gbps/UE in cellular systems: Understanding ultra-dense small cell deployments," *IEEE Communications Surveys Tutorials*, vol. 17, no. 4, pp. 2078–2101, Fourthquarter 2015.

[85] P. Kela, J. Turkka, and M. Costa, "Borderless mobility in 5G outdoor ultra-dense networks," *IEEE Access*, vol. 3, pp. 1462–1476, Sep. 2015.

[86] H. Zhang, C. Jiang, J. Cheng, and V. C. M. Leung, "Cooperative interference mitigation and handover management for heterogeneous cloud small cell networks," *IEEE Wireless Commun.*, vol. 22, no. 3, pp. 92–99, Jun. 2015.

[87] L. Yang and M. S. Alouini, "Performance comparison of different selection combining algorithms in presence of co-channel interference," *IEEE Trans. Veh. Technol.*, vol. 55, no. 2, pp. 559–571, Mar. 2006.

[88] H. Yang and M. S. Alouini, "Outage probability of dual-branch diversity systems in presence of co-channel interference," *IEEE Trans. Wireless Commun.*, vol. 2, no. 2, pp. 310–319, Mar. 2003.

[89] A. Nezampour, A. Nasri, R. Schober, and Y. Ma, "Asymptotic BEP and SEP of quadratic diversity combining receivers in correlated ricean fading, non-gaussian noise, and interference," *IEEE Trans. Commun.*, vol. 57, no. 4, pp. 1039–1049, Apr. 2009.

[90] A. Nasri, R. Schober, and I. F. Blake, "Performance and optimization of amplify-and-forward cooperative diversity systems in generic noise and interference," *IEEE Trans. Wireless Commun.*, vol. 10, no. 4, pp. 1132–1143, Apr. 2011.

[91] M. A. Ruder, A. M. Lehmann, R. Schober, and W. H. Gerstacker, "Single antenna interference cancellation for GSM/VAMOS/EDGE using l_p-norm detection and decoding," *IEEE Trans. Wireless Commun.*, vol. 14, no. 5, pp. 2413–2425, May 2015.

[92] M. Kang, L. Yang, and M. S. Alouini, "Outage probability of MIMO optimum combining in presence of unbalanced co-channel interferers and noise," *IEEE Trans. Wireless Commun.*, vol. 5, no. 7, pp. 1661–1668, Jul. 2006.

[93] K. Gulati, B. L. Evans, J. G. Andrews, and K. R. Tinsley, "Statistics of co-channel interference in a field of Poisson and Poisson-Poisson clustered interferers," *IEEE Trans. Signal Process.*, vol. 58, no. 12, pp. 6207–6222, Dec. 2010.

[94] C. Feng, H. Cui, M. Ma, and B. Jiao, "On statistical properties of co-channel interference in OFDM systems," *IEEE Commun. Lett.*, vol. 17, no. 12, pp. 2328–2331, Dec. 2013.

[95] D. B. da Costa and M. D. Yacoub, "Outage performance of two hop AF relaying systems with co-channel interferers over Nakagami-m fading," *IEEE Commun. Lett.*, vol. 15, no. 9, pp. 980–982, Sep. 2011.

[96] S. S. Ikki, P. Ubaidulla, and S. Aissa, "Regenerative cooperative diversity networks with co-channel interference: Performance analysis and optimal energy allocation," *IEEE Trans. Veh. Technol.*, vol. 62, no. 2, pp. 896–902, Feb. 2013.

[97] E. Soleimani-Nasab, M. Matthaiou, M. Ardebilipour, and G. K. Karagiannidis, "Two-way AF relaying in the presence of co-channel interference," *IEEE Trans. Commun.*, vol. 61, no. 8, pp. 3156–3169, Aug. 2013.

[98] J. H. Yun and K. G. Shin, "Adaptive interference management of OFDMA femtocells for co-channel deployment," *IEEE J. Sel. Areas Commun.*, vol. 29, no. 6, pp. 1225–1241, Jun. 2011.

[99] K. I. Pedersen, Y. Wang, S. Strzyz, and F. Frederiksen, "Enhanced inter-cell interference coordination in co-channel multi-layer LTE-advanced networks," *IEEE Wireless Commun.*, vol. 20, no. 3, pp. 120–127, Jun. 2013.

[100] Y. R. Huang, C. C. Fung, and K. T. Wong, "Interference suppression for OFDM systems with insufficient guard interval using null subcarriers," *IEEE Signal. Proc. Let.*, vol. 16, no. 11, pp. 929–932, Nov. 2009.

[101] D. Cox, "Cochannel interference considerations in frequency reuse small-coverage-area radio systems," *IEEE Trans. Commun.*, vol. 30, no. 1, pp. 135–142, Jan. 1982.

[102] R. Muammar and S. Gupta, "Cochannel interference in high-capacity mobile radio systems," *IEEE Trans. Commun.*, vol. 30, no. 8, pp. 1973–1978, Aug. 1982.

[103] K. Daikoku and H. Ohdate, "Optimal channel reuse in cellular land mobile radio systems," *IEEE Trans. Veh. Technol.*, vol. 32, no. 3, pp. 217–224, Aug. 1983.

[104] R. Prasad and A. Kegel, "Effects of Rician faded and log-normal shadowed signals on spectrum efficiency in microcellular radio," *IEEE Trans. Veh. Technol.*, vol. 42, no. 3, pp. 274–281, Aug. 1993.

[105] Y. D. Yao and A. U. H. Sheikh, "Investigations into cochannel interference in microcellular mobile radio systems," *IEEE Trans. Veh. Technol.*, vol. 41, no. 2, pp. 114–123, May 1992.

[106] S. M. Barta and M. L. Honig, "Analysis of a demand assignment TDMA blocking system," *AT&T Bell Laboratories Technical Journal*, vol. 63, no. 1, pp. 89–114, Jan. 1984.

[107] H. Ghafouri-Shiraz and M. M. Karbassian, *Optical CDMA Review*. Wiley-IEEE Press, 2011, pp. 115–131.

[108] D. S. K.-A. A. Boulogeorgos and F. N. Pavlidou, "Comparative analysis of medium access techniques in wireless body area networks," in *5th International Conference on Modern Circuits and Systems Technologies (MOCAST)*. Thessaloniki, GR: IEEE, May 2016, pp. 1–4.

[109] D. S. Kaitalidou, A.-A. Boulogeorgos, and F. N. Pavlidou, "Comparison of CSMA/CA protocols applied in wireless body area network standards," in *18th Mediterranean Electrotechnical Conference (MELECON)*. Limassol, CY: IEEE, Apr. 2016, pp. 1–6.

[110] R. C. T. Lee, M.-C. Chiu, and J.-S. Lin, *Spread spectrum communications*. Wiley-IEEE Press, 2007, pp. 209–230.

[111] A. F. Molisch, *Equalizers*. Wiley-IEEE Press, 2011, pp. 343–361.

[112] M. F. Bugallo, J. Miguez, and L. Castedo, "A maximum likelihood approach to blind multiuser interference cancellation," *IEEE Trans. Signal Process.*, vol. 49, no. 6, pp. 1228–1239, Jun. 2001.

[113] B. C. W. Lo and K. B. Letaief, "Adaptive equalization and interference cancellation for wireless communication systems," *IEEE Trans. Commun.*, vol. 47, no. 4, pp. 538–545, Apr. 1999.

[114] S. Chen, S. McLaughlin, B. Mulgrew, and P. M. Grant, "Bayesian decision feedback equaliser for overcoming co-channel interference," *IEE Proceedings - Communications*, vol. 143, no. 4, pp. 219–225, Aug. 1996.

[115] H. Son, S. Kim, and S. Lee, "Maximum SINR-based receive combiner for cognitive MU-MIMO systems," *IEEE Trans. Veh. Technol.*, vol. 64, no. 9, pp. 4344–4350, Sep. 2015.

[116] Federal Standard, "1037c: Glossary of telecommunications terms," *The Institute for Telecommunication Sciences*, Oct. 2006.

[117] A. F. Molisch, *Wireless Communications*, 2nd ed. John Wiley & Sons, Nov. 2010.

[118] P. Stavroulakis, *Interference analysis and reduction for wireless systems*. Artech House, 2003.

[119] S. Golestaneh, H. M. Hafez, and S. A. Mahmoud, "The effect of adjacent channel interference on the capacity of FDMA cellular systems," *IEEE Trans. Veh. Technol.*, vol. 43, no. 4, pp. 946–954, Nov. 1994.

[120] K. Heiska, H. Posti, P. Muszynski, P. Aikio, J. Numminen, and M. Hamalainen, "Capacity reduction of WCDMA downlink in the presence of interference from adjacent narrow-band system," *IEEE Trans. Veh. Technol.*, vol. 51, no. 1, pp. 37–51, Jan. 2002.

[121] W. Li, J. Chen, H. Long, and B. Wu, "Performance and analysis on LTE system under adjacent channel interference of broadcasting system," in *IEEE 12th International Conference on Computer and Information Technology (CIT)*. Chengdu, CN: IEEE, Oct. 2012, pp. 290–294.

[122] H. Haas and S. McLaughlin, "A derivation of the PDF of adjacent channel interference in a cellular system," *IEEE Commun. Lett.*, vol. 8, no. 2, pp. 102–104, Feb. 2004.

[123] L. Milstein, R. Pickholtz, and D. Schilling, "Comparison of performance of digital modulation techniques in the presence of adjacent channel interference," *IEEE Trans. Commun.*, vol. 30, no. 8, pp. 1984–1993, Aug. 1982.

[124] I. Korn, "Differential phase shift keying in two-path rayleigh channel with adjacent channel interference," *IEEE Trans. Veh. Technol.*, vol. 40, no. 2, pp. 461–471, May 1991.

[125] A. Goldsmith, *Wireless Communications*. New York, NY, USA: Cambridge University Press, Aug. 2005.

[126] Z. Zhang, X. Chai, K. Long, A. V. Vasilakos, and L. Hanzo, "Full duplex techniques for 5G networks: self-interference cancellation, protocol design, and relay selection," *IEEE Commun. Mag.*, vol. 53, no. 5, pp. 128–137, May 2015.

[127] Fempto Forum, "Interference management in UMTS femtocells," Feb. 2010.

[128] J. I. Choi, M. Jain, K. Srinivasan, P. Levis, and S. Katti, "Achieving single channel, full duplex wireless communication," in *Sixteenth Annual International Conference on Mobile Computing and Networking*, ser. MobiCom '10. New York, NY, USA: ACM, Sep. 2010, pp. 1–12.

[129] M. Duarte and A. Sabharwal, "Full-duplex wireless communications using off-the-shelf radios: Feasibility and first results," in *Forty Fourth Asilomar Conference on Signals, Systems and Computers*. Pacific Grove, CA: IEEE, Nov. 2010, pp. 1558–1562.

[130] V. Syrjala, M. Valkama, L. Anttila, T. Riihonen, and D. Korpi, "Analysis of oscillator phase-noise effects on self-interference cancellation in full-duplex OFDM radio transceivers," *IEEE Trans. Wireless Commun.*, vol. 13, no. 6, pp. 2977–2990, Jun. 2014.

[131] S. P. Herath and T. Le-Ngoc, "Sum-rate performance and impact of self-interference cancellation on full-duplex wireless systems," in *IEEE 24th Annual International Symposium on Personal, Indoor, and Mobile Radio Communications (PIMRC)*. London, UK: IEEE, Sep. 2013, pp. 881–885.

[132] Z. Tong and M. Haenggi, "Throughput analysis for full-duplex wireless networks with imperfect self-interference cancellation," *IEEE Trans. Commun.*, vol. 63, no. 11, pp. 4490–4500, Nov. 2015.

[133] T. Riihonen, S. Werner, and R. Wichman, "Mitigation of loopback self-interference in full-duplex mimo relays," *IEEE Trans. Signal Process.*, vol. 59, no. 12, pp. 5983–5993, Dec. 2011.

[134] Z. He, S. Shao, Y. Shen, C. Qing, and Y. Tang, "Performance analysis of RF self-interference cancellation in full-duplex wireless communications," *IEEE Wireless Commun. Lett.*, vol. 3, no. 4, pp. 405–408, Aug. 2014.

[135] I. Atzeni and M. Kountouris, "Full-duplex mimo small-cell networks: Performance analysis," in *IEEE Global Communications Conference (GLOBECOM)*. San Diego, CA: IEEE, Dec. 2015, pp. 1–6.

[136] M. A. Ahmed, C. C. Tsimenidis, and A. F. A. Rawi, "Performance analysis of full-duplex-MRC-MIMO with self-interference cancellation using null-space-projection," *IEEE Trans. Signal Process.*, vol. 64, no. 12, pp. 3093–3105, Jun. 2016.

[137] D. S. Michalopoulos, J. Schlenker, J. Cheng, and R. Schober, "Error rate analysis of full-duplex relaying," in *International Waveform Diversity and Design Conference*. Niagara Falls, ON: IEEE, Aug. 2010, pp. 165–168.

[138] M. Khafagy, A. Ismail, M. S. Alouini, and S. Aissa, "On the outage performance of full-duplex selective decode-and-forward relaying," *IEEE Commun. Lett.*, vol. 17, no. 6, pp. 1180–1183, Jun. 2013.

[139] T. K. Baranwal, D. S. Michalopoulos, and R. Schober, "Outage analysis of multihop full duplex relaying," *IEEE Commun. Lett.*, vol. 17, no. 1, pp. 63–66, Jan. 2013.

[140] L. J. Rodriguez, N. H. Tran, and T. Le-Ngoc, "Performance of full-duplex AF relaying in the presence of residual self-interference," *IEEE J. Sel. Areas Commun.*, vol. 32, no. 9, pp. 1752–1764, Sep. 2014.

[141] I. Krikidis, H. A. Suraweera, P. J. Smith, and C. Yuen, "Full-duplex relay selection for amplify-and-forward cooperative networks," *IEEE Trans. Wireless Commun.*, vol. 11, no. 12, pp. 4381–4393, Dec. 2012.

[142] H. Cui, M. Ma, L. Song, and B. Jiao, "Relay selection for two-way full duplex relay networks with amplify-and-forward protocol," *IEEE Trans. Wireless Commun.*, vol. 13, no. 7, pp. 3768–3777, Jul. 2014.

[143] W. C. Babcock, "Intermodulation interference in radio systems," *Bell System Technical Journal*, vol. 32, no. 1, pp. 63–73, Jan. 1953.

[144] M. Grimm, M. Allen, J. Marttila, M. Valkama, and R. Thoma, "Joint mitigation of nonlinear RF and baseband distortions in wideband direct-conversion receivers," *IEEE Trans. Microw. Theory Tech.*, vol. 62, no. 1, pp. 166–182, Jan. 2014.

[145] E. Rebeiz, A. Ghadam, M. Valkama, and D. Cabric, "Spectrum sensing under RF non-linearities: Performance analysis and DSP-enhanced receivers," *IEEE Trans. Signal Process.*, vol. 63, no. 8, pp. 1950–1964, Apr. 2015.

[146] G. L. Heiter, "Characterization of nonlinearities in microwave devices and systems," *IEEE Trans. Microwave Theory Tech.*, vol. 21, no. 12, pp. 797–805, Dec. 1973.

[147] A. Chorti and M. Brookes, "On the effects of memoryless nonlinearities on M-QAM and DQPSK OFDM signals," *IEEE Trans. Microwave Theory Tech.*, vol. 54, no. 8, pp. 3301–3315, Aug. 2006.

[148] Z. Shuang, C. Sunzeng, K. Kai, and Q. Hua, "Optimal transmission power in a nonlinear VLC system," *ZTE Communications*, vol. 14, no. 2, pp. 23–28, Apr. 2016.

[149] A. Kiayani, M. Abdelaziz, L. Anttila, V. Lehtinen, and M. Valkama, "Digital mitigation of transmitter-induced receiver desensitization in carrier aggregation FDD transceivers," *IEEE Trans. Microwave Theory Tech.*, vol. 63, no. 11, pp. 3608–3623, Nov. 2015.

[150] J. B. Tsui, *Digital techniques for wideband receivers*. SciTech Publishing, 2004, vol. 2.

[151] M. Frerking, *Digital signal processing in communications systems*. Springer Science & Business Media, 2013.

[152] J. C. Pedro and N. B. Carvalho, *Intermodulation distortion in microwave and wireless circuits*. Artech House, 2002.

[153] S. C. Cripps, *Advanced techniques in RF power amplifier design*. Artech House, 2002.

[154] A. Shahed hagh ghadam, "Contributions to analysis and DSP-based mitigation of nonlinear distortion in radio transceivers," Ph.D. dissertation, Tampere University of Technology, Faculty of Computing and Electrical Engineering, Department of Communications Engineering, Oct. 2011.

[155] M. Aaron and D. Tufts, "Intersymbol interference and error probability," *IEEE Trans. Inf. Theory*, vol. 12, no. 1, pp. 26–34, Jan. 1966.

[156] W. M. Hubbard, "The effect of intersymbol interference on error rate in binary differentially-coherent phase-shift-keyed systems," *The Bell System Technical Journal*, vol. 46, no. 6, pp. 1149–1172, Jul. 1967.

[157] W. Hirt and J. L. Massey, "Capacity of the discrete-time Gaussian channel with intersymbol interference," *IEEE Trans. Inf. Theory*, vol. 34, no. 3, pp. 38–38, May 1988.

[158] O. Shimbo, R. Fang, and M. Celebiler, "Performance of M-ary PSK systems in Gaussian noise and intersymbol interference," *IEEE Trans. Inf. Theory*, vol. 19, no. 1, pp. 44–58, Jan. 1973.

[159] J. Nowakowski and I. Protasewicz, "Performance of an M-ary p.s.k. system in the presence of additive noise, intersymbol interference and fading," *Radio Electron. Eng.*, vol. 46, no. 2, pp. 83–91, Feb. 1976.

[160] H. Vikalo, B. Hassibi, B. Hochwald, and T. Kailath, "On the capacity of frequency-selective channels in training-based transmission schemes," *IEEE Trans. Signal Process.*, vol. 52, no. 9, pp. 2572–2583, Sep. 2004.

[161] H. Ma, N. Shehadeh, and J. Vanelli, "Effects of intersymbol interference on a Rayleigh fast-fading channel," *IEEE Trans. Commun.*, vol. 28, no. 1, pp. 128–131, Jan. 1980.

[162] A. J. Goldsmith and M. Effros, "The capacity region of broadcast channels with intersymbol interference and colored Gaussian noise," *IEEE Trans. Inf. Theory*, vol. 47, no. 1, pp. 219–240, Jan. 2001.

[163] C. Choudhuri and U. Mitra, "Capacity bounds for relay channels with intersymbol interference and colored gaussian noise," *IEEE Trans. Inf. Theory*, vol. 60, no. 9, pp. 5639–5652, Sep. 2014.

[164] M. A. Smadi, V. K. Prabhu, and A. K. S. Al-Bayati, "Performance analysis of optimum diversity combining for partially coherent frequency-selective fading channel with intersymbol interference," *IEEE Trans. Veh. Technol.*, vol. 57, no. 6, pp. 3589–3597, Nov. 2008.

[165] S. N. Diggavi, N. Al-Dhahir, and A. R. Calderbank, "Algebraic properties of space-time block codes in intersymbol interference multiple-access channels," *IEEE Trans. Inf. Theory*, vol. 49, no. 10, pp. 2403–2414, Oct. 2003.

[166] H. Q. Lai, W. P. Siriwongpairat, and K. J. R. Liu, "Performance analysis of multiband OFDM UWB systems with imperfect synchronization and intersymbol interference," *IEEE J. Sel. Top. Signal Process.*, vol. 1, no. 3, pp. 521–534, Oct. 2007.

[167] L. Dai, B. Wang, Y. Yuan, S. Han, C. l. I, and Z. Wang, "Non-orthogonal multiple access for 5G: Solutions, challenges, opportunities, and future research trends," *IEEE Commun. Mag.*, vol. 53, no. 9, pp. 74–81, Sep. 2015.

[168] Y. Saito, A. Benjebbour, Y. Kishiyama, and T. Nakamura, "System-level performance evaluation of downlink non-orthogonal multiple access (NOMA)," in *IEEE 24th Annual International Symposium on Personal, Indoor, and Mobile Radio Communications (PIMRC)*. London, UK: IEEE, Sep. 2013, pp. 611–615.

[169] Y. Liu, Z. Ding, M. Elkashlan, and H. V. Poor, "Cooperative non-orthogonal multiple access with simultaneous wireless information and power transfer," *IEEE J. Sel. Areas Commun.*, vol. 34, no. 4, pp. 938–953, Apr. 2016.

[170] Z. Ding, P. Fan, and V. Poor, "Impact of user pairing on 5G non-orthogonal multiple access downlink transmissions," *IEEE Trans. Veh. Technol.*, vol. PP, no. 99, pp. 1–1, 2015.

[171] Z. Ding, F. Adachi, and H. V. Poor, "The application of MIMO to non-orthogonal multiple access," *IEEE Trans. Wireless Commun.*, vol. 15, no. 1, pp. 537–552, Jan. 2016.

[172] M. F. Hanif, Z. Ding, T. Ratnarajah, and G. K. Karagiannidis, "A minorization-maximization method for optimizing sum rate in the downlink of non-orthogonal multiple access systems," *IEEE Trans. Signal Process.*, vol. 64, no. 1, pp. 76–88, Jan. 2016.

[173] Y. Yuan, Z. Yuan, G. Yu, C. h. Hwang, P. k. Liao, A. Li, and K. Takeda, "Non-orthogonal transmission technology in LTE evolution," *IEEE Commun. Mag.*, vol. 54, no. 7, pp. 68–74, Jul. 2016.

[174] P. Diamantoulakis, K. Pappi, Z. Ding, and G. Karagiannidis, "Wireless powered communications with non-orthogonal multiple access," *IEEE Trans. Wireless Commun.*, vol. PP, no. 99, pp. 1–1, 2016.

[175] P. D. Diamantoulakis, K. N. Pappi, Z. Ding, and G. K. Karagiannidis, "Optimal design of non-orthogonal multiple access with wireless power transfer," in *IEEE International Conference on Communications (ICC)*. Kuala Lumpur, MY: IEEE, May 2016, pp. 1–6.

[176] W. Shin, M. Vaezi, B. Lee, D. J. Love, J. Lee, and V. Poor, "Coordinated beamforming for Multi-Cell MIMO-NOMA," *IEEE Commun. Lett.*, vol. PP, no. 99, pp. 1–1, 2016.

[177] F.-L. Luo and C. Zhang, *Non-Orthogonal Multiple Access (NOMA): Concept and Design*. Wiley-IEEE Press, 2016.

[178] Y. Liu, Z. Ding, M. Elkashlan, and J. Yuan, "Non-orthogonal multiple access in large-scale underlay cognitive radio networks," *IEEE Trans. Veh. Technol.*, vol. PP, no. 99, pp. 1–1, 2016.

[179] Z. Ding, Z. Yang, P. Fan, and H. V. Poor, "On the performance of non-orthogonal multiple access in 5G systems with randomly deployed users," *IEEE Signal. Proc. Let.*, vol. 21, no. 12, pp. 1501–1505, Dec. 2014.

[180] N. Zhang, J. Wang, G. Kang, and Y. Liu, "Uplink nonorthogonal multiple access in 5G systems," *IEEE Commun. Lett.*, vol. 20, no. 3, pp. 458–461, Mar. 2016.

[181] T. S. Rappaport, *Wireless communications: Principles and practice*. Prentice Hall PTR New Jersey, 1996, vol. 2.

[182] A. Sheikh, *Wireless communications: theory and techniques*. Springer Science & Business Media, 2011.

[183] W. C. Y. Lee, "Elements of cellular mobile radio systems," *IEEE Trans. Veh. Technol.*, vol. 35, no. 2, pp. 48–56, May 1986.

[184] J. P. M. G. Linnartz, R. Hekmat, and R. J. Venema, "Near-far effects in land mobile random access networks with narrow-band rayleigh fading channels," *IEEE Trans. Veh. Technol.*, vol. 41, no. 1, pp. 77–90, Feb. 1992.

[185] W. M. Lovelace and J. K. Townsend, "Threshold discrimination and blanking for large near-far power ratios in UWB networks," *IEEE Trans. Commun.*, vol. 53, no. 9, pp. 1447–1450, Sep. 2005.

[186] V. Chandrasekhar, M. Kountouris, and J. G. Andrews, "Coverage in multi-antenna two-tier networks," *IEEE Trans. Wireless Commun.*, vol. 8, no. 10, pp. 5314–5327, Oct. 2009.

[187] P. Xia, V. Chandrasekhar, and J. G. Andrews, "Open vs. closed access femtocells in the uplink," *IEEE Trans. Wireless Commun.*, vol. 9, no. 12, pp. 3798–3809, Dec. 2010.

[188] S. L. Miller, "An adaptive direct-sequence code-division multiple-access receiver for multiuser interference rejection," *IEEE Trans. Commun.*, vol. 43, no. 2/3/4, pp. 1746–1755, Feb. 1995.

[189] B. Hombs and J. S. Lehnert, "Multiple-access interference suppression for MC-CDMA by frequency-domain oversampling," *IEEE Trans. Commun.*, vol. 53, no. 4, pp. 677–686, Apr. 2005.

[190] U. Madhow and M. L. Honig, "MMSE interference suppression for direct-sequence spread-spectrum CDMA," *IEEE Trans. Commun.*, vol. 42, no. 12, pp. 3178–3188, Dec. 1994.

[191] Samsung Electronics, "Design considerations for CoMP joint transmission," R1-091232, 3GPP TSG RAN WG1 Meeting #56bis, Mar. 2009.

[192] LG Electronics, "CoMP configurations and UE/eNB behaviors in LTE-advanced," R1-090782,3GPP TSG RAN WG1 Meeting #56, Feb. 2009.

[193] Alcatel-Lucent Shanghai Bell, Alcatel-Lucent, "Uplink coordinated multi-point reception with distributed inter-cell interference suppression for LTE-A," R1-090770, 3GPP TSG RAN WG1 Meeting #56, Feb. 2009.

[194] U. Jang, H. Son, J. Park, and S. Lee, "CoMP-CSB for ICI nulling with user selection," *IEEE Trans. Wireless Commun.*, vol. 10, no. 9, pp. 2982–2993, Sep. 2011.

[195] W. Nam, D. Bai, J. Lee, and I. Kang, "Advanced interference management for 5G cellular networks," *IEEE Commun. Mag.*, vol. 52, no. 5, pp. 52–60, May 2014.

[196] M. R. Akdeniz and S. Rangan, "Optimal wireless scheduling with interference cancellation," in *IEEE International Symposium on Information Theory Proceedings (ISIT)*. Istanbul, TR: IEEE, Jul. 2013, pp. 246–250.

[197] V. Abdrashitov, W. Nam, and D. Bai, "Rate and UE selection algorithms for interference-aware receivers," in *IEEE 79th Vehicular Technology Conference (VTC Spring)*. Seoul, KR: IEEE, May 2014, pp. 1–5.

[198] N. Souto, R. Dinis, A. Correia, and C. Reis, "Interference-aware iterative block decision feedback equalizer for single-carrier transmission," *IEEE Trans. Veh. Technol.*, vol. 64, no. 7, pp. 3316–3321, Jul. 2015.

[199] S. t. Brink, J. Speidel, and R.-H. Yan, "Iterative demapping and decoding for multilevel modulation," in *IEEE Global Telecommunications Conference*, vol. 1. Sydney, AU: IEEE, Nov. 1998, pp. 579–584.

[200] B. Lu and X. Wang, "Iterative receivers for multiuser space-time coding systems," *IEEE J. Sel. Areas Commun.*, vol. 18, no. 11, pp. 2322–2335, Nov. 2000.

[201] L. Boher, R. Rabineau, and M. Helard, "FPGA implementation of an iterative receiver for MIMO-OFDM systems," *IEEE J. Sel. Areas Commun.*, vol. 26, no. 6, pp. 857–866, Aug. 2008.

[202] J. Choi, "A correlation based analysis for approximate MAP detectors and iterative receivers," *IEEE Trans. Wireless Commun.*, vol. 6, no. 5, pp. 1764–1773, May 2007.

[203] G. Dietl and W. Utschick, "Complexity reduction of iterative receivers using low-rank equalization," *IEEE Trans. Signal Process.*, vol. 55, no. 3, pp. 1035–1046, Mar. 2007.

[204] J. Choi, Y. Hong, and J. Yuan, "An approximate MAP-based iterative receiver for MIMO channels using modified sphere detection," *IEEE Trans. Wireless Commun.*, vol. 5, no. 8, pp. 2119–2126, Aug. 2006.

[205] CMCC (Rapporteur), "Summary of the description of candidate eICIC solutions," R1b•"104968,3GPP TSG-WG1 #62, Aug. 2010.

[206] Austin, TX, "Evaluations of RSRP/RSRQ measurement," R4-110284, 3GPP TSG-WG1, Jan. 2011.

[207] H. Holma, A. Toskala, and J. Reunanen, *LTE Small Cell Optimization: 3GPP Evolution to Release 13*. John Wiley & Sons, 2016.

[208] A. Damnjanovic, J. Montojo, Y. Wei, T. Ji, T. Luo, M. Vajapeyam, T. Yoo, O. Song, and D. Malladi, "A survey on 3gpp heterogeneous networks," *IEEE Wireless Commun. Mag.*, vol. 18, no. 3, pp. 10–21, Jun. 2011.

[209] LG Electronics, "Comparison of time-domain eICIC solutions," R1-104661, 3GPP TSG RAN WG1 Meeting #62, Aug. 2010.

[210] D. Lopez-Perez, I. Guvenc, G. de la Roche, M. Kountouris, T. Q. S. Quek, and J. Zhang, "Enhanced intercell interference coordination challenges in heterogeneous networks," *IEEE Wireless Commun.*, vol. 18, no. 3, pp. 22–30, Jun. 2011.

[211] M. Baker, S. Sesia, and I. Toufik, *LTE:The UMTS Long Term Evolution From Theory to Practice*. Chichester: John Wiley & Sons Ltd, 2011.

[212] Nokia Siemens Networks, Nokia, "HeNB power setting performance under different access constraints," R1-103823, 3GPP TSG RAN WG1 #61bis Meeting, Jun. 2010.

[213] CATT , "Dl power setting in macro-femto," R1-103495, 3GPP TSG RAN WG1 meeting #61bis, Jul. 2010.

[214] S. Sun, Q. Gao, Y. Peng, Y. Wang, and L. Song, "Interference management through CoMP in 3GPP LTE-advanced networks," *IEEE Wireless Commun.*, vol. 20, no. 1, pp. 59–66, Feb. 2013.

[215] Samsung Electronics, "Performance evaluation of CoMP2JT for scenario 2," R1-091232, 3GPP TSG RAN WG1 Meeting #55, May 2011.

[216] D. Lee, H. Seo, B. Clerckx, E. Hardouin, D. Mazzarese, S. Nagata, and K. Sayana, "Coordinated multipoint transmission and reception in LTE-advanced: deployment scenarios and operational challenges," *IEEE Commun. Mag.*, vol. 50, no. 2, pp. 148–155, Feb. 2012.

[217] S. Annapureddy, A. Barbieri, S. Geirhofer, S. Mallik, and A. Gorokhov, "Coordinated joint transmission in WWAN," *IEEE Commun. Theory Wksp*, May 2010.

[218] P. Marsch and G. Fettweis, "Uplink CoMP under a constrained backhaul and imperfect channel knowledge," *IEEE Trans. Wireless Commun.*, vol. 10, no. 6, pp. 1730–1742, Jun. 2011.

[219] M. A. Maddah-Ali, A. S. Motahari, and A. K. Khandani, "Communication over MIMO X channels: Interference alignment, decomposition, and performance analysis," *IEEE Trans. Inf. Theory*, vol. 54, no. 8, pp. 3457–3470, Aug. 2008.

[220] V. R. Cadambe and S. A. Jafar, "Interference alignment and degrees of freedom of the K-user interference channel," *IEEE Trans. Inf. Theory*, vol. 54, no. 8, pp. 3425–3441, Aug. 2008.

[221] O. E. Ayach, S. W. Peters, and R. W. Heath, "The practical challenges of interference alignment," *IEEE Wireless Commun.*, vol. 20, no. 1, pp. 35–42, Feb. 2013.

[222] P. Mohapatra, K. E. Nissar, and C. R. Murthy, "Interference alignment algorithms for the K user constant MIMO interference channel," *IEEE Trans. Signal Process.*, vol. 59, no. 11, pp. 5499–5508, Nov. 2011.

[223] H. Ning, C. Ling, and K. K. Leung, "Feasibility condition for interference alignment with diversity," *IEEE Trans. Inf. Theory*, vol. 57, no. 5, pp. 2902–2912, May 2011.

[224] S. A. Jafar, *Interference alignment: A new look at signal dimensions in a communication network*. Boston-Delft: Now Publishers Inc, 2011.

[225] N. Zhao, F. R. Yu, M. Jin, Q. Yan, and V. C. M. Leung, "Interference alignment and its applications: A survey, research issues and challenges," *IEEE Communications Surveys Tutorials*, vol. PP, no. 99, pp. 1–1, 2016.

[226] C. M. Yetis, T. Gou, S. A. Jafar, and A. H. Kayran, "On feasibility of interference alignment in MIMO interference networks," *IEEE Trans. Signal Process.*, vol. 58, no. 9, pp. 4771–4782, Sep. 2010.

[227] M. Razaviyayn, G. Lyubeznik, and Z. Q. Luo, "On the degrees of freedom achievable through interference alignment in a MIMO interference channel," *IEEE Trans. Signal Process.*, vol. 60, no. 2, pp. 812–821, Feb. 2012.

[228] K. Kim, S. W. Jeon, and D. K. Kim, "The feasibility of interference alignment for full-duplex MIMO cellular networks," *IEEE Commun. Lett.*, vol. 19, no. 9, pp. 1500–1503, Sep. 2015.

[229] Z. Liu and D. Sun, "Relay-assisted opposite directional interference alignment: Feasibility condition and achievable degrees of freedom," *IEEE Commun. Lett.*, vol. 19, no. 1, pp. 66–69, Jan. 2015.

[230] L. Mroueh and J. C. Belfiore, "Feasibility of interference alignment in the time-frequency domain," *IEEE Trans. Wireless Commun.*, vol. 11, no. 11, pp. 3932–3941, Nov. 2012.

[231] M. El-Absi, S. Galih, M. Hoffmann, M. El-Hadidy, and T. Kaiser, "Antenna selection for reliable MIMO-OFDM interference alignment systems: Measurement-based evaluation," *IEEE Trans. Veh. Technol.*, vol. 65, no. 5, pp. 2965–2977, May 2016.

[232] A. Ghasemi, A. S. Motahari, and A. K. Khandani, "Interference alignment for the K user MIMO interference channel," in *IEEE International Symposium on Information Theory*. Austin, TX: IEEE, Jun. 2010, pp. 360–364.

[233] D. Bharadia, E. McMilin, and S. Katti, "Full duplex radios," *SIGCOMM Comput. Commun. Rev.*, vol. 43, no. 4, pp. 375–386, Aug. 2013.

[234] S. Hong, J. Brand, J. I. Choi, M. Jain, J. Mehlman, S. Katti, and P. Levis, "Applications of self-interference cancellation in 5G and beyond," *IEEE Commun. Mag.*, vol. 52, no. 2, pp. 114–121, Feb. 2014.

[235] B. Debaillie, D. J. van den Broek, C. LavG•n, B. van Liempd, E. A. M. Klumperink, C. Palacios, J. Craninckx, B. Nauta, and A. PG•rssinen, "Analog/RF solutions enabling compact full-duplex radios," *IEEE J. Sel. Areas Commun.*, vol. 32, no. 9, pp. 1662–1673, Sep. 2014.

[236] S. Chen, M. A. Beach, and J. P. McGeehan, "Division-free duplex for wireless applications," *Electron. Lett.*, vol. 34, no. 2, pp. 147–148, Jan. 1998.

[237] M. Duarte, A. Sabharwal, V. Aggarwal, R. Jana, K. K. Ramakrishnan, C. W. Rice, and N. K. Shankaranarayanan, "Design and characterization of a full-duplex multiantenna system for WiFi networks," *IEEE Trans. Veh. Technol.*, vol. 63, no. 3, pp. 1160–1177, Mar. 2014.

[238] M. Jain, J. I. Choi, T. Kim, D. Bharadia, S. Seth, K. Srinivasan, P. Levis, S. Katti, and P. Sinha, "Practical, real-time, full duplex wireless," in *17th Annual International Conference on Mobile Computing and Networking*, ser. MobiCom '11. New York, NY, US: ACM, 2011, pp. 301–312.

[239] A. Sahai, G. Patel, C. Dick, and A. Sabharwal, "On the impact of phase noise on active cancelation in wireless full-duplex," *IEEE Trans. Veh. Technol.*, vol. 62, no. 9, pp. 4494–4510, Nov. 2013.

[240] J. Sangiamwong, T. Asai, J. Hagiwara, Y. Okumura, and T. Ohya, "Joint multi-filter design for full-duplex MU-MIMO relaying," in *IEEE 69th Vehicular Technology Conference (VTC) Spring*. Barcelona, ES: IEEE, Apr. 2009, pp. 1–5.

[241] B. P. Day, A. R. Margetts, D. W. Bliss, and P. Schniter, "Full-duplex bidirectional MIMO: Achievable rates under limited dynamic range," *IEEE Trans. Signal Process.*, vol. 60, no. 7, pp. 3702–3713, Jul. 2012.

[242] A. K. Khandani, "Two-way (true full-duplex) wireless," in *13th Canadian Workshop on Information Theory (CWIT)*. Toronto, ON: IEEE, Jun. 2013, pp. 33–38.

[243] E. Everett, A. Sahai, and A. Sabharwal, "Passive self-interference suppression for full-duplex infrastructure nodes," *IEEE Trans. Wireless Commun.*, vol. 13, no. 2, pp. 680–694, Feb. 2014.

[244] M. Duarte, C. Dick, and A. Sabharwal, "Experiment-driven characterization of full-duplex wireless systems," *IEEE Trans. Wireless Commun.*, vol. 11, no. 12, pp. 4296–4307, Dec. 2012.

[245] A. Sabharwal, P. Schniter, D. Guo, D. W. Bliss, S. Rangarajan, and R. Wichman, "In-band full-duplex wireless: Challenges and opportunities," *IEEE J. Sel. Areas Commun.*, vol. 32, no. 9, pp. 1637–1652, Sep. 2014.

[246] E. Aryafar, M. A. Khojastepour, K. Sundaresan, S. Rangarajan, and M. Chiang, "MIDU: Enabling MIMO full duplex," in *18th Annual International Conference on Mobile Computing and Networking*, ser. Mobicom '12. New York, NY, USA: ACM, Aug. 2012, pp. 257–268.

[247] A.-A. A. Boulogeorgos, N. D. Chatzidiamantis, and G. K. Karagiannidis, "Spectrum sensing with multiple primary users over fading channels," *IEEE Commun. Lett.*, vol. 20, no. 7, pp. 1457–1460, Jul. 2016.

[248] R. Engelman, K. Abrokwah, G. Dillon, G. Foster, G. Godfrey, T. Hanbury, C. Lagerwerff, W. Leighton, M. Marcus, R. Noel, J. Payton, J. Tomchin, J. Williams, and A. Yang, "Report of the spectrum efficiency working group," Federal Communications Commission-Spectrum Policy Task Force, Tech. Rep. 02-135, Nov. 2002.

[249] N. Devroye, M. Vu, and V. Tarokh, "Cognitive radio networks," *IEEE Signal. Proc. Mag.*, vol. 25, no. 6, pp. 12–23, Nov. 2008.

[250] S. Haykin, "Cognitive radio: brain-empowered wireless communications," *IEEE J. Sel. Areas Commun.*, vol. 23, no. 2, pp. 201–220, Feb. 2005.

[251] L. Fan, X. Lei, T. Q. Duong, R. Q. Hu, and M. Elkashlan, "Multiuser cognitive relay networks: Joint impact of direct and relay communications," *IEEE Trans. Wireless Commun.*, vol. 13, no. 9, pp. 5043–5055, Sep. 2014.

[252] A. Le, S. Herath, N. Tran, T. Duong, and S. Shetty, "Achievable rates and outage probability of cognitive radio with dynamic frequency hopping under imperfect spectrum sensing," *IET Communications*, vol. 9, no. 17, pp. 2160–2167, Nov. 2015.

[253] T. Duong, P. L. Yeoh, V. N. Q. Bao, M. Elkashlan, and N. Yang, "Cognitive relay networks with multiple primary transceivers under spectrum-sharing," *IEEE Signal Process. Lett.*, vol. 19, no. 11, pp. 741–744, Nov. 2012.

[254] Y. Liu, L. Wang, T. T. Duy, M. Elkashlan, and T. Duong, "Relay selection for security enhancement in cognitive relay networks," *IEEE Wireless Communications Letters*, vol. 4, no. 1, pp. 46–49, Feb. 2015.

[255] E. Benitez Olivo, D. Moya Osorio, D. da Costa, and J. Silveira Santos Filho, "Outage performance of spectrally efficient schemes for multiuser cognitive relaying networks with underlay spectrum sharing," *IEEE Trans. Wireless Commun.*, vol. 13, no. 12, pp. 6629–6642, Dec. 2014.

[256] C. Zhong and T. Ratnarajah, "Performance of user selection in cognitive broadcast channels," *IEEE Trans. Commun.*, vol. 60, no. 12, pp. 3529–3534, Dec. 2012.

[257] T. Yucek and H. Arslan, "A survey of spectrum sensing algorithms for cognitive radio applications," *IEEE Commun. Surveys Tuts.*, vol. 11, no. 1, pp. 116–130, Mar. 2009.

[258] K. Letaief and W. Zhang, "Cooperative communications for cognitive radio networks," *Proc. IEEE*, vol. 97, no. 5, pp. 878–893, May 2009.

[259] S. Chaudhari, J. Lunden, V. Koivunen, and H. Poor, "Cooperative sensing with imperfect reporting channels: Hard decisions or soft decisions?" *IEEE Trans. Signal Process.*, vol. 60, no. 1, pp. 18–28, Jan. 2012.

[260] S. Atapattu, C. Tellambura, and H. Jiang, "Energy detection based cooperative spectrum sensing in cognitive radio networks," *IEEE Trans. Commun.*, vol. 10, no. 4, pp. 1232–1241, Apr. 2011.

[261] D. Hamza, S. Aissa, and G. Aniba, "Equal gain combining for cooperative spectrum sensing in cognitive radio networks," *IEEE Trans. Wireless Commun.*, vol. 13, no. 8, pp. 4334–4345, Aug. 2014.

[262] M. Z. Shakir, A. Rao, and M.-S. Alouini, "Generalized mean detector for collaborative spectrum sensing," *IEEE Trans. Commun.*, vol. 61, no. 4, pp. 1242–1253, Apr. 2013.

[263] A. Kortun, T. Ratnarajah, M. Sellathurai, C. Zhong, and C. Papadias, "On the performance of eigenvalue-based cooperative spectrum sensing for cognitive radio," *IEEE J. Sel. Topics Signal Process.*, vol. 5, no. 1, pp. 49–55, Feb. 2011.

[264] E. H. Gismalla and E. Alsusa, "On the performance of energy detection using Bartlett's estimate for spectrum sensing in cognitive radio systems," *IEEE Trans. Signal Process.*, vol. 60, no. 7, pp. 3394–3404, Jul. 2012.

[265] R. Fan and H. Jiang, "Optimal multi-channel cooperative sensing in cognitive radio networks," *IEEE Trans. Wireless Commun.*, vol. 9, no. 3, pp. 1128–1138, Mar. 2010.

[266] W. Zhang, R. Mallik, and K. Letaief, "Optimization of cooperative spectrum sensing with energy detection in cognitive radio networks," *IEEE Trans. Wireless Commun.*, vol. 8, no. 12, pp. 5761–5766, Dec. 2009.

[267] A. Al Hammadi, O. Alhussein, P. Sofotasios, S. Muhaidat, M. Al-Qutayri, S. Al-Araji, G. Karagiannidis, and J. Liang, "Unified analysis of cooperative spectrum sensing over composite and generalized fading channels," *IEEE Trans. Veh. Technol.*, vol. PP, no. 99, pp. 1–1, Oct. 2015.

[268] A. Mariani, A. Giorgetti, and M. Chiani, "Effects of noise power estimation on energy detection for cognitive radio applications," *IEEE Trans. Commun.*, vol. 59, no. 12, pp. 3410–3420, Dec. 2011.

[269] E. Dahlman, S. Parkvall, and J. Skold, *4G: LTE/LTE-Advanced for Mobile Broadband*, 1st ed. Academic Press, Mar. 2011.

[270] "IEEE standard for air interface for broadband wireless access systems," *IEEE Std 802.16-2012 (Revision of IEEE Std 802.16-2009)*, pp. 1–2542, Aug. 2012.

[271] J. L. Burbank, J. Andrusenko, J. S. Everett, and W. T. M. Kasch, *Third-Generation (3G) Cellular Communications.* Wiley-IEEE Press, 2013, ch. 7, pp. 366–468.

[272] B. Zhao, Y. Chen, C. He, and L. Jiang, "Performance analysis of spectrum sensing with multiple primary users," *IEEE Trans. Veh. Technol.*, vol. 61, no. 2, pp. 914–918, Feb. 2012.

[273] A. S. Cacciapuoti and M. Caleffi, "Spectrum sensing in small-scale networks: Dealing with multiple mobile pus," *Ad Hoc Networks*, vol. 33, pp. 209–220, May 2015.

[274] I. S. Gradshteyn and I. M. Ryzhik, *Table of Integrals, Series, and Products*, 6th ed. New York: Academic, 2000.

[275] A. Chaudhry and S. Zubair, *On a Class of Incomplete Gamma Functions with Applications.* CRC Press, 2001.

[276] G. K. Karagiannidis, N. C. Sagias, and T. A. Tsiftsis, "Closed-form statistics for the sum of squared Nakagami-m variates and its applications," *IEEE Trans. Commun.*, vol. 54, no. 8, pp. 1353–1359, Aug. 2006.

[277] A.-A. A. Boulogeorgos, N. D. Chatzidiamantis, and G. K. Karagiannidis, "Energy detection spectrum sensing under RF imperfections," *IEEE Trans. Commun.*, vol. 64, no. 7, pp. 2754–2766, Jul. 2016.

[278] A.-A. A. Boulogeorgos, N. Chatzidiamantis, G. K. Karagiannidis, and L. Georgiadis, "Energy detection under RF impairments for cognitive radio," in *IEEE International Conference on Communications - Workshop on Cooperative and Cognitive Networks (ICC - CoCoNet).* London, UK: IEEE, Jun. 2015, pp. 955–960.

[279] A. Gokceoglu, S. Dikmese, M. Valkama, and M. Renfors, "Energy detection under IQ imbalance with single- and multi-channel direct-conversion receiver: Analysis and mitigation," *IEEE J. Sel. Areas Commun.*, vol. 32, no. 3, pp. 411–424, Mar. 2014.

[280] J. Lee, Y. Kim, Y. Kwak, J. Zhang, A. Papasakellariou, T. Novlan, C. Sun, and Y. Li, "LTE-advanced in 3GPP Rel-13/14: an evolution toward 5G," *IEEE Commun. Mag.*, vol. 54, no. 3, pp. 36–42, Mar. 2016.

[281] T. A. Levanen, J. Pirskanen, T. Koskela, J. Talvitie, and M. Valkama, "Radio interface evolution towards 5G and enhanced local area communications," *IEEE Access*, vol. 2, pp. 1005–1029, Sep. 2014.

[282] M. Dohler, T. Nakamura, A. Osseiran, J. F. Monserrat, O. Queseth, and P. Marsch, *5G Mobile and Wireless Communications Technology.* Cambridge University Press, 2016.

[283] K. David, D. Dixit, and N. Jefferies, "2020 vision. The wireless world research forum looks to the future," *IEEE Veh. Technol. Mag.*, vol. 5, no. 3, pp. 22–29, Sep. 2010.

[284] Cisco, *Cisco visual network index: Global mobile traffic forecast update, 2015-2020.*, Feb. 2012. [Online]. Available: http://www.cisco.com/c/en/us/solutions/collateral/service-provider/visual-networking-index-vni/mobile-white-paper-c11-520862.html

[285] 5GPPP, *5G Vision: The 5G infrastructure public private partership: the next generation of communication networks and services*, Feb. 2015. [Online]. Available: https://5g-ppp.eu/wp-content/uploads/2015/02/5G-Vision-Brochure-v1.pdf

[286] M. Agiwal, A. Roy, and N. Saxena, "Next generation 5G wireless networks: A comprehensive survey," *IEEE Communications Surveys Tutorials*, vol. PP, no. 99, pp. 1–1, Feb. 2016.

[287] B. Bangerter, S. Talwar, R. Arefi, and K. Stewart, "Networks and devices for the 5G era," *IEEE Commun. Mag.*, vol. 52, no. 2, pp. 90–96, Feb. 2014.

[288] J. Thompson, X. Ge, H.-C. Wu, R. Irmer, H. Jiang, G. Fettweis, and S. Alamouti, "5G wireless communication systems: prospects and challenges [guest editorial]," *IEEE Commun. Mag.*, vol. 52, no. 2, pp. 62–64, Feb. 2014.

[289] J. G. Andrews, S. Buzzi, W. Choi, S. V. Hanly, A. Lozano, A. C. K. Soong, and J. C. Zhang, "What will 5G be?" *IEEE J. Sel. Areas Commun.*, vol. 32, no. 6, pp. 1065–1082, Jun. 2014.

[290] Q. C. Li, H. Niu, A. T. Papathanassiou, and G. Wu, "5G network capacity: Key elements and technologies," *IEEE Veh. Technol. Mag.*, vol. 9, no. 1, pp. 71–78, Mar. 2014.

[291] ITU-R, "Requirements related to technical performance for IMT-advanced radio interface(s)," ITU, Tech. Rep. M.2134, Nov. 2008.

[292] G. D. Ntouni, A.-A. A. Boulogeorgos, D. S. Karas, T. A. Tsiftsis, F. Foukalas, V. M. Kapinas, and G. K. Karagiannidis, "Inter-band carrier aggregation in heterogeneous networks: Design and assessment," in *Proc. International Symposium on Wireless Communication Systems (ISWCS).* Barcelona, ES: IEEE, Aug. 2014, pp. 1–6.

[293] A.-A. A. Boulogeorgos, G. D. Ntouni, D. S. Karas, T. A. Tsiftsis, F. Foukalas, G. K. Karagiannidis, and C. Thomos, "MIMO link adaptation with carrier aggregation in LTE-A heterogeneous networks," in *European Conference on Networks and Communications (EuCNC)*, Paris, FR, Jun. 2015, pp. 765–767.

[294] I. Chih-Lin, S. Han, Z. Xu, Q. Sun, and Z. Pan, "5G: Rethink mobile communications for 2020+," *Philosophical Transactions of the Royal Society of London A: Mathematical, Physical and Engineering Sciences*, vol. 374, no. 2062, pp. 1–13, Feb. 2016. [Online]. Available: http://rsta.royalsocietypublishing.org/content/374/2062/20140432

[295] X. Li and M. Ismail, *Multi-Standard CMOS Wireless Receivers: Analysis and Design*, ser. The Springer International Series in Engineering and Computer Science. Springer US, 2002, no. 675.

[296] C. Chien, *Digital radio systems on a chip: A systems approach.* Springer Science & Business Media, 2001.

[297] W. H. Tuttlebee, *Software defined radio: Enabling technologies.* John Wiley & Sons, 2003.

[298] S. Chakraborty, V. Ivanov, J. Einzinger, R. P. Aditham, D. LeDeaut, J. F. Ren, H. S. Kim, C. Kuch, G. Dietz, M. Goel, and J. Graul, "An ultra-low power, low-cost, multi-standard transceiver," in *Texas Symposium on Wireless and Microwave Circuits and Systems (WMCS).* Waco, TX: IEEE, Apr. 2015, pp. 1–5.

[299] L. Anttila, M. Valkama, and M. Renfors, "Circularity-based I/Q imbalance compensation in wideband direct-conversion receivers," *IEEE Trans. Veh. Technol.*, vol. 57, no. 4, pp. 2099–2113, Jul. 2008.

[300] L. Anttila, "Digital front-end signal processing with widely-linear signal models in radio devices," Ph.D. dissertation, Tampere University of Technology, Finland, Oct. 2011.

[301] S. Spiridon, *Toward 5G Software Defined Radio Receiver Front-Ends.* Springer, 2016.

[302] O. Font-Bach, N. Bartzoudis, X. Mestre, D. Lopez-Bueno, P. Mege, L. Martinod, V. Ringset, and T. A. Myrvoll, "When SDR meets a 5G candidate waveform : Agile use of fragmented spectrum and interference protection in PMR networks," *IEEE Wireless Commun.*, vol. 22, no. 6, pp. 56–66, Dec. 2015.

[303] J. Mitola and G. Q. Maguire, "Cognitive radio: Making software radios more personal," *IEEE Pers. Commun.*, vol. 6, no. 4, pp. 13–18, Aug. 1999.

[304] B. A. Fette, *Cognitive radio technology.* Academic Press, 2009.

[305] M. Mueck, A. Piipponen, K. Kalliojarvi, G. Dimitrakopoulos, K. Tsagkaris, P. Demestichas, F. Casadevall, J. Perez-Romero, O. Sallent, G. Baldini, S. Filin, H. Harada, M. Debbah, T. Haustein, J. Gebert, B. Deschamps, P. Bender, M. Street, S. Kandeepan, J. Lota, and A. Hayar, "ETSI reconfigurable radio systems: status and future directions on software defined radio and cognitive radio standards," *IEEE Commun. Mag.*, vol. 48, no. 9, pp. 78–86, Sep. 2010.

[306] M. Brandolini, P. Rossi, D. Manstretta, and F. Svelto, "Toward multistandard mobile terminals - fully integrated receivers requirements and architectures," *IEEE Trans. Microwave Theory Tech.*, vol. 53, no. 3, pp. 1026–1038, Mar. 2005.

[307] S. Mirabbasi and K. Martin, "Classical and modern receiver architectures," *IEEE Commun. Mag.*, vol. 38, no. 11, pp. 132–139, Nov. 2000.

[308] L. Maurer, R. Stuhlberger, C. Wicpalek, G. Haberpeuntner, and G. Hueber, "Be flexible," *IEEE Microwave Mag.*, vol. 9, no. 2, pp. 83–95, Apr. 2008.

[309] P. I. Mak, S. P. U, and R. P. Martins, "Transceiver architecture selection: Review, state-of-the-art survey and case study," *IEEE Circuits Syst. Mag.*, vol. 7, no. 2, pp. 6–25, Second 2007.

[310] "5G white paper," *Next Generation Mobile Networks, White paper*, 2015.

[311] H. H. Cho, C. F. Lai, T. K. Shih, and H. C. Chao, "Integration of SDR and SDN for 5G," *IEEE Access*, vol. 2, pp. 1196–1204, Oct. 2014.

[312] H. Zamat and C. R. Nassar, "Introducing software defined radio to 4G wireless: Necessity, advantage, and impediment," *J. Commun. Netw.*, vol. 4, no. 4, pp. 1–7, Dec. 2002.

[313] J. Mitola, "Software radios: Survey, critical evaluation and future directions," *IEEE Aerosp. Electron. Syst. Mag.*, vol. 8, no. 4, pp. 25–36, Apr. 1993.

[314] A.-A. A. Boulogeorgos, V. M. Kapinas, R. Schober, and G. K. Karagiannidis, "I/Q-imbalance self-interference coordination," *IEEE Trans. Wireless Commun.*, vol. 15, no. 6, pp. 4157–4170, Jun. 2016.

[315] J. Savoj and B. Soltanian, "LO generation and distribution in a multi-band transceiver," Apr. 2014, US Patent 8.699.548.

[316] A. A. Abidi, "Evolution of a software-defined radio receiver's rf front-end," in *IEEE Radio Frequency Integrated Circuits (RFIC) Symposium, 2006.* San Francisco, CA: IEEE, Jun. 2006, pp. 4–7.

[317] R. Bagheri, A. Mirzaei, M. E. Heidari, S. Chehrazi, M. Lee, M. Mikhemar, W. K. Tang, and A. A. Abidi, "Software-defined radio receiver: dream to reality," *IEEE Commun. Mag.*, vol. 44, no. 8, pp. 111–118, Aug. 2006.

[318] A. Abidi, "Direct-conversion radio transceivers for digital communications," *IEEE J. Solid-State Circuits*, vol. 30, no. 12, pp. 1399–1410, Dec. 1995.

[319] M. Valkama, M. Renfors, and V. Koivunen, "Advanced methods for I/Q imbalance compensation in communication receivers," *IEEE Trans. Signal Process.*, vol. 49, no. 10, pp. 2335–2344, Aug. 2001.

[320] T. Schenk, *RF Imperfections in High-Rate Wireless Systems.* The Netherlands: Springer, 2008.

[321] B. Razavi, *RF Microelectronics.* Upper Saddle River, NJ, USA: Prentice-Hall, Inc., 1998.

[322] T. T. Duy, T. Duong, D. Benevides da Costa, V. N. Q. Bao, and M. Elkashlan, "Proactive relay selection with joint impact of hardware impairment and co-channel interference," *IEEE Trans. Commun.*, vol. 63, no. 5, pp. 1594–1606, May 2015.

[323] B. Razavi, "A study of phase noise in CMOS oscillators," *IEEE J. Solid-State Circuits*, vol. 31, no. 3, pp. 331–343, Mar. 1996.

[324] P. Banelli, G. Baruffa, and S. Cacopardi, "Effects of HPA nonlinearity on frequency multiplexed OFDM signals," *IEEE Trans. Broadcast.*, vol. 47, no. 2, pp. 123–136, Jun. 2001.

[325] D. Dardari, V. Tralli, and A. Vaccari, "A theoretical characterization of nonlinear distortion effects in OFDM systems," *IEEE Trans. Commun.*, vol. 48, no. 10, pp. 1755–1764, Oct. 2000.

[326] R. Stuhlberger, R. Krueger, B. Adler, J. Kissing, L. Maurer, G. Hueber, and A. Springer, "LTE-downlink performance in the presence of RF-impairments," in *European Conference on Wireless Technologies.* Munich, DE: IEEE, Oct. 2007, pp. 189–192.

[327] P. Rykaczewski, M. Valkama, and M. Renfors, "On the connection of I/Q imbalance and channel equalization in direct-conversion transceivers," *IEEE Trans. Veh. Technol.*, vol. 57, no. 3, pp. 1630–1636, May 2008.

[328] A. Gokceoglu, Y. Zou, M. Valkama, P. Sofotasios, P. Mathecken, and D. Cabric, "Mutual information analysis of OFDM radio link under phase noise, IQ imbalance and frequency-selective fading channel," *IEEE Trans. Wireless Commun.*, vol. 12, no. 6, pp. 3048–3059, Jun. 2013.

[329] C. Studer, M. Wenk, and A. Burg, "MIMO transmission with residual transmit-RF impairments," in *Proc. International ITG Workshop on Smart Antennas (WSA).* Bremen, DE: IEEE, Feb. 2010, pp. 189–196.

[330] D. K. Nguyen, M. Matthaiou, T. Q. Duong, and H. Ochi, "RF energy harvesting two-way cognitive df relaying with transceiver impairments," in *IEEE International Conference on Communication Workshop (ICCW)*. London, UK: IEEE, Jun. 2015, pp. 1970–1975.

[331] E. Bjornson, M. Matthaiou, and M. Debbah, "A new look at dual-hop relaying: Performance limits with hardware impairments," *IEEE Trans. Commun.*, vol. 61, no. 11, pp. 4512–4525, Nov. 2013.

[332] J. Zhang, L. Dai, X. Zhang, E. Bjornson, and Z. Wang, "Achievable rate of rician large-scale MIMO channels with transceiver hardware impairments," *IEEE Trans. Veh. Technol.*, vol. PP, no. 99, pp. 1–1, 2015.

[333] B. E. Priyanto, T. B. Sorensen, O. K. Jensen, T. Larsen, T. Kolding, and P. Mogensen, "Assessing and modeling the effect of RF impairments on UTRA LTE uplink performance," in *IEEE 66th Vehicular Technology Conference*. Baltimore, MD: IEEE, Sep. 2007, pp. 1213–1217.

[334] R. Hamila, O. Ozdemir, and N. Al-Dhahir, "Beamforming OFDM performance under joint phase noise and I/Q imbalance," *IEEE Trans. Veh. Technol.*, vol. PP, no. 99, pp. 1–1, 2015.

[335] E. Björnson, P. Zetterberg, M. Bengtsson, and B. Ottersten, "Capacity limits and multiplexing gains of MIMO channels with transceiver impairments," *IEEE Commun. Lett.*, vol. 17, no. 1, pp. 91–94, Jan. 2013.

[336] H. Mehrpouyan, M. Matthaiou, R. Wang, G. K. Karagiannidis, and Y. Hua, "Hybrid millimeter-wave systems: A novel paradigm for hetnets," *IEEE Commun. Mag.*, vol. 53, no. 1, pp. 216–221, Jan. 2015.

[337] C.-L. Liu, "Impacts of I/Q imbalance on QPSK-OFDM-QAM detection," *IEEE Trans. Consum. Electron.*, vol. 44, no. 3, pp. 984–989, Jun. 1998.

[338] M. Valkama, M. Renfors, and V. Koivunen, "Compensation of frequency-selective I/Q imbalances in wideband receivers: models and algorithms," in *IEEE Third Workshop on Signal Processing Advances in Wireless Communications (SPAWC)*. Taiwan, TW: IEEE, Mar. 2001, pp. 42–45.

[339] G. Xing, M. Shen, and H. Liu, "Frequency offset and I/Q imbalance compensation for direct-conversion receivers," *IEEE Trans. Wireless Commun.*, vol. 4, no. 2, pp. 673–680, Mar. 2005.

[340] M. Windisch and G. Fettweis, "Performance degradation due to I/Q imbalance in multi-carrier direct conversion receivers: A theoretical analysis," in *IEEE International Conference on Communications (ICC)*, vol. 1. Istanbul, TR: IEEE, Jun. 2006, pp. 257–262.

[341] Y. Zou, M. Valkama, and M. Renfors, "Digital compensation of I/Q imbalance effects in space-time coded transmit diversity systems," *IEEE Trans. Signal Process.*, vol. 56, no. 6, pp. 2496–2508, Jun. 2008.

[342] L. Anttila, M. Valkama, and M. Renfors, "Frequency-selective I/Q mismatch calibration of wideband direct-conversion transmitters," *IEEE Trans. Circuits Syst. II Express Briefs*, vol. 55, no. 4, pp. 359–363, Apr. 2008.

[343] C. P. Yen, Y. Tsai, G. Zhang, and R. Olesen, "Blind estimation and compensation of frequency-flat I/Q imbalance using cyclostationarity," in *IEEE 68th Vehicular Technology Conference (VTC 2008)-Fall*. Calgary, BC: IEEE, Sep. 2008, pp. 1–5.

[344] S. A. Bassam, S. Boumaiza, and F. M. Ghannouchi, "Block-wise estimation of and compensation for I/Q imbalance in direct-conversion transmitters," *IEEE Trans. Signal Process.*, vol. 57, no. 12, pp. 4970–4973, Dec. 2009.

[345] W. R. Peng, B. Zhang, X. Wu, K. M. Feng, A. E. Willner, and S. Chi, "Compensation for I/Q imbalances and bias deviation of the Mach-Zehnder modulators in direct-detected optical OFDM systems," *IEEE Photonics Technol. Lett.*, vol. 21, no. 2, pp. 103–105, Jan. 2009.

[346] S. Traverso, M. Ariaudo, I. Fijalkow, J.-L. Gautier, and C. Lereau, "Decision-directed channel estimation and high I/Q imbalance compensation in OFDM receivers," *IEEE Trans. Commun.*, vol. 57, no. 5, pp. 1246–1249, May 2009.

[347] B. Narasimhan, D. Wang, S. Narayanan, H. Minn, and N. Al-Dhahir, "Digital compensation of frequency-dependent joint Tx/Rx I/Q imbalance in OFDM systems under high mobility," *IEEE J. Sel. Topics Signal Process.*, vol. 3, no. 3, pp. 405–417, Jun. 2009.

[348] K. Y. Sung and C. c. Chao, "Estimation and compensation of I/Q imbalance in OFDM direct-conversion receivers," *IEEE J. Sel. Top. Signal Process.*, vol. 3, no. 3, pp. 438–453, Jun. 2009.

[349] P. Rabiei, W. Namgoong, and N. Al-Dhahir, "Low-complexity OFDM channel estimation in the presence of I/Q imbalance and phase noise," in *IEEE Global Telecommunications Conference*. Honolulu, HI: IEEE, Nov. 2009, pp. 1–5.

[350] J. Qi and S. Aissa, "Analysis and compensation of I/Q imbalance in MIMO transmit-receive diversity systems," *IEEE Trans. Commun.*, vol. 58, no. 5, pp. 1546–1556, May 2010.

[351] Y. Tsai, C.-P. Yen, and X. Wang, "Blind frequency-dependent I/Q imbalance compensation for direct-conversion receivers," *IEEE Trans. Wireless Commun.*, vol. 9, no. 6, pp. 1976–1986, Jun. 2010.

[352] J. Gao, X. Zhu, H. Lin, and A. K. Nandi, "Independent component analysis based semi-blind I/Q imbalance compensation for mimo ofdm systems," *IEEE Trans. Wireless Commun.*, vol. 9, no. 3, pp. 914–920, Mar. 2010.

[353] H. Minn and D. Munoz, "Pilot design for channel estimation of MIMO OFDM systems with frequency-dependent I/Q imbalance," *IEEE Trans. Commun.*, vol. 58, no. 8, pp. 2252–2264, Aug. 2010.

[354] B. Narasimhan, S. Narayanan, H. Minn, and N. Al-Dhahir, "Reduced-complexity baseband compensation of joint Tx/Rx I/Q imbalance in mobile MIMO-OFDM," *IEEE Trans. Wireless Commun.*, vol. 9, no. 5, pp. 1720–1728, May 2010.

[355] Y. Zhou and Z. Pan, "Impact of LPF mismatch on I/Q imbalance in direct conversion receivers," *IEEE Trans. Wireless Commun.*, vol. 10, no. 6, pp. 1702–1708, Jun. 2011.

[356] J. Qi, S. Aissa, and M.-S. Alouini, "Analysis and compensation of I/Q imbalance in amplify-and-forward cooperative systems," in *IEEE Wireless Communications and Networking Conference (WCNC)*. Shanghai, CN: IEEE, Apr. 2012, pp. 215–220.

[357] W. Nam, H. Roh, J. Lee, and I. Kang, "Blind adaptive I/Q imbalance compensation algorithms for direct-conversion receivers," *IEEE Signal. Proc. Let.*, vol. 19, no. 8, pp. 475–478, Aug. 2012.

[358] B. Maham, O. Tirkkonen, and A. Hjorungnes, "Impact of transceiver I/Q imbalance on transmit diversity of beamforming OFDM systems," *IEEE Trans. Commun.*, vol. 60, no. 3, pp. 643–648, Mar. 2012.

[359] H. Lin and K. Yamashita, "Time domain blind I/Q imbalance compensation based on real-valued filter," *IEEE Trans. Wireless Commun.*, vol. 11, no. 12, pp. 4342–4350, Dec. 2012.

[360] O. Semiari, B. Maham, and C. Yuen, "Effect of I/Q imbalance on blind spectrum sensing for ofdma overlay cognitive radio," in *IEEE International Conference on Communications in China (ICCC)*. Beijing, CN: IEEE, Aug. 2012, pp. 433–437.

[361] W. H. Yu, C. F. Cheang, P. I. Mak, W. F. Cheng, K. F. Un, U. W. Lok, and R. P. Martins, "A nonrecursive digital calibration technique for joint elimination of transmitter and receiver I/Q imbalances with minimized add-on hardware," *IEEE Trans. Circuits Syst. II Express Briefs*, vol. 60, no. 8, pp. 462–466, Aug. 2013.

[362] J. Luo, A. Kortke, W. Keusgen, and M. Valkama, "A novel adaptive calibration scheme for frequency-selective I/Q imbalance in broadband direct-conversion transmitters," *IEEE Trans. Circuits Syst. II Express Briefs*, vol. 60, no. 2, pp. 61–65, Feb. 2013.

[363] O. Ozdemir, R. Hamila, and N. Al-Dhahir, "I/Q imbalance in multiple beamforming OFDM transceivers: SINR analysis and digital baseband compensation," *IEEE Trans. Commun.*, vol. 61, no. 5, pp. 1914–1925, May 2013.

[364] H. Li, X. Wang, and Y. Zou, "Exploiting transmitter I/Q imbalance for estimating the number of active users," in *IEEE Global Communications Conference (GLOBECOM)*. Atlanta, GA, US: IEEE, Dec. 2013, pp. 3318–3322.

[365] J. Luo, A. Kortke, W. Keusgen, and M. Valkama, "Efficient estimation and pilot-free online re-calibration of I/Q imbalance in broadband direct-conversion transmitters," *IEEE Trans. Veh. Technol.*, vol. 63, no. 6, pp. 2506–2520, Jul. 2014.

[366] O. Ozgur, R. Hamila, and N. Al-Dhahir, "Exact average OFDM subcarrier SINR analysis under joint transmit-receive I/Q imbalance," *IEEE Trans. Veh. Technol.*, no. 8, pp. 4125–4130, Oct. 2014.

[367] M. Mokhtar, A.-A. A. Boulogeorgos, G. K. Karagiannidis, and N. Al-Dhahir, "OFDM opportunistic relaying under joint transmit/receive I/Q imbalance," *IEEE Trans. Commun.*, vol. 62, no. 5, pp. 1458–1468, May 2014.

[368] S. Zarei, W. Gerstacker, and R. Schober, "I/Q imbalance aware widely-linear precoding for downlink massive mimo systems," in *IEEE Globecom Workshops (GC Wkshps)*. Austin, TX: IEEE, Dec. 2014, pp. 301–307.

[369] J. Li, M. Matthaiou, and T. Svensson, "I/Q imbalance in two-way AF relaying: Performance analysis and detection mode switch," in *IEEE Global Communications Conference*. Austin, TX: IEEE, Dec. 2014, pp. 4001–4007.

[370] P. Hao, X. Wang, and A. Behnad, "Relay authentication by exploiting I/Q imbalance in amplify-and-forward system," in *IEEE Global Communications Conference*. Austin, TX: IEEE, Dec. 2014, pp. 613–618.

[371] A. Hakkarainen, J. Werner, K. Dandekar, and M. Valkama, "Analysis and augmented spatial processing for uplink OFDMA MU-MIMO receiver with transceiver I/Q imbalance and external interference," *IEEE Trans. Wireless Commun.*, vol. PP, no. 99, pp. 1–1, Jan. 2016.

[372] S. Zarei, W. Gerstacker, J. Aulin, and R. Schober, "I/Q imbalance aware widely-linear receiver for uplink multi-cell massive MIMO systems: Design and sum rate analysis," *IEEE Trans. Wireless Commun.*, vol. PP, no. 99, pp. 1–1, Jan. 2016.

[373] M. Sakai, H. Lin, and K. Yamashita, "Joint estimation of channel and I/Q imbalance in OFDM/OQAM systems," *IEEE Commun. Lett.*, vol. 20, no. 2, pp. 284–287, Feb. 2016.

[374] A.-A. A. Boulogeorgos, P. C. Sofotasios, S. Muhaidat, M. Valkama, and G. K. Karagiannidis, "The effects of RF impairments in Vehicle-to-Vehicle communications," in *IEEE 25th International Symposium on Personal, Indoor and Mobile Radio Communications - (PIMRC): Fundamentals and PHY (IEEE PIMRC 2015 - Fundamentals and PHY)*. Hong Kong, CN: IEEE, Aug. 2015, pp. 840–845.

[375] A.-A. A. Boulogeorgos, P. C. Sofotasios, B. Selim, S. Muhaidat, G. K. Karagiannidis, and M. Valkama, "Outage probability under I/Q imbalance and cascaded fading effects," in *International Conference on Telecommunications (ICT)*. Thessaloniki, GR: IEEE, May 2016, pp. 1–5.

[376] A.-A. A. Boulogeorgos, Karas, and G. K. Karagiannidis, "How much does I/Q imbalance affect secrecy capacity?" *IEEE Commun. Lett.*, vol. 20, no. 7, pp. 1305–1308, Jul. 2016.

[377] A. A. Boulogeorgos, H. B. Salameh, and G. Karagiannidis, "Spectrum sensing in full-duplex cognitive radio networks under hardware imperfections," *IEEE Trans. Veh. Technol.*, vol. PP, no. 99, pp. 1–1, 2016.

[378] A.-A. A. Boulogeorgos, H. Bany Salameh, and G. K. Karagiannidis, "On the effects of I/Q imbalance on sensing performance in Full-Duplex cognitive radios," in *IEEE Wireless Communications and Networking Conference WS 8 : IEEE WCNC'2016 International Workshop on Smart Spectrum (IWSS) (IEEEWCNC2016-IWSS)*. Doha, QA: IEEE, Apr. 2016, pp. 361–366.

[379] A.-A. A. Boulogeorgos, P. D. Diamantoulakis, and G. K. Karagiannidis, "Optimal power allocation for OFDMA systems under I/Q imbalance," *IEEE Signal. Proc. Let.*, vol. PP, no. 99, 2016.

[380] M. Lont, D. Milosevic, G. Dolmans, and A. H. M. van Roermund, "Implications of I/Q imbalance, phase noise and noise figure for SNR and BER of FSK receivers," *IEEE Trans. Circuits Syst. I Regul. Pap.*, vol. 60, no. 8, pp. 2187–2198, Aug. 2013.

[381] J. Crols and M. Steyaert, *CMOS Wireless Transceiver Design*. Norwell, MA, USA: Kluwer Academic Publishers, 1997.

[382] A.-A. A. Boulogeorgos, P. C. Sofotasios, B. Selim, S. Muhaidat, G. K. Karagiannidis, and M. Valkama, "Effects of RF impairments in communications over cascaded fading channels," *IEEE Trans. Veh. Technol.*, vol. PP, no. 99, 2016.

[383] M. Mokhtar, A.-A. A. Boulogeorgos, G. K. Karagiannidis, and N. Al-Dhahir, "Dual-hop OFDM opportunistic AF relaying under joint transmit/receive I/Q imbalance," in *IEEE Global Telecommunications Conference (GLOBECOM)*. Atlanta, US: IEEE, Dec. 2013, pp. 4287–4292.

[384] B. Razavi, "Design considerations for direct-conversion receivers," *IEEE Trans. Circuits Syst. II, Analog Digit. Signal Process.*, vol. 44, no. 6, pp. 428–435, Jun. 1997.

[385] Z. Zhu, X. Huang, and H. Leung, "Blind compensation of frequency-dependent I/Q imbalance in direct conversion OFDM receivers," *IEEE Commun. Lett.*, vol. 17, no. 2, pp. 297–300, Feb. 2013.

[386] T. H. Lee and A. Hajimiri, "Oscillator phase noise: a tutorial," *IEEE J. Solid-State Circuits*, vol. 35, no. 3, pp. 326–336, Mar. 2000.

[387] W. Lindsey and K. Tu, "Phase noise effects on space shuttle communications link performance," *IEEE Trans. Commun.*, vol. 26, no. 11, pp. 1532–1541, Nov. 1978.

[388] Y.-C. Tseng, W. M. Huang, E. Spears, D. Spooner, D. Ngo, J. M. Ford, and J. C. S. Woo, "Phase noise characteristics associated with low-frequency noise in submicron SOI MOSFET feedback oscillator for RF IC's," *IEEE Electron Device Lett.*, vol. 20, no. 1, pp. 54–56, Jan. 1999.

[389] R. Corvaja and S. Pupolin, "Phase noise effects in QAM systems," in *8th IEEE International Symposium on Personal, Indoor and Mobile Radio Communications (PIMRC '97)*, vol. 2. Helsinki, FI: IEEE, Sep. 1997, pp. 452–456.

[390] N. C. Sagias and G. K. Karagiannidis, "Effects of carrier phase error on EGC receivers in correlated Nakagami-m fading," *IEEE Commun. Lett.*, vol. 9, no. 7, pp. 580–582, Jul. 2005.

[391] L. Tomba, "On the effect of Wiener phase noise in OFDM systems," *IEEE Trans. Commun.*, vol. 46, no. 5, pp. 580–583, May 1988.

[392] L. Tomba and W. A. Krzymien, "Sensitivity of the MC-CDMA access scheme to carrier phase noise and frequency offset," *IEEE Trans. Veh. Technol.*, vol. 48, no. 5, pp. 1657–1665, Sep. 1999.

[393] A. G. Armada, "Understanding the effects of phase noise in orthogonal frequency division multiplexing (OFDM)," *IEEE Trans. Broadcast.*, vol. 47, no. 2, pp. 153–159, Jun. 2001.

[394] Y. Zhang and H. Liu, "MIMO-OFDM systems in the presence of phase noise and doubly selective fading," *IEEE Trans. Veh. Technol.*, vol. 56, no. 4, pp. 2277–2285, Jul. 2007.

[395] A. Pitarokoilis, E. Bjornson, and E. G. Larsson, "ML detection in phase noise impaired SIMO channels with uplink training," *IEEE Trans. Commun.*, vol. 64, no. 1, pp. 223–235, Jan. 2016.

[396] S. Wu and Y. Bar-Ness, "OFDM systems in the presence of phase noise: Consequences and solutions," *IEEE Trans. Commun.*, vol. 52, no. 5, pp. 855–855, May 2004.

[397] A. Gomaa and N. Al-Dhahir, "SC-FDMA performance in presence of oscillator impairments: EVM and subcarrier mapping impact," in *IEEE Global Telecommunications Conference (GLOBECOM 2011)*. Houston, TX, USA: IEEE, Dec. 2011, pp. 1–5.

[398] A. Hajimiri and T. H. Lee, "A general theory of phase noise in electrical oscillators," *IEEE J. Solid-State Circuits*, vol. 33, no. 2, pp. 179–194, Feb. 1998.

[399] B. Razavi, *A General Theory of Phase Noise in Electrical Oscillators*. Wiley-IEEE Press, 2003, pp. 189–204. [Online]. Available: http://ieeexplore.ieee.org/xpl/articleDetails.jsp?arnumber=5311468

[400] P. Liu, S. Wu, and Y. Bar-Ness, "A phase noise mitigation scheme for MIMO WLANs with spatially correlated and imperfectly estimated channels," *IEEE Commun. Lett.*, vol. 10, no. 3, pp. 141–143, Mar. 2006.

[401] R. Krishnan, G. Colavolpe, A. G. i Amat, and T. Eriksson, "Algorithms for joint phase estimation and decoding for MIMO systems in the presence of phase noise and quasi-static fading channels," *IEEE Trans. Signal Process.*, vol. 63, no. 13, pp. 3360–3375, Jul. 2015.

[402] F. Munier, T. Eriksson, and A. Svensson, "An ICI reduction scheme for OFDM system with phase noise over fading channels," *IEEE Trans. Commun.*, vol. 56, no. 7, pp. 1119–1126, Jul. 2008.

[403] Z. Jianhua, H. Rohling, and Z. Ping, "Analysis of ICI cancellation scheme in OFDM systems with phase noise," *IEEE Trans. Broadcast.*, vol. 50, no. 2, pp. 97–106, Jun. 2004.

[404] V. Syrjala, M. Valkama, L. Anttila, T. Riihonen, and D. Korpi, "Analysis of oscillator phase-noise effects on self-interference cancellation in full-duplex OFDM radio transceivers," *IEEE Trans. Wireless Commun.*, vol. 13, no. 6, pp. 2977–2990, Jun. 2014.

[405] M. K. Lee, S. C. Lim, and K. Yang, "Blind compensation for phase noise in OFDM systems over constant modulus modulation," *IEEE Trans. Commun.*, vol. 60, no. 3, pp. 620–625, Mar. 2012.

[406] R. Wang, H. Mehrpouyan, M. Tao, and Y. Hua, "Channel estimation, carrier recovery, and data detection in the presence of phase noise in OFDM relay systems," *IEEE Trans. Wireless Commun.*, vol. 15, no. 2, pp. 1186–1205, Feb. 2016.

[407] J. Tubbax, B. Come, L. V. der Perre, S. Donnay, M. Engels, H. D. Man, and M. Moonen, "Compensation of IQ imbalance and phase noise in OFDM systems," *IEEE Trans. Wireless Commun.*, vol. 4, no. 3, pp. 872–877, May 2005.

[408] Q. Zou, A. Tarighat, and A. H. Sayed, "Compensation of phase noise in OFDM wireless systems," *IEEE Trans. Signal Process.*, vol. 55, no. 11, pp. 5407–5424, Nov. 2007.

[409] J. Shentu, K. Panta, and J. Armstrong, "Effects of phase noise on performance of OFDM systems using an ICI cancellation scheme," *IEEE Trans. Broadcast.*, vol. 49, no. 2, pp. 221–224, Jun. 2003.

[410] M. R. Khanzadi, R. Krishnan, and T. Eriksson, "Estimation of phase noise in oscillators with colored noise sources," *IEEE Commun. Lett.*, vol. 17, no. 11, pp. 2160–2163, Nov. 2013.

[411] A. Georgiadis, "Gain, phase imbalance, and phase noise effects on error vector magnitude," *IEEE Trans. Veh. Technol.*, vol. 53, no. 2, pp. 443–449, Mar. 2004.

[412] S. Sancho, A. Suarez, and F. Ramirez, "General phase-noise analysis from the variance of the phase deviation," *IEEE Trans. Microwave Theory Tech.*, vol. 61, no. 1, pp. 472–481, Jan. 2013.

[413] J.-A. Huang, K.-P. Ho, H.-K. Chen, S. K. Liaw, and H.-C. Wang, "Impact of nonlinear phase noise to DPSK signals: experimental verification of a simplified theoretical model," *IEEE Photonics Technol. Lett.*, vol. 17, no. 10, pp. 2236–2238, Oct. 2005.

[414] Q. Zou, A. Tarighat, and A. Sayed, "Joint compensation of IQ imbalance and phase noise in OFDM wireless systems," *IEEE Trans. Commun.*, vol. 57, no. 2, pp. 404–414, Feb. 2009.

[415] H. Mehrpouyan, A. A. Nasir, S. D. Blostein, T. Eriksson, G. K. Karagiannidis, and T. Svensson, "Joint estimation of channel and oscillator phase noise in mimo systems," *IEEE Trans. Signal Process.*, vol. 60, no. 9, pp. 4790–4807, Sep. 2012.

[416] E. Bjornson, M. Matthaiou, and M. Debbah, "Massive MIMO systems with hardware-constrained base stations," in *IEEE International Conference on Acoustics, Speech and Signal Processing (ICASSP)*. Florence, IT: IEEE, May 2014, pp. 3142–3146.

[417] A. Gokceoglu, Y. Zou, M. Valkama, and P. C. Sofotasios, "Multi-channel energy detection under phase noise: Analysis and mitigation," *ACM/Springer Mob. Netw Appl.*, vol. 19, no. 4, pp. 473–486, Aug. 2014.

[418] E. Ahmed and A. M. Eltawil, "On phase noise suppression in full-duplex systems," *IEEE Trans. Wireless Commun.*, vol. 14, no. 3, pp. 1237–1251, Mar. 2015.

[419] P. Mathecken, T. Riihonen, S. Werner, and R. Wichman, "Performance analysis of OFDM with Wiener phase noise and frequency selective fading channel," *IEEE Trans. Commun.*, vol. 59, no. 5, pp. 1321–1331, May 2011.

[420] H.-G. Ryu and Y.-S. Lee, "Phase noise analysis of the OFDM communication system by the standard frequency deviation," *IEEE Trans. Consum. Electron.*, vol. 49, no. 1, pp. 41–47, Feb. 2003.

[421] A. A. Abidi, "Phase noise and jitter in CMOS ring oscillators," *IEEE J. Solid-State Circuits*, vol. 41, no. 8, pp. 1803–1816, Aug. 2006.

[422] S. Wu, P. Liu, and Y. Bar-Ness, "Phase noise estimation and mitigation for OFDM systems," *IEEE Trans. Wireless Commun.*, vol. 5, no. 12, pp. 3616–3625, Dec. 2006.

[423] A. A. Nasir, H. Mehrpouyan, R. Schober, and Y. Hua, "Phase noise in MIMO systems: Bayesian Cramer-Rao bounds and soft-input estimation," *IEEE Trans. Signal Process.*, vol. 61, no. 10, pp. 2675–2692, May 2013.

[424] M. R. Khanzadi, R. Krishnan, J. Soder, and T. Eriksson, "On the capacity of the Wiener phase-noise channel: Bounds and capacity achieving distributions," *IEEE Trans. Commun.*, vol. 63, no. 11, pp. 4174–4184, Nov. 2015.

[425] A. Chorti and M. Brookes, "A spectral model for RF oscillators with power-law phase noise," *IEEE Trans. Circuits Syst. I Regul. Pap.*, vol. 53, no. 9, pp. 1989–1999, Sep. 2006.

[426] Y. Li, H. Jacobsson, M. Bao, and T. Lewin, "High-frequency SiGe MMICs-an industrial perspective," in *GigaHerz 2003 symp.* Linkoping, SE: IEEE, Nov. 2003, pp. 1–4.

[427] L. Smaini, *RF Analog Impairments Modeling for Communication Systems Simulation: Application to OFDM-Based Transceivers.* John Wiley & Sons, Ltd, Aug. 2012.

[428] A. Demir, A. Mehrotra, and J. Roychowdhury, "Phase noise in oscillators: a unifying theory and numerical methods for characterization," *IEEE Transactions on Circuits and Systems I: Fundamental Theory and Applications*, vol. 47, no. 5, pp. 655–674, May 2000.

[429] S. Bay, C. Herzet, J. M. Brossier, J. P. Barbot, and B. Geller, "Analytic and asymptotic analysis of bayesian cramer-rao bound for dynamical phase offset estimation," *IEEE Trans. Signal Process.*, vol. 56, no. 1, pp. 61–70, Jan. 2008.

[430] G. V. Klimovitch, "A nonlinear theory of near-carrier phase noise in free-running oscillators," in *Third IEEE International Caracas Conference on Devices, Circuits and Systems.* Cancun, MX: IEEE, Mar. 2000, pp. T80/1–T80/6.

[431] S. Wu and Y. Bar-Ness, "A phase noise suppression algorithm for OFDM-based WLANs," *IEEE Commun. Lett.*, vol. 6, no. 12, pp. 535–537, Dec. 2002.

[432] H. Meyr, M. Moeneclaey, and S. A. Fechtel, *Digital Communication Receivers, Synchronization, Channel Estimation, and Signal Processing.* John Wiley & Sons, Inc., New York, NY, 1988.

[433] A. G. Armada and M. Calvo, "Phase noise and sub-carrier spacing effects on the performance of an OFDM communication system," *IEEE Commun. Lett.*, vol. 2, no. 1, pp. 11–13, Jan. 1998.

[434] J. Bussgang, "Crosscorrelation functions of amplitude-distorted gaussian signals. research lab. electron," 1952.

[435] ——, "Cross-correlation functions of amplitude-distorted gaussian inputs," *Nonlinear systems. Stroudsburg, PA: Dowdon, Hutchinson & Ross*, 1975.

[436] A. Papoulis and S. Pillai, *Probability, Random Variables, and Stochastic Processes*, ser. McGraw-Hill series in electrical engineering: Communications and signal processing. Tata McGraw-Hill, Jan. 2002.

[437] J. Minkoff, "The role of AM-to-PM conversion in memoryless nonlinear systems," *IEEE Trans. Commun.*, vol. 33, no. 2, pp. 139–144, Feb. 1985.

[438] P. Banelli and S. Cacopardi, "Theoretical analysis and performance of OFDM signals in nonlinear AWGN channels," *IEEE Trans. Commun.*, vol. 48, no. 3, pp. 430–441, Mar. 2000.

[439] H. Ochiai and H. Imai, "Performance analysis of deliberately clipped OFDM signals," *IEEE Trans. Commun.*, vol. 50, no. 1, pp. 89–101, Jan. 2002.

[440] K. Bae, C. Shin, and E. J. Powers, "Performance analysis of OFDM systems with selected mapping in the presence of nonlinearity," *IEEE Trans. Wireless Commun.*, vol. 12, no. 5, pp. 2314–2322, May 2013.

[441] T. K. Helaly, R. M. Dansereau, and M. El-Tanany, "Analysis of BER performance in presence of nonlinear distortion due to PD-HPA in downlink DS-CDMA signals," *IEEE Commun. Lett.*, vol. 14, no. 4, pp. 273–275, Apr. 2010.

[442] H.-G. Ryu, T. P. Hoa, N. T. Hieu, and J. Jianxue, "BER analysis of clipping process in the forward link of the OFDM-FDMA communication system," *IEEE Trans. Consum. Electron.*, vol. 50, no. 4, pp. 1058–1064, Nov. 2004.

[443] A. R. S. Bahai, M. Singh, A. J. Goldsmith, and B. R. Saltzberg, "A new approach for evaluating clipping distortion in multicarrier systems," *IEEE J. Sel. Areas Commun.*, vol. 20, no. 5, pp. 1037–1046, Jun. 2002.

[444] R. Price, "A useful theorem for nonlinear devices having Gaussian inputs," *IRE Transactions on Information Theory*, vol. 4, no. 2, pp. 69–72, Jun. 1958.

[445] A. Abdi and M. Kaveh, "K distribution: an appropriate substitute for rayleigh-lognormal distribution in fading-shadowing wireless channels," *Electronics Letters*, vol. 34, no. 9, pp. 851–852, Apr. 1998.

[446] P. Bithas, N. Sagias, P. Mathiopoulos, G. Karagiannidis, and A. Rontogiannis, "On the performance analysis of digital communications over generalized-K fading channels," *IEEE Commun. Lett.*, vol. 10, no. 5, pp. 353–355, May 2006.

[447] A. Laourine, M.-S. Alouini, S. Affes, and A. Stephenne, "On the performance analysis of composite multipath/shadowing channels using the g-distribution," *IEEE Trans. Commun.*, vol. 57, no. 4, pp. 1162–1170, Apr. 2009.

[448] P. Bithas, "Weibull-gamma composite distribution: alternative multipath/shadowing fading model," *Electronics Letters*, vol. 45, no. 14, pp. 749–751, Jul. 2009.

[449] C. Zhong, M. Matthaiou, G. Karagiannidis, A. Huang, and Z. Zhang, "Capacity bounds for af dual-hop relaying in cal G fading channels," *IEEE Trans. Veh. Technol.*, vol. 61, no. 4, pp. 1730–1740, May 2012.

[450] P. C. Sofotasios, T. Tsiftsis, M. Ghogho, L. Wilhelmsson, and M. Valkama, "The $\eta - \mu$/IG distribution: A novel physical multipath/shadowing fading model," in *IEEE International Conference on Communications (ICC)*. Budapest, HU: IEEE, Jun. 2013, pp. 5715–5719.

[451] P. Bithas, N. Sagias, and P. Mathiopoulos, "The bivariate generalized-$X(X_g)$ distribution and its application to diversity receivers," *IEEE Trans. Commun.*, vol. 57, no. 9, pp. 2655–2662, Sep. 2009.

[452] J. Zhang, M. Matthaiou, Z. Tan, and H. Wang, "Performance analysis of digital communication systems over composite $\eta-\mu$ /gamma fading channels," *IEEE Trans. Veh. Technol.*, vol. 61, no. 7, pp. 3114–3124, Sep. 2012.

[453] J. F. Paris, "Advances in the statistical characterization of fading: from 2005 to present," *Hindawi International Journal on Antennas and Propagation - Special Issue, Article ID 258308*, pp. 1–5, 2014.

[454] P. C. Sofotasios, T. Tsiftsis, K. H. Van, S. Freear, L. Wilhelmsson, and M. Valkama, "The $\kappa - \mu$/inverse-gaussian composite statistical distribution in rf and fso wireless channels," in *IEEE 78th Vehicular Technology Conference (VTC Fall)*. Las Vegas, NV, US: IEEE, Sep. 2013, pp. 1–5.

[455] J. Paris, "Statistical characterization of $\kappa - \mu$ shadowed fading," *IEEE Trans. Veh. Technol.*, vol. 63, no. 2, pp. 518–526, Feb. 2014.

[456] J. B. Andersen, "Statistical distributions in mobile communications using multiple scattering," in *27th URSI General Assembly*, Jan. 2002.

[457] G. K. Karagiannidis, N. C. Sagias, and P. T. Mathiopoulos, "N*Nakagami: A novel stochastic model for cascaded fading channels," *IEEE Trans. Commun.*, vol. 55, no. 8, pp. 1453–1458, Aug. 2007.

[458] P. C. Sofotasios, L. Mohjazi, S. Muhaidat, M. Al-Qutayri, and G. Karagiannidis, "Energy detection of unknown signals over cascaded fading channels," *IEEE Antennas Wireless Propag. Lett.*, vol. 15, pp. 135–138, Feb. 2016.

[459] V. Erceg, S. Fortune, J. Ling, A. Rustako, and R. Valenzuela, "Comparisons of a computer-based propagation prediction tool with experimental data collected in urban microcellular environments," *IEEE J. Sel. Areas Commun.*, vol. 15, no. 4, pp. 677–684, May 1997.

[460] E. Bjornson, P. Zetterberg, and M. Bengtsson, "Optimal coordinated beamforming in the multicell downlink with transceiver impairments," in *IEEE Global Communications Conference*. Anaheim, CA: IEEE, Dec. 2012, pp. 4775–4780.

[461] E. Bjornson, A. Papadogiannis, M. Matthaiou, and M. Debbah, "On the impact of transceiver impairments on AF relaying," in *IEEE International Conference on Acoustics, Speech and Signal Processing (ICASSP)*. Vancouver, BC: IEEE, May 2013, pp. 4948–4952.

[462] A. Tarighat, R. Bagheri, and A. Sayed, "Compensation schemes and performance analysis of IQ imbalances in OFDM receivers," *IEEE Trans. Signal Process.*, vol. 53, no. 8, pp. 3257–3268, Aug. 2005.

[463] J. Qi, S. Aissa, and M.-S. Alouini, "Impact of I/Q imbalance on the performance of two-way CSI-assisted AF relaying," in *IEEE Wireless Communications and Networking Conf.* Shanghai, CN: IEEE, Apr. 2013, pp. 2507–2512.

[464] ——, "Dual-hop amplify-and-forward cooperative relaying in the presence of Tx and Rx in-phase and quadrature-phase imbalance," *IET Commun.*, vol. 8, no. 3, pp. 287–298, Feb. 2014.

[465] J. Li, M. Matthaiou, and T. Svensson, "I/Q imbalance in AF dual-hop relaying: Performance analysis in Nakagami-m fading," *IEEE Trans. Commun.*, vol. 62, no. 3, pp. 836–847, Mar. 2014.

[466] ——, "I/Q imbalance in two-way AF relaying," *IEEE Trans. Commun.*, vol. 62, no. 7, pp. 2271–2285, Jul. 2014.

[467] T. C. W. Schenk, E. R. Fledderus, and P. F. M. Smulders, "Performance analysis of zero-IF MIMO OFDM transceivers with IQ imbalance," *J. Commun.*, vol. 2, no. 7, pp. 9–19, 2007.

[468] S. J. Grant and J. K. Cavers, "Analytical calculation of outage probability for a general cellular mobile radio system," in *IEEE Vehicular Technology Conf.*, vol. 3. Amsterdam, NL: IEEE, Sep. 1999, pp. 1372–1376.

[469] H. Seo, K. D. Lee, S. Yasukawa, Y. Peng, and P. Sartori, "LTE evolution for vehicle-to-everything services," *IEEE Commun. Mag.*, vol. 54, no. 6, pp. 22–28, Jun. 2016.

[470] D. W. Matolak and J. Frolik, "Worse-than-Rayleigh fading: Experimental results and theoretical models," *IEEE Commun. Mag.*, vol. 49, no. 4, pp. 140–146, Apr. 2011.

[471] K. C. Dey, A. Mishra, and M. Chowdhury, "Potential of intelligent transportation systems in mitigating adverse weather impacts on road mobility: A review," *IEEE Trans. Intell. Transp. Syst.*, vol. 16, no. 3, pp. 1107–1119, Jun. 2015.

[472] P. Papadimitratos, A. D. L. Fortelle, K. Evenssen, R. Brignolo, and S. Cosenza, "Vehicular communication systems: Enabling technologies, applications, and future outlook on intelligent transportation," *IEEE Commun. Mag.*, vol. 47, no. 11, pp. 84–95, Nov. 2009.

[473] H. Ilhan, M. Uysal, and I. Altunbas, "Cooperative diversity for intervehicular communication: Performance analysis and optimization," *IEEE Trans. Veh. Commun.*, vol. 58, no. 7, pp. 3301–3310, Sep. 2009.

[474] A. Molisch, F. Tufvesson, J. Karedal, and C. Mecklenbrauker, "A survey on vehicle-to-vehicle propagation channels," *IEEE Wireless Commun. Mag.*, vol. 16, no. 6, pp. 12–22, Dec. 2009.

[475] M. Kihl, K. Bur, F. Tufvesson, and J. Aparicio Ojea, "Simulation modelling and analysis of a realistic radio channel model for V2V communications," in *Int. Congr. on Ultra Modern Telecommunications and Control Systems and Workshops*. Moscow, RU: IEEE, Oct. 2010, pp. 981–988.

[476] M. K. Simon and M.-S. Alouini, *Digital Communication over fading channels*. John Wiley & Sons, Ltd., 2005, vol. 95.

[477] A. P. Prudnikov, Y. A. Brychkov, and O. I. Marichev, *Inegrals and Series, Vol. 2: Special Functions*. Gordon and Breach Science Publishers, 1992.

[478] H. Hadizadeh, S. Muhaidat, and I. Bajic, "Impact of imperfect channel estimation on the performance of inter-vehicular cooperative networks," in *IEEE Biennial Symposium on Communications*. Kingston, GB: IEEE, May 2010, pp. 373–376.

[479] M. Shirkhani, Z. Tirkan, and A. Taherpour, "Performance analysis and optimization of two-way cooperative communications in inter-vehicular networks," in *IEEE Int. Conf. on Wireless Communications Signal Processing*. Huangshan, CN: IEEE, Oct. 2012, pp. 1–6.

[480] J. Xiao, R. Hu, Y. Qian, L. Gong, and B. Wang, "Expanding LTE network spectrum with cognitive radios: From concept to implementation," *IEEE Wireless Commun. Mag.*, vol. 20, no. 2, pp. 12–19, Apr. 2013.

[481] M. Sherman, A. Mody, R. Martinez, C. Rodriguez, and R. Reddy, "IEEE standards supporting cognitive radio and networks, dynamic spectrum access, and coexistence," *IEEE Commun. Mag.*, vol. 46, no. 7, pp. 72–79, Jul. 2008.

[482] W. Afifi and M. Krunz, "Incorporating self-interference suppression for full-duplex operation in opportunistic spectrum access systems," *IEEE Trans. Wireless Commun.*, vol. 14, no. 4, pp. 2180–2191, Apr. 2015.

[483] O. Altrad, S. Muhaida, A. Al-Dweik, A. Shami, and P. D. Yoo, "Opportunistic spectrum access in cognitive radio networks under imperfect spectrum sensing," *IEEE Trans. Veh. Technol.*, vol. 63, no. 2, pp. 920–925, Feb. 2014.

[484] S. Huang, X. Liu, and Z. Ding, "Optimal sensing-transmission structure for dynamic spectrum access," in *IEEE Conference on Computer Communications (INFOCOM)*. Rio de Janeiro, BR: IEEE, Apr. 2009, pp. 2295–2303.

[485] B. Razavi, "Cognitive radio design challenges and techniques," *IEEE J. Solid-State Circuits*, vol. 45, no. 8, pp. 1542–1553, Aug. 2010.

[486] J. Verlant-Chenet, J. Renard, J.-M. Dricot, P. D. Doncker, and F. Horlin, "Sensitivity of spectrum sensing techniques to RF impairments," in *Proc. IEEE Vehicular Technology Conference (VTC-Spring)*. Taipei, CN: IEEE, May 2010, pp. 1–5.

[487] A. Zahedi-Ghasabeh, A. Tarighat, and B. Daneshrad, "Cyclo-stationary sensing of OFDM waveforms in the presence of receiver RF impairments," in *IEEE Wireless Communications and Networking Conference (WCNC)*. Sydney, NSW: IEEE, Apr. 2010, pp. 1–6.

[488] A. ElSamadouny, A. Gomaa, and N. Al-Dhahir, "Likelihood-based spectrum sensing of OFDM signals in the presence of Tx/Rx I/Q imbalance," in *Proc. IEEE Global Communications Conference (GLOBECOM)*. Anaheim, CA: IEEE, Dec. 2012, pp. 3616–3621.

[489] G. Zheng, I. Krikidis, and B. Ottersten, "Full-duplex cooperative cognitive radio with transmit imperfections," *IEEE Trans. Wireless Commun.*, vol. 12, no. 5, pp. 2498–2511, May 2013.

[490] Y. Yuan, P. Bahl, R. Chandra, T. Moscibroda, and Y. Wu, "Allocating dynamic time-spectrum blocks in cognitive radio networks," in *Proceedings of the 8th ACM International Symposium on Mobile Ad Hoc Networking and Computing*, ser. MobiHoc '07. New York, NY, USA: ACM, Sep. 2007, pp. 130–139.

[491] H. Bany Salameh and M. Krunz, "Channel access protocols for multihop opportunistic networks: Challenges and recent developments," *IEEE Network*, vol. 23, no. 4, pp. 14–19, Jul. 2009.

[492] S. Chatterjee, S. Maity, and T. Acharya, "Energy efficient cognitive radio system for joint spectrum sensing and data transmission," *IEEE Journal on Emerging and Selected Topics in Circuits and Systems*, vol. 4, no. 3, pp. 292–300, Sep. 2014.

[493] H. Bany Salameh, M. Krunz, and O. Younis, "Cooperative adaptive spectrum sharing in cognitive radio networks," *IEEE/ACM Trans. Netw.*, vol. 18, no. 4, pp. 1181–1194, Aug. 2010.

[494] H. Bany Salameh and M. El-Attar, "Cooperative ofdm-based virtual clustering scheme for distributed coordination in cognitive radio networks," *IEEE Trans. Veh. Technol.*, vol. 64, no. 8, pp. 3624–3632, Aug. 2015.

[495] J. Lunden, M. Motani, and H. V. Poor, "Distributed algorithms for sharing spectrum sensing information in cognitive radio networks," *IEEE Trans. Wireless Commun.*, vol. 14, no. 8, pp. 4667–4678, Aug. 2015.

[496] K. Bian, J. M. Park, and R. Chen, "Control channel establishment in cognitive radio networks using channel hopping," *IEEE J. Sel. Areas Commun.*, vol. 29, no. 4, pp. 689–703, Apr. 2011.

[497] IEEE 802.16 Working Group on Broadband Wireless Access, "IEEE standard for air interface for broadband wireless access systems," *IEEE Std 802.16-2012 (Revision of IEEE Std 802.16-2009)*, pp. 1–2542, Aug. 2012.

[498] 3GPP, "Reconfigurable radio systems (RRS); Feasibility study on control channels for cognitive radio systems," ETSI, Tech. Rep. 102.684, Apr. 2012.

[499] M. Seyf, S. Muhaidat, and J. Liang, "Relay selection in cognitive radio networks with interference constraints," *IET Commun.*, vol. 7, no. 10, pp. 922–930, Jul. 2013.

[500] W. Xu, W. Xiang, M. Elkashlan, and H. Mehrpouyan, "Spectrum sensing of OFDM signals in the presence of carrier frequency offset," *IEEE Trans. Veh. Technol.*, no. 99, pp. 1–1, Sep. 2015.

[501] A. Ebrahimzadeh, M. Najimi, S. Hosseini Andargoli, and A. Fallahi, "Sensor selection and optimal energy detection threshold for efficient cooperative spectrum sensing," *IEEE Trans. Veh. Technol.*, vol. 64, no. 99, pp. 1565 – 1577, Apr. 2014.

[502] M. Wenk, *MIMO-OFDM Testbed: Challenges, Implementations, and Measurement Results*, ser. Series in Microelectronics. ETH, 2010.

[503] C. Studer, M. Wenk, and A. Burg, "System-level implications of residual transmit-RF impairments in MIMO systems," in *European Conference on Antennas and Propagation (EUCAP)*. Rome, IT: IEEE, Apr. 2011, pp. 2686–2689.

[504] S. Heinen and R. Wunderlich, "High dynamic range RF frontends from multiband multistandard to cognitive radio," in *Semiconductor Conference Dresden (SCD)*. Dresden, DE: IEEE, Sep. 2011, pp. 1–8.

[505] D. Cabric, S. Mishra, and R. Brodersen, "Implementation issues in spectrum sensing for cognitive radios," in *Conference Record of the Thirty-Eighth Asilomar Conference on Signals, Systems and Computers*, vol. 1. Pacific Grove, CA: IEEE, Nov. 2004, pp. 772–776.

[506] H. Urkowitz, "Energy detection of unknown deterministic signals," *Proc. IEEE*, vol. 55, no. 4, pp. 523–531, Apr. 1967.

[507] F. Digham, M.-S. Alouini, and M. K. Simon, "On the energy detection of unknown signals over fading channels," *IEEE Trans. Commun.*, vol. 55, no. 1, pp. 21–24, Jan. 2007.

[508] P. Zetterberg, "Experimental investigation of TDD reciprocity-based zero-forcing transmit precoding," *EURASIP J. Adv. Signal Process.*, vol. 2011, no. 1, p. 137541, Jan. 2011.

[509] Y. Yoshida, K. Hayashi, H. Sakai, and W. Bocquet, "Analysis and compensation of transmitter IQ imbalances in OFDMA and SC-FDMA systems," *IEEE Trans. Signal Process.*, vol. 57, no. 8, pp. 3119–3129, Aug. 2009.

[510] M. Valkama, J. Pirskanen, and M. Renfors, "Signal processing challenges for applying software radio principles in future wireless terminals: an overview," *Int. J. Commun. Syst.*, vol. 15, no. 8, pp. 741–769, Sep. 2002.

[511] C. Sun, X. Gao, S. Jin, M. Matthaiou, Z. Ding, and C. Xiao, "Beam division multiple access transmission for massive MIMO communications," *IEEE Trans. Commun.*, vol. 63, no. 6, pp. 2170–2184, Jun. 2015.

[512] X. Zhang, M. Matthaiou, M. Coldrey, and E. Bjornson, "Energy efficiency optimization in hardware-constrained large-scale MIMO systems," in *11th International Symposium on Wireless Communications Systems (ISWCS)*. Barcelona: IEEE, Aug. 2014, pp. 992–996.

[513] E. Björnson, L. Sanguinetti, J. Hoydis, and M. Debbah, "Optimal design of energy-efficient multi-user MIMO systems: Is massive MIMO the answer?" *IEEE Trans. Wireless Commun.*, vol. 14, no. 6, pp. 3059–3075, Jun. 2015.

[514] C. Guo, B. Liao, L. Huang, X. Lin, and J. Zhang, "On Convexity of Fairness-Aware Energy-Efficient Power Allocation in Spectrum-Sharing Networks," *IEEE Commun. Letters*, vol. 20, no. 3, pp. 534–537, Mar. 2016.

[515] S. Boyd and L. Vandenberghe, *Convex Optimization*. Cambridge University Press, 2009.

[516] P. D. Diamantoulakis, K. N. Pappi, G. K. Karagiannidis, and H. V. Poor, "Autonomous Energy Harvesting Base Stations With Minimum Storage Requirements," *IEEE Wireless Commun. Lett.*, vol. 4, no. 3, pp. 265–268, Jun. 2015.

[517] P. D. Diamantoulakis, K. N. Pappi, S. Muhaidat, G. K. Karagiannidis, and T. Khattab, "Underlay cognitive radio: What is the impact of carrier aggregation and relaying on throughput?" in *IEEE Wireless Communications and Networking Conference (WCNC)*. Doha, Qatar: IEEE, Apr. 2016, pp. 1–6.

[518] P. D. Diamantoulakis, G. D. Ntouni, K. N. Pappi, G. K. Karagiannidis, and B. S. Sharif, "Throughput maximization in multicarrier wireless powered relaying networks," *IEEE Wireless Commun. Lett.*, vol. 4, no. 4, pp. 385–388, Aug. 2015.

[519] L. Ju-hu and W. Wei-ling, "Performance of MIMO-OFDM systems with phase noise at transmit and receive antennas," in *Proc. International Conference on Wireless Communications, Networking and Mobile Computing (WiCOM)*. Wuhan, CN: IEEE, Sep. 2011, pp. 1–4.

[520] H. Zareian and V. Vakili, "Analytical BER performance of M-QAM-OFDM systems in the presence of IQ imbalance," in *Proc. IFIP International Conference on Wireless and Optical Communications Networks (WOCN)*. Singapore, SG: IEEE, Jul. 2007, pp. 1–5.

[521] J. Qi and S. Aissa, "Compensation for HPA nonlinearity and I/Q imbalance in MIMO beamforming systems," in *IEEE International Conference on Wireless and Mobile Computing, Networking and Communications (WiMob)*. Niagara Falls, ON: IEEE, Oct. 2010, pp. 78–82.

[522] T. C. Schenk, E. R. Fledderus, and P. F. Smulders, "Performance impact of IQ mismatch in direct-conversion MIMO OFDM transceivers," in *Proc. IEEE Radio and Wireless Symposium (RWS)*. Long Beach, CA: IEEE, Jan. 2007, pp. 329–332.

[523] G.-T. Gil, I.-H. Sohn, jin Kyu Park, and Y. H.Lee, "Joint ML estimation of carrier frequency, channel, I/Q mismatch, and DC offset in communication receivers," *IEEE Trans. Veh. Technol.*, vol. 54, no. 1, pp. 338–349, Jan. 2005.

[524] Y. Jin, J. Kwon, Y. Lee, J. Ahn, W. Choi, and D. Lee, "Additional diversity gain in OFDM receivers under the influence of IQ imbalances," in *IEEE International Conference on Communications (ICC)*. Glasgow, GB: IEEE, Jun. 2007, pp. 5915–5920.

[525] E. Au, Z. Lei, and F. Chin, "Exploiting the diversity gain of transmitter I/Q imbalance in single-antenna OFDM systems," in *IEEE Global Telecommunications Conference (GLOBECOM)*. Honolulu, HI: IEEE, Nov. 2009, pp. 1–5.

[526] S. Alamouti, "A simple transmit diversity technique for wireless communications," *IEEE J. Sel. Areas Commun.*, vol. 16, no. 8, pp. 1451–1458, Oct. 1998.

[527] B. Xu, C. Yang, and G. Bi, "Frequency-time block code for frequency diversity in UWB-OFDM systems," *Journal of Electronics (China)*, vol. 23, no. 4, pp. 481–484, Jul. 2006.

[528] D. Bartolome and A. Perez-Neira, "MMSE techniques for space diversity receivers in OFDM-based wireless LANs," *IEEE J. Sel. Areas Commun.*, vol. 21, no. 2, pp. 151–160, Feb. 2003.

[529] T. Cui and C. Tellambura, "Joint frequency offset and channel estimation for OFDM systems using pilot symbols and virtual carriers," *IEEE Trans. Wireless Commun.*, vol. 6, no. 4, pp. 1193–1202, Apr. 2007.

[530] Y.-F. Chen and C.-S. Wang, "Adaptive antenna arrays for interference cancellation in OFDM communication systems with virtual carriers," *IEEE Trans. Veh. Technol.*, vol. 56, no. 4, pp. 1837–1844, Jul. 2007.

[531] H. Stark and J. Woods, *Probability, Statistics, and Random Processes for Engineers*, 4th ed. Prentice Hall, 2012.

[532] M. K. Simon and M. S. Alouini, *Digital Communication over Fading Channels: A Unified Approach to Performance Analysis*, 1st ed. New York: Wiley, 2000.

[533] G. Stuber, J. Barry, S. McLaughlin, Y. Li, M. Ingram, and T. Pratt, "Broadband MIMO-OFDM wireless communications," *Proc. IEEE*, vol. 92, no. 2, pp. 271–294, Feb. 2004.

[534] Y. Li, L. Wang, and Z. Ding, "An integrated linear programming receiver for LDPC coded MIMO-OFDM signals," *IEEE Trans. Commun.*, vol. 61, no. 7, pp. 2816–2827, Jul. 2013.

[535] J. Proakis and M. Salehi, *Digital Communications*, ser. McGraw-Hill higher education. McGraw-Hill Education, 2007.

[536] M. Mokhtar, A. Gomaa, and N. Al-Dhahir, "OFDM AF relaying under I/Q imbalance: Performance analysis and baseband compensation," *IEEE Trans. Commun.*, vol. 61, no. 4, pp. 1304–1313, Apr. 2013.

[537] 3GPP Technical Specification Group Radio Access Network, "Study on UMTS/LTE in 900 MHz band and coexistence with 850 MHz band," 3 GPP, TR 37.804, 2012.

[538] B. Crow, I. Widjaja, J. G. Kim, and P. Sakai, "IEEE 802.11 wireless local area networks," *IEEE Commun. Mag.*, vol. 35, no. 9, pp. 116–126, Sep. 1997.

[539] A. Goldsmith and S. Wicker, "Design challenges for energy-constrained ad hoc wireless networks," *IEEE Wireless Commun. Mag.*, vol. 9, no. 4, pp. 8–27, Aug. 2002.

[540] M. Dohler and Y. Li, *Cooperative Communications: Hardware, Channel and PHY*. Wiley, 2010.

[541] T.-D. Nguyen, O. Berder, and O. Sentieys, "Cooperative MIMO schemes optimal selection for wireless sensor networks," in *IEEE Vehicular Technology Conference (VTC-Spring)*. Dublin, IE: IEEE, Apr. 2007, pp. 85–89.

[542] G. Y. Li, Z. Xu, C. Xiong, C. Yang, S. Zhang, Y. Chen, and S. Xu, "Energy-efficient wireless communications: tutorial, survey, and open issues," *IEEE Wireless Commun.*, vol. 18, no. 6, pp. 28–35, Dec. 2011.

[543] Y. E. Lin, K. H. Liu, and H. Y. Hsieh, "On using interference-aware spectrum sensing for dynamic spectrum access in cognitive radio networks," *IEEE Trans. Mob. Comput.*, vol. 12, no. 3, pp. 461–474, Mar. 2013.

[544] M. Lopez-Benitez and F. Casadevall, "Signal uncertainty in spectrum sensing for cognitive radio," *IEEE Trans. Commun.*, vol. 61, no. 4, pp. 1231–1241, Apr. 2013.

[545] L. Shen, H. Wang, W. Zhang, and Z. Zhao, "Blind spectrum sensing for cognitive radio channels with noise uncertainty," *IEEE Trans. Wireless Commun.*, vol. 10, no. 6, pp. 1721–1724, Jun. 2011.

[546] R. Tandra and A. Sahai, "Snr walls for signal detection," *IEEE J. Sel. Top. Signal Process.*, vol. 2, no. 1, pp. 4–17, Feb. 2008.

[547] D. Tsonev, S. Sinanovic, and H. Haas, "Complete modeling of nonlinear distortion in OFDM-based optical wireless communication," *J. Lightwave Technol.*, vol. 31, no. 18, pp. 3064–3076, Sep. 2013.

[548] S. Dimitrov and H. Haas, "Information rate of OFDM-based optical wireless communication systems with nonlinear distortion," *J. Lightwave Technol.*, vol. 31, no. 6, pp. 918–929, Mar. 2013.

[549] J. Armstrong, "OFDM for optical communications," *J. Lightwave Technol.*, vol. 27, no. 3, pp. 189–204, Feb. 2009.

[550] M. Abramowitz and I. A. Stegun, *Handbook of Mathematical Functions with Formulas, Graphs, and Mathematical Tables*. New York: Dover Publications, 1965.